



The University of  
**Nottingham**

ON BITUMEN MICROSTRUCTURE AND  
THE EFFECTS OF CRACK HEALING

by

Joshua Gaskin

Thesis submitted to the University of Nottingham

For the degree of Doctor of Philosophy

July 2013

# ABSTRACT

When an asphalt pavement is subjected to repeated traffic loads punctuated by rest periods, the acquisition of damage is interrupted by molecular relaxation and healing: the restoration of continuity across fractured interfaces. The healing effect is responsible for improved fatigue performance at high temperatures and dominates the laboratory-to-field shift factor in design. The mechanism of healing is not well understood, however. To describe this process, myriad investigations are collated with healing in high polymers, but neglect microstructural changes due to the damage processes that precipitate fracture. Yet, the remnants of deformation drive healing phenomena. An enhanced knowledge of healing and the effect of fracture could allow for the direct application of laboratory fatigue in pavement performance prediction.

This thesis develops an understanding of the interrelation between binder structure and crack healing, using electron microscopy and mechanical analyses. Cryogenic microscopy indicates that the bulk is amorphous: phase separation in the form of bi-continuous or discrete structure is catalysed by surface effects including composition-dependent short-range interactions and thermal gradients. Environmental microscopy shows that the creation of a free surface during fracture perturbs the bulk solubility continuum, which stimulates phase separation in the form of interconnected fibrils. This system is sensitive to molecular scission and precludes healing by spatial interference and by reduced potential interaction.

Rheological tests confirm the space-bound character of the microstructure and emphasise the requirement for an efficient method to quantify healing. Vialit pendulum tests validate the use of cohesive energy for this purpose and define the effect of fracture temperature: the capacity for healing is reduced by rupture of glassy fractions. Although susceptible to high variability, the outcome of direct tension testing confirms the involvement of crystallisable materials and the reduced proliferation of interfacial molecular interaction due to main-chain scission.

# CONTENTS

Abstract .....	i
Contents .....	ii
List of tables .....	viii
List of figures .....	x
1 Introduction .....	1
1.1 Background .....	1
1.2 Defining the problem .....	2
1.3 Research aim and scope .....	3
2 Bitumen constitution.....	5
2.1 Elemental composition of bitumen .....	5
2.2 Characteristic molecular structures in bitumen .....	6
2.3 Fractional composition of bitumen .....	7
2.4 Intermolecular interactions .....	12
2.5 Bitumen structure .....	15
2.5.1 Colloidal model.....	16
2.5.2 Microstructural model.....	19
2.6 Microscopy investigations .....	21
2.6.1 Atomic force microscopy .....	23
2.6.2 Scanning electron microscopy .....	33
2.6.3 Discussion on microscopy literature .....	44
2.7 Chapter summary.....	45
2.8 Conclusions and approach.....	46
3 A review on bitumen healing.....	47

3.1	Introductory remarks .....	47
3.2	A review on fatigue and fracture .....	48
3.3	Postulations on the healing mechanism .....	49
3.3.1	Preamble .....	49
3.3.2	The interdiffusion concept .....	50
3.3.3	The multi-step concept for fatigue and healing .....	57
3.3.4	The dissipative thermodynamic concept .....	58
3.3.5	The pseudo variable concept .....	60
3.3.6	The thermodynamic model of fracture and healing .....	63
3.3.7	Thixotropic effects .....	65
3.4	Historical work on damage healing in asphalt .....	66
3.4.1	Preamble .....	66
3.4.2	A review of fatigue- and fracture-healing tests on asphalt .....	66
3.4.3	A review of techniques used to quantify healing .....	67
3.4.4	Developments in research regarding asphalt healing .....	70
3.5	Historical work on damage healing in bitumen .....	77
3.5.1	Preamble .....	77
3.5.2	A review of fracture-healing tests on bitumen .....	77
3.5.3	Developments in research affecting bitumen healing .....	78
3.6	Chapter summary .....	86
3.7	Conclusions and approach .....	87
4	Research approach .....	88
4.1	Introductory remarks .....	88
4.2	Experimental materials .....	89
4.2.1	Bitumen fractionation .....	90

4.2.2	Laboratory ageing of sampled bitumens .....	91
4.2.3	Conventional physical property tests .....	91
4.2.4	Rheological property tests .....	92
4.3	Research diagram .....	103
4.3.1	Introductory remarks .....	103
4.3.2	Explanation of the research process .....	104
5	A study on bitumen and its fractions by SEM .....	106
5.1	Environmental scanning electron microscopy .....	107
5.1.1	Background .....	107
5.1.2	Sample preparation .....	107
5.1.3	Sample testing .....	109
5.1.4	Radiation effects in ESEM .....	110
5.1.5	The morphology of bitumen .....	116
5.1.6	The morphology of bitumen fractions .....	125
5.1.7	Discussion .....	130
5.1.8	Summary .....	131
5.2	Cryogenic scanning electron microscopy .....	132
5.2.1	Background .....	132
5.2.2	Review of pertinent literature .....	132
5.2.3	Sample preparation .....	134
5.2.4	Sample testing .....	135
5.2.5	The morphology of bitumen .....	135
5.2.6	The morphology of maltenes .....	141
5.2.7	Summary .....	142
5.3	Cryogenic focused ion beam microscopy .....	144

5.3.1	Background .....	144
5.3.2	Review of pertinent literature .....	145
5.3.3	Sample testing.....	148
5.3.4	FIB etching of bitumen .....	148
5.3.5	FIB etching of maltenes .....	153
5.3.6	Summary.....	154
5.4	Conclusions and recommendations .....	155
5.4.1	Conclusions from microscopy studies.....	155
5.4.2	Recommended further electron microscopy studies.....	156
6	A study on fracture healing in bitumen .....	158
6.1	Introductory remarks .....	159
6.2	Direct tension testing.....	159
6.2.1	Background .....	159
6.2.2	Review of pertinent literature .....	159
6.2.3	Sample preparation.....	161
6.2.4	Sample testing.....	162
6.2.5	Results and discussion .....	163
6.2.6	Electron microscopy study on short-term healing .....	168
6.2.7	Summary.....	170
6.3	Dynamic shear rheometry .....	172
6.3.1	Background .....	172
6.3.2	Fatigue-healing tests.....	172
6.3.3	Fracture-healing tests .....	178
6.3.4	Correlation of fatigue- and fracture-healing .....	180
6.3.5	Summary.....	181

6.4	Vialit pendulum test.....	182
6.4.1	Background .....	182
6.4.2	Sample preparation.....	183
6.4.3	Sample testing.....	183
6.4.4	Results and discussion .....	184
6.4.5	Summary.....	192
6.5	Collation of mechanical test data .....	193
6.6	Electron microscopy study on fracture healing .....	195
6.6.1	Preamble.....	195
6.6.2	Precursory cryo-SEM study on healing.....	195
6.6.3	ESEM study on healing.....	196
6.6.4	ESEM study on fracture .....	198
6.6.5	A comment on the effects on microstructure .....	199
6.6.6	Discussion on the effects of microstructure .....	199
6.6.7	Summary.....	201
6.7	Conclusions and recommendations .....	202
6.7.1	Conclusions from mechanical analyses of crack healing .....	202
6.7.2	Conclusions from microscopic analyses of crack healing.....	203
6.7.3	Recommended further studies on healing .....	203
7	Conclusions .....	204
7.1	Conclusions from microscopy studies.....	205
7.2	Conclusions from mechanical studies.....	206
7.3	Overall conclusion.....	208
7.4	Conclusions with regard to asphalt pavements .....	209
	List of references.....	211



# LIST OF TABLES

Table 2-1: Summary of composition as derived from a typical 85/100 bitumen (Corbett, 1969) .....	8
Table 2-2: Effect of polarity on the viscosity of asphalt fractions (Peterson, 2009).....	15
Table 2-3: A chronological summary on the composition of the bee-like structuring by AFM.	26
Table 2-4: A summary of the mechanisms potentially involved in the bee-like structuring .....	29
Table 2-5: A chronological summary on bitumen structure by ESEM at ambient temperatures .....	36
Table 2-6: The thermal behaviour of chromatographic fractions as characterised by differential scanning calorimetry (DSC) and thermogravimetry (TGA). After Jiménez-Mateos et al. (1996) .....	40
Table 3-1: Mixture stiffness effect on improvement in fatigue life for a rest-to-load cycle period ratio of 25 (Bonnaure et al., 1982) .....	72
Table 3-2: Life ratio values on the basis of regression (Awanti et al., 2007) .....	75
Table 3-3: Life ratio values on the basis of intermittent fatigue tests (Lu et al., 2003) .....	81
Table 3-4: Healing rates for different testing conditions (Shen et al., 2010).....	82
Table 4-1: A summary cross-referencing prominent physical-chemical theories on healing with the structure of bitumen, which is recovered by this process (thesis page references included) .....	89
Table 4-2: Physical properties and basic chemical composition of sampled bitumens .....	90
Table 4-3: SHRP suggested disc diameters for DSR rheology testing (Anderson et al., 1994) .....	93
Table 4-4: A chronological summary on bitumen structure by ESEM at ambient temperatures .....	96
Table 4-5: DSR test conditions for sample geometry .....	96
Table 5-1: A summary of key preparation methods with benefits (ben.) and drawbacks (dra.) .....	107
Table 5-2: A summary of radiation effects in bitumen with varying asphaltene (asph.) content .....	110

Table 5-3: Parameters developed for ESEM quantification of sample microstructure at 25°C .....	117
Table 5-4: Summary of geometrical properties of dispersed bee-like structures at 5°C .....	119
Table 5-5: A summary of the morphology of bitumen fractions using ESEM .....	125
Table 5-6: Chronological summary of ESEM literature on asphaltene morphology .....	126
Table 5-7: Geometrical properties of un-etched and etched bee-like structures.....	151
Table 6-1: Variability of failure properties at 3%/min and -25°C (bitumen B) .....	165
Table 6-2: Parameters for ESEM quantification of sample microstructure (bitumen B) .....	165
Table 6-3: Parameters developed for the modified Christensen-Anderson Model.....	167
Table 6-4: Parameters for ESEM quantification of healed and initial structuring in bitumen B .....	170
Table 6-5: Parameters developed for the healing function for bitumen B .....	177
Table 6-6: Parameters developed for the modified Christensen-Anderson Model.....	186
Table 6-7: Parameters for the Christensen-Anderson model at a healing temperature of 40°C .....	188
Table 6-8: Parameters for ESEM quantification of healed and initial structuring in bitumen B (data derived from micrographs produced at 20°C).....	197
Table 6-9: Parameters for ESEM quantification of fractured and poured structure in bitumen B (data derived from micrographs produced at 20°C).....	199
Table 6-10: Parameters for ESEM quantification of the effects of fracture-delay-healing on the microstructure of bitumen B (data derived from micrographs produced at 20°C) .....	200
Table 6-11: Parameters for ESEM quantification of initial structure and healing (data derived from micrographs produced at 20°C and using the Christensen-Anderson model).....	200
Table 7-1: Summary of the important novel findings of this research .....	204

# LIST OF FIGURES

Figure 1-1: Flow diagram of the research to correlate bitumen structure and healing .....	4
Figure 2-1: Ball-and-stick diagram of a typical bitumen molecule, after Redelius (2011) .....	6
Figure 2-2: Ball-and-stick diagrams of characteristic molecules found in bitumen, developed from Airey (1997); Read and Whiteoak (2003); Hornback (2006); and Redelius (2011) .....	7
Figure 2-3: Schematic of Corbett chromatography (Read and Whiteoak, 2003).....	8
Figure 2-4: Plate-stack model for asphaltenes, after Dickie and Yen (1967), Porte et al. (2003) and Read and Whiteoak (2003) .....	9
Figure 2-5: Parallel-displaced pi stacking of the benzene dimer .....	14
Figure 2-6: A simplified notion of the colloidal structure of bitumen: the micelles are pictured as spherical to illustrate the solvation layer. The schematic transverse cut of a micelle shows a perynaphthyl radical trapped by a transition from even aromatics and stacked asphaltenes to resins. After Dickie and Yen (1967), Acevedo et al. (1997) and Lesueur (2009) .....	17
Figure 2-7: Schematic of: (a) sol bitumen, and (b) gel bitumen (Read and Whiteoak, 2003) .	18
Figure 2-8: The microstructural model, showing chain building between active sites (denoted by stars) in polar molecules associating into different shapes, after Jones and Kennedy (1991).....	20
Figure 2-9: Schematic assembly of an atomic force microscope, with a magnification of the interaction of the tip and sample atoms. Developed from Rugar and Hansma (1990) and Adamsmaier (2008).....	24
Figure 2-10: Atomic force microscopy topography image of bitumen AAK-1 (Pauli et al., 2011) .....	25
Figure 2-11: AFM scan of AAA-1 doped with tetratetracontane (Pauli et al., 2011).....	28
Figure 2-12: Schematic of a chain folded lamella with periodic undulations in which chain tilting occurs, and the solid-liquid interface with intermediate order (Mehta et al., 2004).....	30
Figure 2-13: Schematic of a scanning electron microscope, with secondary electron (SE) and backscattered electron (BSE) detectors. Encyclopaedia Britannica (2008) .....	33

Figure 2-14: Possible interactions of the electron beam impinging with the surface of a solid sample: the most important signals are secondary electrons, backscattered electrons and X-rays, shown in magnifications. Developed from Johnson (1966) and Poulikakos (2011) .....	34
Figure 2-15: Micrograph of bitumen after several minutes irradiation (Rozeveld et al., 1997)	37
Figure 2-16: Micrograph of strained bitumen after electron irradiation (Rozeveld et al., 1997) .....	39
Figure 2-17: SEM of fractured surface of HDPE/33EVA blend along flow (Na et al., 2003) ...	44
Figure 3-1: Schematic of fracture propagation and chain separation by loss of entanglement, developed from Kausch and Dettenmaier (1982) .....	49
Figure 3-2: Schematic of chain motion during healing of a fractured interface (Wool, 1995). Stages: (I) rearrangement, (II) approach, (III) wetting, (IV) diffusion and (V) randomisation ..	50
Figure 3-3: Variation of strength with rearrangement time (Wool, 1995).....	51
Figure 3-4: Disengagement of a molecule from its initial conformation near an interface, the increasing spherical envelopes of minor chains and entanglement formation (Wool, 1995) ..	53
Figure 3-5: PB healing using a double cantilever beam test (Wool and O'Connor, 1981) .....	54
Figure 3-6: The effect of pressure on the recovery of fracture toughness (Jud et al., 1981) ..	56
Figure 3-7: The multi-stage model for fracture and healing, postulated by Phillips (1999) .....	57
Figure 3-8: Stress-strain and transformed stress-pseudo strain loops for two loading cycles (Kim et al., 2003).....	61
Figure 3-9: (I) Change in pseudo stiffness due to a rest period (Lee and Kim, 1998) and (II) Conceptual diagram for damage healing (Roque et al., 2010).....	62
Figure 3-10: Schematic RDEC plot showing the three zones of behaviour, Shen et al. (2009) .....	69
Figure 3-11: Recovery master curve for asphalt mixtures at a reference temperature of 15°C, produced by the author of this thesis from data reported by Bazin and Saunier (1967) .....	70
Figure 3-12: Variation of healing index with MMHC ratio for bitumens (Kim et al., 1990).....	73
Figure 3-13: Variation of recovery of DCSE with healing temperature, produced by the author of this thesis using data reported by Kim and Roque (2006).....	76
Figure 3-14: Schematic of repeated local failure test, after from de la Roche et al. (2003) ....	77
Figure 3-15: Schematic of the intrinsic two-piece healing test (Bommavaram et al., 2009)....	78

Figure 3-16: Evolution of force versus displacement during stage two (displacement controlled) tests on 50/70 penetration grade bitumen at 0°C (Maillard et al., 2004) .....	79
Figure 3-17: Variation of healing with time and surface energy (Bommavaram et al., 2009)..	80
Figure 3-18: Variation of (I) complex modulus and (II) sample temperature during fatigue and healing cycles of the intermittent loading test (Bodin et al., 2004) .....	81
Figure 3-19: Fatigue life and healing time for three binders <i>in duplo</i> (Phillips, 1999) .....	83
Figure 3-20: The effect of rest periods in storage recuperation tests on bitumen complex modulus and fatigue life (Lu et al., 2003).....	84
Figure 4-1: Example strain sweep for selected bitumens, tested at 10°C and frequency of 1Hz .....	97
Figure 4-2: Isochrones of complex modulus for bitumen and maltenes (mal.) at 1Hz shear ..	98
Figure 4-3: Isochrones of phase angle for bitumen and maltenes (mal.) at 1Hz oscillation ....	98
Figure 4-4: Isotherms of complex modulus for bitumen and maltenes (mal.) at 15°C and 35°C .....	99
Figure 4-5: Isotherms of complex modulus for bitumen and maltenes (mal.) at 15°C and 35°C .....	99
Figure 4-6: Master curves of complex modulus ( $G^*$ ) for the reference temperature of 25°C	100
Figure 4-7: Master curves of phase angle ( $\delta$ ) for the reference temperature of 25°C.....	101
Figure 4-8: Black diagram for bitumen and maltenes (using Peltier (P) and fluid (F) cooling) .....	101
Figure 4-9: Fatigue (continuous shear) curves for maltenes and bitumen. Complex modulus is normalised to the initial (for the maltenes mean initial modulus is 17.8kPa).....	102
Figure 4-10: Schematic of structural failure of an asphalt pavement and stresses induced by the moving wheel load. Developed from Read and Whiteoak (2003) .....	104
Figure 4-11: Research diagram for the experimental study on bitumen structure and healing .....	105
Figure 5-1: Conceptual representation of the research approach for the microscopy section .....	106
Figure 5-2: (a) ESEM micrograph of bitumen D after 2 minutes irradiation at 25°C. (b) Beam .....	111

Figure 5-3: Beam effects due to discontinuous irradiation of bitumen D at 10keV and 25°C. .....	112
Figure 5-4: (a) Image of bubble formation and rupture in bitumen D at 25°C. (b) Distortion of entangled network components due to metallic precipitates. ....	113
Figure 5-5: (a) Image of charging in bitumen B, irradiated at 10keV and 25°C for 10 minutes. (b) Micrograph of bitumen B irradiated at 20keV and 25°C for 5 minutes. ....	114
Figure 5-6: Micrograph of bitumen A following irradiation at 20keV and 25°C for 20 minutes. .....	115
Figure 5-7: Example of quantification of properties of bitumen structure from an ESEM image .....	116
Figure 5-8: (a) Micrograph of bitumen D following irradiation at 10keV and 0°C for 2 minutes. (b) Micrograph of bitumen D following irradiation at 10keV and 5°C for 2 minutes. ....	120
Figure 5-9: (a) Micrograph of bitumen D following irradiation at 10keV and 10°C for 2 minutes. (b) Micrograph of bitumen D following irradiation at 10keV and 15°C for 2 minutes. ....	120
Figure 5-10: (a) Micrograph of bitumen D after irradiation at 10keV and 20°C for 2 minutes. (b) Micrograph of bitumen D captured at 0°C after the thermal cycle (0°C to 25°C to 0°C)..	120
Figure 5-11: (a) Image of bitumen D (aged) after irradiation at 10keV and 0°C for 2 minutes. (b) Micrograph of bitumen D (aged) following irradiation at 10keV and 5°C for 2 minutes. ..	122
Figure 5-12: (a) Image of bitumen D (aged) after irradiation at 10keV and 10°C for 2 minutes. (b) Micrograph of bitumen D (aged) following irradiation at 10keV and 15°C for 2 minutes.	122
Figure 5-13: (a) Image of bitumen D (aged) after irradiation at 10keV and 20°C for 2 minutes. (b) Micrograph of bitumen D (aged) following irradiation at 10keV and 25°C for 2 minutes.	122
Figure 5-14: Image of bitumen D (aged) at 0°C after the thermal cycle (0°C to 25°C to 0°C). .....	123
Figure 5-15: Micrographs of bitumen C after irradiation at 10keV and 0°C for 2 minutes. ....	124
Figure 5-16: (a) Micrograph of bitumen C after irradiation at 10keV and 0°C for 2 minutes. (b) Micrograph of bitumen C following irradiation at 10keV and 15°C for 2 minutes. ....	124
Figure 5-17: (a) Micrograph of bitumen C after irradiation at 10keV and 20°C for 2 minutes. (b) Micrograph of bitumen C following irradiation at 10keV and 25°C for 2 minutes. ....	125

Figure 5-18: (a) Micrograph of asphaltenes after irradiation at 10keV and 25°C for 2 minutes.  
(b) Image of fracture detail in asphaltenes after irradiation at 10keV and 25°C for 2 minutes.  
..... 127

Figure 5-19: (a) Micrograph of maltenes after irradiation at 10keV and -10°C for 1 minute. (b)  
Micrograph of maltenes after irradiation at 10keV and -10°C for 2 minutes..... 128

Figure 5-20: (a) Low resolution image of wax after irradiation at 10keV and 5°C for 1 minute.  
(b) High resolution micrograph of wax after irradiation at 10keV and 5°C for 1 minute. .... 129

Figure 5-21: (a) Micrograph of waxes after irradiation at 10keV and 20°C for 1 minute. (b)  
Micrograph of waxes after irradiation at 10keV and 0°C for 1 minute. .... 130

Figure 5-22: Image of thin bitumen D sample after irradiation at 10keV and 20°C for 1 minute.  
..... 131

Figure 5-23: Sample pressed between two rivet mounts for fracture under cryo conditions. 135

Figure 5-24: (a) Electron micrograph of bitumen D showing the effects of freezing in the slush.  
(b) Electron micrograph of bitumen D showing bee-like structures and cracking..... 136

Figure 5-25: (a) Electron micrograph of bitumen D showing an aborted secondary crack. (b)  
Electron micrograph of bitumen D showing cracked bee-like structures..... 136

Figure 5-26: Schematic of overlapping depletion layers and unbalanced osmotic pressure  
(Lekkerkerker and Tunier, 2011)..... 137

Figure 5-27: Electron micrograph of near-surface bee-type structuring in bitumen D at a crack.  
..... 138

Figure 5-28: (a) Cryo-SEM micrograph of the bulk of bitumen D, produced by *in situ* fracture.  
(b) Micrograph of bitumen D showing the fragmented structure of the fractured surface. .... 139

Figure 5-29: (a) Micrograph of the bulk of bitumen D showing pyramidal instabilities and  
planar layering. (b) Micrograph of parabolic cast marks in the bulk of bitumen D..... 139

Figure 5-30: Schematic illustration of phase separation by spinodal decomposition (Masson et  
al., 2003; Wei et al., 2010) ..... 140

Figure 5-31: (a) Cryo-SEM micrograph of maltenes showing ice crystal growth at the surface.  
(b) Micrograph of maltenes indicating columnar ice crystal growth due to freezing in the slush.  
..... 141

Figure 5-32: (a) Low magnification image of the surface of quenched maltenes with cleavage cracks. (b) Cryo-SEM micrograph of the amorphous surface of gradually-cooled maltenes. 141

Figure 5-33: (a) Micrograph of topographic detail in the bulk of maltenes produced by fracture. (b) Cryo-SEM micrograph of planar layering in the bulk of the maltenes, exposed *in situ*. ... 142

Figure 5-34: Possible interactions of the incident ion beam with a solid sample; the most important process is the release of target atoms: physical sputtering (Orloff et al., 2006).... 145

Figure 5-35: Diagram of the evolution of the surface of vitreous ice with beam incidence angle (Fu et al., 2008)..... 147

Figure 5-36: (a) Cryo-SEM image of the effects of ion bombardment of bitumen D at 1nA and 0° incidence. (b) Image of the effects of ion irradiation in bitumen D at 3nA and 0° incidence. .... 149

Figure 5-37: (a) Micrograph of peripheral effects of ion bombardment of bitumen D at 3nA and 0° incidence. (b) Image of the effects of ion irradiation in bitumen D at 3nA and 20° incidence. .... 150

Figure 5-38: (a) Micrograph of the effects of ion bombardment of bitumen D at 3nA and 52° incidence. (b) Image of the effects of ion irradiation in bitumen D at 3nA, 52° incidence and a dwell time 20µs. .... 150

Figure 5-39: (a) Micrograph of the effects of ion bombardment bee-type structure 30pA and 0° incidence. (b) Image of the effects of prolonged FIB irradiation of another bee-type structure. .... 152

Figure 5-40: (a) Image of the effects of ion irradiation of structured and amorphous domains at 30pA and 0° incidence. (b) Image of the effects of ion irradiation in the bulk of bitumen D. .... 152

Figure 5-41: (a) Micrograph of the effect of ion bombardment of the surface of quench-cooled maltenes. (b) Image of near-surface phase separation in gradually-cooled maltenes..... 153

Figure 5-42: (a) High-magnification of the phase separation along the ion-eroded edge of the surface in gradually-cooled maltenes. (b) Micrograph of the effects of ion bombardment in the bulk of quench-cooled maltenes ..... 154

Figure 6-1: Conceptual representation of the research approach for the mechanical section ..... 158

Figure 6-2: Various stress-strain behaviours of bitumen in the DTT, where the failure stress in each example is denoted by grey circles .....	160
Figure 6-3: Direct tension test aluminium mould and sample geometry (AASHTO T 314-02) .....	161
Figure 6-4: Schematic of the healing test on bitumen using the DTT .....	163
Figure 6-5: Repeatability of DTT at -25°C after one hour annealing at 25°C .....	164
Figure 6-6: Repeatability of DTT at -25°C after 24 hours annealing at 25°C .....	164
Figure 6-7: Repeatability of DTT at -25°C after 48 hours annealing at 25°C .....	164
Figure 6-8: Profile photograph of a fractured, healed and re-fractured DTT sample. Note the two crack trajectories: the healed crack near the right end-tab, and the central re-fracture. ....	166
Figure 6-9: Variation of strength recovery with time modelled using the modified Christensen-Anderson Model, for healing temperatures of 20°C and 40°C and fracture at -25°C .....	167
Figure 6-10: The effect of repeated fracture-healing on recovered strength: healing cycles are 24 hours at 20°C, and fracture is at -25°C .....	168
Figure 6-11: (a) Image of the bridge-healing mechanism in bitumen B (10 seconds exposure). (b) Micrograph of the interfacial bridge after 5 minutes irradiation at 20keV and 20°C .....	169
Figure 6-12: (a) Low magnification image of interruption to healing due to potassium crystals. (b) High resolution of disruption to microstructure due to potassium crystals. ....	170
Figure 6-13: Strain sweep for bitumen B at 20°C and 25Hz, using a Bohlin Gemini rheometer .....	173
Figure 6-14: Variation of normalised complex modulus ( $G^*(n) / G^*(i)$ ) in continuous oscillation, showing the fatigue failure point defined by Rowe and Bouldin (2000) .....	174
Figure 6-15: Complex modulus recovery plots for healing at 20°C from various damage levels .....	175
Figure 6-16: Variation of complex modulus recovery with the fourth root of healing time .....	175
Figure 6-17: Recovery rate of complex modulus with damage level at the onset of healing .....	175
Figure 6-18: Variation of complex modulus recovery with time modelled using the equation by Bhasin et al. (2009), for healing temperatures of 20°C and 40°C and fatigue at 20°C .....	177
Figure 6-19: The effect of repeated fatigue-healing cycles on rheological property recovery .....	178

Figure 6-20: Schematic of the (tensile) fracture (shear) healing test on bitumen B using the dynamic shear rheometer .....	179
Figure 6-21: Recovery of complex modulus at 20°C for samples fractured in tension at 5°C .....	180
Figure 6-22: Data for complex modulus recovery from fatigue-healing tests for healing at 20°C and 40°C, and a fracture-healing test on 3.4mm thick samples at 20°C .....	181
Figure 6-23: Schematic of Vialit pendulum cohesion test (developed from EN 13588:2008)	182
Figure 6-24: Profile photograph of a fractured Vialit pendulum sample (bitumen A).....	184
Figure 6-25: Vialit pendulum curve for bitumen A: the variation of cohesion with temperature .....	185
Figure 6-26: Cohesion recovery curves for bitumen A at 20°C, 30°C, 40°C and 50°C.....	186
Figure 6-27: Cohesion recovery master curve produced for bitumen A at 40°C .....	186
Figure 6-28: The effect of delay between re-contact of fracture surfaces on asymptotic healing .....	187
Figure 6-29: Cohesion recovery curves for virgin and oxidised bitumens healed at 40°C ....	188
Figure 6-30: Cohesion recovery curves produced by healing the bitumen softening points .	189
Figure 6-31: The effect of base plate roughness on the healing of bitumen A at 50°C.....	190
Figure 6-32: The effect of fracture temperature on restored cohesion for healing of bitumen A at 40°C .....	191
Figure 6-33: Variation of Christensen-Anderson model parameters with asphaltene content (m is denoted by the open squares, and n is denoted by the filled diamonds).....	191
Figure 6-34: Collation of data for bitumen B healed at 40°C, and tested using Vialit pendulum (cohesion), DSR (complex modulus and fatigue life) and DTT (strength).....	193
Figure 6-35: Variation of healing asymptote (strength and cohesion) with fracture temperature for bitumens A and B healed at 40°C.....	194
Figure 6-36: Schematic of the approach used to prepare fractured-healed samples for electron microscopy studies.....	195
Figure 6-37: Cryo-SEM images of bitumen B fractured and healed for 0.25 hours at 40°C .	196
Figure 6-38: (a) Low magnification image of a crack interface after 0.5 hours healing at 40°C. (b) High magnification micrograph of the crack interface after 0.5 hours healing at 40°C. ...	197

Figure 6-39: (a) Low magnification image of a crack interface after 6.0 hours healing at 40°C.

(b) High magnification micrograph of the crack interface after 6.0 hours healing at 40°C. ... 197

Figure 6-40: (a) Low magnification image of a crack surface after 0.1hours exposure at 20°C.

(b) High magnification micrograph of the crack surface after 0.1hours exposure at 20°C. .... 198

# 1 INTRODUCTION

## 1.1 BACKGROUND

In the UK, from the late 1700s, Thomas Telford and his contemporary John Loudon McAdam perfected the construction of roads with graded crushed stones, without any medium to bind them together. Yet, under the action of large volumes of traffic these broken-stone roads were liable to be ground into dust that was expelled from the surface in dry weather, and converted into mud in the wet. This inhibited access in these streets (Gillespie, 1855). In 1832 therefore, coal tar was introduced into macadam pavements as a binder: to seal the surface and protect the pavement from water percolation (Abraham, 1838). Tar macadam paving was born and in 1848 its use to construct Lincoln Road in Nottinghamshire heralded the start of the bituminous paving era (Hubbard, 1910; Collins and Hart, 1936). Realising additional benefits of coal tar, road engineers subsequently developed a range of coated-stone materials in which it was the binder. In 1913 coal tar was replaced by refinery bitumen, which is produced from compliant crude oils using the processes of distillation, blowing and blending (RBA, 2011).

Use of refinery bitumen in asphalt paving is preeminent (Kriech et al., 1992). The versatility of bitumen derives from its complex rheology: as a thermoplastic, its deformation properties are sensitive to the rate and temperature at which it is loaded. In two extremes, bitumen behaves as a solid purely elastic material, or as a purely viscous liquid. The brittle characteristics of the solid dominate during rapid loading and at low temperature, whereas the material flows under slow loading and at high temperature (Airey, 1997). This behaviour is separated roughly by its glass transition temperature: the temperature through which heating causes its transformation from the glassy to the liquid state and which is between  $-40^{\circ}\text{C}$  and  $0^{\circ}\text{C}$  (Cheung and Cebon, 1997). At normal in-service temperatures bitumen has a viscous and elastic response to load therefore (Dukatz and Anderson, 1980), and a time-dependent relationship between load and induced strain. This behaviour is controlled by chemistry and microstructure (Peterson, 1984).

Repeated traffic and thermal loading of an asphalt pavement provokes structural degradation: the loss of capacity to maintain compliance with performance requirements. One of the critical

modes of structural distress is fatigue, which is the phenomenon of fracture due to repetitive stress at a magnitude less than the strength of the material. The capacity of laboratory tests to predict fatigue performance is limited however: asphalt fatigue life is miscalculated by up to 2000% (Al-Balbissi and Little, 1990). This difference is ascribed to (Kim and Little, 1990):

1. Rest periods that occur under the compound-loading conditions in the field but not in the (normal) continuous cyclic tests in the laboratory.
2. A sequence of load applications of varying magnitude.
3. Reactions or friction encountered in the field between the asphalt surface and base.

When an asphalt pavement is subjected to repetitive applications of traffic loads interspersed with rest periods, the accumulation of damage is interrupted by relaxation of stress due to the viscoelasticity of bitumen, and the phenomena of adhesive and cohesive healing.

## **1.2 DEFINING THE PROBLEM**

Cohesive healing is the partial restoration of intrinsic bitumen structure across adjacent crack surfaces: a process that reverses crack growth and so extends fatigue life (Little et al., 1999). The nature of binder structure is ambiguous: a network of entangled viscous fibrils embedded in an oily layer to a depth of 400nm is resolved by electron irradiation (Stangl et al., 2006), yet research by atomic force microscopy reports on striped ellipsoidal structures dispersed at the surface (Loeber et al., 1996). Besides morphological differences, there is ambivalence about the composition of this structuring. The network structure is thought (Rozeveld et al., 1997) to be exposed by volatilisation of oils concentrated at the surface: the chemistry of the dispersed phase was initially thought to be of polyaromatics flocculated from an aliphatic moiety (Jäger et al., 2004), but more recently of crystallised fractions. Yet, it is the morphology of the bulk of the material that governs its behaviour, but the structure of this phase remains unresolved.

Notwithstanding microstructural ambiguity, bitumen healing is not yet well understood and the literature is devoid of effective measurement: mechanical analysis of the healing phenomenon is susceptible to testing methods. To develop an understanding of healing kinetics in bitumen,

comparison with high molecular weight polymers is used. Viscous flow and molecular mixing in warm periods or between two axes are thus thought to restore the continuity of the binder, which tends to crack at interparticle contacts in cold weather (Thom, 2008). While discourse on the similitude of the phenomena is instructive and provides understanding of the effects of temperature and time, the problem of evaluating fracture effects in bitumen precludes elegant analogy. Further research is required to study healing in fractured bitumen, which is driven by the remnants of the deformation process (Wool, 1995).

### **1.3 RESEARCH AIM AND SCOPE**

The principal aim of this research is to define the relationship between bitumen microstructure and fracture-healing (refer to Figure 1-1). This thesis focuses accordingly on three aspects:

1. The bulk structure of bitumen and structure-sustaining fractions.
2. The healing phenomenon in bitumen and how it can be measured effectively.
3. The effects of fracture and healing on bitumen microstructure and *vice versa*.

The scope of this thesis consists of a literature review followed by three chapters, focusing on the aspects of this work, and lastly a chapter reporting the conclusions and recommendations.

The literature review presents the principal findings with regards to the chemical composition, physical properties of and intermolecular associations in bitumen. This review also introduces bitumen microstructure, which is historically identified as a three-dimensional network of polar fractions diluted by a less-polar solvent. In this review a proof of structures involving non-polar fractions is summarised. This review lastly presents the healing phenomenon in bitumen, and includes models of this process, methods of characterisation, and influential parameters.

The following three chapters explain the materials selected for this thesis, and introduce novel microscopy and healing studies. Chapter 4 provides a physical description of the investigated bitumens, and introduces the conceptual representation for the research approach. Chapter 5 introduces electron microscopy studies of structuring in bitumen and its fractions. It is shown

that cryogenic preparation enables the first study of internal morphology. Chapter 6 examines the healing phenomenon using three new tests: dynamic shear rheometry, direct tension and Vialit pendulum tests. This thesis emphasises the use of fracture testing, and correlates these with an original microscopy study on the response of bitumen to fracture and healing.

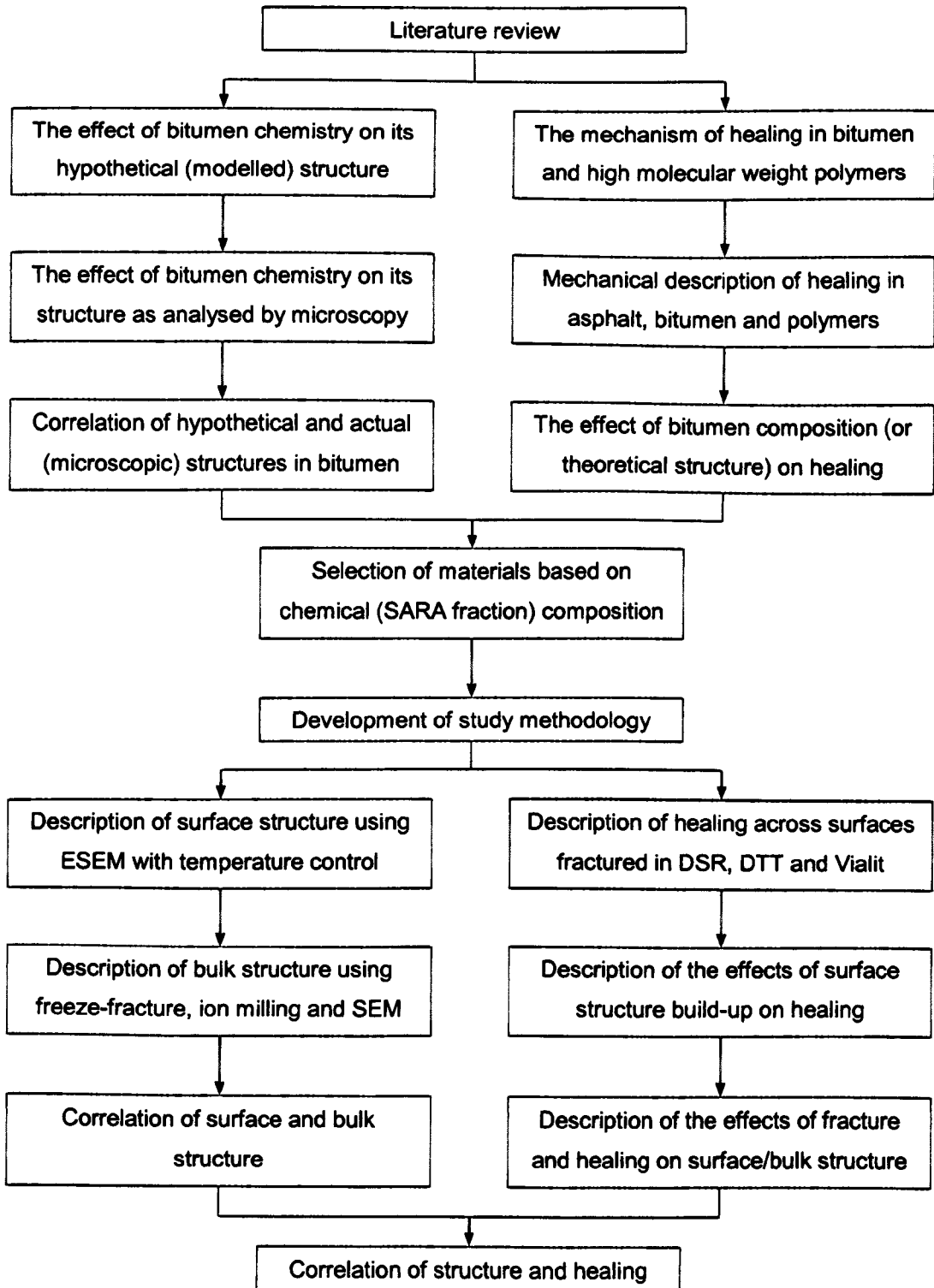


Figure 1-1: Flow diagram of the research to correlate bitumen structure and healing

## 2 BITUMEN CONSTITUTION

In this chapter a review is presented of the elemental, molecular and fractional composition of bitumen and of two models derived to explain molecular associations. A critique of the current microscopy evidence for each model is introduced, from which the third chapter is developed.

### 2.1 ELEMENTAL COMPOSITION OF BITUMEN

The chemical composition and physical properties of refinery bitumen are dependent on the conditions used during its manufacture, and on the crude oil source: the Middle East, Russia, the USA and the Caribbean countries (EIA, 2009). Generally, bitumen constitutes a mixture of highly-polar to neutral hydrocarbon molecules, with a size from about 20 carbons and higher (Redelius, 2011); minor quantities of mono-, di- and poly-substituted heterocyclic molecules<sup>1</sup>; functional groups or heteroatoms containing sulphur, nitrogen and oxygen; and trace metals including vanadium, nickel and iron, which commonly occur in the form of inorganic salts and oxides (Traxler, 1936; Lancaster, 2006).

The functional groups impart functionality<sup>2</sup> and polarity to the hydrocarbons, and thus modify the physical properties of the binder disproportionately to their concentration (Peterson, 1984; Lancaster, 1996). Carboxylic acids for example, which are polar hydrocarbons defined by the incidence of carboxyl functional groups, alter molecular interactions that control flow. Namely, they control viscosity through the formation of hydrogen bonds (Cheung and Cebon, 1997).

Moreover, elemental analyses of bitumens manufactured from a variety of crude sources, with different physical characteristics, have demonstrated that most contain (by weight):

- |             |           |
|-------------|-----------|
| 1. Carbon   | 82% - 88% |
| 2. Hydrogen | 8% - 11%  |

---

<sup>1</sup> Organic compounds with a closed ring of atoms, at least one of which is not carbon

<sup>2</sup> Reactions between bitumen molecules and their interactions with other molecules

3. Sulphur            0% - 6%
4. Oxygen            0% - 1.5%
5. Nitrogen           0% - 6%

Understanding the effect of this composition on bitumen performance derives from knowledge of how these elements interact to form the millions of similar but distinct molecules in bitumen, the architecture by which they are differentiated and the interactions that occur between them.

## 2.2 CHARACTERISTIC MOLECULAR STRUCTURES IN BITUMEN

The complex chemistry of bitumen renders the separation and identification of hydrocarbons infeasible: less than 3% have hitherto been isolated and characterised (Redelius, 2011). Yet, together with heteroatoms and trace metals, bitumen molecules are pseudo-polymers formed of combinations of four broadly-defined organic structures: aliphatic, olefinic, naphthenic and aromatic groups (Breen and Stevens, 1967; Strausz, 1977) (refer to Figures 2-1 and 2-2).

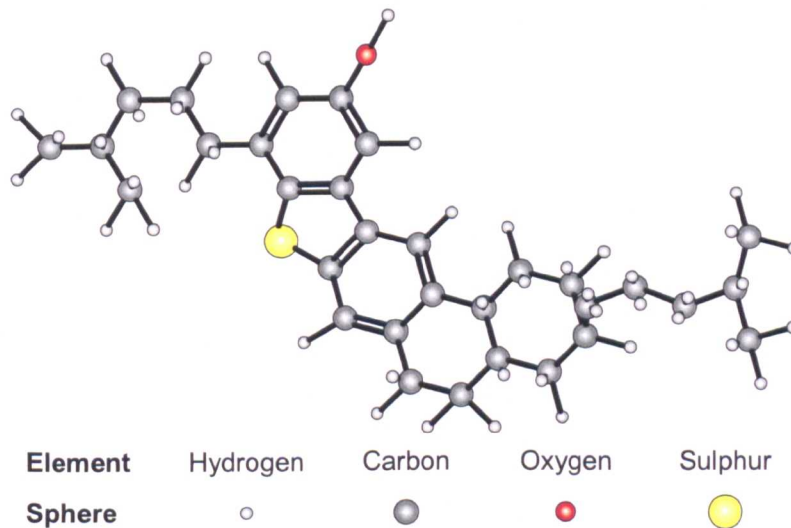


Figure 2-1: Ball-and-stick diagram of a typical bitumen molecule, after Redelius (2011)

Arguably the simplest organic compounds in bitumen, the aliphatics are formed of saturated<sup>3</sup> carbon atoms linked in straight or branched chains in an open structure. Olefins contain one or more carbon-carbon double bonds, are unsaturated and thus more reactive with hydrogen

<sup>3</sup> The condition in which the compound will no longer react with hydrogen (Hornback, 2006)

than aliphatics (Hornback, 2006). In naphthenic groups the carbon atoms are linked in simple or complex saturated rings (Wu, 2009). The aromatic ring systems are distinguished from the naphthenics by the presence of at least one especially stable six-atom ring, such as benzene or toluene (Airey, 1997). Both the aromatic and naphthenic species could have attached side chains: branches off the main chain that affect the behaviour of the bitumen (Quddus, 1992).

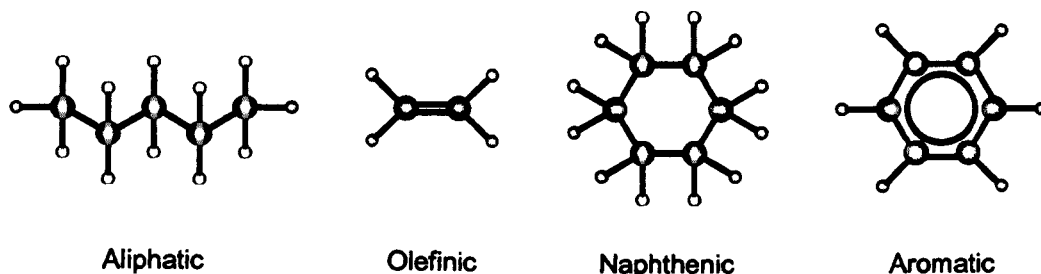


Figure 2-2: Ball-and-stick diagrams of characteristic molecules found in bitumen, developed from Airey (1997); Read and Whiteoak (2003); Hornback (2006); and Redelius (2011)

### 2.3 FRACTIONAL COMPOSITION OF BITUMEN

Through weak chemical bonds (Airey, 1997), these systems form flexible repeating units with a molecular weight between 36 and 91g/mol. The monomers interact to produce a distribution of oligomeric molecules (Masson and Polomark, 2001) that is continuous over a broad range of polarity and molecular weight (Redelius, 2011). This multi-component material is normally examined by one of various fractionation techniques that separate bitumen by molecular size, reactivity or polarity into discrete and less complex fractions. This arbitrary classification yields the proportion and properties of each fraction dependent on the solvent used (Goodrich et al., 1986). Moreover, bitumen fractionation methods are developed in copious published studies.

Perhaps the foremost study was by Boussingault (1837) on the bitumen of Bechelbronn [sic. Merkwiller-Pechelbronn] in Alsace, France. The research separated the material by distillation into two parts: brittle solids called asphaltenes due to a composition similar to natural asphalt (Lesueur, 2009); and distillable volatile oils that serve as a solvent to that phase: petrolene. In a similar manner, Richardson (1910) defined the asphaltenes as the part insoluble in naphtha from petroleum of 62 or 88° Baumé. By its resemblance to maltha: a soft natural bitumen, the author named the insoluble parts malthenes [sic. maltenes] (Lesueur, 2009). With the advent

of modern chromatography, Corbett (1969) defined his often used fractionation scheme (refer to Figure 2-3). This technique firstly separates the asphaltenes as the precipitate on dilution of bitumen in *n*-heptane or *n*-pentane (Redelius, 2011), then subdivides the solute (maltenes) by adsorption-desorption into three fractions with rising polarity: saturates, aromatics and resins.

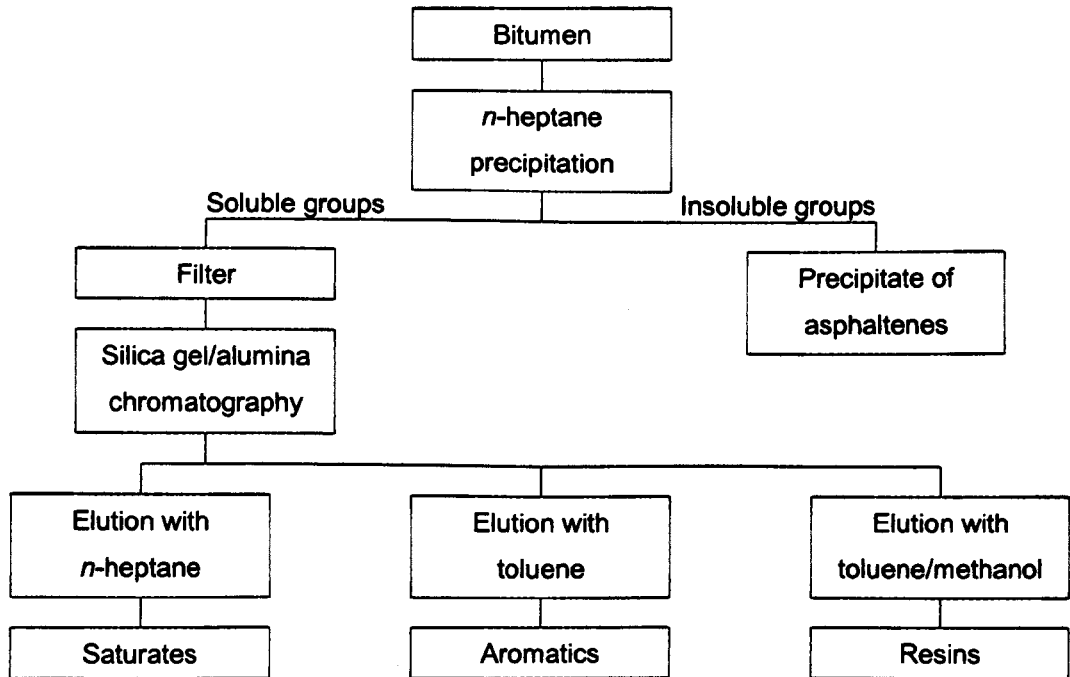


Figure 2-3: Schematic of Corbett chromatography (Read and Whiteoak, 2003)

It is pertinent that the SARA fractions are arbitrarily extracted from a continuous distribution of molecules with differences ascribed to solubility or polarity. While each fraction is more simple and homogeneous than the binder from which it is separated, the fractions overlap and share (Redelius, 2011) the physicochemical properties introduced below (refer also to Table 2-1).

Table 2-1: Summary of composition as derived from a typical 85/100 bitumen (Corbett, 1969)

Component	Weight (%)	MW (g/mol)	Physical nature	Chemical structure
Asphaltenes	5-20	3500	Brown to black solid	Mixed paraffin-naphthene-aromatics in polycyclic structures with sulphur, oxygen and nitrogen
Resins	30-45	1150	Black solid	Mixed paraffin-naphthene-aromatics in multi-ring structures with sulphur, oxygen and nitrogen
Aromatics	30-45	725	Yellow to red liquid	Mixed paraffin-naphthene-aromatics with sulphur-containing compounds
Saturates	5-15	650	Colourless liquid	Pure paraffins, pure naphthenes and mixed paraffin-naphthenes

## Asphaltenes

The asphaltenes are the fraction insoluble in heptane but soluble in toluene, which precipitate as black solids and from high wax content binders perhaps jointly with crystalline wax (Thanh et al., 1999). This component notionally forms as a by-product of the polymerisation of heteroatomic aromatic macro-cyclic structures by sulphide linkages (Becker, 1997), and is protected from secondary alteration in an oil reservoir by its colloidal nature (Ancheyta et al., 2010). The asphaltenes are hence distinguished by a high concentration of polar heteroatom-containing functional compounds, highly condensed polarisable aromatic rings and particularly by fused aromatic structures (Lesueur, 2009). An abundance of aliphatic moieties bond covalently to this polyaromatic core (Liao et al., 2006), curling to form a vesicle with high bending flexibility (Porte et al., 2003). This cavity may cage radicals with the structural features of perynaphthyl or transition metals in the form of metallo-porphyrin complexes (Acevedo et al., 1997; Gondal et al., 2010). The amphiphilic nature of asphaltenes is ascribed thus, to this presence of polar and apolar components (Pernyeszi et al., 1997).

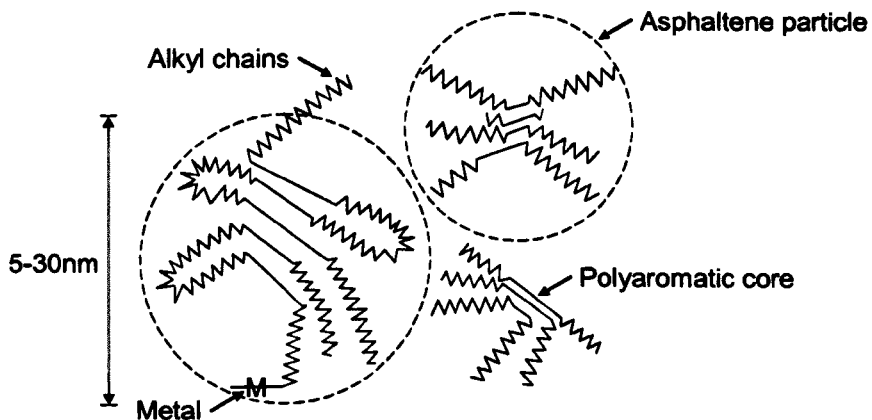


Figure 2-4: Plate-stack model for asphaltenes, after Dickie and Yen (1967), Porte et al. (2003) and Read and Whiteoak (2003)

By the fused unsaturated structure of the porphyrin rings, the polydisperse asphaltenes derive a planar molecular geometry (Becker, 1997). By attractive pi bonds these structures can stack to form graphite-like systems (Schabron and Speight, 1998; Lesueur, 2009) with an average of five sheets (Scotti and Montanari, 1998) and peripheral alkyl chains (Dickie and Yen, 1967) (refer to Figure 2-4). This oligomer formation may be enhanced by polar interactions between oxygen functional groups (Akbarzadeh et al., 2005), enabling stacks of up to eight sheets that

are stabilised by hydrogen bonds (Pernyeszi et al., 1997; Di Primio et al., 2000). The average molecular weight for an asphaltene sheet has been estimated by vapour pressure osmometry at 800-3500g/mol (Lesueur, 2009), and for the aggregations: 600-300000g/mol (Airey, 1997).

Strong dispersive interactions develop by the occurrence of the heteroatoms and by electron delocalisation due to asphaltene aggregation (Becker, 1997). These contribute to the surface stability and activity of bitumen, and to adhesion and cohesion (Peterson and Plancher, 1998; Bauget et al., 2001). Thus, with increasing asphaltene content between the typical proportions of 5% and 20% by weight, bitumen exhibits increasing viscosity and decreasing penetration.

### **Resins**

Purified with a toluene-methanol blend, resins are red to brown solids at ambient temperature (Mack, 1932; Corbett, 1969). This fraction is an intermediate product of the oxidation process of the oils, which transform into asphaltenes (Mack, 1932). The basic hydrocarbon skeleton of the compounds is similar to the asphaltenes therefore (Koots and Speight, 1975) but with less advanced aromatisation, and thus fewer condensed and fused aromatic rings. Moreover, the most probable structure corresponds to between two and four rings compared with five in an asphaltene (Koots and Speight, 1975; Piéri, 1995; Redelius, 2006). The extent of substitution reactions in the aromatic nuclei of the resins is lower than in the asphaltenes, but side chains attached to these components are usually longer (Koots and Speight, 1975).

The resins contain heteroatoms of sulphur or oxygen (Mack, 1932; Koots and Speight, 1975), various functional groups (Moschopedis and Speight, 1976) and both acids and bases. These impart polarity that enables molecular interaction through hydrogen bonding, which contribute to the adhesive properties of bitumen (Airey, 1997; Osman, 2004). In the lyophobic model, the resins limit the surface activity of the asphaltenes by clustering about them (Leontaritis, 1989). Moreover, by an affinity for paraffinic compounds in the oil the resins solvate and disperse the asphaltenes through the oils (Witherspoon and Munir, 1960). The stability of these clusters is altered by the addition of light paraffins to the solution, which produces a better solvent for the resins that dissociate from the asphaltenes that hence flocculate (Porte et al., 2003). The ratio

of resins to asphaltenes and aromatics to saturates (Diallo et al., 2000) therefore governs the solution (sol) or gelatinous (gel) character of bitumen (Airey, 1997) (refer also to Section 2-5).

### **Aromatics**

The aromatics fractionate as dark brown viscous liquids, which form a plasticising oil with the saturates in which the resin-peptised asphaltenes are dispersed (Corbett, 1969). This fraction forms by cracking and reactions including the hydrogenation of naphthenes, the aromatisation of aliphatics and the dealkylation of unsaturated molecules (Alsabei, 2011). The hydrocarbon backbone of these compounds is hence slightly aliphatic, with naphthenics branching (Gluyas and Swarbrick, 2004) off lightly condensed aromatic and non-aromatic rings (Piéri, 1995). The rings can occlude heteroatoms of sulphur, oxygen and nitrogen, which impart weak polarity to the chains (Peterson, 2000). The mean molecular weight is 300-2000g/mol (Airey, 1997).

### **Saturates**

Desorbed from a chromatographic column with heptane, saturates form a colourless or lightly-coloured liquid at room temperature (Corbett, 1969). The viscosity of this oil is lower than that of the aromatics at equi-temperature conditions due to a lower glass transition temperature: at about -70°C compared to -20°C (Lesueur, 2009). This fraction forms either as a by-product of asphaltene polymerisation, during which bridging methylene chains and appendages break to produce smaller saturated molecules (Kashir et al., 2007), or by cracking and isomerisation of paraffins, olefins, naphthenes and aromatics (Alsabei, 2011). These compounds are primarily aliphatic therefore (Lesueur, 2009), constituting saturated linear and branched-chain organics with negligible quantities of saturated cyclics and mono-ring aromatics (Peterson, 1984). This hydrocarbon backbone has a molecular weight of 600g/mol and is non-polar (Airey, 1997).

Depending on the paraffinic content of the crude oil from which the bitumen residue is distilled (Edwards, 2005), this fraction can include waxy (crystallisable) hydrocarbons in the proportion of 0-15% by weight (Claudy et al., 1992). These molecules are normally categorised as either macrocrystalline or microcrystalline (Kané et al., 2003). Macrocrystalline (paraffin) waxes are distributions of alkanes with a carbon number of C<sub>15</sub> to C<sub>57</sub> (Lu and Redelius, 2006), few or no

branches, and minor amounts of iso- and cyclo-paraffins (Edwards and Redelius, 2003). This wax type crystallises as large flat plates and needles in bitumen when cooled below about 20-50°C (Edwards and Redelius, 2003; Dorset, 2005). Microcrystalline waxes are differentiated by the prevalence of aliphatics and non-normal, iso- and cyclo-alkanes and naphthenes, high molecular weight and crystallisation as microscopic needles (Srivastava et al., 1993; Edwards and Redelius, 2003). Moreover, the crystallisable fractions have a negative effect on bitumen-stone adhesion and reduce cohesion, due to their hydrophobic property and inhomogeneities in the bitumen caused by wax crystals, respectively (Edwards and Redelius, 2003).

## **2.4 INTERMOLECULAR INTERACTIONS**

Chromatographic separation of bitumen evidences the disparate chemical functionality of the fractions; the asphaltenes and oils are incompatible (Davison et al., 1991). Yet, compositional stability is assured by solubilisation through the formation of colloidal solutions and continuum of intermolecular forces, which extend from the core of the colloid into the solvent (Peterson, 2000; Lesueur, 2009). These forces are hence important to the physical properties of bitumen (Barbour and Peterson, 1974; Ensley, 1975), and include London-dispersion, dipole-dipole or Keesom interactions, hydrogen and pi-pi bonds (Jones, 1992; Hansen, 2007).

### **London-dispersion interactions**

The dispersive interactions originate from atomic forces: irregularities in electron density that produce temporary and fluctuating dipoles in the outer shell of atoms, and thus exist between polar and non-polar molecules (Burke, 1984). Whilst these short-range forces are weak, their strength increases with molecular weight due to an increase in polarisability (Hefer and Little, 2005). Moreover, for non-polar alkanes and cyclo-alkanes these are the only cohesive forces present (O dian and Blei, 1994). Among the linear alkanes dominating the saturates therefore, this intermolecular friction explains the fluidity of this fraction (Peterson, 2009).

### **Dipole-dipole (Keesom) interactions**

The second type of intermolecular cohesion is the dipole-dipole type: an electrostatic friction that develops between opposite charges of permanent imbalances in electron density, which

derives from polar bonds (Burke, 1984). The kinetics of this interaction requires the preferred orientation of the polar compounds (Ensley, 1975), which align themselves to reduce potential energy and hence increase cohesion (Dunningham and Vedral, 2011). Moreover, as the polar groups diffuse and approach non-polar molecules they induce temporary dipoles therein, due to momentary attractive or repulsive distortions in their electric field (Kotz et al., 2010): this is entitled induction (Dunningham and Vedral, 2011). It is thought (Ensley, 1975) that the dipole-dipole interaction contributes extensively to the association of conjugated asphaltene.

### **Hydrogen bonds**

The third source of intermolecular cohesion is the hydrogen bond (Hansen, 2007): a stronger form of Keesom interaction caused by highly electronegative atoms (Dunningham and Vedral, 2011). This force has qualities similar to covalent bonds: it is directional; produces interatomic distances shorter than the sum of van der Waals radii; and involves a few interaction partners, which is understood as valency (Gargaud et al., 2011). This non-ionic friction occurs between the highly-polar, residually-positive pair of hydrogen's covalently-bonded to oxygen, nitrogen or fluorine (defined as the hydrogen-bonding acid), and an atom of residually-negative nature (the hydrogen-bonding base) (Burke, 1984).

A research has demonstrated the occurrence of hydrogen-bonding acids in bitumen, including carboxylic acids, phenols, amides and pyrroles (Barbour and Peterson, 1974). Another study has shown the capacity for aromatic systems in asphaltenes to participate in hydrogen bonds as electron-donor bases (Yen, 1971). It is among the bitumen fractions with highly-condensed aromatics, heteroatoms and functionalities that hydrogen bonding therefore occurs (Peterson, 2000). This facilitates elasticity-building networks (Jones, 1992). The high melting point of the asphaltenes is also attributed to this intermolecular interaction (Peterson, 2000).

### **pi-pi bonds**

The pi-pi bond is unique to the aromatic hydrocarbons and constitutes one of two overlapping atomic orbitals in carbon-carbon double bonds (Hart et al., 2012). Three of the carbon orbitals combine to form  $sp^2$  hybridised orbitals that produce sigma bonds with three atoms by end-on

overlap. The fourth valence electron in the un-hybridised  $2p$  orbital on each trigonal carbon is perpendicular to the single plane cast by the  $sp^2$  orbitals and, if two carbon atoms are aligned with each  $p$  orbital parallel, pi bonds may thus occur by lateral overlap (Hart et al., 2012). This interaction confers the capacity for aromatics to form a stacked configuration therefore, which in bitumen enables the stacking of asphaltene molecules that is evidenced by X-ray diffraction patterns (Peterson, 2000) (refer to Figure 2-5). It is also instructive to observe that the carbon-carbon double bond is stronger and shorter than a single bond and that, for rotation around it, the pi-pi bond must be broken (Hart et al., 2012).

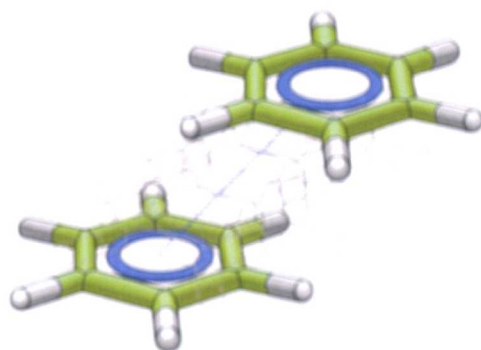


Figure 2-5: Parallel-displaced pi stacking of the benzene dimer

### Effects of molecular interactions on the properties of bitumen

The forces by which the molecules interact are reversible and in dynamic equilibrium between the bonded and un-bonded states, they break and reform in response to fluctuations in stress or temperature (Jones, 1992, Peterson, 2009). These bonds control the physical properties of bitumen therefore (Mohamed and Gamal, 2010). Notably, interactions in the non-polar solvent impart the viscous properties, and networks of polar molecules formed by hydrogen and pi-pi bonds contribute to elastic properties (Airey, 1997). In consequence of the size (20-30Å) and volume (35-65%) of the network particles, vast coagulation points exist. Strong intermolecular bonds are realised at these inter-particle contacts, due to interaction distances comparable to the molecular radius (10Å). According to one study therefore (Gokhman, 2000), this dispersed polar phase contributes highly to bitumen's strength. Moreover, the intensity of intermolecular bonds differs between the bitumen fractions: pure hydrocarbon molecules interact with forces of less than 10kcal/mol, and those including heteroatoms interact with forces of 12-15kcal/mol (Peterson, 1984, Hefer and Little, 2005). One effect of polarity is exemplified in Table 2-2: the

data are selected by Griffen et al. (1959) from profiles of molecular weight versus viscosity for the fractions at the same true molecular weight (Peterson, 2009). It is also instructive to note, although perhaps contradictorily, that the strength of the interactions also varies with type. For example, the London-dispersive component is  $18.4\text{MPa}^{0.5}$  and about five times stronger than dipole-dipole and hydrogen types, respectively  $3.9\text{MPa}^{0.5}$  and  $3.6\text{MPa}^{0.5}$  (Redelius, 2011).

Table 2-2: Effect of polarity on the viscosity of asphalt fractions (Peterson, 2009)

Fraction	Molecular weight (g/mol)	Viscosity at 25°C (Pa-s)
Saturates	500	10
Aromatics	500	1000
Resins	500	1000000

The effect of the intermolecular attractions on the physical and chemical properties of bitumen is limited by many factors but primarily by temperature (Peterson, 1984). As the kinetic energy of the system is minimised at low temperatures, there is a tendency for the bitumen molecules to associate into immobilised structures which produce an ordered composition. This ordering strongly affects the material's behaviour (Peterson, 2000) (refer to Section 2.5). Although this spatial configuration is partly influenced by molecular polarity, the crucial variable is geometry (O dian and Blei, 1994). As a molecule develops a less spherical or more cylindrical geometry with increased branching, the area for coagulation is minimised from a line to a point and the intermolecular attraction reduced (O dian and Blei, 1994). The effect of cyclisation is contrary: cyclic compounds are more rigid than linear alkanes and so approach other molecules more closely to enable strong interactions. The linear molecules pass continuously through various conformations due to free rotation about single carbon-carbon bonds, thus inhibiting effective association and producing weak interactions (Peterson, 1984). For temperatures in the region of Newtonian behaviour, this effect is minimised and polarity is decisive (Peterson, 2000).

## 2.5 BITUMEN STRUCTURE

The function and interaction of the SARA compounds in contributing to bitumen compatibility are characterised by different models: the micellar colloidal model by Nellensteyn (1924); the

steric colloidal and continuous thermodynamic models by Park and Mansoori (1988); and the microstructural model developed during the Strategic Highways Research Program (SHRP).

### **2.5.1 Colloidal model**

In 1861 Thomas Graham studied the rate at which the molecules of organic materials diffused through porous membranes of parchment, for example. Graham concluded that the diffusivity of solutions of starch and gelatine and like substances was reduced due to their large size: he conjectured that these constituted clusters of small molecules, or colloids (Gratzer, 2009).

Rosinger (1914) and Nellensteyn (1924) were among the first researchers to define bitumens as colloidal compounds of asphaltenes dispersed in maltenes. The latter author cited Tyndall scattering of asphaltene solutions, microscopy observations of Brownian motion of asphaltene particles, and the inability of such solutions to diffuse through porous membranes as evidence for this theory (Lesueur, 2009). More rigorous validation for the aggregation of asphaltenes in organic solvent derives from electron microscopy (Katz, 1945), X-ray (Pollack and Yen, 1970) and neutron (Sheu, 1998) scattering techniques. Moreover, work to refine this model by Mack (1932) and Pfeiffer and Saal (1939) in particular, to explain differences in the rheology of sol or gel bitumen by measurements of penetration and viscosity, has since established it as the most successful for bitumen structure (Little et al., 2003; Redelius, 2007).

In this heterogeneous system, discrete dispersions of polyaromatic molecules are dissolved in aliphatic solvent (Pfeiffer and Saal, 1939). The dispersed phase is thought to consist of a core of free radicals caged by asphaltenes of even aromatic character and low solubility (Acevedo et al, 1997). This core is enveloped by a molecular continuum of reducing aromaticity: from an adsorbed sheath of highly polar resins to films of less polar naphthenes and aromatics, and a diffuse periphery of saturates that extends into the oily solvent from within which it aggregates (Peterson, 1984). Colloidal stability is ensured by the resins, which act as a solvating layer to peptise the asphaltenes in the maltenes and thus prevent the retrogression of this dispersion process (Svedberg, 1921). The compatibility of each of the contacting fractions: the adsorbed aromatic compounds with both the asphaltenes and the solvent, produces a system in which

there are no interfaces between SARA fractions with significant differences in surface tension (Redelius, 2011). It is instructive to note also that the colloids (schematised in Figure 2-6) are porous (Acevedo et al., 1997). In a suspension therefore, the solvent could penetrate the core and react with the radicals, causing aromatisation and the decay of intermolecular bonds.

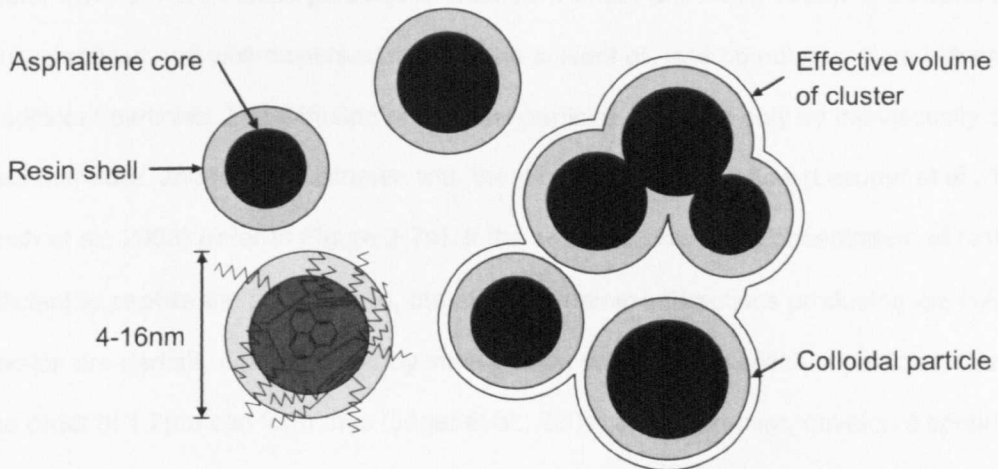


Figure 2-6: A simplified notion of the colloidal structure of bitumen: the micelles are pictured as spherical to illustrate the solvation layer. The schematic transverse cut of a micelle shows a perynaphthyl radical trapped by a transition from even aromatics and stacked asphaltenes to resins. After Dickie and Yen (1967), Acevedo et al. (1997) and Lesueur (2009)

Though this aggregation of asphaltenes and resins is widely-accepted (Porte et al., 2003) and the colloidal chemistry is well-defined, the particle shape is elusive (Lesueur, 2009). Dwiggin (1978) observed colloidal particles in crude oil using small angle X-ray scattering, and argued that the scattering intensity indicated either a monodisperse ellipsoidal macrostructure for the colloids, or a polydisperse spherical geometry with a radii of gyration of 30-40Å. Later, Herzog (1987) used this method to study asphaltene dispersions in benzene and maltene and defined the colloids as a distribution of discs, with the thickness of 3.4Å and radius of 13-800Å. Ravey et al. (1988) used small angle neutron scattering to study asphaltenes in solution in benzene, pyridine and tetrahydrofuran, and similarly concluded that the scattering intensity was typical of monodisperse discs with a constant thickness of 3.4Å and radius of 130-850Å. The authors postulated that the scattering intensity may indicate instead colloidal particles with a flattened spheroidal profile, with a large dimension in the range of 80-190Å (Storm and Sheu, 1994). In the research by Overfield et al. (1989), small angle neutron scattering was used to investigate

asphaltene colloids in toluene over the temperature range of 25-250°C. The authors proposed an elongated cylindrical shape for the particles (Lesueur, 2009).

In bitumen with sufficient aromatics and resins of adequate solvating power, the formation of the outer layer of the colloidal particles is ensured (Pfeiffer and Saal, 1939). The asphaltenes are fully peptised and well-dispersed through the solvent oil, and do not associate extensively with adjacent particles. The diffusion of colloidal particles is limited only by the viscosity of the solvent therefore, and form sol bitumen with the property of viscous flow (Lesueur et al., 1996; Muench et al., 2003) (refer to Figure 2-7a). If the solvating power or concentration of resins is insufficient to peptise the asphaltenes, the electrodynamic interactions producing the colloidal dispersion are partially compensated by mutual attraction between colloidal particles. Clusters on the order of 1.2µm can form thus (Jäger et al., 2004) and, moreover, develop a continuous viscosity-building network that further reduces the solvating ability of the maltenes (Read and Whiteoak, 2003) (refer to Figure 2-7b). This gel bitumen is characterised by an irregular open-packed structure therefore, and may exhibit non-Newtonian flow (Pfeiffer and Saal, 1939). If this structure becomes very organised and rigid, an external stress may cause the network to fracture rather than to deform elastically (Read and Whiteoak, 2003). The range of chemical composition of bitumens refined from different petroleum crudes means that in practice, their microstructure and physical behaviour is intermediate between sol and gel (Lesueur, 2009).

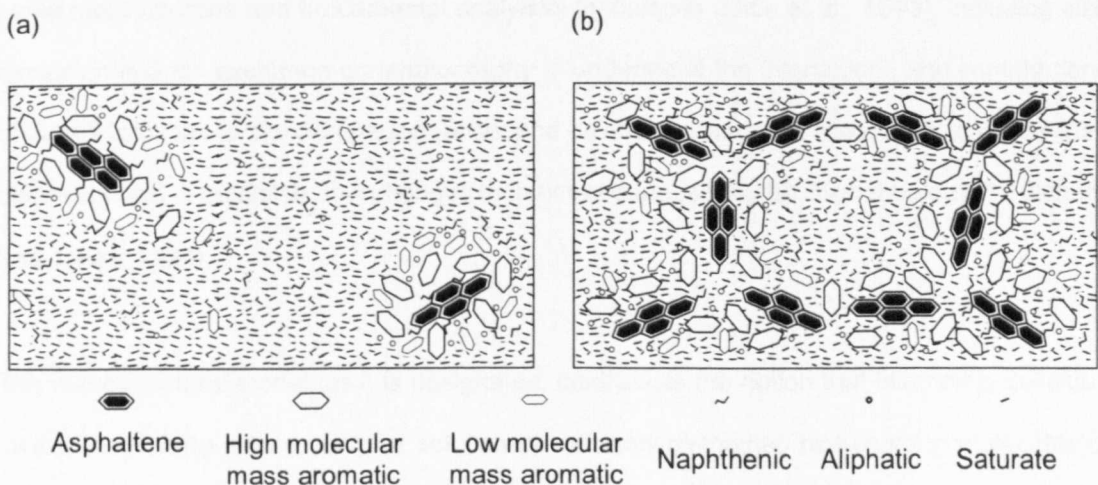


Figure 2-7: Schematic of: (a) sol bitumen, and (b) gel bitumen (Read and Whiteoak, 2003)

While many often competing models have been proposed to explain the viscoelastic response of bitumen (Ostwald, 1921; Katz and Beu, 1945; Monismith, 1961; Leontaritis and Mansoori; 1987), the notion of a colloidal structure was long-sustained by a lack of definitive proof to the contrary (Little et al., 2003). The accuracy of a colloidal dispersion of asphaltenes in maltenes stirred passionate debate though: the occurrence of colloidal dispersions of organic molecules through other organic molecules rarely occurs in non-polymeric systems (Hansen, 2007). It is also dubious if there is enough difference in the chemistry of the asphaltenes and maltenes to permit the formation of dispersions instead of solutions (Schmets et al., 2010). Recent models therefore, including the microstructural model and the solubility model, describe bitumen as a simple homogenous liquid in which the hydrocarbons are evenly distributed and stabilised by their mutual solubility in each other (Peterson et al., 1994; Redelius, 2006).

### **2.5.2 Microstructural model**

Although the colloidal model is in many ways similar to the discussions of Boussingault (1837) on the composition of bitumen (Youtcheff and Jones, 1994), it is emphasised (Peterson et al., 1994) that it was developed differently to contemporary theory on the character of colloids. An alternative model was postulated by the SHRP in response to studies proving the inadequacy of colloidal theory to explain chemical-physical relationships in bitumen, including the absence of rubber elasticity and an elastic plateau for gels (Lesueur, 2009). This model was conceived using more rigorous and fundamental analytical techniques (Little et al., 1993), including size exclusion and ion exchange chromatography to understand the interactions and contributions of SARA fractions to bitumen performance; and by nuclear magnetic resonance to define their chemistry and to establish how changes in their structure modify bitumen rheology (Youtcheff and Jones, 1994).

The microstructural model, as it is designated, contradicts the notion that bitumen is colloidal, instead describing it as a complex solution of uniformly distributed hydrocarbon molecules of widely varying molecular weight and polarity (Redelius, 2011), roughly half of which are polar and half neutral (Robertson et al., 1992). The non-volatile polar components are in such close proximity that they interact by various non-covalent bonds, with a rather uniform distribution of

bond energy up to a maximum of about 30kcal/mol (Robertson et al., 1992). Though there are no true phases in this system therefore, multiple sulphur, nitrogen or oxygen functional groups attached to some hydrocarbons impart hydrogen-bonding acidic and basic behaviour, and the ability to form dipolar intermolecular bonds with molecules of opposite polarity (Youtcheff and Jones, 1994). The polar molecules interact thus, and by pi-pi bonding of aromatic rings or by dispersive interactions between aliphatic parts (Airey, 1997), forming localised concentrations or primary microstructures within the non-polar aliphatic moiety. Under proper conditions, the microstructures may associate to develop chains and continuous three-dimensional networks of weak polar-polar bonds, which reduce the free volume of the bitumen (Jones and Kennedy, 1991) (refer to Figure 2-8). This three-dimensional structuring requires at least two points of attachment per molecule. This may be achieved by the dipolar interaction of functional groups but more likely, across multifunctional molecules such as amphoteric: molecules with a high aromatic content, which in addition to interactions by hydrogen bonds, may thus associate by pi-pi bonds (Peterson et al., 1994). The aromatic character of the polar molecules, in addition to the strength and number of polar sites thereon, is therefore of particular importance in the microstructural model. The type and location of heteroatoms on a molecule control its polarity and influence the planarity of the molecular system, which reduces its aromaticity and retards the delocalisation process of electrons in pi-pi bonds (Mehta and Mehta, 2005) and, therefore, directly influences the formation of any network (Youtcheff and Jones, 1994).

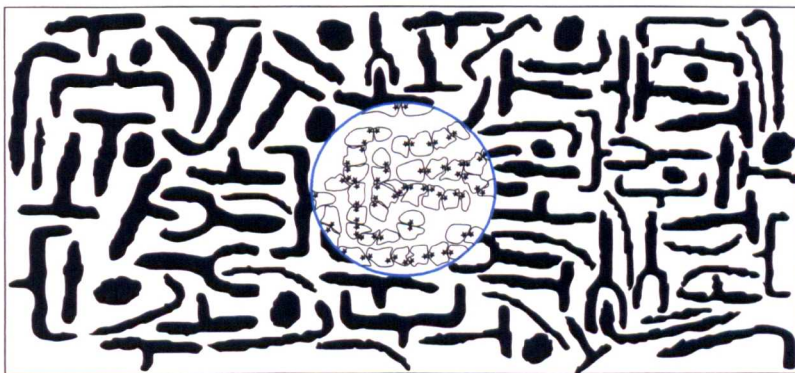


Figure 2-8: The microstructural model, showing chain building between active sites (denoted by stars) in polar molecules associating into different shapes, after Jones and Kennedy (1991)

This model rationalises the elastic property of bitumen by the formation of a three-dimensional network: physical chemistry suggests that molecules of higher molecular weight than present

in bitumen are responsible for this property (Peterson et al., 1994). It is thought therefore, that the network formed by the association of the relatively small bitumen molecules behaves as if high in molecular weight (Robertson et al., 1992). Under the action of thermal or shear stress however, viscous flow develops from an apparent decrease in molecular weight (Robertson et al., 1992). This is explained by reorientation of polar molecules by stress-induced breaking of the network of intermolecular associations. From the constant breaking and reformation of the bonds, bitumen derives a viscoelastic response to stress and metastability that is a function of its thermal and shear history (Robertson et al., 1992; Little et al., 2001). The molecular weight distribution and proportion of the plasticising non-polar fractions with which the network mixes are also important: physical properties are described in this model by the effectiveness of the solvent oil to disperse the microstructures rather than by elemental composition (Airey, 1997).

## 2.6 MICROSCOPY INVESTIGATIONS

The association of hydrocarbons in bitumen is the mechanism by which the material develops its intrinsic structure. The literature has shown that this structuring acquires spatial properties beyond the resolution<sup>4</sup> of a healthy human eye: one arc minute (Kalloniatis and Luu, 2007) or 75µm at a normal distance of 0.25m (Poulikakos, 2011). To visualise this structure therefore, researchers first used simple reflected-light microscopy, which manipulates light in the visible spectrum to achieve a resolution of 200nm (Morris et al., 1999). In their research for example, Goodarzi and Macqueen (1990) used optical dispersion based on reflectance of white light to define the maturity of natural bitumen, and to investigate the morphology of bituminous shale. While reflected-light microscopy has also since resolved the morphology of refinery bitumens (Jäger et al., 2004), its ability to successfully investigate *in situ* structure is often limited by the opaque property of bitumen (Masson et al., 2006). This inhibits strong contrast and precludes investigations without solvent-extraction of its components (Li and Wan, 1995; Bearsley et al., 2004). To improve image contrast light microscopy is supplemented with transillumination and fluorescence methods, yet literature on bitumen fluorescence is contradictory. Notably, Collins et al. (1991) stated that under blue and UV light with wavelengths of 400–440nm, the aromatic

---

<sup>4</sup> The shortest distance between two points identifiable as separate entities (Davidson, 2010)

and resin fractions fluoresce but asphaltenes and saturates do not, at filtered wavelengths of above 470nm. Loeber et al. (1996) noted that for bitumen fluorescent light emission is modest because the oily phase is mixed with an asphaltene and resins phase that does not fluoresce. Contrary to these studies Li and Wan (1995) concluded that when irradiated using an incident light source with a wavelength of 568nm, fluorescent excitation of highly conjugated aromatic structures is a distinct possibility. Bearsley et al. (2004) reported that asphaltenes fluoresce in the 515-545nm wavelength range, when irradiated with light with a wavelength of 488nm. The authors also postulated that bitumen fluorescence in the research by Loeber et al. (1996) was obscured by unfiltered reflected light. Moreover, fluorescence microscopy has been applied in petroleum geology since the late 1930s, in studies on organic matter including coal, shale oils and natural bitumen (Rost, 1995; Diessel and Gammidge, 1998; Bearsley et al., 2004).

Cross-polarised light microscopy has more recently been applied in the petroleum industry, to better understand the formation of wax-oil gels: deposits with volume-spanning networks that inhibit oil flow in pipelines and processing plant (Senra et al., 2009). Academic-level research has also used optical microscopy with the aim to define the structure of bitumen. Claudy et al. (1992) for example used polarised light microscopy to examine notions of the bi-phasic nature of this material. The authors described it thus, as a solvent in which are dispersed birefringent crystalline domains of up to 15µm in length. The well-organised parts, it was concluded, form as the aliphatic groups in paraffinic waxes and attached side chains precipitate from within the solvent upon cooling, and then form aggregations by van der Waals forces. The authors also used phase contrast microscopy at 25°C, and resolved poorly-organised amorphous domains of polar molecules dispersed in a glass. These regions were typically 1 to 3µm in width. In the research it was argued that the mechanism for this separation is not crystallisation but instead spinodal decomposition: the spontaneous formation of two-phases by diffusive aggregation of atoms uniformly throughout the solution due to compositional fluctuations (Campbell, 2008).

Lu et al. (2005) applied confocal-laser scanning microscopy to produce high-resolution optical images of bitumen structure. The authors reported flake-like and ellipsoidal heterogeneities in an amorphous matrix, which decreased in length as sample thickness reduced. The repeating

well-organised internal structure of the 2 to 15 $\mu$ m long dispersions, and a melting temperature similar to paraffin waxes, led the authors to conclude that this phase forms of non-interacting waxes. An absence of such domains in otherwise comparable but non-waxy bitumens verified their theory. The published research also recognised that this conclusion could not explain the amorphous crescent-shaped phase in both waxy and non-waxy bitumen, which were ascribed instead to clustered asphaltenes. This validated the research by Bearsley et al. (2004), which identified 2 to 7 $\mu$ m long structures as asphaltenes, defined by their fluorescent wavelength. It is notable that, while wax occurs throughout the bulk phase of bitumen (Schmets et al., 2010), crystallisation phenomena are thermodynamically favourable at the air-bitumen interface. The proportion of crystallisable material that wets the surface, by diffusion, thermal convection and interfacial effects, is thus related to the volume of liquid-phase wax in the bulk as a function of sample thickness (Pauli et al., 2011). This explains the sample thickness-structure geometry relationship that Lu et al. (2005) reported.

In parallel with optical techniques, research on bitumen structure by atomic force and electron microscopy has been published since 1996, and is reviewed below.

### **2.6.1 Atomic force microscopy**

The basic principle of atomic force microscopy (AFM) imaging is to measure the interactions between a sharp probe and the surface of a sample. By digitising the deflection-response of the cantilever to which the probe is attached, high resolution images of topography, magnetic domain wall structure and charge distribution (Meyer, 1992).

In force microscopy, a probe is attached to the free end of a cantilever beam that is fabricated using photolithography from silicon, silicon oxide or silicon nitride (Rugar and Hansma, 1990). The fine tip of this probe, with a diameter in the range of 10-60nm (Braga and Ricci, 2004), is scanned across the sample in a raster pattern, to develop a false colour image of its surface (Bryant et al., 1988) (refer to Figure 2-9). Two force regimes are recognised: non- contact and contact. In the non-contact regime the probe is held between tens and hundreds of angstroms of the surface (Kumaraguruparan, 2010). Attractive electrostatic and capillary forces of nano

or pico Newton's occur between the probe and atoms, molecules and particles in the surface (Meyer, 1992). In the contact mode, the attractive forces are negated by repulsive short-range ionic interactions (Adamsmair, 2008). The presence of a force induces deflections of the static cantilever beam in this regime, and modifies the amplitude of the driven cantilever oscillation in the non-contact mode (Rugar and Hansma, 1990). This is measured by the reflectance of a laser beam, and then processed to produce an image of the surface (Galloway Group, 2004).

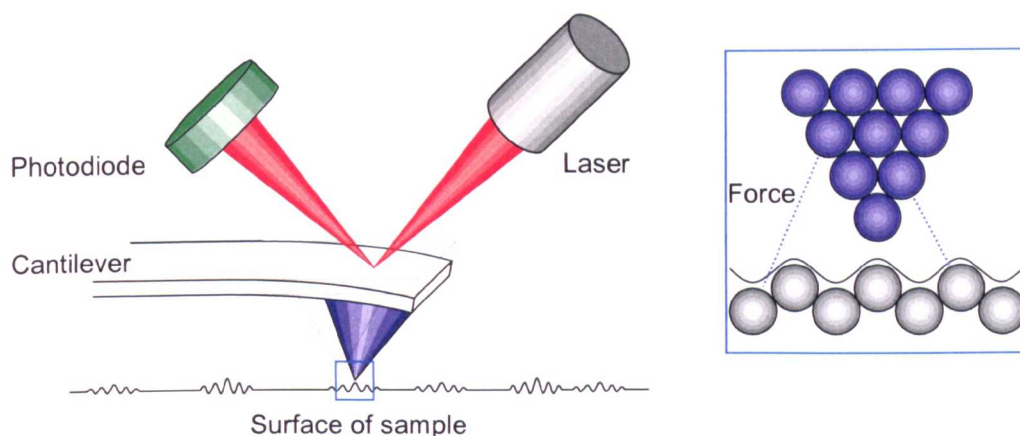


Figure 2-9: Schematic assembly of an atomic force microscope, with a magnification of the interaction of the tip and sample atoms. Developed from Rugar and Hansma (1990) and Adamsmair (2008)

The basic morphology of bitumen as obtained by AFM at ambient temperature, and observed repeatedly in the literature, shows a flat matrix within which is dispersed a catana phase (refer to Figure 2-10). This phase is identified by its ellipsoidal geometry and striped topography: a series of light and dark lines from which the impression of peculiar bee-like structures derives (Loeber et al., 1996). The light and dark parts of the dispersions are created by an undulating surface texture: by thin parts that emerge from the surface due to an inhomogeneous volume contraction on cooling, and by the broad immersing strips between which they occur (Masson et al., 2002). This rippled texture spans several micrometres and is bitumen-specific (Masson et al. 2007), but also depends on sample thickness. This structuring is essentially constant for films thicker than 10 $\mu$ m, with three-dimensional out-of-plane ripples favourable due to a high volume of crystallisable material available in the bulk for wetting. As the specimen thickness is decreased, two-dimensional lenticular structures tend to develop (Pauli et al., 2011). Notably, the rippled structures usually comprise between two and five high parts: 20 to 300nm in width

and up to 85nm in height, between the low parts that are often 550nm wide and 40 to 50nm lower than the mean surface of the specimen (Masson et al., 2006; Le Guern et al., 2011).

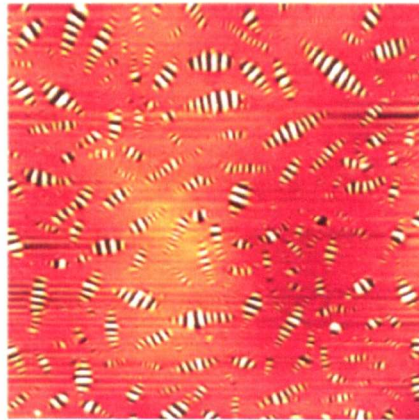


Figure 2-10: Atomic force microscopy topography image of bitumen AAK-1 (Pauli et al., 2011)

Masson et al. (2007) examined low temperature ( $-72^{\circ}\text{C}$  to  $-10^{\circ}\text{C}$ ) structuring in bitumen using AFM in phase detection mode. This method produces a phase-contrast image of a surface by differentiating mechanical properties, using analyses of the harmonics of an oscillating probe. The authors established that the bee-like structures are stable on cooling to  $-72^{\circ}\text{C}$ , and noted a secondary phase separation in the matrix. The published study thus indicated the presence of at least three temperature-dependent phases in bitumen. By correlating the morphological changes to endothermic and exothermic phase transitions, the authors indicated that domains around the rippled dispersions are rich in naphthene and polar aromatics. Moreover, viscous areas adjacent to this so-called paraphase were postulated to be rich in non-polar saturates, and to retain liquid-like properties to temperatures far below that of bitumen's glass transition.

While AFM research has clearly identified phase separation in bitumens, understanding of the chemical composition of the bee-like structures is divisive (refer to Table 2-3). Among the first to analyse this structuring with AFM, Loeber et al. (1996) initially resolved the dispersions only in gel bitumens and thus related their composition to colloidal asphaltenes. Pauli et al. (2001) also concluded that the structures form by clustering of asphaltenes: they doped samples with asphaltenes and identified an increase in the density of the dispersed phase. However, Pauli and Grimes (2003) observed this phase to be dissolved repetitive scanning and proposed that this order-disorder transition denotes a crystallisation process, which undergoes retrogression

through heating. In accordance with Loeber et al. (1996) however, the authors also concluded that asphaltenes are involved in the formation of these crystallised structures, conceivably by co-precipitation and aggregation. Using AFM in pulsed force mode, an intermediate-contact regime in which a sample is oscillated beneath the probe, Jäger et al. (2004) established the stiffness of the matrix and the bee-like structures. The viscous domains and high parts of the dispersed structures were respectively, 30% and 45% stiffer than the paraphase and the low parts of the undulating ellipsoids. The authors concluded that the viscous phase and arch-like structuring are formed of highly polar components: asphaltenes and resins, which act to focus a physical and chemical transition within the matrix that hence dips and decreases in polarity away from these concentrations.

Table 2-3: A chronological summary on the composition of the bee-like structuring by AFM

<b>Author</b>	<b>Observations on the chemistry of the dispersed structures</b>
Loeber et al. (1996;1998)	Larger quantities in higher asphaltene bitumen: authors suggested their composition is hence related to colloidal asphaltene particles.
Pauli et al. (2001)	Correlated the area of bee microstructures to asphaltene content.
Pauli and Grimes (2003)	Dispersed structures dissolved or melted under repeated scans of the AFM: a crystallisation theory was suggested for the structures.
Jäger et al. (2004)	Peaks of the rippled interior formed by asphaltenes and resins that effect a chemical transition in the matrix that decreases in polarity.
Masson et al. (2006)	Rejected relation between asphaltene content and bee structures, instead related the catana phase to metallo-porphyrin complexes.
Wu et al. (2009)	Simulated long-term ageing and observed increased structuring: ascribed to the growth and clustering of asphaltene-resin micelles.
De Moraes et al. (2010)	Showed the profile of bee-like structures changed at temperatures of wax crystallisation, and alluded to their formation by paraffinics. Suggested asphaltene aggregation to the wax altered their profile.
Kringos et al. (2011)	Pronounced bee-like structure to be similar to model paraffin wax.
Pauli et al. (2011)	From thermal cycling: interactions between crystallising paraffins and non-waxy fractions cause structuring in the non-polar moiety. From wax-doping: the appearance of surface structuring relates to wax type and concentration, and crystallising conditions.

Subsequent to the research published by Pauli and Grimes (2003), only Wu et al. (2009) have concluded that structuring at the bitumen surface is due to the interaction of chromatographic fractions. Notably, the authors used AFM to characterise pure and styrene-butadiene-styrene polymer modified bitumens that had oxidised using the rolling thin film oven test and pressure ageing vessel test. The research showed that the density and length of the bee-like structures increased after oxidation, which was ascribed to the production of asphaltenes and functional groups by ageing processes. In the intervening and subsequent period, different explanations of the composition of this structuring have been developed, as follows.

Masson et al. (2006) used AFM in phase detection mode to image the surfaces of the twelve SHRP bitumens. Thin-film samples were prepared by heat-casting to maintain their solid-state structure. The authors rejected previous correlations between the bee-like structuring and the SARA composition of the bitumen. Instead, the research defined a linear relationship between the proportion of the surface covered by the bee-like structures, and the nickel and vanadium content of the bitumen. Elemental analyses established that the nickel content varied between 14ppm and 141ppm, and the vanadium component was in the range of 28ppm to 1499ppm. A noteworthy correspondence was also found between the dispersed area and the average size of fused molecular structures. The study hence concluded that the bee-like structures consist of stacks of fused aromatic molecules bonded by cationic nickel and vanadium complexes.

Research on low-wax content bitumen by Pauli et al. (2011), among others, has prompted the return to the interpretation firstly suggested by Claudy et al. (1992): that the bee-like structure is formed by the diffusive precipitation of paraffin waxes. Pauli et al. (2011) used AFM to show an absence of the rippled dispersions in low-wax content bitumens, and the occurrence of this phase in the maltenes. The authors concluded that this illustrates that the bee-like structure is not formed by asphaltenes and applied this to reject the correlation proposed by Masson et al. (2006). Namely, metallic chelates associate with and concentrate in the asphaltenes (Speight, 1999) and would thus be removed indirectly on precipitation of this fraction. Pauli et al. (2011) also performed wax-doping experiments to establish the effect of wax additives on the surface structures of two bitumens, with naturally-low wax content. Samples with 2% by weight of wax

were firstly prepared by spin-casting solutions of bitumen-toluene and wax-toluene, and then by thermal conditioning. The waxes included four normal paraffin waxes with carbon numbers  $C_{28}$ ,  $C_{44}$ ,  $C_{50}$  and  $C_{60}$ , and one microcrystalline wax. In each sample the addition of model wax produced some bee-like structures, which were otherwise absent from the base bitumens. In both bitumens doped with the same concentration of different paraffin waxes, this structuring differed: from typical bee-like structures to dendritic forms and crab-like clusters constituting a broad and rippled segment, from which short protrusions occur (refer to Figure 2-11). Diverse structuring was also resolved when the same paraffin wax was doped into both bitumens. The authors concluded therefore, that although waxes are mostly responsible for the structuring of the dispersed phase, many interrelated variables affect the geometry of the dispersions.

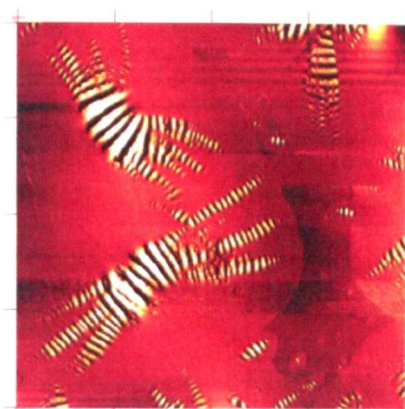


Figure 2-11: AFM scan of AAA-1 doped with tetratetracontane (Pauli et al., 2011)

Research on thermally conditioned samples lends credence to the correlation between waxes and bee-like structuring. Notably, De Moraes et al. (2010) indicated that the dispersed phase dissolved or melted as samples were heated to  $70^{\circ}\text{C}$ . When cooled through temperatures of wax crystallisation, bee-like structures nucleated from stable embryos that developed distinct phase boundaries. Le Guern et al. (2011) similarly reported that the length of the dispersions increased as temperature reduced: from  $1.7\mu\text{m}$  at  $33^{\circ}\text{C}$ , to  $2.8\mu\text{m}$  at  $21^{\circ}\text{C}$ . This is consistent with the concept that a bitumen fraction is crystallising (Singh et al., 2001a).

The suggested explanation for this crystallisation depends upon the tenet that high molecular weight *n*-alkanes are of a lower solubility compared to, and crystallise more readily than, other fractions in bitumen (Senra et al., 2009). As bitumen cools therefore, the solubility of the high carbon number paraffin waxes greatly reduces, and thus the *n*-alkanes solidify from within the

matrix to form an incipient gel layer. Driven by dispersive interactions, long-chained *n*-alkanes align and organise within this layer at the expense of lower carbon number components. This causes the solid content of the wax gel to increase, towards the formation of a fractal network of microscopic crystals (Vignati et al., 2005). The widely-accepted mechanism for the ordering process is molecular diffusion (Singh et al., 2001b) to a limited depth in the bulk (Bée, 1988). The crystalline phase is hence not imaged in rapidly-quenched bitumen (Kringos et al., 2011).

### **Review of paraffin wax morphology in the literature**

The preceding literature review establishes that structuring at the bitumen surface is produced by interactions between chromatographic fractions or by crystallising wax. The mechanism by which the dispersed phase develops its distinctive internal undulations is not fully understood, however. A description of the mechanisms potentially involved in the formation of this texture may be developed by reviewing literature on paraffin crystallisation in other systems, and then on polymer crystallisation kinetics. This treatise does not preclude structural variations due to wax type and crystallisation temperature, nor due to cluster-formations of different paraffins in the solid state (Turner, 1971; Briard et al., 2006). The potential for such groupings arises from the Gaussian distribution of petroleum waxes (Tegelaar et al., 1989). Notably, lattice structure in these clusters is affected by differences in molecular weight and solubility of co-crystallised paraffin molecules, which may produce contortions (Dorset and Snyder, 1996). A summary of the treatise that follows is presented below in Table 2-4.

Table 2-4: A summary of the mechanisms potentially involved in the bee-like structuring

<b>Potential mechanism</b>	<b>Effect on the geometry of the dispersed microstructures</b>
Localised changes in the kinetics of crystal growth	The ease with which the alkanes crystallise suggests their nuclei contain dislocations that drive local variations in growth kinetics or a three-dimensional conformation, which introduces sectorisation.
Sectorisation or division of lamella by chain folding	A single paraffin crystal may acquire local undulation at its surface by the packing of long molecules that directs an oblique tilt axis. Differences in tilt angle precipitate an alternating light-dark texture.
Viscous stress relaxation by curvature elasticity	A periodic instability transverse to the main axis of a crystal may form by relaxation of internal local stress by non-linear elasticity. The creation of this oscillation develops a sectorised morphology.

Transitions in the surface of paraffin crystals precipitated from hexane solutions are observed frequently in the literature, wherein they are ascribed to local changes in the kinetics of crystal growth (Bennema et al., 1992; Liu et al., 1992). The mechanisms that drive the abrupt change differ among crystallographic planes, and can thus induce divisions of the lamella that appear as discrete sectors at the surface of crystals (Tsukruk and Reneker, 1995; Sunagawa, 2003). Evidence for this so-called sectorisation phenomenon derives notably from electron diffraction microscopy (Dorset, 1986), and decoration techniques (Lotz, 1994).

The ease with which paraffins crystallise is thought to suggest that the original nuclei and the crystals formed hence contain imperfections or screw dislocations (Dawson, 1952; 1954). The dislocations provide a spiral path for growth (Mott, 1950) that produces local accumulation of material and a three-dimensional conformation. Paraffin crystals thus acquire a tent, chair-like or pyramid structure (Toda et al., 2005), for which each quadrant exhibits alternating light and dark bands in micrographs under bright-field and electron diffraction (Dorset et al., 1990). This repeating texture is a consequence of the differences in tilt angle of aligned paraffin chains in adjacent sectors. Namely, low molecular weight and odd-numbered paraffins are un-tilted and thus planar, but the packing of long even-numbered chains directs an energetically-favourable oblique tilt axis. This creates a three-dimensional crystal habit that emerges as a local surface undulation (Dorset et al., 1993) (refer to Figure 2-12). Moreover, the molecular packing of the nucleus determines sectorisation. For folded molecules, a collapse of their three-dimensional folds has a secondary role in defining this structuring (Dorset et al. 1993).

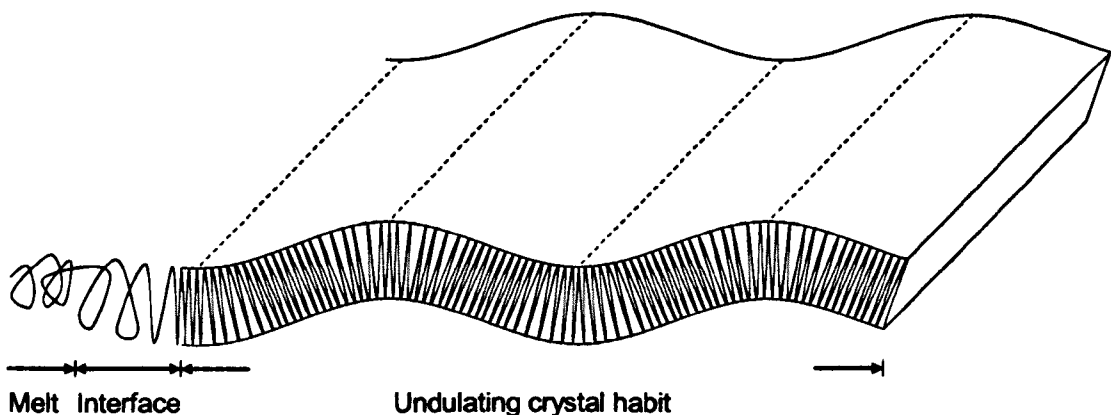


Figure 2-12: Schematic of a chain folded lamella with periodic undulations in which chain tilting occurs, and the solid-liquid interface with intermediate order (Mehta et al., 2004)

Sectorisation is also often observed in syndiotactic polypropylene (sPP) (Bu et al., 1996; Zhou et al., 2000) and polyethylene (Toda et al., 2003; 2005) single-crystals, in which the division of lamellae is a phenomenon consequential of different chain folding behaviour (Wiley, 2008). In controlled crystallisation of these polymers, single crystals grow with rectangular and lozenge-like geometries (Geil, 1963) and generally arrange in a radial pattern from undeveloped nuclei (Tsukruk and Reneker, 1995; Zhou et al., 2000). The growth of these crystals under quiescent conditions may be described by the Lauritzen-Hoffman model (Ratta, 1999): the deposition of a single polymer stem onto a smooth substrate initiates the growth of a single lamella (Hu et al., 2002), which then spreads by reeling-in chains along the growth face (Hoffman and Miller, 1997). As they reach a lamella surface, these molecules fold back (Bassett, 1981) and, where regularity of folding varies (Bassett, 1988), form distinct sectors with different thermodynamic stabilities (Zhou et al., 2000). The mechanical integrity of adjacent sectors is assured by tie-molecules that do not fold at the growth face, but instead pass between lamella (Wiley, 2008).

Perhaps the most interesting phenomenon associated with sectorised polymer single-crystals; among them sPP, is the formation of a sinusoidal-like surface profile, by periodic ridges which run transverse to the main axis of the crystals (Tsukruk and Reneker, 1995). This texture was first observed about fifty years ago in solution-grown polyethylene single-crystals (Bassett and Keller, 1961) and unlike sectorisation does not simply reflect the trajectories of different chain orientation (Guenther and Kyu, 2000). It is contended instead, that it is by the creation of a corrugated profile that this sectorised morphology develops (Donald and Windle, 1983; Viney et al., 1985; Viney and Windle, 1986). The rippled surface instability however, is attributed to the viscous relaxation of internal local stresses (Mehta et al., 2004) that develop during cooling to ambient temperatures: by thermal shrinkage of lamellae (Lovinger et al., 1994); by differential contraction between the lamellae and the amorphous substrate (Tsukruk and Reneker, 1995); and by the impeded self-extension of random-coils into straight segments, which also causes these chains to experience buckling (Fischer et al., 1996). Such stresses may be accentuated in sectorised single-crystals by differential chain tilt between sectorised planes (Lotz et al., 1988), and by the presence of a viscoelastic network: a system of rogue molecules that failed to form an integral part of the crystalline domain, but which when relaxed after straining could exert a

compressive stress to produce buckling (Fischer et al., 1996).

While the stress relaxation effect is accepted (Guenther and Kyu, 2000), it is questioned why crystals deform with a periodic habit (Mehta et al., 2004). For low molecular weight nematics<sup>5</sup> this periodic order emerges as a transient response to the reorientation of an external electric or magnetic field. This structure evolves rapidly to the homogenous state or to form a wall-like morphology (Lonberg et al., 1984). Similar periodic distortion is observed using microscopy in other polymer-like systems, and is known to possess greater stability (Chang and Han, 1996). In the absence of pre-existing surface structure, elastic anisotropy at local dynamic distortions in the molecular structure produces this periodic texture parallel to the long axis of the crystals (Lonberg and Meyer, 1985). This contrasts to the bee-like structuring observed in bitumen.

In the phase field model proposed by Guenther and Kyu (2000), the emergence of banding parallel to the short growth axis of a crystal was explained by coupling stress relaxation due to ordinary rubber-like elasticity, with a higher-order mechanism for bending: curvature elasticity. This nonlinear deformation includes bulk flow or affine centre-of-mass motion and the periodic rotation of physical elements, and dominates the linear deformation (Lonberg et al., 1984). An oscillatory wavefront may develop hence and propagate through the crystal by overall rotation of chain segments, which produces the periodic structure (Mehta et al., 2004). For systems in which this time-dependent process is suppressed, banded textures can also develop; instead, by the growth of weakly-bound isolated surface kinks due to thermal fluctuations (Guenther and Kyu, 2000).

The kinetics of sectorisation and curvature elasticity could be responsible for the structure and formation of the dispersed phase in bitumen. However, the correlation between the chemistry of the interacting solvent phase and the appearance of the surface structuring that is reported in the literature review is not fully explained by these concepts (Pauli et al., 2011). Moreover, it is unknown if this bee-like morphology is present within the bulk.

---

<sup>5</sup> Liquid crystals formed of elongated molecules with anisotropic viscosity (de Gennes, 1982)

## 2.6.2 Scanning electron microscopy

The scanning electron microscope (SEM) produces atomic-resolution images of a surface by analysing its electromagnetic response to electron irradiation (Egerton, 2005).

The incident electrons are focused at the surface to a diameter of 1-10nm and raster-scanned across the sample (Qi, 2007). The probe penetrates the surface and experiences decelerating collisions and elastic interactions with sample atoms, which produce a pear-shaped diffraction pattern and the dissipation of kinetic energy as radiation (Li, 2003; Swapp, 2011). Detectors in the sample chamber collect the quanta emitted (Reimer, 1998; Qi, 2007) (refer to Figure 2-13) and, although any emitted signal could be used to develop an image of the surface, greyscale topographical micrographs are frequently acquired from backscattered or secondary electrons (Oatley, 1982; Ruska, 1986; McMullan, 1993; Johnson, 1996; Goldstein et al., 2003).

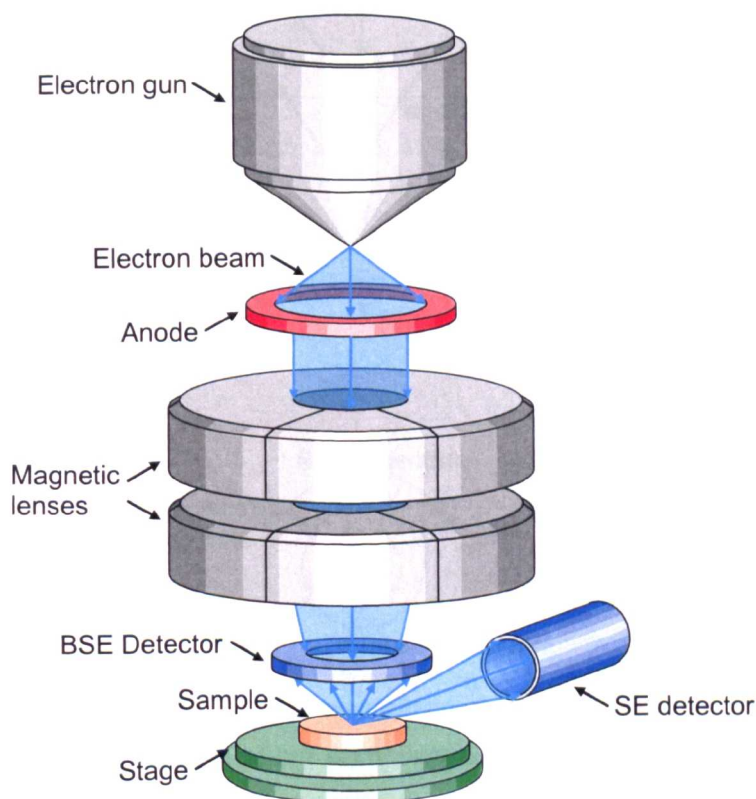


Figure 2-13: Schematic of a scanning electron microscope, with secondary electron (SE) and backscattered electron (BSE) detectors. Encyclopaedia Britannica (2008)

The backscattered fraction forms as the trajectory of the incident electrons is rotated through more than  $90^\circ$  without a significant loss of kinetic energy (Goodge, 2011). The intensity of this

signal is proportional to atomic number and image contrast hence derives from compositional variations (Swapp, 2011). The inelastic collision of incident signals with sample atoms causes ionisation, as K-orbital electrons are excited in a cascade process and then ejected from the sample as secondary electrons (Wang et al., 2003; Hanke et al., 2009). The escape depth of these particles is limited to the upper ten nanometres of the specimen due to their low energy, which is of the order of 5eV (Voutou and Stefaniki, 2008). The intensity of this signal varies in response to surface topography, and is captured to create high-resolution micrographs of fine surface texture (Hanke et al., 2009). A significant percentage of secondary electrons (40% in aluminium (Kanter, 1960a)) may derive from below this secondary escape region, by inelastic scattering of sample atoms caused by backscattered electrons exiting the sample from within the bulk (Kanter, 1960b). The interactions are schematised below, in Figure 2-14.

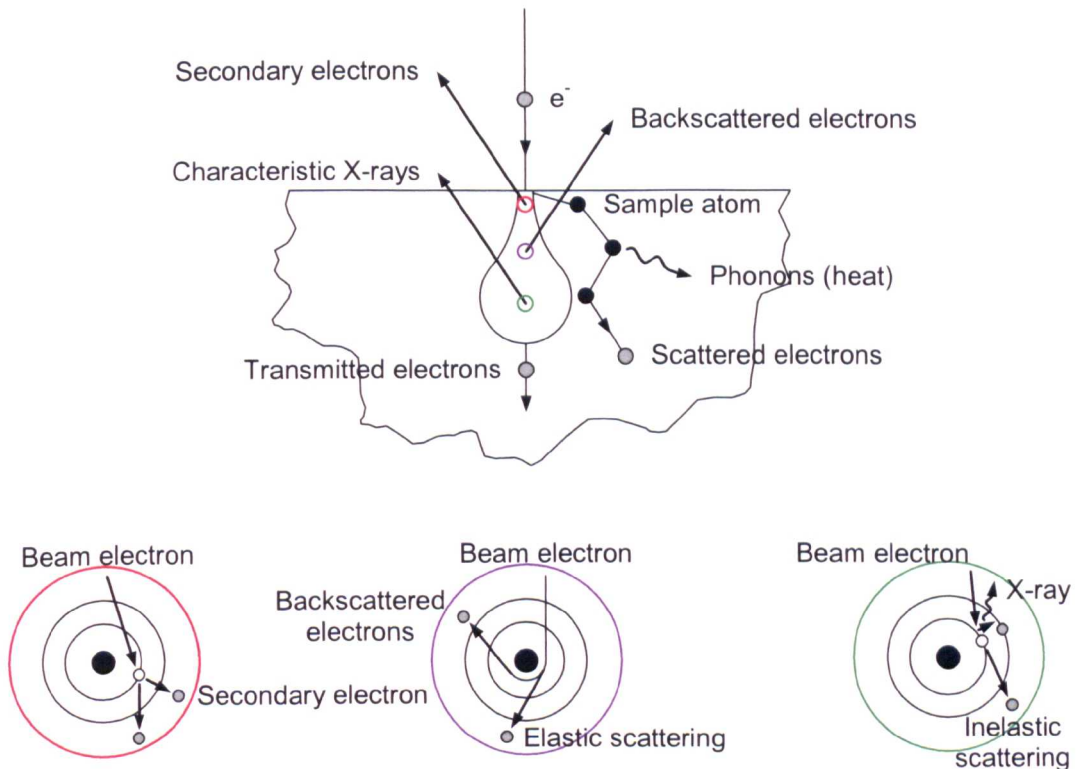


Figure 2-14: Possible interactions of the electron beam impinging with the surface of a solid sample: the most important signals are secondary electrons, backscattered electrons and X-rays, shown in magnifications. Developed from Johnson (1966) and Poulikakos (2011)

The irradiation of materials in the conventional SEM requires that they are observed in a high-vacuum environment, for the propagation of an electron beam without significant scatter in the presence of gas molecules (Danilatos, 1985). This condition necessitates that electrically non-conductive samples are coated with a film of metal, to dissipate artefact-inducing electrostatic

charge deposited by the electron beam (Egerton, 2005). Hydrated, vaporous and oily samples are either desiccated or chemically-fixed, to purge or suspend volatile parts that could outgas and degrade the vacuum (Li, 2003). These modifications preclude the direct observation of the natural surface of such materials though (Danilatos, 1989), which are instead often examined in an environmental SEM (ESEM). This microscope uses a high-pressure gas in the chamber to provide a relatively benign environment in which materials may be imaged analogously to a conventional SEM, but without routine preparation for compatibility (Hachenberg and Beaver, 1959; Goldstein, 1976; Johnson, 1996; Bhurke et al., 1997; Benawra et al., 2007).

The ESEM provides the unique opportunity to image living matter, including aphids and mealy bugs feeding on biological material (Miller, 2011), and the dynamic characteristics of materials such as swelling of hydrogel (Thomann and Thomann, 2011). However, the complex question arises as to what extent the uncoated sample is physically or chemically modified by electron irradiation, whether beneficially or detrimentally (Danilatos, 1986; 1987).

There is extensive literature on the effects of beam irradiation in ESEM, which in observations on fibres of Lincoln and Merino wool evolve with exposure time and system parameters. From the etching of an atomic layer of the material at low accelerating voltage (5kV), high pressure (3 Torr) and prolonged exposure (31 minutes), to a severe loss of surface mass, wrinkling and an increased density of bubble-like formations at high accelerating voltage (20kV), low vapour pressure (0.15 Torr) and short exposure (4 minutes) (Danilatos, 1985). During the irradiation process, the fibre surfaces were in some way also rendered resistant to radiation: successive observations did not produce severe irradiation effects in the usual manner (Danilatos, 1985). This response has been used to increase the level of photo-protection of such fibres (Milligan, 1980). The consequences of other irradiation effects have established theories valuable to the understanding of polymers (Rask et al., 1993; Rozeveld et al., 1997) amongst other materials. The effects of beam exposure are not necessarily detrimental, therefore (Danilatos, 1986).

The etching effect of beam irradiation has been used to reveal the crystalline structure of films of polypropylene and polybutylene (Rask et al., 1993). In that study, the authors exposed an area of each uncoated sample to repeated scans of the beam, which eroded amorphous parts

in preference to the more-resistant crystalline domains. This revealed the spherulitic texture of both polymers. In contrast to polypropylene, which exhibited internal details of the spherulites after five minutes exposure, polybutylene was difficult to etch and required two hours in order to expose this structure. In addition to molecular organisation, the chemical composition of the material thus influences the irradiation effect. Perhaps the added resistance of polybutylene to beam etching is precipitated by surface energy, which is high relative to that of polypropylene (Assanta et al., 1998; Markgraf, 2005). Notably, the spherulitic structure captured by ESEM is consistent with images of polypropylene from optical microscopy (Rask et al., 1993), and with studies using chemical etching methods (Bartosiewicz and Mencik, 1974; Kojima and Satake, 1982). This prompted the conclusion that the structure is not an artefact of electron irradiation. A complementary study by Rozeveld et al. (1997) on polypropylene confirmed that the original structure is maintained during exposure. The authors also noted that localised surface melting by beam heating may introduce artefacts roughly parallel to the direction of beam scan.

A review of published research on the electron irradiation response of bitumen establishes an understanding of its structuring that ostensibly verifies the microstructural model. The treatise that follows is summarised below, in Table 2-5.

Table 2-5: A chronological summary on bitumen structure by ESEM at ambient temperatures

Author	Observations on the morphology of bitumen
Shin et al. (1996)	A highly entangled fibrillar network in both pure and polymer modified bitumen that is altered by strain and by interactions with the polymer.
Rozeveld et al. (1997)	After several minutes of exposure, an entangled network of fibrils that coarsened on ageing, from 10 $\mu$ m to 15 $\mu$ m, and packed more closely. Ageing-induced coarsening of asphaltene particles: 0.2 $\mu$ m to 1.2 $\mu$ m. The alignment of this network parallel to the axis of tensile strain.
Stangl et al. (2006)	The densification and coarsening of the fibrillar network on short-term ageing, in which the fibril diameter increased from 8.6 $\mu$ m to 14.2 $\mu$ m. A hackled system on long-term ageing with a fibril diameter of 5.8 $\mu$ m. A depth of fibril embedment of the order of 400nm below the surface. The effects of styrene-butadiene-styrene modification: an increase of fibril diameter by 12% due to styrene block-asphaltene interactions.

The irradiation response of bitumen is comparable to polyethylene and polypropylene: under prolonged exposure to an electron beam at ambient temperatures, the amorphous surface is modified to expose a three-dimensional network of entangled fibrillar structures. This random string-like system is embedded within the upper surface in a featureless substance (Rozeveld et al., 1997; Stangl et al., 2006) (refer to Figure 2-15). In their published study, Rozeveld et al. (1997) postulated that this etching is caused by local heating of the sample due to interactions between the impinging electrons and bitumen atoms. The authors concluded that this causes the preferential volatilisation of low molecular weight oils, which reveals high molecular weight fractions that remain associated in the form of strands. The mean diameter of this component is about  $10\mu\text{m}$  (Stangl et al., 2006).

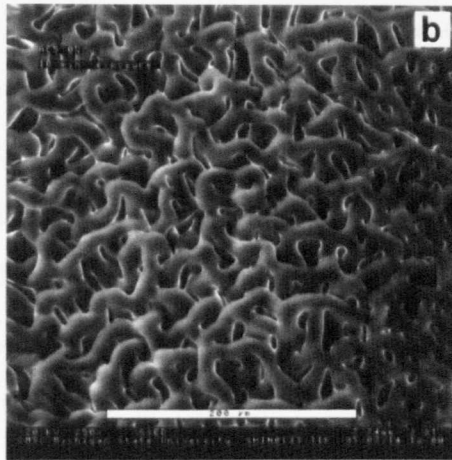


Figure 2-15: Micrograph of bitumen after several minutes irradiation (Rozeveld et al., 1997)

Similar structure is visible in asphaltene precipitates, in which platelets with diameters of 110-260nm cluster to form particles on the order of  $0.2\text{-}1.2\mu\text{m}$  (Stulirova and Pospisil, 2008). This provides some verification for the postulated chemistry of the fibrils. Moreover, the theoretical concentration of high molecular weight fractions into the network structures is corroborated by reviewing literature on ageing-induced chemical and physical modifications, as follows.

The process of bitumen ageing is the most important aspect affecting the durability of asphalt pavements (Peterson, 1984): degradation by environmental factors is the subject of continued laboratory simulation. The mechanisms of ageing vary with time: evolving from volatilisation of oily components during mixing and paving, to the seasonal and progressive oxidation of polar

fractions in-service (Airey, 2003). Notably, the saturate component is inert in oxygen and thus essentially unaltered by oxidation (Chipperfield et al., 1970; Isacsson and Zeng, 1997). Cyclic aromatics are more reactive with oxygen and, during ageing, polymerise into resins and then asphaltenes. This introduces chemical and rheological changes (Becker, 1997). The formation of highly polar and strongly interacting oxidised functions and ketones, due to the degradation of naphthenic rings and the oxidation of methylene, also contributes (Lu and Isacsson, 2002).

These irreversible phenomena increase the length and number of the asphaltene molecules, and thus the overall polarity of bitumen (Lu and Isacsson, 2002; Benbouzid and Hafsi, 2008). This contributes to the capacity of this fraction to establish an increasingly-organised network, which manifests itself as a concomitant increase in viscosity and decay in penetration (Stangl et al., 2006). The increased packing density of the string-like network captured in micrographs of oxidised bitumens reflects these changes, and renders the strands to be composed mainly of resins and asphaltenes (Stangl et al., 2006). The concurrent coarsening of these fibrils, to a mean diameter of about 15µm (Rozeveld et al., 1997), correlates with an increased molecular weight of the asphaltenes that is encountered on oxidation and derived using gel permeation chromatography (Stangl et al., 2006). This provides validation for the inherency of the network and for its formation by the clustering of oxidisable polar compounds.

The theory that the entangled network is exposed by the volatilisation of low molecular weight saturates, and is developed by polar interactions between high molecular weight asphaltenes and resins, is published by Rozeveld et al. (1997) and Stangl et al. (2006). This change in the structure of bitumen is potentially an ESEM construct: disruption of intermolecular bonds and ionisation of sample atoms associated with mass loss alters the thermodynamic energy of the system (Aguilera and Stanley, 1999). This could drive the rearrangement of surface and sub-surface particles into an otherwise absent morphology (Nix, 2009). Rozeveld et al. (1997) and Stangl et al. (2006) hence tested the inherency of the network, by strain and nanoindentation.

From their study on polypropylene, Rozeveld et al. (1997) postulated that the alignment of an artefact depends on the scan direction of the electron beam: inherent structuring does not but

may be modified by strain previous to irradiation. The authors therefore strained rolled films of bitumen under uniaxial tension at room temperature, and exposed the network structure using electron etching. Moreover, the axis of tension for one sample was perpendicular to the scan direction of the electron beam, and for a second was inclined at an angle of  $45^\circ$  to that plane. In both samples, the average diameter of the fibrils was the same as for unstrained bitumen: about  $10\mu\text{m}$ , but the random network was more ordered. Notably, the long fibrils were aligned parallel to the axis of tension and the shorter chains perpendicular thereto. This modification is shown in Figure 2-16, and indicates that the network structure is not an ESEM construct but an inherent microstructural feature (Rozeveld et al., 1997).

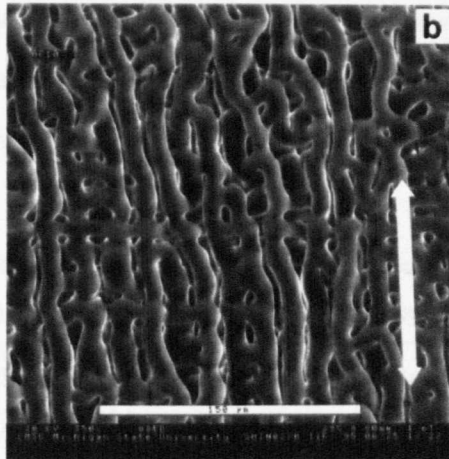


Figure 2-16: Micrograph of strained bitumen after electron irradiation (Rozeveld et al., 1997)

Stangl et al. (2006) defined bitumen structure by deriving a viscoelastic solution for the single dash-pot model for deviatoric creep using nanoindentation. In this depth-sensing technique, a tip penetrates the sample under a trapezoidal load profile: indents consist of loading, dwelling and unloading phases. The response of nanoscopic regions of the surface is quantified by the penetration depth of this tip, which is measured with time and load during a test and used with analytical solutions to back-analyse the parameters of the viscoelastic model (Tarefder et al., 2010). Stangl et al. (2006) defined a structural profile of pure and polymer modified bitumen at  $5^\circ\text{C}$  by the viscosity of the dashpot model, extracted by indentation in a grid scheme: adjacent indents were performed at intervals of  $5\mu\text{m}$  using a Berkovich tip with a maximum penetration depth of  $400\text{nm}$ . The plots of viscosity confirmed the texture imaged using ESEM: a bi-phasic

structure consisting of a high-viscosity part with a dimension of 10 $\mu$ m, which is embedded in a low-viscosity material. The authors also informed on the sub-surface depth of this structuring.

### Review of the thermoanalytical behaviour of bitumen

The literature review lends credence to the inherency of the network and to its chemistry, and proffers evaporation of the oils during irradiation as the mechanism by which this structuring is exposed. This volatilisation is thought to occur due to the elevation of surface temperature to 200 °C (Rozeveld et al., 1997), where incident electrons are decelerated in bitumen and their energy is converted by inelastic scattering into heat. Yet, evidence of liquid-to-gas transitions or other structural changes and kinetic parameters associated with the thermal decomposition of bitumen is elusive in SEM studies. This is resolved by a review of low-temperature changes of structure using differential scanning calorimetry, and of high-temperature modifications by thermogravimetry (Guillén et al., 1996). This treatise is expressed succinctly in Table 2-6.

Table 2-6: The thermal behaviour of chromatographic fractions as characterised by differential scanning calorimetry (DSC) and thermogravimetry (TGA). After Jiménez-Mateos et al. (1996)

Fraction	Glassy characteristics (DSC)		Volatile characteristics (TGA)	
	Glass transition temperature (°C)	Crystallised fraction (wt. %)	Pyrolysis onset temperature (°C)	Mass loss (wt. %)
Bitumen	-22.9	4.5	284.4	13.3
Saturates	-61.0	20.0	279.6	71.3
Aromatics	-19.6	3.6	303.1	32.8
Resins	14.7	0.9	246.8	6.4
Asphaltenes	70.0	0.0	268.4	2.3

Differential scanning calorimetry is a technique that measures the temperatures and enthalpic changes of physical transitions or chemical reactions in a system as a function of temperature and time (Collins, 2010). By modulating the otherwise linear heating rate to carry a sinusoidal profile (Price, 1998), endothermic and exothermic reactions are deconvoluted into reversing and non-reversing signals. These describe, respectively, kinetic processes or glass transitions in amorphous domains, and irreversible transitions by oxidation, evaporation, relaxation and

crystallisation (Reading, 1993; Wunderlich et al., 1998; Kriz et al., 2008).

The reversing thermal profile of bitumen shows several broad glass transitions, which indicate a complex mixture of crystalline, glassy and non-glassy amorphous phases (Kriz et al., 2008). Moreover, the transition to the glassy state relates inverse-linearly to bitumen penetration (du Bois, 1996) and depends on the polarity, complexity, flexibility and solubility of the component fractions (Eisenberg, 1993). For the maltenes the glass transition temperature of  $-30.8^{\circ}\text{C}$  (Kriz et al., 2008) is assigned to the convolution of the vitrification of the saturates at  $-60^{\circ}\text{C}$ , and the aromatics at  $-20^{\circ}\text{C}$  (Claudy et al., 1992). The asphaltene glass transition temperature is  $70^{\circ}\text{C}$ , but is lowered relative to its temperature of vitrification as a separate entity by the interference of lighter fractions (Masson and Polomark, 2006). Namely, the asphaltenes can be mobilised and entrapped in the lattice of crystallisable compounds or diluted by the oils, and may hence be inhibited from packing into a glass by the other fractions in bitumen (Kriz et al., 2008).

The non-reversing thermal profile of bitumen reveals the disordered phases to be metastable: at isothermal temperatures in the glass transition range they evolve with time to a more stable thermodynamic state (Masson and Polomark, 2001). The metastability of bitumen is governed by three overlapping phenomena. Namely, physical transitions in the temperature envelope of  $-42^{\circ}\text{C}$  to  $92^{\circ}\text{C}$  are controlled by the conversion of structured amorphous domains of alkylated and naphthene aromatics into anisotropic phases. The second process stems from materials that melt at higher temperatures: inhomogeneous waxes and crystalline fractions, which are neither completely crystalline nor completely amorphous in nature (Noel and Corbett, 1970). This transition occurs at temperatures of  $-10^{\circ}\text{C}$  to  $45^{\circ}\text{C}$  (Redelius, 2011), though melting may persist to  $90^{\circ}\text{C}$  (Bahia and Anderson, 1992). The dissolution of structured but non-interacting domains of asphaltenes and resins, by disruption to Keesom interactions (Ensley, 1975), is a concomitant modification of structure between  $40^{\circ}\text{C}$  and  $50^{\circ}\text{C}$  (Masson and Polomark, 2006).

Knowledge of high-temperature kinetic behaviour is acquired by thermogravimetric analysis: a technique for measuring the mass of a material as a function of temperature, whilst its sample is the subject of a controlled temperature regime in inert gas (Earnest, 1988). Measured thus,

pyrolysis of refinery bitumen starts at temperatures of between 170°C and 200°C (Benbouzid and Hafsi, 2008; Kopsch, 2008). Though complicated by consecutive reactions of the colloidal fractions, this temperature is governed by the volatilisation of saturates, the scission of single bonds of carbon with sulphur or nitrogen heteroatoms, and the cracking of aromatics (Qing et al., 2007; Guo et al., 2008). This temperature is affected by the varying degree of volatilisation of different volatile fractions therefore, by fluxing and by decomposition of oxidation products (Benbouzid and Hafsi, 2008; Kopsch, 2008; Murugan et al., 2012).

The sequence of thermal reaction following this onset of mass loss is governed by aromaticity and molecular weight. This reflects the activation energy required to crack the hydrocarbons before they are volatilised, and the relative differences in their oxygen susceptibility (King and Corbett, 1969; Guo et al., 2008). This sequence often conforms to the order of: saturates, that primarily distil at below 350°C; aromatics and resins, which distil mainly in the range of 350°C to 450°C; and asphaltenes, which distil at temperatures above 450°C (Xu and Huang, 2012). The thermal decomposition of specific resins and asphaltenes may contribute paradoxically to the onset of pyrolysis: high reactivity of these components in oxygen (King and Corbett, 1969) is related to highly functional groups and longer bridging carbon chains.

Notably, this literature review indicates that mass flux from bitumen occurs by the emission of saturates and aromatics, when the sample temperature is increased to above 200°C. This is similar to the elevation in surface temperature that is caused by electron irradiation, and could confirm the theory that the network is exposed by the volatilisation of oily fractions. Moreover, cracking of saturates produces free radicals and fragmental alkanes, which abstract hydrogen from the other fractions. This reaction inhibits the dispersion of the solute phase and produces an increase in molecular interactions therefore (Peterson et al., 1994), which could establish a cause-effect relationship for the observed structuring. Although the decomposition of specific asphaltenes and resins may occur at a temperature below which the oils are retained in liquid phase, they are highly susceptible to oxygen adsorption. These components readily-coke and contribute to structural modifications in the form of a concentrated residual fraction rather than of a vapour therefore, which is the destination of the saturates and aromatics.

## **Review of comparable phase morphology**

The network structuring in bitumen that is resolved by ESEM is similar to multiphase polymer composites described in the literature. The structure of two synthetic composites investigated using electron microscopy is summarised below, to provide additional insight of the properties potentially influencing bitumen structure and of other techniques available for this research.

Erdmann et al. (2007) characterised the morphology of clay-based high density polyethylene (HDPE) and polyamide 6 (PA 6) blends by SEM. Films were prepared for imaging by fracture under cryogenic conditions, and then by vapour phase-etching with boiling toluene to remove HDPE. Micrographs reveal the phases to be well-separated due to poor compatibility: HDPE forms non-polar parts by van der Waals type forces, which do not interact with the continuous PA 6-silicate polar phase that is strongly bonded by hydrogen transfer (Erdmann et al., 2007). After extraction of HDPE therefore, voids of the order of 0.4–4.0 $\mu\text{m}$  form by lixiviation, and are separated by channels in the continuous phase of about 8.5 $\mu\text{m}$  across.

Na et al. (2003) investigated phase morphology in injection moulded HDPE and ethylene vinyl acetate (EVA) blends using SEM. Samples were prepared firstly by fracture in liquid nitrogen, and then by benzene-etching. Blends with up to 20% by weight EVA and fractured transverse to the direction of flow exhibited sponge-like texturing: 0.5-1.0 $\mu\text{m}$  diameter voids formed in the position of benzene-extracted EVA particles. These circular voids deformed to ellipses under shear force. As EVA content approached 40%, the texture of samples fractured perpendicular to flow direction evolved, firstly to a sea-island structure and then a co-continuous morphology with irregular voids up to 20 $\mu\text{m}$  in length. Phase morphology in such blends was anisotropic: a highly-oriented layered structure was observed in the direction of flow (refer to Figure 2-17).

From this summary, it is evident that the morphology of a synthetic composite depends on the volume ratio of its components and their rheological and interfacial properties. Notably, strong interfacial interaction is required between the components to ensure compatibility: in blends of incompatible systems phase separation often occurs. After removal of the incompatible phase a porous structure is imaged using electron microscopy. The similarity of this effect to that of

physical etching of the weakly-bound saturate fraction in bitumen perhaps provides evidence for arguments (Redelius, 2006; 2011) on the incompatibility of the chromatographic fractions. Moreover, the use of cryogenic fracture techniques in petroleum microscopy is yet to be fully exploited, and may offer the opportunity to study bulk structure of samples from this industry.

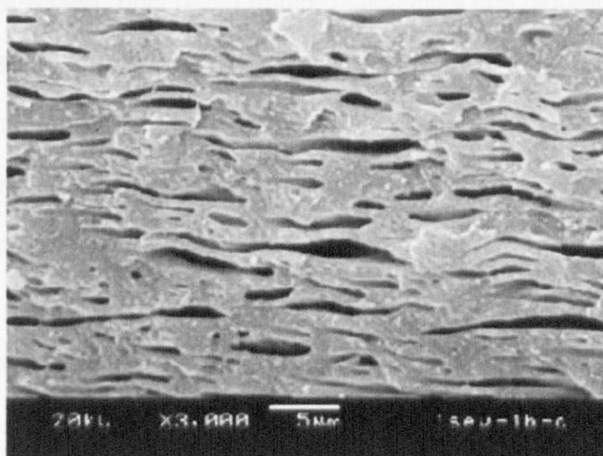


Figure 2-17: SEM of fractured surface of HDPE/33EVA blend along flow (Na et al., 2003)

### 2.6.3 Discussion on microscopy literature

Microscopy studies published in the literature indicate that the interaction of chromatographic and crystalline fractions produces bitumen structure. Moreover, this structure is dependent on the microscopy technique used to image it: in the AFM randomly-dispersed ellipsoidal clusters of rippled wax are imaged at the surface, and in the ESEM polar molecules align to develop a continuous network that is immersed in light oils. It may be that the surface-dispersions are an expression of this network or reflect ambiguities in the structure of pseudo-crystalline fractions (Noel and Corbett, 1970). The structural inconsistency could instead render the dispersions to be produced by crystallisable sections of molecules that concentrate at a surface by a tension effect, and which extend into the smooth peripheral regions. Therein, the amorphous sections of the pseudo-crystalline molecules develop intermolecular associations that contribute to the sub-surface network. The undulating structure could then be absent from ESEM micrographs due to an apparent incapacity to limit sample instability during irradiation.

## 2.7 CHAPTER SUMMARY

Bitumen is a viscous fluid that was exploited in antiquity from seepages of subterranean crude oil along geological fault planes, and which is presently manufactured for use as an adhesive in the construction of pavements by the distillation of specific crude oils. Although its chemical composition has hitherto been only partly defined, analytical techniques characterise bitumen as a complex and heterogeneous mixture of thousands of similar but unique hydrocarbons, of varying polarity and molecular weight. Heteroatoms of sulphur, oxygen and nitrogen are also often present, in addition to trace quantities of nickel and vanadium complexes that contribute to intermolecular interactions.

Electrodynamic interactions between the molecules are of critical importance to defining the properties of bitumen. Namely, high strength dispersive forces between polar fractions confer to bitumen its elasticity and dark colour, and the interaction of these molecules with non-polar compounds gives bitumen its viscous characteristics. In specific conditions, these interactions drive the formation of clusters of polar molecules, which are solvated in a non-polar moiety in the form of discrete islands or interconnected chains. The distribution and organisation of the clusters is correlated with the mechanical behaviour of the material, and is conceptualised by several models.

In the revered colloidal model, the displacement of well-dispersed parts at high temperatures is limited only by the viscosity of the non-polar matrix, and the material hence exhibits viscous fluid-like behaviour. At low temperatures however, and in the absence of a sufficient quantity of the fraction that peptises the dispersions, these clusters associate to develop a continuous rigid network that may deform elastically or fracture when stressed. The microstructural model also describes the capacity of polar molecules to form chains of weak polar-polar interactions. From the continuous breakage and reformation of these secondary bonds bitumen derives its viscoelastic behaviour; the unique way that they reform explains temperature-sensitivity.

Debate pervades the literature regarding the simplistic nature of the colloidal model and of the thermodynamic capacity for phase separation. The validity of the microstructural model is also

questioned, as are the interpretations of structure as represented by different microscopes. In an AFM, randomly-dispersed ellipsoidal groups of thin strands of interacting hydrocarbons are resolved at the surface. The literature concludes that waxes associating with chromatographic fractions or these fractions themselves are responsible for this structure. In an ESEM, surface oils precluding the analysis of bitumen structure are volatilised by beam irradiation, to expose a continuous fibrillar network of polar molecules. Notably therefore, a complete understanding of these structures is elusive, and moreover, of evidence of the bulk morphology of bitumen.

## **2.8 CONCLUSIONS AND APPROACH**

In consideration of the preceding literature review and the aim of this thesis, it was decided to use electron microscopy to analyse the structure of bitumen. The primary differences between the published AFM and ESEM studies are the representation of the surface, and the changes in morphology with variations in temperature. Notably, it is thought that elevated temperatures under the electron beam volatilise oils and therefore preclude images of the surface. To arrest the volatile fractions and preserve the physicochemical state of bitumen during irradiation, this novel study proposes to use an ESEM equipped with a Peltier cooling stage. By this approach it is aimed to enable unique images of the surface to be produced using electron microscopy, and hence develop unprecedented knowledge of thermal-structural transitions at and near the surface of bitumen.

Although significant research has developed knowledge of the chemistry of surface structure, the literature is devoid of any clarity on how these systems relate to bulk morphology. For this thesis, it is proposed to supplement ESEM research with insights acquired of bulk structuring using two new approaches. Namely, a cryogenic fracture preparation technique similar to that used effectively to examine the internal morphology of polymer composites, and an ion milling process to study near-surface morphology of amorphous and structured domains.

By this research approach, it is aimed to correlate bitumen structuring at the surface and in its bulk, which is absent from the literature and unrivalled by available AFM methods.

### **3 A REVIEW ON BITUMEN HEALING**

Bitumen fracture is ubiquitous at temperatures near the glass transition, where the dissipation of strain energy by plasticity is negligible (Moavenzadeh, 1967), and the prevalent mechanism of damage during fatigue. Molecular restructuring, relaxation and healing of fractured surfaces that contain the remnants of this deformation zone partially restore the mechanical properties of the material. To describe the healing phenomenon, myriad studies on bitumen are collated with healing in long-chain polymers. Recent published research aims to mimic this process by joining two samples of bitumen under compression, and measuring changes in strength using faint shear stress. This approach neglects however, the modifications in molecular weight that occur due to the microscopic deformations that precede and precipitate fracture.

#### **3.1 INTRODUCTORY REMARKS**

Traffic and environmental loading of an asphalt pavement establish stress distributions in the binder that peak at aggregate contacts. These initiate and propagate cracks where the energy of intermolecular bonding is exceeded (Cherry, 1981). Moavenzadeh (1967) concluded that in asphalt it is generally inconceivable for a crack to propagate through the solid phase, because the bonding of crystalline solids is much stronger than that of amorphous bitumen. Moreover, in asphalts with poor binder-aggregate adhesion: a consequence of high permeability (Thom, 2008), low aggregate roughness (Yang and Al-Qadi, 2009), or low acid component of bitumen surface energy (Bhasin et al., 2007) the interface establishes a preferential fracture trajectory.

The mechanism of failure also depends on the thickness of the bitumen film around the stone particles. Little and Jones (2001) used triaxial tests to demonstrate that at aggregate contacts with thin bitumen films ( $< 35\mu\text{m}$ ) rupture occurs at the binder-stone interface (adhesively), but thicker films fail in the bitumen-filler matrix (cohesively). With respect to temperature, Babcock et al. (1998) studied bitumen using lap shear bonds and defined an adhesive-cohesive failure transition at  $6^\circ\text{C}$ . Mo et al. (2007) reported tensile fatigue tests at  $5^\circ\text{C}$  and  $25^\circ\text{C}$ , and ascribed cohesive failure at both temperatures to a synergistic rise of cohesive strength and interfacial bonding. Frolov et al. (1983) published tensile studies of bitumen samples adhered to marble

and steel substrates. The authors indicated that the adhesive bond strength exceeds the work of cohesion of bitumen by 10% to 50%, and therefore concluded that cracks in asphalt usually traverse in close proximity to but around aggregates. This was confirmed by Read (1999).

Fractures through the solid asphalt phase are primarily attributed to the pre-existence of flaws and cracks in such pieces (Genin and Cebon, 2000). In consideration of the preceding review, it can therefore be assumed that the fracture behaviour of bitumen controls the cracking of the mixture. In the study of healing this thesis focuses on the restoration of bitumen structure and mechanical properties by viscous flow and molecular remixing, which defines asphalt healing.

### **3.2 A REVIEW ON FATIGUE AND FRACTURE**

The mechanism by which repeated stress propagates fatigue within bitumen is known to vary with temperature. In the glassy regime, the fluid non-polar fractions are immobilised and form a structured network with a rigid character. This originates the proclivity for structural damage by brittle fracture (Castro and Sánchez, 2006). The modulus of this gel system is controlled by the stretching and bending of intermolecular bonds (refer to Section 2.6), and is hence related directly to the stiffness thereof (Cheung and Cebon, 1997). As the temperature is increased to above the glass transition, chain separation due to thermal expansion or mechanical agitation reduces and then melts van der Waals restoring forces. This enables sliding of the previously elastically-bonded network segments that manifests macroscopically as viscoelastic response to load, and then plastic flow from regions of low to high stress (Harvey and Cebon, 2003).

The molecular response of polymers to external stimuli is established in the literature (Kausch et al., 1991; Perkins et al., 1994) and summarised below, providing a substantive contribution to the review. In dilute solutions of long polymers molecular dislocation is governed by friction. Namely, from a relaxed amorphous state, the transmission of load between polymer sections that cross a load-bearing plane occurs by viscous interactions between adjacent random-coil chains (Kausch et al., 1991), which readily slip apart by Rouse diffusion (Wool, 1993). Hence, the depth of penetration of the oriented molecules crossing this plane is reduced, and fracture occurs by pullout (Kline and Wool, 1988). The molecular weight distribution within the surface

layer is relatively unaffected therefore (Wool, 1995). In concentrated solutions and semi-dilute regions, additional resistance to motion stems from mechanical interaction or interpenetration of coiled molecules. This is explained by the concept of entanglement (Graessley, 1974). The drop in entropy that occurs as polymers are strained between affinely-displace entanglements concentrates stress (Hoy and Robbins, 2007). Where unreleased by creep or diffusion due to topological constraints, this stress may excite a main-chain bond between an adjacent pair of entanglements to the quantum state of separation; energy in the remaining bonds dissipates as heat (Sperling, 2006). Low molecular weight fragments are created by this scission event, which align with ruptured ends normal to the crack surface (Wool, 1995) (refer to Figure 3-1). The response of polymers to mechanical or thermal stimuli is thus limited by the strength of a single chain or chain segment but also depends on multi-chain interactions including diffusion, conformational change, and the alignment of structural elements (phase-separated domains) with respect to the deformation field (Bueche, 1955; Wool, 1995).

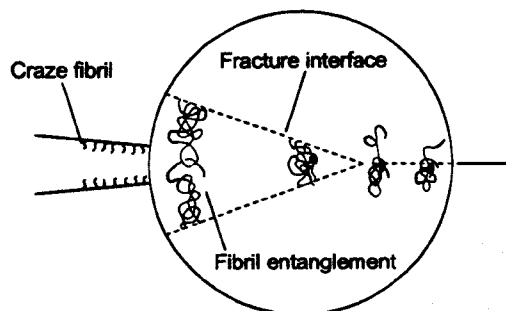


Figure 3-1: Schematic of fracture propagation and chain separation by loss of entanglement, developed from Kausch and Dettenmaier (1982)

### 3.3 POSTULATIONS ON THE HEALING MECHANISM

#### 3.3.1 Preamble

For polymers, healing is defined thus: when two fractured surfaces are brought into contact at a temperature above the glass transition, the junction becomes indiscernible from any surface located within the bulk and develops increasing mechanical strength until the properties of the virgin material are achieved (Jud and Kausch, 1979; Prager and Tirrell, 1981; Wool, 1995). In the field of pavement engineering healing is described as the partial restoration of the intrinsic

bitumen structure across adjacent crack surfaces (Little et al., 1999). To explicate the healing process in bitumen, it is firstly instructive to review published theories on healing of polymers.

### 3.3.2 The interdiffusion concept

In brevity, this model defines healing by the restoration of secondary bonds among molecules or microstructural components, and the formation of mechanical force-transmitting bridges at the interface by Rouse diffusion or by reptation. This model is schematised in Figure 3-2.

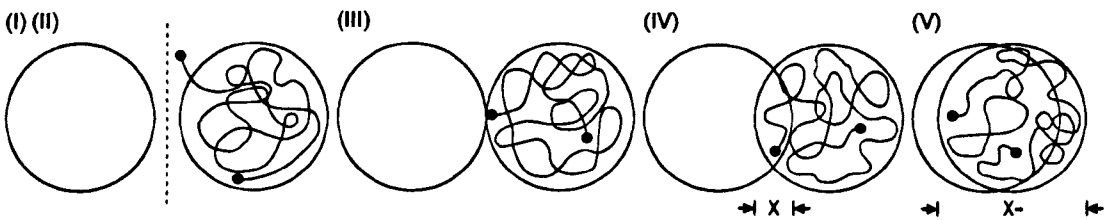


Figure 3-2: Schematic of chain motion during healing of a fractured interface (Wool, 1995). Stages: (I) rearrangement, (II) approach, (III) wetting, (IV) diffusion and (V) randomisation

The theory of interdiffusion indicates that healing involves five consecutive stages. The stages describe the conditions necessary to establish intimate interfacial contact between adhering surfaces and to restore the characteristic strength of the material, as identified by microscopic and mechanical measurements. The first two stages of this model are ubiquitously ignored in bitumen healing studies, which stems from the aim to minimise the time-dependence of initial cohesion. This may instead yield a solution to the fundamentally different problem of welding: the contact of two surfaces with uniform molecular weight distribution (Wool, 1995). However, surface concentrations of chain ends (pullout) and fragments (scission) affects the increase of interfacial strength by molecular diffusion (Wool, 1995). Moreover, during fracture propagation the configuration of chains in contact with the interface is compressed. The relaxation of these drives healing by Rouse motion (Rouse, 1953). This overview compels scrutiny of each stage.

#### Stage one: surface rearrangement

Surface rearrangement phenomena, which could include relaxation, diffusive inward migration or chemical reaction of chains with atmospheric gas, impede interfacial diffusion. The duration required for the microscopic sequences to restore mechanical properties thus increases. Jud

and Kausch (1979) studied surface rearrangement in poly(methyl methacrylate) by separating for several days samples fractured in single-edge notch and compact tension tests. The study reported a 95% reduction in the rate of fracture toughness recovery compared to control tests, in which crack surfaces were instantly rejoined.

Barber and Atkinson (1972) also showed that cohesive bond strength was reduced by surface rearrangement effects, namely inhomogeneous near-surface structure produced by cooling in air. O'Connor (1984) identified a limit on the availability of hydroxyl-terminated polybutadiene molecules to initiate healing after contact is established. This corresponded to the recovery of fracture strength in edge-notched samples equal to that acquired by cohesion (refer to Figure 3-3). The authors also concluded that the effects of surface rearrangement are reversible.

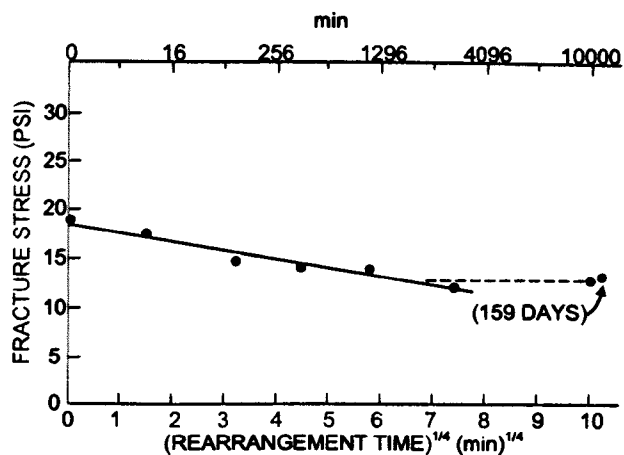


Figure 3-3: Variation of strength with rearrangement time (Wool, 1995)

### Stage two: surface approach

Partial mechanical contact at the interface is established by bulk translation of microstructural components. This occurs by flow of molecular segments when they possess sufficient thermal energy to overcome energy barriers (Jud et al., 1981; Kline and Wool, 1988), or driving forces including connected chains and stored strain energy in the bulk (Wool, 1995). The orientation and interpenetration of the flowing material are reported to influence the strength of the crack healing effect (de Gennes, 1983; Shim and Kim, 1997). Where polymer viscosity is high, the inability of fractured surfaces to interpenetrate and establish uniform contact at the interface produces a system that is weakened by imbibed air or non-contacting regions (Bucknall et al., 1980). For low viscosity polymers, a large volume of material may be displaced to peripheral

regions of the interface. This causes chain alignment parallel to the surface and normal to the bulk, thereby reducing the contribution of chemical bonds and chain segment interconnection to strength (Barber and Atkinson, 1972; Wool and O'Connor, 1981; Shim and Kim, 1997). It is notable that this stage constitutes a boundary value problem to crack healing, which requires contact between the fractured surfaces at distances of the order of 10nm (Fourche, 1995).

### **Stage three: wetting**

Surface forces, electrostatic forces and hydrogen bonds induce adhesive healing by a gradual reduction of surface irregularities, through elastic-plastic deformation of the fractured surfaces (Briscoe, 1978; Jud et al., 1981). By this phenomenon (wetting), potential barriers associated with inhomogeneities disappear and chains can diffuse across the interface (Wool, 1995). The restoration of long-range attractive (electrostatic) interactions between non-bonded segments at the interface drives adsorption. This defines the adhesive area (Krupp, 1976) to separation distances of about 0.3nm to 10nm (Fourche, 1995). Short-range attractive interactions (acid-base or hydrogen bonds) are established at distances of less than 0.3nm, and assure transfer of matter between adhering surfaces (Sharpe and Schonhorn, 1963). Cohesion in elastomers is also defined by the viscoelastic properties of the hinterland adjacent to the interface, which interact with the surface forces to augment cohesive strengths (Krupp, 1976 Cherry, 1981).

### **Stages four and five: diffusion and randomisation**

The ability of a partially-healed interface to transmit stresses that exceed the thermodynamic work of cohesion is assured by intermolecular entanglements, which are formed at chain ends and transferred along the chain (Kausch and Dettenmaier, 1982; Kim and Wool, 1983) (refer to Figure 3-1). The mechanism of chain interpenetration, namely the method by which chains condense and entangle, was defined by Kim and Wool (1983) in the minor chain model.

In this model of an isothermal matrix dominated by entanglement, chain motion is confined to an un-deformable tube that acquires a conformation equivalent to the current curvilinear path of the molecule. In this tube, one-dimensional chain motion occurs due to thermal fluctuations and reduced surface entropy. The driving mechanisms include rotation, segmental transverse reorganisation and reptation: longitudinal snake-like displacement (de Gennes, 1971) (refer to

Figure 3-4). It is by the accumulation of these random back-and-forth wriggling motions, and three-dimensional swimming in semi-dilute domains (Rouse, 1953), that the chain disengages from its initial conformation (de Gennes, 1971; Prager and Tirrell, 1981). Kim and Wool (1983) define the escaped chain segments as minor chains (refer to Figure 3-4), which assume new random Gaussian conformations as they diffuse and penetrate the interface. These segments entangle with low energy chain ends to restore the virgin molecular configuration (Wool, 1979; Liang et al., 2004), when the initial conformations have evaporated (Wool, 1990).

Notably, crack healing seldom occurs by reformation of broken bonds in the polymer skeleton. In semi-crystalline homopolymers and multiphase block copolymers, static forces at interfaces are transmitted by van der Waals attraction between contacting segments and molecules that are entangled in the two phases forming at the interface (Jud and Kausch, 1979; Wool, 1995).

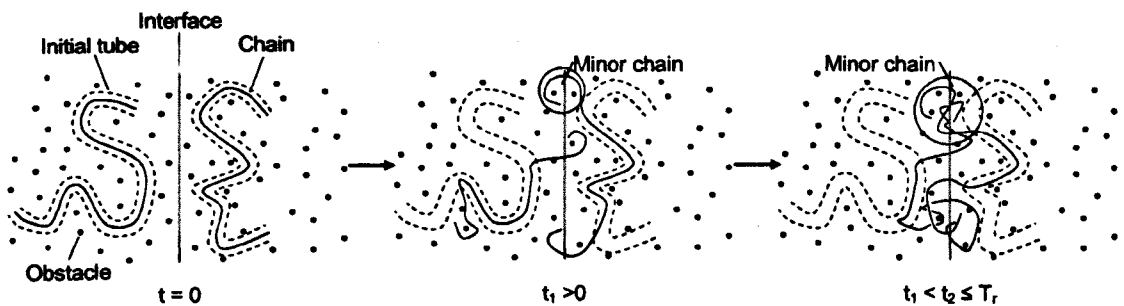


Figure 3-4: Disengagement of a molecule from its initial conformation near an interface, the increasing spherical envelopes of minor chains and entanglement formation (Wool, 1995)

Jud and Kausch (1979) reported macro-mechanical development for the minor chain concept. Using fracture toughness experiments and the Einstein relation the authors correlated healing with chain ends or kinks in the chains constituting 5% of the length thereof, which cross-link in the matrix. Moreover, it was concluded that interfacial diffusion of entire molecules is unlikely.

### The time dependence of the healing process

Jud and Kausch (1979) stated that voids formed in PMMA by constant strain compact tension tests optically-healed in three minutes. The study characterised the development of interfacial adhesion by energy release rate, and showed that interfacial bond strength on closure of the fracture exceeded the contribution from surface tension.

O'Connor and Wool (1980) studied isothermal healing in styrene-isoprene-styrene using light-transmitted photometry. The authors reported a sigmoidal recovery of transmittance with time, on a logarithmic axis. Later, Jud et al. (1981) produced a double logarithmic graph correlating the fracture toughness of PMMA with healing period, and observed a straight-line relationship with an exponent of 0.25. Wool and O'Connor (1981) revealed independently this relationship for fracture stress and healing time (refer to Figure 3-5) using double cantilever beam tests on polybutadiene. These data compelled Prager and Tirrell (1981) to conclude that a single time-scaling law applies over the entire healing period. Wool and O'Connor (1981) defined this by the convolution product of intrinsic healing and wetting functions:

$$R = \int_{\tau=-\infty}^{t-t} R_h(t-\tau) \frac{d\varphi(t,X)}{d\tau} d\tau \quad \text{Equation 3-2}$$

$$R_h(t) = R_0 + Kt^{1/4} \cdot \varphi(t) \quad \text{Equation 3-3}$$

where  $R$  is the macroscopic healing function,  $R_h(t)$  is the intrinsic healing function that defines instantaneous strength gain by cohesion ( $R_0$ ) and time-dependent strength gain by interfacial diffusion ( $K$  is constant),  $\varphi(t, X)$  is the wetting function,  $\tau$  is the time variable and  $t$  is present time (Wool and O'Connor, 1981).

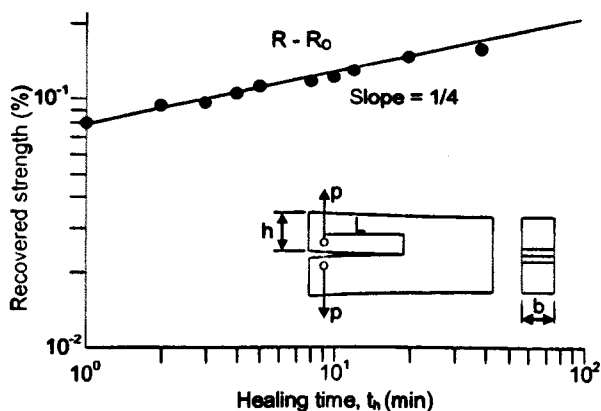


Figure 3-5: PB healing using a double cantilever beam test (Wool and O'Connor, 1981)

Prager and Tirrell (1981) studied healing phenomena at polymer interfaces using the reptation model derived by de Gennes (1971). The study concluded that at fixed healing time, strength is proportional to chain weight. Namely, if the adhering surfaces contain molecules terminated there, as evident at brittle fractures in glasses, then healing strength is defined using Equation

3-4. However, if the contact is between surfaces equilibrated against a gas phase the number of bridges across the joint is described by Equation 3-5. Kausch and Dettenmaier (1982) and Kausch et al. (1991) also noted that healing depends on chain length. Wool (1995) concluded that the reptation time scale, which is proportional to the cube of chain length, is adequate for molecular interpenetration and entanglement. It is known however, that long chains increase the healed fracture energy more efficiently than short chains (Jud et al., 1981): the curvilinear depth and volume of interpenetration required for complete transfer of interfacial stress varies inversely with chain weight (Kausch et al., 1991).

$$\sigma \sim t^{1/4} M^{-1/4} \quad \text{Equation 3-4}$$

$$\sigma \sim t^{1/2} M^{-3/2} \quad \text{Equation 3-5}$$

where  $\sigma$  is the re-fracture stress,  $t$  is the duration of healing and  $M$  is molecular weight.

It is notable that in compact tension and double cantilever beam tests on the fracture process in healed PMMA (Jud and Kausch, 1979) and polystyrene (Wool, 1995), crack propagation is a more rapid phenomenon than in virgin polymer. Jud and Kausch (1979) reported specimens thought to be completely healed, from the aspect of fracture toughness, failed ten times faster than in the first test. Namely, original samples fractured under constant load after 70 minutes, whereas the apparently fully-healed samples broke under the same conditions after some 2 to 5 minutes. The authors proposed therefore, that chemical cross-linking reactions between the adhering surfaces contribute negligibly, if at all, to the bond at the interface. However, similar observations and reduced crack re-propagation times in polystyrene were explained by Wool (1995) by change in the physical attitude of nucleating particles at the original nucleation site.

#### **The temperature dependence of the healing process**

Succinctly, a higher temperature during healing shifts the recovery response to shorter times. Specifically, temperature modifies wetting by changing the nucleation density and propagation rate of wetted areas; the initiation and rate of diffusion via surface rearrangement phenomena and molecular mobility; and the depth of chain penetration by conformation effects (Wool and O'Connor, 1981). Jud and Kausch (1979) also reported that mechanical interaction in PMMA

healed below its glass transition is limited by secondary bonds at points of contact. To enable diffusion, interpenetration and temporary cross-linking (Bueche, 1995) of chain segments, the temperature was raised by 10K. Complete recovery of fracture resistance in compact tension tests required higher temperatures, however. The temperature-sensitivity of polymer healing has been reported in other research (Bucknall et al., 1980; Bastien and Gillespie, 1991; Shim and Kim, 1997; Boiko, 2000). Interestingly, Wool and O'Connor (1981) produced a sigmoidal healing master curve using time-temperature superposition (refer to page 94 for description).

**The effect of pressure on the healing process**

Using compact tension tests in PMMA (Jud and Kausch, 1979) and polystyrene (Wool, 1995), the effect of pressure on the healing process has been studied: an interface-normal pressure shifts recovery to shorter times (refer to Figure 3-6). Chuang et al. (2000) simulated this effect for wetting of two polymer globules. The authors noted that, in absentia of an external force to move the particles together previous to reptation, the equilibration of repulsive and attractive forces establishes a nuclear separation that precludes interpenetration and interfacial strength development. However, Wool and O'Connor (1981) concluded the time required for maximum interpenetration increased as an exponential function of pressure. Pressure to assist wetting, which then relaxes to zero, is therefore recommended.

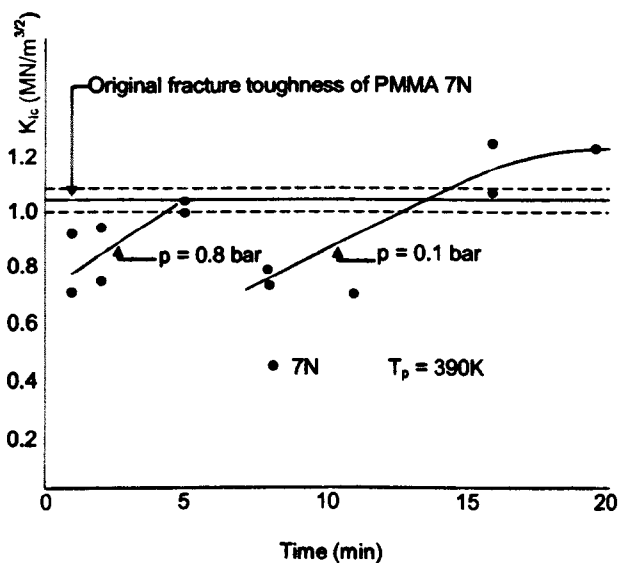


Figure 3-6: The effect of pressure on the recovery of fracture toughness (Jud et al., 1981)

### A comment on fatigue crack healing

Klosterman (1984) studied healing in polystyrene and polystyrene reinforced with glass fibres, using compact tension samples fatigued in constant displacement control. The healed crack growth rate in polystyrene was restored to the virgin response at times shorter than required to achieve complete interpenetration and fracture strength, and was devoid of significant time dependence. Wool (1995) ascribed this juxtaposition to the ability of cracks to grow remotely to the original interface, and the contribution of low molecular weight species to rapid healing. In the fibre-reinforced polymer, permanent fibre damage and fibre-matrix debonding reduced the load-carrying capacity of the healed polystyrene matrix and established additional sites for crack nucleation upon re-fatiguing (Wool, 1995).

### 3.3.3 The multi-step concept for fatigue and healing

Recognising analogy between the healing phenomenon in bitumen and high molecular weight polymers, Phillips (1999) developed a three-stage model to describe the processes of fatigue healing. The healing mechanism consists of macrocrack closure due to consolidation stresses and flow; microcrack closure and adhesion driven by wetting; and rejuvenation of mechanical properties by diffusion-limited build-up of asphaltenic structures (refer to Figure 3-7). Although incongruous analysis was reported, the rate of healing was thought to decrease with time and to restore modulus firstly and subsequently strength. It should be noted that the original figure published by Phillips (1999) contained a typographic error: the order of strength and modulus loss during the fatigue process was incorrect.

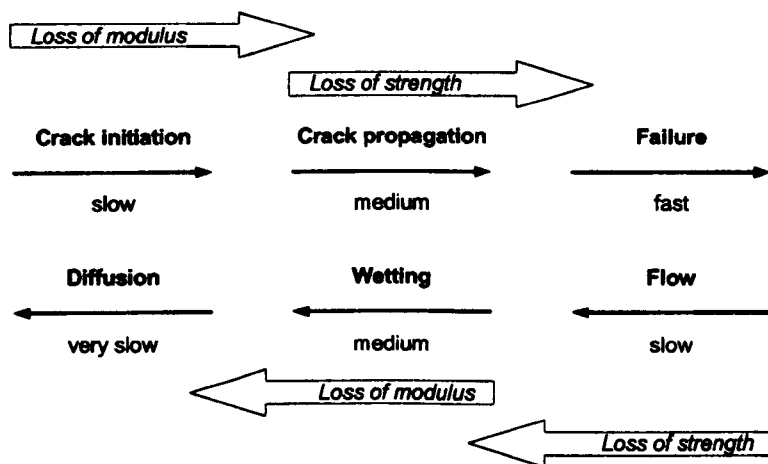


Figure 3-7: The multi-stage model for fracture and healing, postulated by Phillips (1999)

### 3.3.4 The dissipative thermodynamic concept

#### Preamble

To define the fundamental mechanisms of chemical and physical interactions in bitumen that produce fracture healing, Kringos et al. (2009) eschewed comparison with this process in high molecular weight polymers and used on a chemo-mechanics approach. This explains phase change and damage phenomena at a scale where physical chemistry meets mechanics (Silva and Ulm, 2002; Ulm, 2003; Xu and Li, 2010).

From the atomic force microscopy studies published in the literature, it is known that bitumen phase separates under specific kinetic conditions and acquires an inhomogeneous structure. This structure consists of clusters ( $\beta$  phase) dispersed in an amorphous matrix ( $\alpha$  phase). The interface between an elastic cluster and viscoelastic matrix produces a natural stress inducer, which attracts high stresses when the material is exposed to thermal or mechanical load. This yields a crazing pattern of interconnected fibrils that emerges as degraded macro-mechanical properties (Brown, 1991; Schmets et al., 2010). However, if by modifying the thermodynamic conditions of the material the inclusions change, either by rearrangement or by merging into the matrix, then memory of the crazes would dissipate and the bitumen would show recovery of mechanical performance: healing (Kringos et al., 2009).

#### Kinetics of phase separation

In phase equilibrium, for which there is equality of chemical potentials of the  $\alpha$  phase  $\mu_\alpha$  and  $\beta$  phase  $\mu_\beta$ , stable coexistence of both phases occurs. However, when the thermodynamic state of the system is perturbed, a chemical driving force for precipitation or dissolution phenomena develops. The measure of this force is the chemical potential difference, which expresses the energy stored as chemical bonds (Ulm, 2003; Schmets et al., 2011):

$$\Delta\mu = \mu_\alpha - \mu_\beta \quad \text{Equation 3-6}$$

Otherwise stated, for  $\Delta\mu < 0$  the  $\beta$  phase fraction  $c_\beta$  will reduce and the fraction of the  $\alpha$  phase  $c_\alpha$  will increase, but for  $\Delta\mu > 0$  the reverse process occurs. The phase fractions can thus only be changed in non-equilibrium conditions of definite chemo-mechanical driving force (Kringos

et al., 2007). This may be influenced by stored local elastic energy density and pressure due to the biphasic character and deformability of the system (Ulm, 2003).

### **Phase separation in the bulk**

The principle according to which the thermodynamic model was postulated is the existence of phase separation phenomena in bitumen. Knowledge of molecular segregation in the bulk is hence vital. To address this, Schmets et al. (2011) conducted spin-echo small angle neutron scattering (SESANS) experiments complemented by quasi-elastic neutron scattering research using the NEAT spectrometer. The former technique measures the change in polarisation of a transmitted neutron beam by elastic nuclear scattering (Rekveldt et al., 2006). Local structure or variations in the hydrogen-to-carbon ratio of 5% produce contrasting scatter, which defines the presence of phase domain or ordering phenomena in the sample (Li et al., 2010; Schmets et al., 2011). For bitumen with bee-like surface structuring, Schmets et al. (2011) reported that the small angle signal decreased from the length scale of 10 $\mu$ m: comparable to the size of the bee-like domains. The signal was constant for bitumen without surface structures. These data compelled the authors to conclude that bitumens with surface structuring exhibit a chemically-distinct two-phase bulk morphology.

NEAT is a direct time-of-flight neutron spectrometer designed for studies on the dynamics and microscopic structure of materials, for time domains of 0<sup>-13</sup> to 10<sup>-10</sup> seconds and length scales of 0.05 to 50nm (Izaola and Russina, 2010). Using this method, Schmets et al. (2011) showed that the inelastic scattering function for varied bitumens is described by the convolution of two Lorentzian, distributions in energy and an elastic contribution at 0eV. For the studied range of temperatures (10 to 340K) this pattern defines a two-component system in which the diffusing particles are space bound: they are not diffusing throughout the material, but can access only a limited area (Lerf et al., 2006; Schmets et al., 2011). Moreover, with increasing temperature the relaxations are less-strongly suppressed (Cicerone and Soles, 2004), and an asymmetry develops at the neutron energy loss region of the spectrum. This asymmetry is identified with a Boson peak, which is a signature that dynamics resemble those of a typical glass (Kringos et al., 2011; Schmets et al., 2011).

### 3.3.5 The pseudo variable concept

#### Preamble

The mechanical response of a viscoelastic material to fatigue loading traces a hysteretic loop due to structural changes. These changes include the growth of a traction boundary surface, microcrack nucleation and coalescence into a macrocrack, linear viscoelastic contributions to the recovery of strength including steric hardening and healing, and nonlinear viscoelasticity or relaxation (Lee and Kim, 1998; Si et al., 2002a). To eliminate the time-dependent kinetics, researchers have used theory of non-linear viscoelasticity and the correspondence principle.

#### The correspondence principle

Schapery (1984) proposed the extended elastic-viscoelastic correspondence principle using pseudo variables. This may be applied to linear and nonlinear viscoelastic materials in which microstructural details are suppressed. The correspondence principle states that constitutive equations for certain viscoelastic media are identical to those for the elastic case, but stresses and strains are not necessarily physical quantities in the viscoelastic body. Instead, they are pseudo variables that account for hereditary effects of a material through convolution integrals (Lee and Kim, 1998). Developed on Boltzmann superposition (Christensen, 1982), the stress-pseudo strain relationship to transform a viscoelastic problem to the elastic case is defined for homogenous and isotropic materials by Equations 3-7 to 3-9 (Schapery, 1984):

$$\sigma(t) = \int_0^t E(t-\tau) \frac{d\epsilon(\tau)}{d\tau} d\tau \quad \text{Equation 3-7}$$

$$\epsilon_R = \frac{1}{E_R} \int_0^t E(t-\tau) \frac{d\epsilon(\tau)}{d\tau} d\tau \quad \text{Equation 3-8}$$

$$\epsilon_R = \frac{\sigma(t)}{E_R} \quad \text{Equation 3-9}$$

where  $\sigma(t)$  is the linear viscoelastic stress,  $t$  is the present time,  $\tau$  is the time at which strains were measured,  $E(t - \tau)$  is the relaxation modulus in an undamaged state,  $\epsilon(t)$  is the amplitude of strain,  $\epsilon_R$  is the amplitude of pseudo strain and  $E_R$  is the arbitrary reference modulus.

For undamaged linear viscoelastic systems, the stress-pseudo strain graph for cyclic load is a straight line. However, the hysteretic loops for undamaged bitumen indicate that the material

behaviour does not follow exactly the convolution integral: behaviour is nonlinear viscoelastic (Si et al., 2002a) (refer to Figure 3-8). In the general nonlinear case the loop is unchanged by repeated loading, and Schapery's extended correspondence principle remains valid (Lytton, 2000). However, a nonlinear reference modulus is required to collapse the hysteretic curve to a straight line. Moreover, pseudo strain energy dissipated in this corrected pseudo hysteresis cycle describes damage to a material including heat transfer, plastic deformation and fracture, and healing during fatigue (Si, 2001).

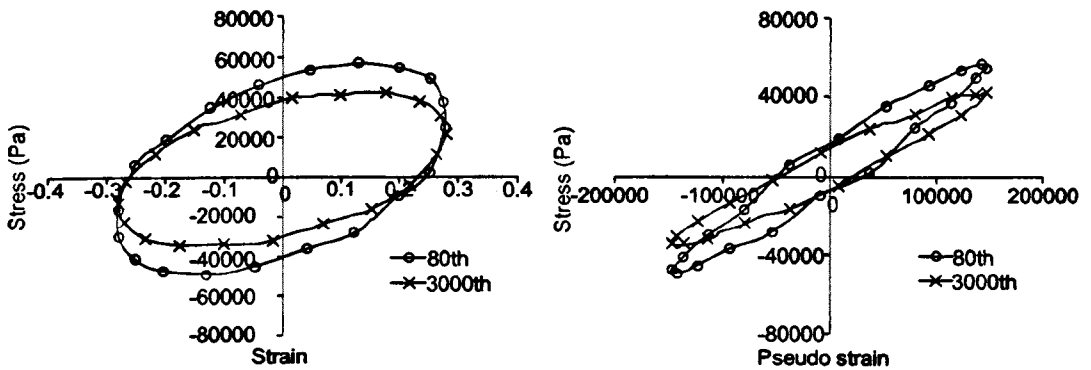


Figure 3-8: Stress-strain and transformed stress-pseudo strain loops for two loading cycles (Kim et al., 2003)

### The viscoelastic continuum damage (VECD) model

To analyse micro-damage due to fatigue, and healing that occurs during rest periods, Lee and Kim (1998) integrated the correspondence principle within work potential theory. Derived from thermodynamic principles of irreversible processes, this theory is used to explain the growing microstructural changes in monolithic and composite elastic media (Schapery, 1990). Lee and Kim (1998) expressed the amount of work required to produce these changes as a function of internal state variables:

$$\text{Pseudo strain energy density: } W_R = W_R(\epsilon_R, S_m) \quad \text{Equation 3-10}$$

where  $W_R$  is the dissipated pseudo strain energy due to structural change,  $\epsilon_R$  is the amplitude of pseudo strain, and  $S_m$  are the internal state variables that account for structural damage.

The structural damage acquired by the material causes the stress-pseudo strain loop to shift from the origin, and its slope to vary with continued loading. This indicates an accumulation of

permanent pseudo strain in the controlled-stress mode, and the reduction of pseudo stiffness.

To describe this response, Lee and Kim (1998) defined a secant pseudo stiffness parameter:

$$S_R = \frac{\sigma_{max}}{\epsilon_{R, max}} \tag{Equation 3-11}$$

where  $\epsilon_{R, max}$  is the peak pseudo strain for each cycle and  $\sigma_{max}$  is the corresponding stress.

Lee and Kim (1998) modified this damage model to explain the microstructural changes due to healing, using two additional internal state variables. The authors proposed  $S_2$  to model the increase in  $S_R$  during a rest period that is ascribed to damage healing, from which the effects of relaxation are separated by use of pseudo strain. The parameter  $S_3$  was included to model the reduction in  $S_R$  on re-loading, due to the re-propagation of damage in healed domains and damage in adjacent material (refer to Figure 3-9(I)). The healing function is then calculated:

For region one:  $H = [S_{RB, i} + C_2(S_{2, i})]C_3(S_{3, i}) - C_1(S_{1, n}) - \sum_{j=1}^{i-1} (S_{RB, j} - S_{RC, j})$  Equation 3-12

For region two:  $H = \sum_{j=1}^i (S_{RB, j} - S_{RC, j})$  Equation 3-13

where  $S_{RB, i}$  is pseudo stiffness before the  $i^{th}$  rest period,  $S_{RC, i}$  is pseudo stiffness without a rest period at the point when  $S_R = S_{RB}$ ,  $C_2(S_{2, i})$  is a function representing healing during the  $i^{th}$  rest period,  $C_3(S_{3, i})$  is a function indicating damage evolution after the  $i^{th}$  rest period, and  $C_1(S_{1, n})$  represents the changes in material stiffness during the initial  $n$  fatigue cycles.

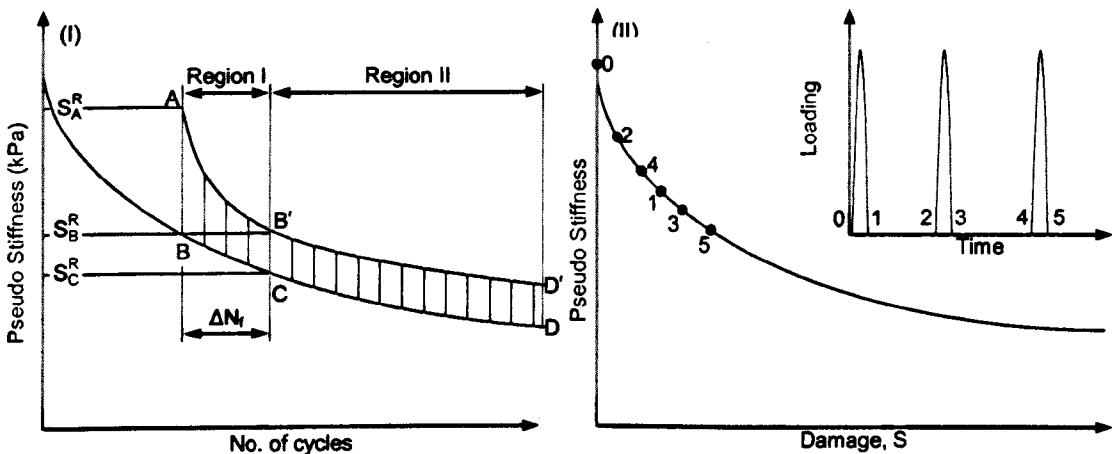


Figure 3-9: (I) Change in pseudo stiffness due to a rest period (Lee and Kim, 1998) and (II) Conceptual diagram for damage healing (Roque et al., 2010)

### The modified VECD model

The continuum damage model reported by Lee and Kim (1998) was modified by Roque et al. (2010) to include ageing and thermal effects. Roque et al. (2010) also simplified the model to use one parameter  $C_1(S_1)$  in order to describe structural changes due to damage and healing. The model is defined in terms of rest period duration, previous load intensity and accumulated damage (Equation 3-14), and is schematised in Figure 3-9(II). In reference to this figure, the model predicts that damage in the first cycle reduces pseudo stiffness along the segment 0-1, which heals during a rest period along the segment 1-2.

$$\frac{\Delta C_{\text{heal}}}{C} = \frac{\kappa}{\left(1 + \left(\frac{\beta}{\xi_{\text{rest}}}\right)^\gamma\right)^{\delta/\gamma}} \quad \text{Equation 3-14}$$

where  $\Delta C_{\text{heal}}$  is the change in pseudo stiffness on healing,  $C$  is the current pseudo stiffness,  $\xi_{\text{rest}}$  is the reduced rest time and the coefficients  $\kappa$ ,  $\beta$ ,  $\gamma$  and  $\delta$  are functions of damage level and energy input (Roque et al., 2010).

### 3.3.6 The thermodynamic model of fracture and healing

Recognising contributions from van der Waals and Lewis acid-base interactions to structural change, Si et al. (2002b) postulated a different fracture-healing model. The authors integrated the correspondence principle with theory of thermodynamic surface energy, as follows.

Lytton et al. (1998) defined a fundamental law for healing (Equation 3-15), which is consistent with fracture theory derived by Schapery (1989) (Equation 3-16):

$$\text{Fundamental law of fracture:} \quad 2\Gamma_f = E_R D_f(t_\alpha) J_v \quad \text{Equation 3-15}$$

$$\text{Fundamental law of healing:} \quad 2\Gamma_h = E_R D_h(t_\alpha) H_v \quad \text{Equation 3-16}$$

where  $\Gamma_f$  is the fracture surface energy density of a crack surface,  $E_R$  is the arbitrary reference modulus,  $D_f(t_\alpha)$  is the tensile creep compliance at time  $t_\alpha$ ,  $J_v$  is the viscoelastic J integral,  $\Gamma_h$  is the healing surface energy density of a crack surface,  $D_h(t_\alpha)$  is compressive creep compliance corresponding to time  $t_\alpha$ , and  $H_v$  is the viscoelastic H integral.

After expanding axioms to healing speed Schapery (1989) defined healing rate as a function of several material properties, including a direct relationship between surface energy and the rate of fracture healing ( $\dot{h}_2$ ) (Equation 3-18). Analogising with rate process theory, Lytton et al. (1998) derived another healing rate function ( $\dot{h}_1$ ) (Equation 3-17). This postulates that surface energy acts instead to impede crack closure and reformation.

$$\text{Short-term healing rate:} \quad \dot{h}_2 = \left[ \frac{2\gamma_m E_R^2 D_{1h} \Gamma_h}{(1-v^2) C_m^{1/m_h} H_v} \right] \beta \quad \text{Equation 3-17}$$

$$\text{Long-term healing rate:} \quad \dot{h}_1 = \left[ \frac{K_h E_R D_{1h} H_v}{2\Gamma_h} \right]^{1/m_h} \beta \quad \text{Equation 3-18}$$

where  $\gamma_m$  and  $C_m$  are functions of the creep compliance gradient  $m_h$ ,  $D_{1h}$  is the compressive creep compliance,  $v$  is Poisson's ratio,  $\beta$  is the size of the crack healing zone and  $K_h$  is a function of  $m_h$  (Si et al., 2002b).

In the course of data analysis, Si et al. (2002b) noted that the healing rates occur concurrently (Equation 3-19). The authors hence ascribed healing to two separate mechanisms, governed in the short-term ( $\dot{h}_1$ ) by non-polar components of surface energy density, but controlled in the long-term ( $\dot{h}_2$ ) by the polar (Lewis acid-base) components.

$$\text{Total healing rate:} \quad \dot{h} = \dot{h}_2 + \frac{\dot{h}_1 - \dot{h}_2}{1 + \frac{\dot{h}_1 - \dot{h}_2}{h_p} (\Delta t)_h} \quad \text{Equation 3-19}$$

Bhasin et al. (2009) pursued an alternative approach, but within the context of surface energy. The authors developed the work by Wool and O'Connor (1981) and by Lytton et al. (1998), to produce a model for healing consistent with the Avrami equation. This model (Equation 3-20) aims to simplify the effects of heterogeneities in bitumen microstructure.

$$R_h(t) = R_0 + p \left( 1 - e^{-qt^r} \right) \quad \text{Equation 3-20}$$

where  $R_h(t)$  is an intrinsic healing function,  $R_0$  is instantaneous healing due to wetting and  $p$ ,  $q$  and  $r$  are material-specific parameters defined using dynamic shear rheometry.

### **3.3.7 Thixotropic effects**

Bitumen viscosity decreases with time when subjected to flow, and increases on cessation of loading (Traxler and Coombs, 1935). This non-Newtonian response (thixotropy) is ascribed to the dissociation and deformation of inter- and intra-molecular bonds: microstructural changes (Tan et al., 2011). Using fatigue tests on asphalt, Verstraeten (1991) established that fatigue at temperatures below 5°C is due to structural damage, and above 15°C is caused mainly by thixotropy. This causes a progressive change from a gel to a sol structure: during rest periods the gel structure is restored (Soltani and Anderson, 2005). While thixotropy is involved in the recovery of mechanical properties (Shan et al., 2010) therefore, this effect is not necessarily related to fracture and the recovery of structural damage would be low. The healing process is instead used to explain the recovery process of structural damage (Qiu, 2012).

### 3.4 HISTORICAL WORK ON DAMAGE HEALING IN ASPHALT

#### 3.4.1 Preamble

Based on controlled displacement crack propagation tests reported in the thesis by Al-Balbissi (1983), Tseng and Lytton (1990) postulated a correlation between crack healing and the shift between laboratory tests and fatigue damage in service. Lytton et al. (1993) decomposed this laboratory-to-field shift factor using mechanics and defined three components: residual stress due to plasticity; dilatancy stress due to the expansion of asphalt under a confining pressure (wheel loads); and damage healing. The healing process is assisted by the pressure induced by dilatancy stresses, which facilitate crack closure (Little et al., 1993). According to literary consensus and extensive research on SHRP pavements, Lytton et al. (1993) emphasised the healing effect in the composite multiplication-form shift factor:

$$\begin{array}{ccccccc} \text{(overall)} & = & \text{(residual stress)} & \times & \text{(resilient dilatancy)} & \times & \text{(healing)} \\ \text{SF} & & \text{SF}_r & & \text{SF}_d & & \text{SF}_h \\ \text{(range: 3 - 100+)} & & \text{(range: 0.3 - 3)} & & \text{(range: 1 - 4)} & & \text{(range: 1 - 10)} \end{array}$$

Research since the 1960s has accordingly aimed to develop a thorough understanding of the theories, mechanisms and observations explaining the healing phenomenon.

#### 3.4.2 A review of fatigue- and fracture-healing tests on asphalt

In absentia of a standard test method for and description of the healing mechanism, recovery of asphalt properties has been studied by various physicochemical and mechanical protocols. Flexural tests on trapezoidal cantilevers or rectangular beams are prevalent (Hsu and Tseng, 1996). Direct axial (Raithby and Sterling, 1970) and indirect diametrical (Grant, 2001) cyclical tension-compression have also been used, but against an unreliable development framework (Bolzan and Huber, 1993; Wagoner et al., 2005). The load-response of sand-asphalt samples has been researched using forced torsional oscillation (Kim et al., 2003) and Izod impact (Kim et al., 1991) methods. These techniques produce a stress state to simulate the complex strain distributions under traffic (Dunhill, 1999), and the mechanism of load-induced cracking.

To simulate accurately the compound-loading condition developed in asphalt under traffic, the continuous sinusoidal or pulsating load applied in fatigue tests is modified to include unloaded (rest) periods. This establishes two procedures:

1. **Storage recuperation:** a sample is fatigued by continuous load repetition to a limiting value of damage, defined by the ratio of current-to-initial mechanical property. Fatigue is then discontinued for a rest period of defined time (Lu et al., 2003), or time required for the damaged property to increase to a predetermined level (Phillips, 1999).
2. **Intermittent loading:** a sample is fatigued by regularly-discontinued load repetitions. The sample is fatigued for a pre-defined number of cycles and then interrupted by the rest period. This process is repeated to define effects on fatigue life (Kim et al., 2003).

Whilst the simulative accuracy of the intermittent method is perhaps superior: the rest periods largely describe headway and temporal or spatial traffic variation (Groenendijk, 1998), the test viability is reduced by the distribution of damage (Bodin et al., 2004). To study crack healing a rest period is inserted between two successive tests on fractured surfaces Bazin and Saunier, 1967; Raithby and Sterling, 1972; Kim et al., 1993).

### **3.4.3 A review of techniques used to quantify healing**

#### **Preamble**

The technique used most simply to define healing during a rest period is a ratio of recovered-to-damaged mechanical property. Bazin and Saunier (1967) for example, defined one healing parameter in terms of tensile strength and a second by tensile strain at rupture. However, the competency of this approach is challenged in fatigue tests (Kim et al., 2003) that elucidate the lag-time dependence of healing conceptualised by Phillips (1999): the healing mechanisms of modulus and rate of damage are not synergistic. Moreover, approaches based on fatigue life are sensitive to ambiguous definitions of fatigue life (Daniel and Kim, 2001), the mode of load control (Westera, 1993), and asphalt-specific trends of modulus loss (Lundstrom et al., 2004). Recently therefore, research has focussed on developing a criterion that encompasses every

fatigue variable, the most promising of which are reviewed below.

### The rate of re-damage

Breyse et al. (2003) studied asphalt healing using two-point (cantilever) flexure. The authors introduced a hyperbolic function (Equation 4-24) to describe stiffness recovery during any rest period. At the beginning of healing, the superposition of temperature (cooling) and mechanical effects originated a fatigue-independent recovery rate. However, the maximal recovery slowly decreased with the repetition of load cycles, due to a reduced healing capacity and increased irrecoverable damage. To quantify the effects of residual damage on the kinetics of re-fatigue, the re-damage rate  $V_{x\%}$  was proffered (Equation 4-25). This was shown to vary exponentially with the preceding level of damage developed in the sample.

$$\Delta E = t / [(1/V_0) + (t/\Delta E_{ULT})] \quad \text{Equation 3-21}$$

where  $\Delta E$  is the stiffness recovery,  $t$  is the recovery time,  $V_0$  is the slope at the origin of the  $t$ - $\Delta E$  diagram and  $E_{ULT}$  is the asymptotic value of stiffness.

$$(V_{x\%})_n = [(E_0)_n - E_{x\%}] / [t_{x\%} - t_0] \quad \text{Equation 3-22}$$

where  $(E_0)_n$  is the normalised stiffness on initiation of the  $n^{\text{th}}$  sequence and  $E_{x\%}$  is the stiffness corresponding to an  $x\%$  loss in time  $[t_{x\%} - t_0]$ .

### The ratio of dissipated energy change (RDEC)

Based on the pioneering work of van Dijk (1969), the concept of dissipated energy has found distinction to define the stress-convoluted load-response of asphalt. In adopting this approach to describe healing, Carpenter and Shen (2005) defined the RDEC parameter (Equation 3-23) to eliminate energy dissipated by passive effects: reversible surface energy, sound emission, viscoelastic damping and heating (Rowe, 1996). The authors hence resolved the incremental amount of energy dissipated by damage: plastic deformation of the material at the crack tip.

$$\text{RDEC}_b = \frac{|DE_b - DE_a|}{DE_a(b-a)} \quad \text{Equation 3-23}$$

where  $DE_n$  is the energy dissipated during the  $n^{\text{th}}$  loading cycle (for  $b > a$ ).

The graph of RDEC against load cycles is divisible into three phases (refer to Figure 3-10), of which the plateau region is most interesting and representative of pavement behaviour during service (Shen et al., 2009). In this central domain, the energy dissipated by successive loads tends to a steady-state: a low RDEC value here indicates low incremental energy for damage. The fatigue resistance in this regime is defined by the plateau value: the RDEC parameter at the 50% loss of initial modulus (Carpenter and Shen, 2005). These data are usually produced using four-point bending tests with an intermittent haversine load protocol (Shen et al., 2009).

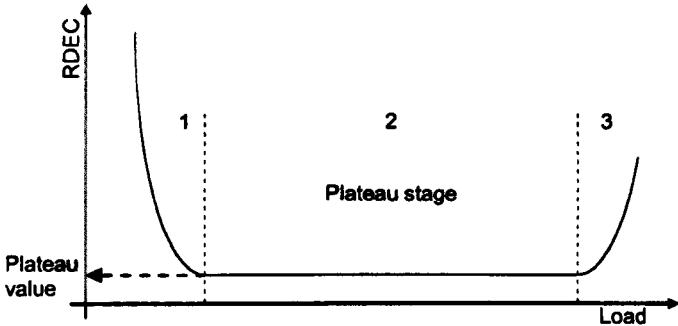


Figure 3-10: Schematic RDEC plot showing the three zones of behaviour, Shen et al. (2009)

**The ratio of dissipated pseudo strain energy**

By the correspondence principle for linear viscoelastic media, Kim and Little (1989) postulated that at high stresses or strains changes in the stress-pseudo strain loop are due to removable nonlinear effects (Si et al., 2002), dissipative behaviours (Bodin et al., 2004) and healing. The authors validated this using uniaxial tension tests with a discontinuous triangular load protocol (rest periods of 30 or 600 seconds), and constant-strain-rate. Recognising the significance of that finding, Little et al. (1999) established a healing index in terms of dissipated pseudo strain energy (Equation 3-24): a parameter similar to the RDEC (Little and Bhasin, 2007). However, the authors reported that this index essentially indicates stiffness recovery. For ageing media, this could be tainted by stiffening or softening phenomena, including molecular structuring or steric hardening, and hysteresis heating or damping.

$$HI = \frac{\varphi_h - \varphi_d}{\varphi_d} \tag{Equation 3-24}$$

where  $\varphi$  is the pseudo strain energy dissipated directly before (d) or after (h) a rest period.

### Dissipated creep strain energy (DCSE)

Kim and Roque (2006) derived a less-rigorous solution to quantify healing in asphalt, using an indirect tensile fatigue test with intermittent load and periodic resilient modulus tests. The rate of healing is quantified in terms of DCSE recovered per unit time, for which this parameter is defined as the fracture energy (FE) minus the elastic energy (EE). The elastic energy is due to the resilient properties of the material.

### 3.4.4 Developments in research regarding asphalt healing

#### Fracture-healing tests

Bazin and Saunier (1967) introduced rest periods to study healing in densely-graded asphalt, which were fractured by uniaxial tension in displacement control. The authors reported on the effects of healing duration (1 to 300 days) and temperature (10°C, 18°C and 25°C). Moreover, the beams were stored vertically, whereby the upper section induced a compressive pressure of 1.48kPa at the ruptured interface, and then re-fractured to describe the recovery of fracture strength. The research reported a logarithmic recovery with time and a shift to shorter healing times at higher temperature. Applying time-temperature superposition to these data produces a recovery master curve that is devoid of the cohesive asymptote, but elucidates the thermal-sensitivity of healing near to the reference temperature (15°C) (refer to Figure 3-11).

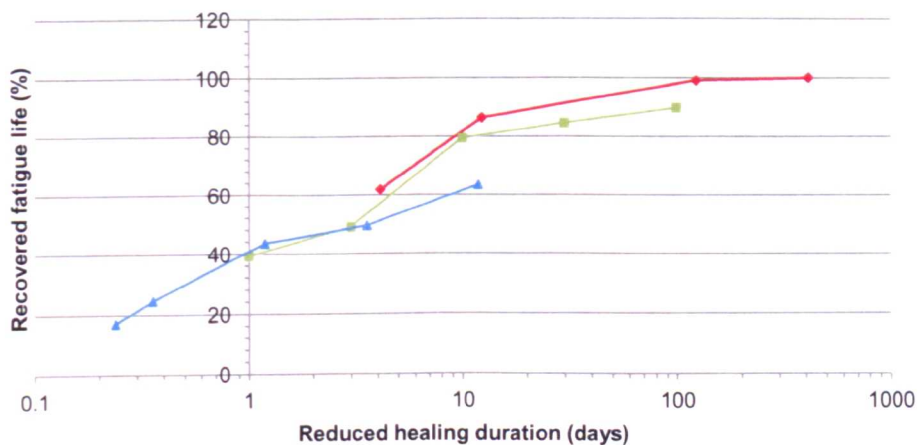


Figure 3-11: Recovery master curve for asphalt mixtures at a reference temperature of 15°C, produced by the author of this thesis from data reported by Bazin and Saunier (1967)

Kim et al. (1991) used scanning electron microscopy to analyse the cracked surfaces of sand-asphalt. The samples were fractured using an Izod impact test and then healed at 20°C for 5, 10 or 20 minutes before re-fracture. The authors philosophised that when a fracture surface is identical to the control (no healing), then the rest period has allowed full healing. The research reported the control fracture surfaces to be composed of two distinct patterns: cleavage-type fracture (sharp lips) and ductile fracture. Following a healing period of 5 minutes the fractured surfaces showed a more ductile pattern with dull lips than the control: the brittle patterns were restored with increased healing time. The authors also noted that asphalt with a high viscosity bitumen required longer healing times, and thus postulated that flow and intermolecular bond energy across the interface contribute decisively to the healing mechanism.

Uchida et al. (2002) applied a composite flexural test to study healing. Asphalt slabs for wheel tracking tests were bent using basally-located steel, and then restored to their initial geometry to produce crack closure. To simulate the healing conditions likely-experienced in service the slabs were stored outside for up to 12 months, and exposed to a passing wheel load at 20°C, 40°C or 60°C to allow for the kneading or compactive action of traffic. The flexural strength of beams cut from the slab was measured under a constant loading rate. Although the effects of exposure are ambiguous, the study noted that healing increased with trafficking temperature.

#### **Intermittent-type fatigue-healing tests**

Raithby and Sterling (1970) conducted uniaxial cyclic tension-compression tests on hot rolled asphalt, using an intermittent loading protocol at loading times of 0.04 to 0.4 seconds and rest times of 0.08 to 4.9 seconds. Defining healing effects by the fatigue life ratio of discontinuous-to-continuous loading, the work reported this parameter increased to an asymptotic value at a rest period-to-loading time ratio of 2.5:1. Raithby and Sterling (1972) noted that the maximum benefit of healing could be achieved at a rest-to-load cycle period of 15:1. The study reported an incongruous variation of healing with temperature: the limiting fatigue life ration was similar for tests at 10°C and 25°C, but markedly-reduced at 40°C. This is ascribed to the convolution of sample variability, applied stress and viscoelasticity, and the mechanism of damage: this is known to vary with temperature, which could affect the healing kinetics (refer to Section 3.3).

van Dijk and Visser (1977) tested rolled asphalt at 20°C using three-point bending beam tests in a constant strain mode of loading, for loading ratios varying from 1 to 25. The investigations showed an increasing fatigue life with increased rest periods and, by extrapolation of data, the authors postulated maximum beneficial effects at a loading ratio of about 50.

Bonnaure et al. (1982) studied fatigue-healing in dense asphalt by three-point bending tests in controlled displacement and controlled force sinusoidal load profiles at 5°C, 20°C and 25°C. It was reported that the beneficial effect of rest periods is significant at load-to-rest period ratios of 10:1 to 25:1, at higher temperatures and for lower mixture stiffness or softer binder (refer to Table 3-1). The authors also noted that this effect is more distinct in force-controlled loading, which is known to define a crack-initiation boundary condition (Tangella et al., 1990). This has inspired the conclusion that healing phenomena contribute principally in this phase of fracture (Lytton et al., 1993). The stress/strain amplitudes were noted to not affect the fatigue life ratio.

Table 3-1: Mixture stiffness effect on improvement in fatigue life for a rest-to-load cycle period ratio of 25 (Bonnaure et al., 1982)

<b>Mixture stiffness (GPa) Fatigue life ratio (<math>N_{rest}/N_{continuous}</math>)</b>	
4	10
6	8
10	5
20	2

Based on the conclusions of Benson (1988), Kim et al. (1990) studied asphalt healing using a fatigue test on notched beams. By Fourier transform infrared spectroscopy, the study defined a phenomenological relationship between healing and the molecular profile of the binder. The authors quantified healing by the ratio of dissipated pseudo strain energy, and reported direct-relation of this index to the amount of long-chain aliphatics in the saturates fraction and long-chain aliphatic side-chains to the polar aromatic and asphaltene molecules. To describe these aliphatic systems, the authors proposed the methylene to methyl hydrogen to carbon (MMHC) ratio, which defines the degree of branching in the alkane material. The diffusivity and rate of

healing was shown to decrease with enhanced branching (Figure 3-12). This was validated by new molecular simulations (Bhasin et al., 2011). The significance of aliphatic chain length and branching is that it is a commonality between polymer and asphalt healing (Little et al., 1993).

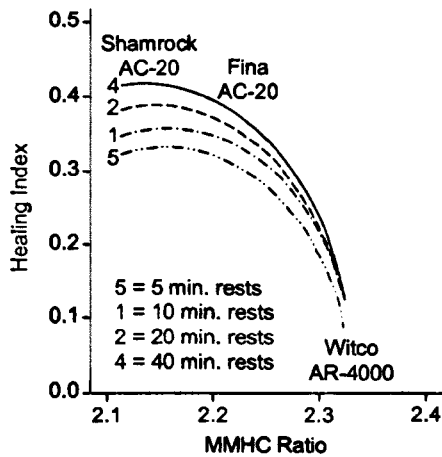


Figure 3-12: Variation of healing index with MMHC ratio for bitumens (Kim et al., 1990)

Hsu and Tseng (1996) reported intermittent three-point bending tests on asphalt under stress-controlled loading at 15°C, 25°C and 40°C. The mixtures with higher loading ratios exhibited a longer fatigue life. The authors ascribed this to healing-induced stiffening, which was verified by the converse softening-effect (shorter fatigue life) at high temperature and binder content.

Little et al. (1999) used controlled-strain tensile tests and the dissipated pseudo strain energy ratio to quantify asphalt healing. The cylindrical samples were prepared with various bitumens in order to evaluate the effects of binder surface energy at 25°C. Based on statistical analysis the authors defined an inverse relationship between short-term healing and the van der Waals component of surface energy. Local secondary forces are viewed (Williams et al., 2001) as an immediate effect therefore, which requires energy to overcome the intermolecular interactions on either face of the closing fracture: an obstacle to the reformation of cohesion. The research also noted a direct relation between the acid-base component and long-term healing. Williams et al. (2001) indicated this to be the driving force to cohesive recovery. Moreover, by Wilhelmy Plate experiments, Williams et al. (2001) concluded logically that aromatic fractions contribute to the acid-base component by pi-pi and multidirectional bonds. The research curiously linked van der Waals interactions to amphoteric structures: molecules with an acidic and basic unit, which allows the molecule to continue interactive or chain-building processes.

Breyse et al. (2003) studied healing in an asphalt mixture at 20°C using two-point bending in controlled strain loading, with rest periods inserted at every 10% stiffness reduction compared to the initial value. The hyperbolic function of rest period-stiffness recovery curves was related to accumulated damage, with recovery asymptotes shifted to low values by prolonged fatigue.

Carpenter et al. (2003) conducted four-point bending tests at 20°C, using haversine loading to induce flexural deformation of 70 to 1000 microstrain. At low strain levels, the RDEC indicated notably-reduced damage per load cycle. The research ascribed this to the near-superposition of energy dissipated by damage and recovered by continuous healing phenomena. Shen and Carpenter (2005) also applied the dissipated energy concept to intermittently-loaded samples, which were fatigued at 500 microstrain with rest times of 0 to 9 seconds. The authors reported more-evident healing in discontinuous fatigue and a decline of plateau value with time.

Kim et al. (2003) studied healing kinetics using dynamic mechanical analysis under controlled strain loading, conducted at 25°C and 2.8% strain. The samples were of fine aggregate mixed with two binders of different properties. Ten two-minute rest periods were included during the tests at equal damage levels for each mixture. This produced an extension in fatigue life that was lower for stiffer binder, which is consistent with low-limited healing kinetics.

Castro and Sánchez (2006) studied the healing properties of dense mix asphalt at 20°C using three-point flexural fatigue under strain control, in continuous and discontinuous loading: rest periods of 1 second separated sinusoidal 0.1 second load cycles. For heavily-loaded samples (amplitude: 400 microstrain), the beneficial effect of intermittent loads was less than in lightly-loaded (amplitude: 200 microstrain) beams. This result is in agreement with Westera (1993).

Awanti et al. (2007) used indirect tensile fatigue tests at 25°C to study fatigue-healing kinetics in asphalt: normal and modified with a styrene-butadiene-styrene (SBS) block copolymer. The stress-controlled loading protocol included rest-to-load ratios of 0 to 8:1. The study noted that polymer modification produced an increase in the fatigue life, but reduced the effect of healing as defined by the fatigue life ratio (refer to Table 3-2). Similar studies by Little et al. (1999), on

asphalt modified with SBS and low density polyethylene (LDPE), prompted the theory that this response is caused by polymer-adsorption of compatible fractions from the binder. To explain, polymer networks in the binder are swollen by the adsorption of compatible components. This establishes a binder that has a higher asphaltene content and reduced capacity for healing by flow. This notwithstanding, Awanti et al. (2007) noted that the effect of discontinuous loading reduced with initial tensile strain, and significantly for the unmodified asphalt. This is related to a change in plastic deformation rates and asphalt stiffness.

Table 3-2: Life ratio values on the basis of regression (Awanti et al., 2007)

Asphalt mixture properties			Fatigue life ratio ( $N_{rest}/N_{cont.}$ ) at load ratio		
Binder type	Stiffness (MPa)	Strain (microstrain)	4	6	8
Polymer-modified	1.32	100	1.87	2.32	2.46
		200	1.74	1.99	2.20
Neat	0.83	100	7.00	8.40	12.13
		200	3.04	3.42	3.83

**Storage recuperation fatigue-healing tests**

Bazin and Saunier (1967) studied healing in dense asphalt at 10°C using two-point bending in stress-controlled loading. Fatigue tests were discontinued immediately before rupture: defined by the amplitude of flexure using an electronic switch. The samples were then stored either in a horizontal or vertical orientation at 10°C for up to 100 days. The study reported that healing post-fatigue is expeditious compared to post-fracture strength recovery and moreover, widely-scattered data for samples stored horizontally; thus, compressive stress promotes healing.

Daniel and Kim (2001) conducted three-point bending tests and studied the healing behaviour of asphalts fatigued thus at 20°C, using an impact resonance method to evaluate the dynamic modulus of elasticity. The damaged samples were healed for four hours at two temperatures, namely 20°C and 60°C, after continuous flexure to low, moderate and high modulus loss. The fatigue life extension due to discontinuous loading was most evident previous to the first point of inflection and increased with thermal softening of the binder, consistent with a flow process.

Grant (2001) and Kim and Roque (2006) evaluated fatigue-healing in asphalt using repeated indirect tensile fatigue and periodic resilient modulus tests at 0°C to 20°C, and the normalised DCSE concept. The authors reported linear accumulation of DCSE on loading and logarithmic recovery during unloading, which indicates healing and nonlinearity. Presenting these data in terms of temperature shows the thermally-nonlinear variation of asphalt healing, in which the asymptotes at low temperature are defined by binder content (refer to Figure 3-13). Moreover, the low mobility of bitumen molecules at these temperatures could involve adhesion, for which small variations are ascribed to changes in surface energy that occur with temperature. These are governed by the Eötvös rule (Devaraj, 1974).

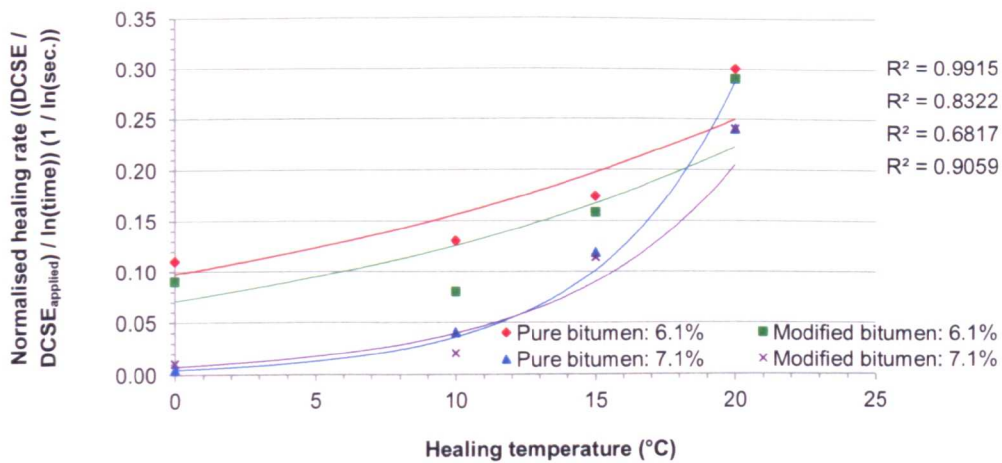


Figure 3-13: Variation of recovery of DCSE with healing temperature, produced by the author of this thesis using data reported by Kim and Roque (2006)

### 3.5 HISTORICAL WORK ON DAMAGE HEALING IN BITUMEN

#### 3.5.1 Preamble

The healing phenomenon of asphalt is dependent on the binder. Knowledge of the restorative properties of pure bitumen is therefore fundamental to understand its contribution during rest periods. Evidenced in the literature review herein, researches on healing behaviour in binders often use dynamic shear rheometry by intermittent or storage recuperation methods. Perhaps the first such study was conducted by Pell (1962) using a constant strain torsional fatigue test. That author demonstrated that a storage recuperation period inserted at half the life to failure enabled an increase in mean life of 55% at  $-4^{\circ}\text{C}$ , and 300% to 655% at ambient temperature.

#### 3.5.2 A review of fracture-healing tests on bitumen

To simulate rupture and healing of binder films in the same configuration as that between two aggregates, de la Roche et al. (2003) proposed a repeated local fracture test. The sample is held between two hemi-spherical protuberances with radii similar to aggregate particles of an intermediate size (Muench et al., 2003), and loaded in tension under displacement-controlled mode (refer to Figure 3-14). After loading, the system is restored to its initial conformation and a rest period is introduced, during which a compressive load of 50N is applied to the sample. The healing response is evaluated by pre- and post-rest period load-displacement graphs.

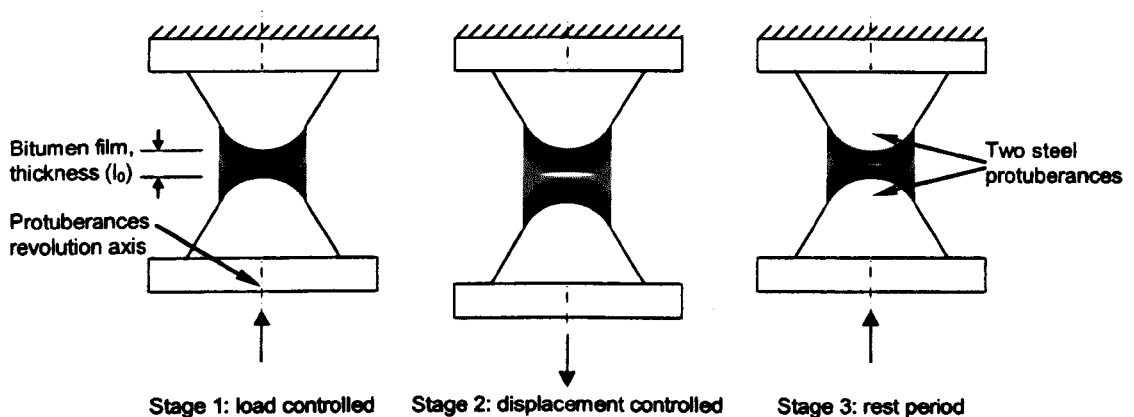


Figure 3-14: Schematic of repeated local failure test, after from de la Roche et al. (2003)

Bommavaram et al. (2009) developed the so-called intrinsic two-piece healing test to simulate directly the interfacial wetting kinetics. Schematised in Figure 3-15, bitumen discs adhered to

the spindle and base plate of a dynamic shear rheometer (DSR) are pressed together in order to mimic crack closure. To obtain complete wetting a normal compressive load is then applied to reduce film thickness. To assess strengthening effects of healing, the evolution of complex modulus is measured by continuous cyclic loading at a strain level of 0.001% and normalised to that from classical tests, to remove stiffening ascribed to steric or geometrical changes. It is questionable however, if this method truly describes healing. Strictly, this scenario is welding, for which uniform molecular weight may modify interfacial behaviour (refer to Section 3.3.2).

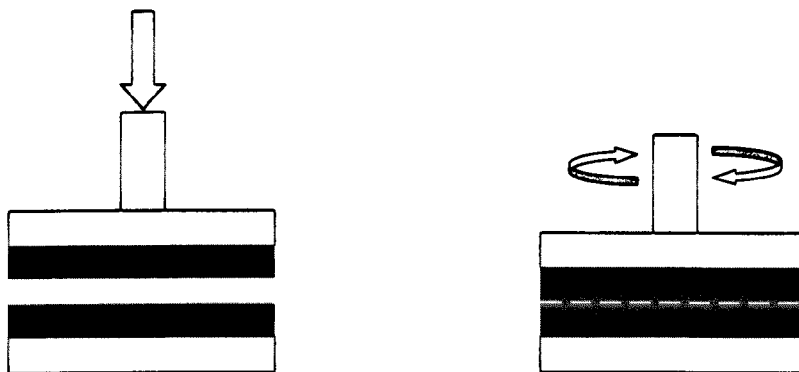


Figure 3-15: Schematic of the intrinsic two-piece healing test (Bommavaram et al., 2009)

### 3.5.3 Developments in research affecting bitumen healing

#### Fracture-healing tests

de la Roche et al. (2003) studied healing from a mechanistic standpoint in a 50/70 penetration grade binder, using the repeated local fracture test and acoustic emissions. The 220 $\mu\text{m}$ -thick films were strained at the rate of 12.5 $\mu\text{m}$  per second for four seconds, after which rest periods of two minutes or four hours preceded secondary loading. For films tested at 0°C, the authors proposed that load-time curves after the long rest period showed complete healing. The initial slope of the curves was coincidental, while the singular load discontinuities indicated an equal number of crack events. Partial healing was shown to occur during the two minute rest period: the recovered stiffness reduced and the rate of fracture initiation and propagation increased. Analogous to the influence of shorter rest periods, lower temperatures were shown to reduce healing. This is consistent with a flow-limited phenomenon (refer to Section 3.2).

Maillard et al. (2004) reported healing in 320 $\mu\text{m}$ -thick films of 50/70 penetration grade binder, which were studied using the local fracture test at a displacement rate of 11.0 $\mu\text{m}$  per second

for ten seconds. The work noted a thermal limit of  $-10^{\circ}\text{C}$  below which damage is irrecoverable and besides, the augmentation of fracture events and highly-reduced stiffness after both rest period durations at  $0^{\circ}\text{C}$  (refer to Figure 3-16). To explain this disparity, the convolution of film thickness, strain rate and magnitude is proffered. Firstly, the film aspect ratio varies inversely with thickness. Assuming the effective diameter to embody the main distribution of strain then, by evaluation with theory published by Harvey and Cebon (2003), the failure mechanisms of the film can be defined. The failure mechanism of the film studied by de la Roche et al. (2003) is voiding and by Maillard et al. (2004) is intermediate between flow and voiding. The different nanoscale damage activities may in-part explain the distinct healing responses. Moreover, in the ductile-brittle failure transition regime, an increased strain rate lowers fracture energy and changes stress distributions (Dieter, 2001; Harvey and Cebon, 2003). This could cause subtle deviations in experimental data. Secondly, it is known that the healing effect decreases with both degree and dispersion of induced damage (Breyse et al., 2003). This is a function of the magnitude of applied strain, which differs between the two published studies.

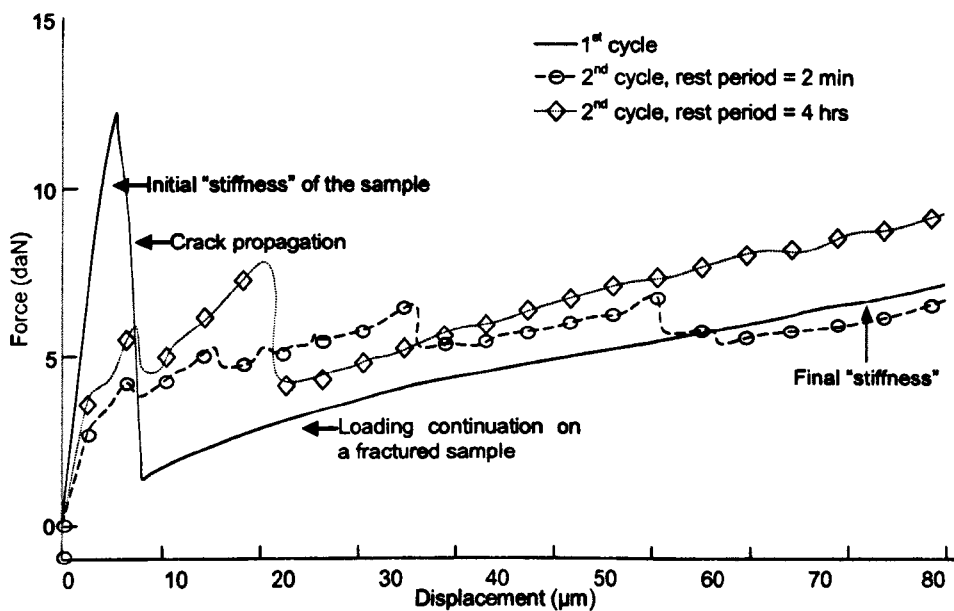


Figure 3-16: Evolution of force versus displacement during stage two (displacement controlled) tests on 50/70 penetration grade bitumen at  $0^{\circ}\text{C}$  (Maillard et al., 2004)

Acoustic emission was adopted by de la Roche et al. (2003) and Maillard et al. (2004) in non-destructive evaluation of sample damage. The temporal progression in acoustic activity allows the pursuit of the cracked condition, to wit, fracture initiation manifests by an intense transient

emission which changes to prolonged activity during propagation. Using acoustic sensors, de la Roche et al. (2003) found that the number of dynamic processes associated with structural degradation increased after a rest period of 35 seconds when compared to the original tensile loading. In the absence of the Kaiser effect, by which materials emit sound waves only under unprecedented stress (Seo and Kim, 2008), the authors argued that post-healing events have lower energy demands and indicate healing in the form of bridges. These appear between the lips of cracks. Conceptually, this is consistent with the kinetics of bridging in polymers (refer to Section 3.3.2). Maillard et al. (2004) defined healing by the transmitted amplitude of ultrasonic signals and correlated stiffness after healing to the dimension of residual macrocracks.

Bommavaram et al. (2009) used the intrinsic two-part healing test to study five SHRP binders at 25°C under controlled strain loading, at a strain of 0.001% and a normal compressive force of 0.4N. The results indicated that the instantaneous healing values rank identically to surface energy (refer to Figure 3-17). This is consistent with initial healing by the thermodynamic work of cohesion (refer to Andrews and King (1978) and Jud et al. (1981)) and the multi-step model postulated for this phenomenon (refer to Section 3.3). It is notable though, that the asymptotic healing limit relates neither to surface energy nor microstructure imaged by Pauli et al. (2011).

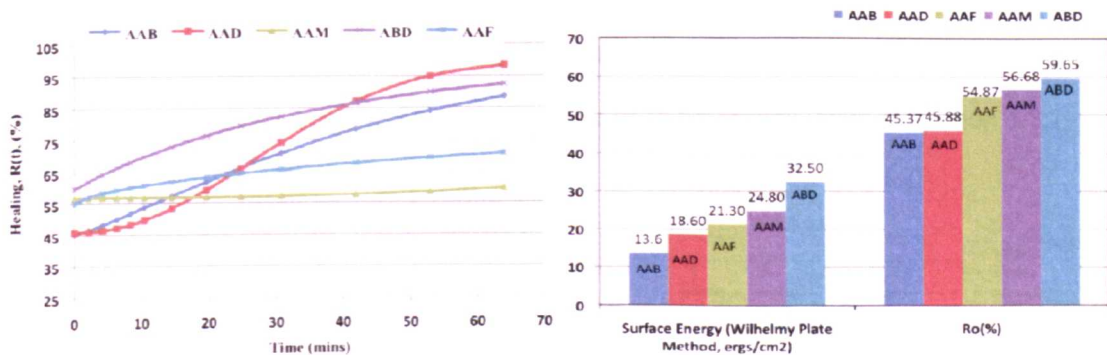


Figure 3-17: Variation of healing with time and surface energy (Bommavaram et al., 2009)

### Intermittent-type fatigue-healing tests

Lu et al. (2003) investigated healing in three binders at 15°C using the DSR in constant stress loading, to produce strain of 1%. Using different combinations of rest-to-load cycle period with an oscillatory loading phase of 20 seconds at 25Hz, the authors showed that the contribution

of rest periods to fatigue life extension depends highly on bitumen type (refer to Table 3-3).

Table 3-3: Life ratio values on the basis of intermittent fatigue tests (Lu et al., 2003)

Bitumen properties				Life ratio ( $N_{rest}/N_{cont.}$ ) at load ratios of				
Stiffness (MPa)	Pen. 25°C (0.1mm)	Softening point (°C)	Stress (kPa)	0.5	1.0	5.0	10.0	20.0
16	86	47.4	184	1.91	> 2.12	> 2.12	-	-
18	86	46.4	210	-	1.50	2.50	-	-
21	87	45.4	237	-	1.07	1.12	1.62	3.12

Bodin et al. (2004) studied healing in a 10/20 penetration grade binder at 15°C using dynamic shear rheometry in strain-controlled loading. The test procedure applied fatigue strain at 1.3% and 25Hz for 500 seconds, succeeded by recovery at 0.05% strain for 500 seconds and three fatigue-rest period cycles thereafter. The authors reported that healing followed a hyperbolic-type time-dependence and ascribed the first section of recovery to temperature effects (rapid cooling) rather than damage recovery. This instead occurs on thermal equilibration. Moreover, it was observed that instantaneous healing, as characterised by recovered complex modulus, decreased with previous loading cycles. This trend may be attributed to an increasingly-partial wetting of crack surfaces, with which an apparent free energy drop less than cohesion occurs (Andrews and King, 1978) and so produces lower instantaneous strength gain (refer to Figure 3-18). Surface energy could also be modified by fracture processes (refer to Section 4.3.2).

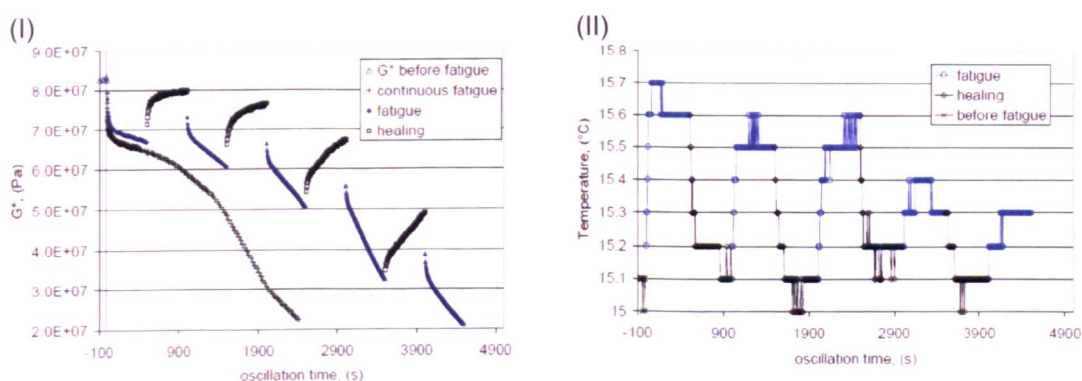


Figure 3-18: Variation of (I) complex modulus and (II) sample temperature during fatigue and healing cycles of the intermittent loading test (Bodin et al., 2004)

Shen et al. (2010) conducted fatigue and healing tests on pure and polymer modified bitumen at 15°C and 25°C, using a DSR in constant stress loading. The intermittent loading sequence involved a short rest period, varying from 0 to 6 seconds, that is inserted after 10 load pulses at a frequency of 10Hz and a stress level of 60 - 230kPa. Under controlled-stress loading, the evolution of dissipated energy is similar to that found in fatigue tests on hot mix asphalt (refer to Figure 3-10), although without the first energy stabilisation stage. The authors hence used the RDEC concept to evaluate binder healing. With increased rest period duration the energy parameter (plateau value) decreased on a straight line in log-log space, conforming to fatigue life extension by the recovery of fracture energy. Moreover, the slope of this unique curve was steepened by bitumen modification with SBS indicating higher healing potential. This could be ascribed to the higher segment mobility of the dispersion medium (refer to Section 3.3.2). Yet, the effect of temperature on pure binder was contradictory to the literature: the healing rate at 15°C was higher than at 25°C (refer to Table 3-4). This phenomenon was explained by strain effects, whereby large deformations at high strain increase the separation between molecules and reduce restoring intermolecular forces. This is validated by the polymer modified binder.

Table 3-4: Healing rates for different testing conditions (Shen et al., 2010)

Bitumen properties		Loading conditions			
Type	Initial G* (MPa)	Temperature (°C)	Stress (kPa)	Initial strain (%)	Healing rate
Neat	1.95	25	60	3.27	1.09
	2.14	25	70	3.45	0.97
	10.85	15	180	1.74	1.49
SBS-modified	1.95	25	60	3.30	1.60
	2.00	25	70	3.75	1.49
	6.75	15	230	3.50	0.50

van den Bergh (2011) studied healing in mortar at 15°C using torque-controlled discontinuous tests on cylindrical virgin and lab-aged samples. The author defined a coefficient to evaluate healing: the number of load cycles to failure in intermittent tests to the number of load cycles to failure in continuous loading tests, where failure occurs at the peak dissipated energy ratio.

The intermittent test consisted of a load period of 3 seconds and 10Hz oscillation for damage, followed by a 9 second rest period for recovery. The author concluded that samples of mortar show healing with the introduction of rest periods and moreover, that higher healing potential is produced by long molecules with few branches. The research confirmed this effect for virgin and specific lab-aged materials.

### Storage recuperation fatigue-healing tests

Bahia et al. (1999) used extensive dynamic shear rheometry to study parametrically the non-linear behaviour of modified bitumens using controlled strain tests at 20°C. The samples were firstly loaded for 5000 cycles at 1.6Hz and 20% strain before the introduction of a rest period, after which fatigue was conducted until failure. The authors reported fatigue life extension due to unloading (0.5 to 12 hours) and significant healing (stiffness recovery) for long rest periods. Moreover, modification with plastomer and elastomer and by oxidation was shown to improve healing, which was defined by larger recovery of stiffness and longer extension of fatigue life.

Phillips (1999) investigated the effect of synthetic wax and SBS modification on binder healing at 10°C, using four-stage storage recuperation tests at constant strain in the DSR. The author defined fatigue and healing by complex modulus loss and recovery. Phillips (1999) concluded that applied strain and induced damage strongly-influence healing phenomena, which remain unaffected by wax gelation and are accelerated by SBS modification (refer to Figure 3-19).

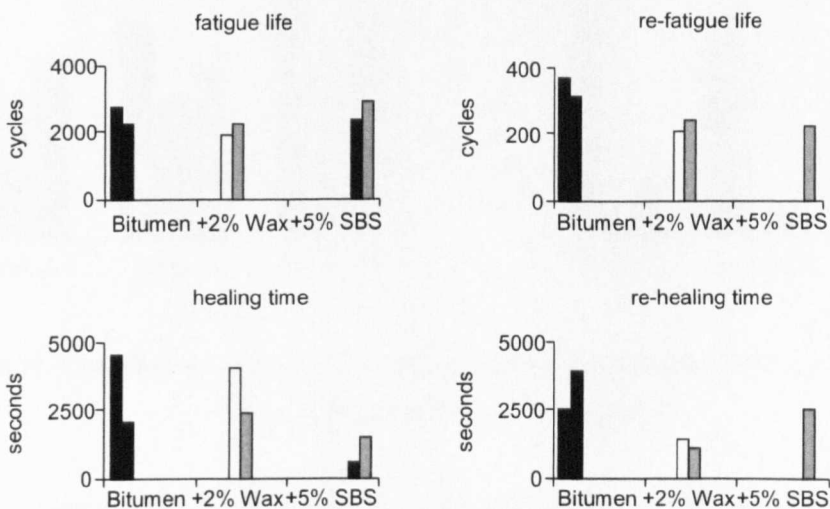


Figure 3-19: Fatigue life and healing time for three binders *in duplo* (Phillips, 1999)

Smith and Hesp (2000b) reported on controlled strain storage recuperation tests conducted in the DSR, to investigate the effect of coarse and fine fillers on healing at 10°C. Specifically, the authors used a two-stage protocol. In the first stage, the mastic was exposed to 0.3% strain in order to introduce fatigue; after stiffness reduced to 50% of the initial value, the second stage (healing) evaluated the change in stiffness at a strain of 0.003% and 40Hz for two hours. The healing effect, defined in terms of the percentage stiffness recovered, was less for the mastics prepared with fine filler than with coarse filler, due to the higher number of fractures pinned by inclusions. This produces a larger number of fracture paths with exposed filler particles. The recovery of mechanical properties is thus retarded by the high proportion of adhesive healing required, which occurs less expeditiously than cohesive healing (Smith and Hesp, 2000a). It is notable that Little et al. (1999) also concluded that filler systems interrupt bitumen healing.

Lu et al. (2003) also studied healing under storage recuperation at 15°C, using dynamic shear rheometry at 0.016% strain and 25Hz oscillation. The three bitumens (refer to Table 3-3) were fatigued to 50% of initial complex modulus, unloaded for four hours, re-fatigued to the pre-rest modulus level, and subsequently unloaded for 17 hours before re-fatigue. Most interestingly, the results confirmed work by Phillips (1999) who indicated that complex modulus recovery is not related directly to fatigue life extension (refer to Figure 3-20).

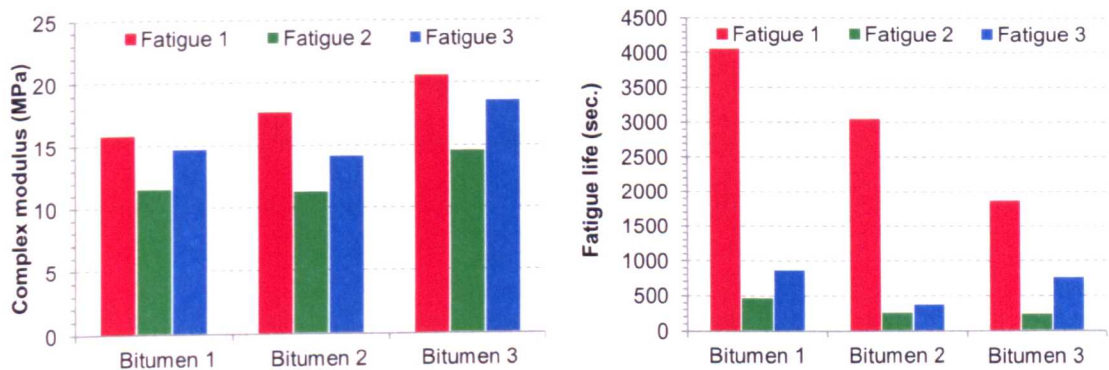


Figure 3-20: The effect of rest periods in storage recuperation tests on bitumen complex modulus and fatigue life (Lu et al., 2003)

Planche et al. (2004) investigated the effect of damage on healing in Superpave 82PG binder, using a DSR in strain-controlled loading. The loss of mechanical properties was introduced by

repeated shear strains of 2%, 5% and 15%, and discontinued for 40 or 360 minutes previous or subsequent to failure. Failure was defined when the cyclic variation of dissipated energy is nonlinear. The study concluded that recovery is inefficient at short rest times and abated after failure. This response could be explained by a convolution of stress concentrations at residual damage, where crack mouth opening exceeds closure by flow, and the incapacity of ruptured molecules to interact and resist additional fatigue (refer to Section 3.3.2).

Santagata et al. (2009) studied damage healing in 70/100 penetration grade bitumen *apropos* of chemical composition and structure, by the combined use of thin-layer chromatography and rheological test protocols using the DSR. The fatigue and healing tests were conducted at iso-stiffness temperatures: 5°C to 9°C with a target value of 25MPa, in the controlled-strain mode at a frequency of 1.59Hz. Moreover, a rest period of two hours separated two loading phases, which were conducted at strain amplitude of 1%. Strain oscillation at 0.01% was used during healing to evaluate stiffness recovery. The authors related bitumen fatigue life to the colloidal instability index, and the healing index (relative change in stiffness due to a rest period) to the saturate-to-aromatic ratio. The authors concluded that this correlation indicates that bitumens constituting a high proportion of low molecular weight fractions have a high healing potential.

### 3.6 CHAPTER SUMMARY

Theories to explain bitumen healing pertain to two types: physicochemical and mechanical. In the first approach the healing phenomenon is described by physical-chemical effects, and the second by nonlinear mechanics. The multi-step model defines two fundamental stages: crack closure under flow and intermolecular attractive forces, which restore stiffness; and interfacial diffusion, during which strength recovers. The viscoelastic continuum damage model applies thermodynamics of irreversible processes to explain structural change, and expresses healing as the recovery of damage parameters. This model evolved in the context of thermodynamic surface energy density, in order to characterise the primary contribution of van der Waals and Lewis acid-base interactions. Bridging the two broad concepts, the dissipative thermodynamic model explains phase change and damage phenomena at a scale where physical chemistry meets mechanics. This theory explains healing by rearrangement of phase-separated waxes.

Healing of bituminous materials has been studied intensely since 1962, using three methods for description: fracture-healing and fatigue-healing using storage recuperation or intermittent loading. It is shown that healing explains strength improvement across crack surfaces when a nominal permanent compressive force is applied thereto. Fatigue-healing tests using storage recuperation protocols have highlighted ambiguity regarding the healing of definition: stiffness recovers rapidly and to about 100% of the initial value, while fatigue life develops more slowly. Moreover, this technique accentuates the effect of damage condition on healing. Intermittent-type testing has identified a boundary condition to life extension and a fatigue endurance limit in asphalt and bitumen, which is sensitive to the control mode and applied stress/strain level.

Using such mechanical tests, the healing behaviour of asphalt is shown to depend critically on the binder and to be retarded by filler materials. In turn, bitumen healing is influenced strongly by intrinsic and extrinsic factors, namely rheology, chemical composition, rest period duration and temperature. Soft binder with a high proportion of long-aliphatic molecules or side-chains and aromatic fractions possesses high healing potential, which can be decreased by polymer modification due to flow-attenuation by adsorption of compatible components (maltenes).

### **3.7 CONCLUSIONS AND APPROACH**

Healing is a fundamental property of asphalt that is dominated by the binder phase but is also influenced by the characterisation method. Three methods are used to describe this process: crack-healing, fatigue-healing by storage recuperation, and fatigue-healing using intermittent loading. Mechanical tests show that healing involves the contact of fracture surfaces by flow, cohesion by wetting, and interfacial transfer of molecular segments by diffusion. Research on the time-dependence of this three-stage phenomenon define sigmoidal variation: a horizontal (cohesive) asymptote at short healing times intersects a tangential limit at long healing times by a (diffusive) transition plane. Healing is accelerated by increased temperature.

Three models are proposed for healing. The viscoelastic continuum damage model includes a compositional variable. The dissipative thermodynamic model emphasises contributions from crystallised molecules, and postulates healing by the rearrangement of this phase-separated domain. The multi-step model, produced from rudiments of polymer theory, defines healing by two critical stages: surface approach under viscous flow and intermolecular attractive forces by which stiffness is restored; and interfacial diffusion during which strength recovers.

In consideration of the preceding literature review and the aim of this thesis, it was decided to use fracture tests to analyse healing. The primary difference between the literature of healing in polymer and bitumen is the testing process. Notably, fatigue tests exemplify the complexity of defining this process mainly with regard to the effect of fracture remnants. By this approach it is aimed to enable a unique study of the effects of fracture temperature and delayed closure of crack surfaces. This will also provide unprecedented insight of the effects of different stress conditions that are experienced by a pavement.

Although research has developed knowledge of fatigue healing, the literature is devoid of any clarity on how this relates to crack healing and recovery of bitumen structure. For this thesis it is proposed to supplement fracture healing tests with fatigue tests, and SEM insights acquired of microstructural recovery. Using this novel approach, it is aimed to correlate bitumen healing with structure, which is absent from the published literature.

## **4 RESEARCH APPROACH**

Published researches of bitumen healing exemplify the complexity of this phenomenon and its dependency on various factors, namely bitumen chemistry and healing time, temperature and the extent of sample damage. The mechanism of healing is poorly defined however and is yet to be correlated with the physical interactions that catalyse healing and impart microstructural properties. To improve knowledge of this phenomenon the research approach derived for this thesis, and developed from preliminary analysis reported in this chapter, therefore focuses on correlating mechanical measurements of healing with microscopic analyses of this process.

This chapter explains the compositional properties that were important to select the materials for this thesis, and then produces a basic physical and rheological characterisation thereof. A conceptual representation of the research approach is then introduced, which is based on the literature review and analyses in Section 4.2.4.

### **4.1 INTRODUCTORY REMARKS**

Theories on the chemical composition of bitumen structure and the physical-chemical kinetics of healing overlap, as defined below and in Table 4-1. Notably, the dissipative thermodynamic model explains healing by the rearrangement of phase separated waxes, which are observed using AFM. This theory is consistent with the studies by Benson (1988) and Kim et al. (1990), who concluded that healing is related directly to the amount of long-chain aliphatic molecules in the crystallisable saturates fraction. Moreover, those researchers also reported that healing is enabled by aliphatic branches to aromatic molecules. This is coherent with AFM studies by Pauli and Grimes (2003) and De Moraes et al. (2010) that describe phase separated domains as wax-asphaltene clusters. Little et al. (1999) defined a direct relationship between aromatic content (in terms of acid-base component of surface energy) and long-term healing rate. This coincides with ESEM images of bitumen by Stangl et al. (2006) for example, which designate bitumen microstructure to be composed of highly-aromatic asphaltene and resin molecules. It has also been established that bitumen constituting a high proportion of low molecular weight oils has a high healing potential (Santagata et al., 2009). This could indicate that the medium

through which this aromatic microstructure is dispersed (the maltenes) modifies healing. More generally, research on healing by Kim et al. (2003) for example, has suggested that healing is inversely proportional to viscosity. Little et al. (1999), Smith and Hesp (2000b) and Qiu (2012) have concluded that polymers and filler materials inhibit bitumen healing. From the literature review on this phenomenon and microstructure, the process of oxidation is also pertinent.

Table 4-1: A summary cross-referencing prominent physical-chemical theories on healing with the structure of bitumen, which is recovered by this process (thesis page references included)

Microscopy studies on bitumen structure		Mechanical studies on bitumen healing	
Author (method)	Conclusion	Author	Conclusion
Claudy et al. (1992) (PLM) (p. 22)	Aliphatic dispersions of birefringent nature	Kim et al. (1990) (p. 72)	Correlated healing to long-chain aliphatics
Pauli et al. (2011) (AFM) (p. 27)	Crystallised paraffins in a non-polar moiety	Santagata et al. (2009) (p. 85)	High saturates content enables higher healing
De Moraes et al. (2010) (AFM) (p. 26)	Phase-separated wax-asphaltene clusters	Kim et al. (1990) (p. 72)	Aliphatic branches on asphaltenes involved
Loeber et al. (1996) (AFM) (p. 24)	Dispersed phase of colloidal asphaltenes	Phillips (1999) (p. 83)	Healing is unaltered by gelation of waxes
Stangl et al. (2006) (ESEM) (p. 36)	Entangled network of asphaltene particles	Williams et al. (2001) (p. 73)	Acid-base interactions drive network recovery

## 4.2 EXPERIMENTAL MATERIALS

In consideration of this review and the aim of this thesis, the sampled bitumens were selected in order to encompass, primarily, a broad range of asphaltene contents. This also provides for variable maltene concentration and bitumen viscosity. In accordance with this review and the proposed microscopy techniques, the secondary criterion for sampling was wax content. The physical properties and basic chemistry of the bitumens are described in Table 4-2. Moreover, the literature review indicated that structuring is caused by asphaltenes, maltenes and waxes, which also contribute to healing phenomena. This thesis also studies the structure-sustaining fractions using microscopy techniques, therefore.

Table 4-2: Physical properties and basic chemical composition of sampled bitumens

Bitumen	Physical properties <sup>6</sup>		Chemical composition		
	Pen. 25°C (0.1mm)	Softening point (°C)	Asphaltenes (%)	Maltenes (%)	Wax (%)
A (RTFOT/PAV)	14 (8)	72.0 (-)	18.3 (26.0)	81.7 (74.0)	-
B (RTFOT/PAV)	52 (17)	51.8 (-)	12.0 (18.1)	88.0 (81.9)	-
C (RTFOT/PAV)	75 (-)	50.0 (-)	11.2 (-)	88.8 (-)	1.26 (-)
D (RTFOT/PAV)	194 (60)	39.2 (-)	7.5 (13.1)	92.5 (86.9)	1.65 (0.12)

#### 4.2.1 Bitumen fractionation

##### Asphaltene and maltene fractionation

Asphaltenes were extracted from bitumens A, B and D using the process defined in BS 2000-143:2004, for determining the asphaltene content in crude petroleum or derivatives. In brevity, duplicates of the sampled bitumen are mixed with *n*-heptane and heated under reflux, and the residue of asphaltenes and inorganic materials is collected using filter paper. The asphaltenes are separated from inorganic compounds by dissolution in toluene, which is then evaporated. The maltenes are recovered from the *n*-heptane eluate by evaporation of the solvent using a boiling water bath, and stored at -30°C to minimise effects of metastability (refer to page 41).

##### Wax fractionation

To separate the waxes from bitumen, the procedure described in EN 12606-1:2007 was used: a specific distillation process obtain these components from the sample. Namely, the bitumen is dissolved in a 50% volume fraction blend of ether and ethane, and then filtered in a vacuum at a temperature of -20°C. The wax extracted using this protocol is solid at room temperature and has a solid-to-liquid phase transition at about 29°C, when the straight-chain Octadecane fraction melts (Messerly et al., 1967). Notably, the distillation process is performed using a lab

<sup>6</sup> Measured by European standard methods: penetration EN 1426; softening point EN 1427

burner with a non-luminous flame, at temperatures potentially above 500°C. This could cause aromatics and cyclo-alkanes substituted with long-chain alkanes to crack, and hence produce extrinsic molecules. The waxes obtained by this method hence show a prevalence of iso- and *n*-alkanes that, with long alkyl chains, are critical to crystal formation (Lu and Redelius, 2006).

#### **4.2.2 Laboratory ageing of sampled bitumens**

In consideration of the literature review in Chapter 2, it is concluded that studying the changes in bitumen structure produced by oxidation provides a subtle method to develop knowledge of the mechanisms involved in its formation. This thesis simulates short-term oxidation using the standard rolling thin film oven test (RTFOT). Defined in EN 12607-1:2007, this ageing process simulates the elevated temperatures during manufacturing and paving, which volatilise a high volume of short-chain fractions (Corbett and Merz, 1975). 35g of sampled bitumen is rotated for 75 minutes at 163°C, in a cylindrical glass jar that is supported in an oven with a constant air supply. To simulate the long-term changes due to in-service ageing, the RTFOT residue is oxidised using a pressure ageing vessel (PAV) in the HiPAT method. 50g samples are poured into stainless steel pans and exposed to the temperature of 85°C at 2.1MPa pressure, for the duration of 65 hours. The effects of this ageing procedure are defined by changes in physical properties, such as penetration and softening point, and chemical composition.

#### **4.2.3 Conventional physical property tests**

##### **Penetration test (EN 1426: 2007)**

Penetration is a measure of the consistency of bitumen expressed as the distance in tenths of a millimetre that a standard needle penetrates vertically into a sample, under a specified load and loading time at a fixed temperature of 25°C. The greater the penetration of the needle the softer the bitumen, therefore (Read and Whiteoak, 2003). The penetration test is considered to be an indirect measurement of bitumen viscosity at a temperature of 25°C (Airey, 1997).

##### **Ring and ball softening point test (EN 1427: 2007)**

The ring and ball softening point test is an empirical test that is used to define the consistency

of bitumen, by measuring the equi-viscous temperature at which behaviour is between solid and liquid. The consistency will be the same for different penetration grade bitumens at their respective softening point temperatures, therefore (Airey, 1997).

#### 4.2.4 Rheological property tests

##### Background

Dynamic shear rheometry is ubiquitous in studies of bitumen rheology. Rheological properties are measured by oscillatory tests conducted in the region of linear viscoelastic behaviour<sup>7</sup>, for analytical accuracy and simplicity (Sybilski et al., 2004). The rheological properties measured include the phase angle  $\delta$ : the viscoelastic balance of rheological behaviour or the phase lag between the applied shear stress and shear strain responses (Airey, 2003; Airey et al., 2008), and the complex modulus  $G^*$ : the ratio of maximums of shear stress and shear strain (Airey, 2003), which provides a measure of the response of the sample to an applied load (Read and Whiteoak, 2003). This modulus constitutes an elastic element: the storage modulus  $G'$ , and a viscous component: the loss modulus  $G''$ . The moduli are correlated by phase angle: a phase angle of  $90^\circ$  is indicative of purely viscous behaviour; an angle of  $0^\circ$  corresponds to the purely elastic response; and between these extremes, a bituminous material is viscoelastic in nature (Airey et al., 2008).

The moduli are susceptible to loading frequency and temperature: a temperature variation of  $\pm 0.1^\circ\text{C}$  evokes an error of  $\pm 2\%$  in the measured complex modulus (Anderson and Knechtel, 1997). Thermal uniformity in the sample and close temperature control are thus vital (Airey et al., 2008). These are acquired by immersing the sample-plate test geometry in the ubiquitous circulating fluid bath, which precludes the formation of temperature gradients within a sample and ensures rigorous temperature control between  $5^\circ$  and  $90^\circ\text{C}$  (Cointe and Monnoye, 1995). Alternatively the less-prevalent Peltier system is used, which applies the thermo-electric effect to heat the lower plate (Airey, 1997; Soenen et al., 2006). Inherently, a temperature gradient sensitive to sample geometry, mainly thickness (Teugels and Gustavsson, 1995), is produced

---

<sup>7</sup> Viscoelastic behaviour is considered linear if the complex modulus is independent of shear stress or strain; to wit, if it has not deviated beyond 5% of its initial value (Becker et al., 2003)

within samples tested using this system. This is hence recommended for low-to-intermediate temperatures only: below 80°C (Teugels and Nilsson, 1995; Soenen et al., 2006).

### Review of pertinent literature

To describe completely the viscoelastic properties of bituminous materials, rheological testing is conducted over a broad range of temperatures and loading frequencies (Airey, 1997) using different test configurations (refer to Table 4-3). For analytical clarity, the properties obtained thus are usually presented in isochronal or isothermal plots, master curves or Black diagrams (Sybilski et al., 2004). Isochrones represent the behaviour of a viscoelastic system at constant frequency; isotherms at constant temperature (Ramond et al., 1993); the master curve, time-temperature equivalency (Loeber et al., 1998); and the Black diagram, its normalised dynamic response independent of time and temperature (Airey, 1997).

Table 4-3: SHRP suggested disc diameters for DSR rheology testing (Anderson et al., 1994)

Disc diameter	Test temperature range	Typical G* range
8 mm	0°C to +40°C	10 <sup>5</sup> Pa to 10 <sup>7</sup> Pa
25 mm	+40°C to +80°C	10 <sup>3</sup> Pa to 10 <sup>5</sup> Pa
40mm	> +80°C	< 10 <sup>3</sup> Pa

For pure bitumens, complex modulus isochrones decrease rapidly with temperature and show highly temperature-sensitive behaviour. Isochrones of phase angle increase along a parabola with temperature to the viscous asymptote, when binder microstructure collapses gradually as temperature rises (Brulé and Gazeau, 1996).

Complex modulus isotherms for manifold pure bitumens increase along unique parabolas with frequency, approaching asymptotically a limiting elastic stiffness of 10<sup>9</sup> Pa (Airey, 1997). Such curves at 60°C are sensitive to asphaltene concentration and structuring (Loeber et al., 1998). Namely, more-flocculated structurally less-homogeneous systems occur at higher asphaltene content, which establishes pervasive stiffening or increased complex modulus across a range of frequencies and reduced thermal susceptibility. This effect is also apparent at 20°C for low-

to-intermediate frequencies: 0.1 to 1.0Hz, where the plastic response of the oily compounds is otherwise dominant for lower asphaltene content bitumens (Loeber et al., 1998). Isotherms of phase angle against frequency also exhibit susceptibility to bitumen chemistry (Soenen et al., 2006). Notably, isothermal crystallisation of waxy compounds at room temperature introduces a trend towards increased elasticity with longer time of exposure, between 0.01 and 0.001Hz. Phase angle is less frequency-dependent thereafter, due to loss of isothermally-formed three-dimensional crystalline structuring at higher load frequencies: 5 to 20Hz (Soenen et al., 2006).

The master curve is a continuous graph of modulus and phase angle measurements on a log-reduced frequency or time scale, for a standard reference temperature of 0°C or 25°C. This is derived using one of various transpositions or shifting techniques (Luminari and Fidato, 1998), usually an Arrhenius function or Williams-Landel-Ferry equation (Marasteanu and Anderson, 1996). For thermorheologically simple bitumen the principle of time-temperature superposition is used to relate equivalency between temperature and loading frequency, and to construct a master curve (Ferry, 1980; Sybilski et al., 2004). The shift factors used to translate individual curves along the time axis indicate the temperature dependency of the viscoelastic behaviour of each material: how the relaxation processes change with temperature (Airey, 1997). Myriad master curves of complex modulus versus reduced frequency in double logarithmic diagrams resemble hyperbolae: a horizontal glassy asymptote at high frequencies intersects a viscous asymptote at low frequencies (inclined at an angle of 45°) by a transition plane (Airey, 1997).

The Black diagram is also used to analyse rheological behaviour, though most often to verify experimental data: to scrutinise measurements for inconsistencies caused by nonlinearity and apparatus compliance (Sybilski et al., 2004). This diagram is complex modulus against phase angle, which circumvents the shifting techniques pursuant to the master curve and elucidates time-temperature equivalency. A smooth curve indicates time-temperature equivalence, while discontinuities describe the antithetical condition (Airey, 1997). The hyperbolic function of the Black curve is related to the hydrogen bonding potential of and polar interactions between the molecules in bitumen (Redelius and Soenen, 2005). Ageing and oxidation phenomena hence shift this curve consistently into the elastic region (lower phase angles) (Wu, 2009), due to the

increased structuring of polar components (Soenen et al., 2006). Loeber et al. (1998) studied the influence of the chromatographic fractions on bitumen rheology. The authors reported that the length and position of the Black curve are related to asphaltene concentration; the graphs are transposed to lower moduli and higher phase angles by reduced asphaltene content; and the unity of the function derives from the resins, which preclude asphaltene structuring. Time-temperature equivalence is also susceptible to crystalline chains: melting of ordered aliphatics at 30 to 70°C invalidates this principle, and discontinuous curves may indicate liquid-liquid demixing (Soenen et al., 2006).

### **Sample preparation**

The procedure used to prepare the specimens for rheological testing conforms to the silicone mould method (Airey and Hunter, 2003). This method consists of pouring a liquid sample into a silicone mould of diameter equal to that of the upper DSR plate: an 8mm or 25mm diameter mould, and of height sufficient to supply a 50% excess sample volume. To ensure a pourable consistency, bitumens are annealed in 10ml vials at 130°C for the minimum duration of fifteen minutes and stirred regularly to ensure homogeneity and remove air. For the maltenes a 10ml sample is heated in a borosilicate glass dish at 40°C for twenty minutes.

To allow for the ordering of molecules involved in the development of microstructure, the filled moulds are passively-cooled, covered and then stored in a dehumidified chamber at 25°C for 24 hours preceding testing (refer to Masson and Polomark (2001)). It was for this preparatory stage that the hot pour technique was eschewed: to negate *ex ante* test variability associated with flow-induced eccentricity in stored mounted specimens. The conditioned disc is removed from the mould at room temperature (for the maltenes at 2°C) and centred on the lower plate. The mounted sample is then heated to its softening point, to allow internal stresses produced during preparation to dissipate prior to testing and to ensure sample-to-plate adhesion (Airey and Hunter, 2003). The interval between the parallel plates is then reduced to 50µm plus the required test gap: 1000µm for the 8mm geometry; 2000µm for the 25mm geometry. Material displaced to the periphery under this compression is trimmed level with the edge of the plates, using a hot spatula. Lastly, the gap is closed by 50µm to acquire the testing separation.

## Sample testing

The dynamic shear rheometer was used for three tests: strain sweeps, frequency sweeps and fatigue. The justification for each type of test is established below, in Table 4-4.

Table 4-4: A chronological summary on bitumen structure by ESEM at ambient temperatures

Test	Justification
Strain sweeps	To ensure that rheological characterisation is conducted in the region of linear viscoelastic response.
Frequency sweeps	To collect data in order to describe the materials using master curves and Black diagrams.
Fatigue tests	To develop insight of the effect of asphaltene-maltene interactions on the phenomenon of damage.

The rheological properties of bitumens and maltenes were acquired using strains confined by the linear viscoelastic limit and strain-controlled loading, under the conditions in Table 4-5.

Table 4-5: DSR test conditions for sample geometry

Parameter	Bitumen		Maltenes	
	Configuration 1	Configuration 2	Configuration 1	Configuration 2
Temperature	5°C to 35°C	25°C to 60°C <sup>8</sup>	5°C to 20°C	5°C to 40°C
Cooling system	Fluid	Fluid	Peltier	Fluid
Plate diameter	8mm	25mm	8mm	25mm
Gap	2mm	1mm	2mm	1mm

### Strain sweeps (stress-strain response)

A binary set of strain sweeps were completed at 10°C and 40°C for the bitumens. To mitigate contamination of the fluid bath by sample flow the strain sweep for the maltenes was acquired at 20°C. The limit of linear viscoelastic response is defined as the point at which the complex modulus has decreased to 95% of its zero-strain level.

<sup>8</sup> Temperature was varied from 60°C to 80°C depending on the sampled bitumen

Amplitude sweeps for the four binders reveal similar strain dependency: a plateau precedes a precipitous decline beyond the linear viscoelastic strain limit, which is a function of stiffness as reported in the literature (Airey et al., 2003) (refer to Figure 4-1). The amplitude sweep for the maltenes shows binary complex modulus at low strain and a broad plateau to the transition to nonlinear viscoelasticity, for which the strain criterion is an outlier in the data for the bitumens. This change in response could be related to the activation of new physical mechanisms or the redistribution of molecular kinetics that contribute to physical processes, due to the extraction of asphaltenes. The response of maltenes in solution with asphaltenes could be dominated by that arising from conformational entropy reduction, as molecules are constrained in motion by the asphaltenes. Analogous behaviour is reported for polymers (Dooling et al., 2002).

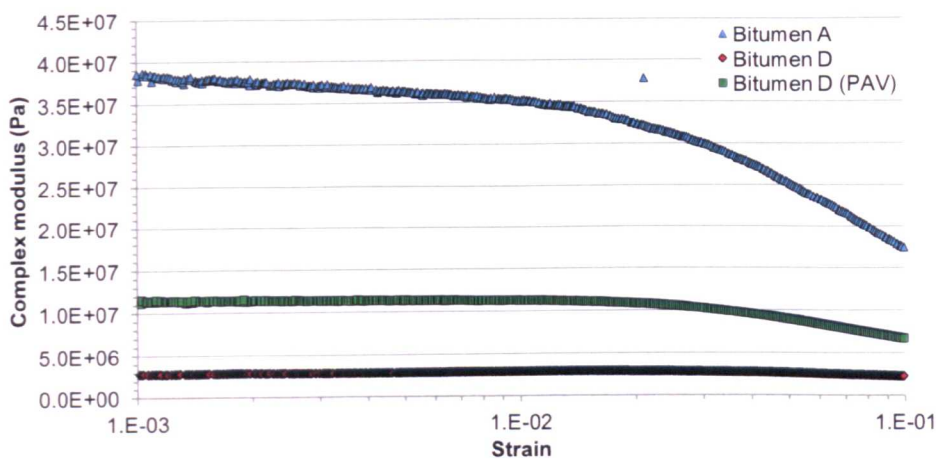


Figure 4-1: Example strain sweep for selected bitumens, tested at 10°C and frequency of 1Hz

### Temperature dependence

The thermal variation of rheological properties is analysed by isochrones of complex modulus and phase angle, plotted at 1Hz (refer to Figures 4-2 and 4-3). The viscoelastic response of the binders is analogous to the literature and is highly temperature-sensitive compared to the maltenes. For this fraction, the isochrone of phase angle is constant at the viscous asymptote. Moreover, the difference in elasticity between the unique phase angle parabolas, produced by measurements using the 8mm and 25mm configurations, increases with asphaltene content.

Complex modulus isochrones decrease continuously with increasing temperature: the notable incongruity for materials thought (Rosinger, 1914) to comprise a gel network is the absence of

a rubbery plateau at moderate temperatures. This region is synonymous with the response of viscoelastic polymer gels subjected to oscillatory strains (Kavanagh and Ross-Murphy, 1998). This is ascribed to a swollen elastic network of topological interactions (Ferry, 1980) between polymer chains, which involves motion-resisting intermolecular entanglements within a three-dimensional matrix of polymers exceeding a critical weight (Wool, 1995). It is also interesting that in the temperature range of 20°C to 60°C, which includes melting of crystalline fractions, there is not an abrupt variation in the gradient of the isochrones. This is observed in modified bitumens comprising pervasive physically cross-linked elastomer (styrene-butadiene-styrene) and semi-crystalline (ethylene-vinyl-acetate copolymer) polymer networks (Airey et al., 2003). To conclude, the isochrones of complex modulus for the sampled bitumens indicate that the contribution of any dispersed asphaltene network is negligible for the studied conditions.

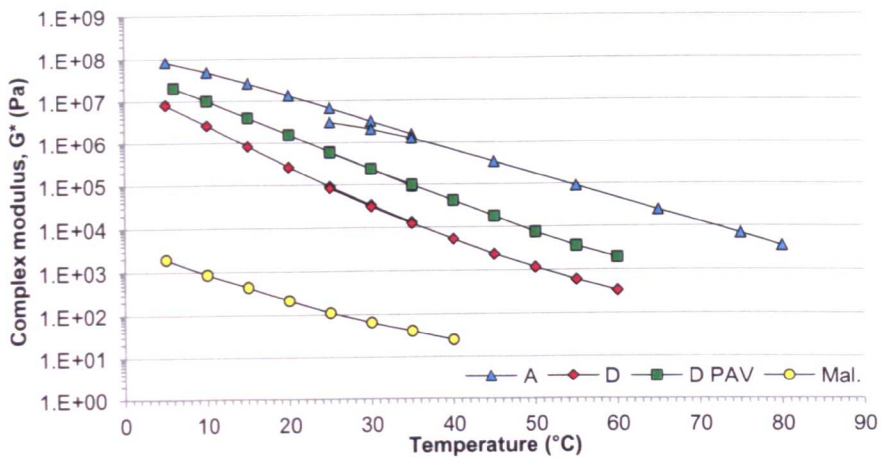


Figure 4-2: Isochrones of complex modulus for bitumen and maltenes (mal.) at 1Hz shear

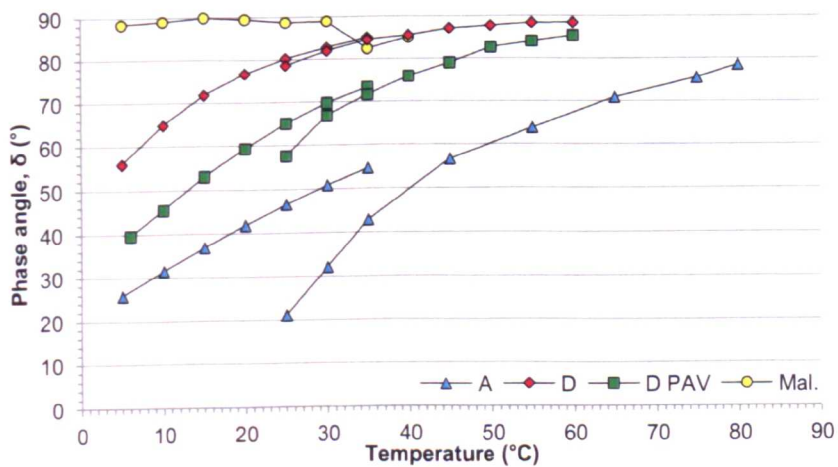


Figure 4-3: Isochrones of phase angle for bitumen and maltenes (mal.) at 1Hz oscillation

## Frequency dependency

The frequency sensitivity of the materials is analysed by isothermal plots of complex modulus and phase angle at 15°C and 35°C, and master curves produced for a reference temperature of 25°C by time-temperature superposition. Complex modulus isotherms increase on unique parabolas with frequency. These curves show stiffening and abated frequency-sensitivity with increasing asphaltene concentration (refer to Figure 4-4). Isotherms of phase angle, which is more sensitive to chemistry (Airey, 1997), show a similar dependency on binder composition: increased elasticity with asphaltene content. Moreover, this graph indicates conformity of low asphaltene content bitumen (D) with the maltenes at low frequencies (high temperature) (refer to Figure 4-5).

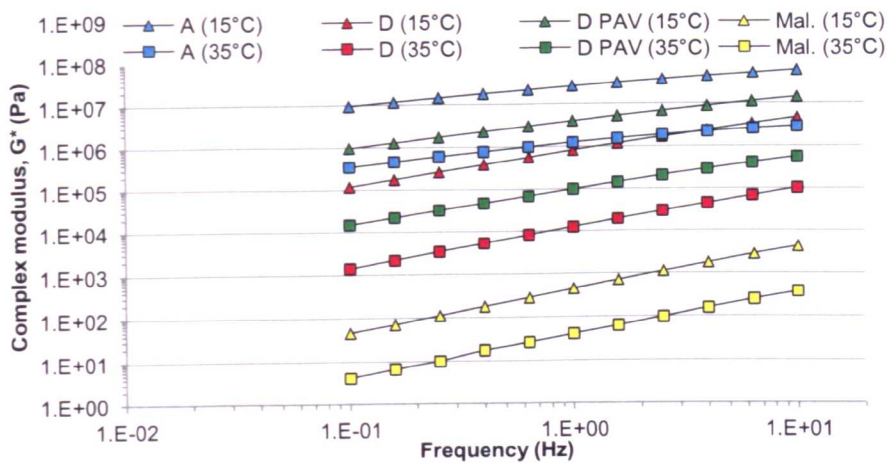


Figure 4-4: Isotherms of complex modulus for bitumen and maltenes (mal.) at 15°C and 35°C

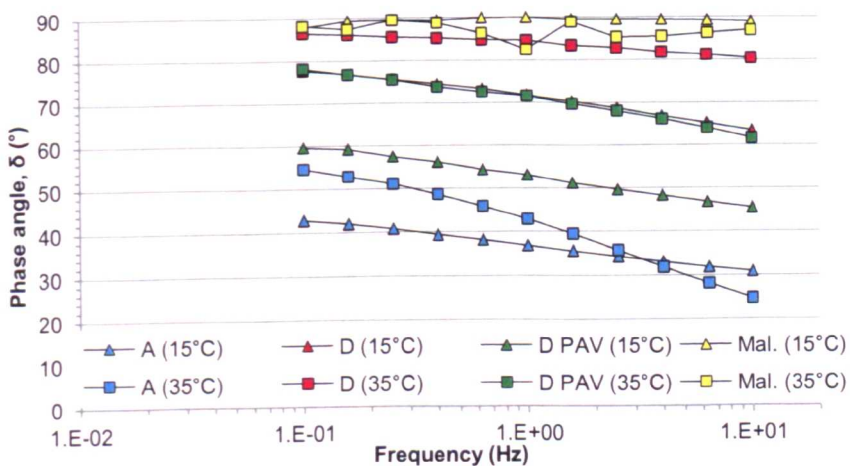


Figure 4-5: Isotherms of complex modulus for bitumen and maltenes (mal.) at 15°C and 35°C

Master curves of complex modulus versus reduced frequency in double logarithmic diagrams for the sampled bitumens resemble the hyperbolae reported in the literature. For the maltenes these data are sited on the viscous asymptote inclined at an angle of 45° (refer to Figure 4-6).

From the viscous asymptote at low frequencies, master curves of phase angle for the binders show smooth and continuously-increasing elasticity with increasing loading frequency. For the maltenes a discontinuous plateau is formed at this asymptote using data from the second test configuration (refer to Table 4-5 and Figure 4-7). The discontinuities punctuate low frequency (high temperature) behaviour, and could be ascribed to a change in sample geometry by flow instability: an edge-effect (Keentok and Xue, 1999) due to circulating fluid, or the invalidation of time-temperature equivalence. This could arise from thermal-structural transitions in waxes and crystallised fractions, which are reported (above) to produce similarly discrete waves. The author suggests that extraction of the asphaltenes concentrates waxes in the maltenes, which are hence more susceptible than the base bitumen to melting phenomena. The Black diagram is used to validate this theory. For the binders data derived at various temperatures indicates moderate overlap: for the maltenes low frequency behaviour is perturbed, perhaps by melting of waxes that crystallised during storage (refer to Figure 4-8). It is interesting that the maltenic rheological fingerprint shows semi-crystalline behaviour on testing in the Peltier DSR: a series of discrete waves in the centre of Black space (Airey et al., 2008). This behaviour may instead indicate inconsistencies caused by apparatus compliance.

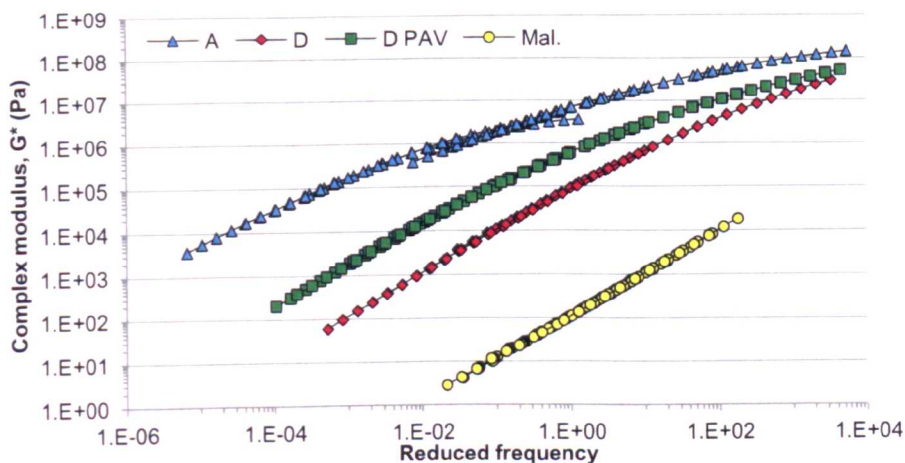


Figure 4-6: Master curves of complex modulus ( $G^*$ ) for the reference temperature of 25°C

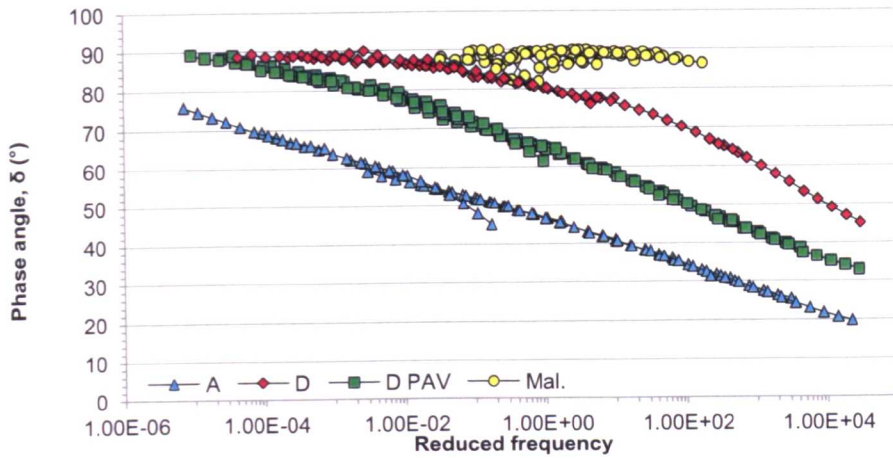


Figure 4-7: Master curves of phase angle ( $\delta$ ) for the reference temperature of 25°C

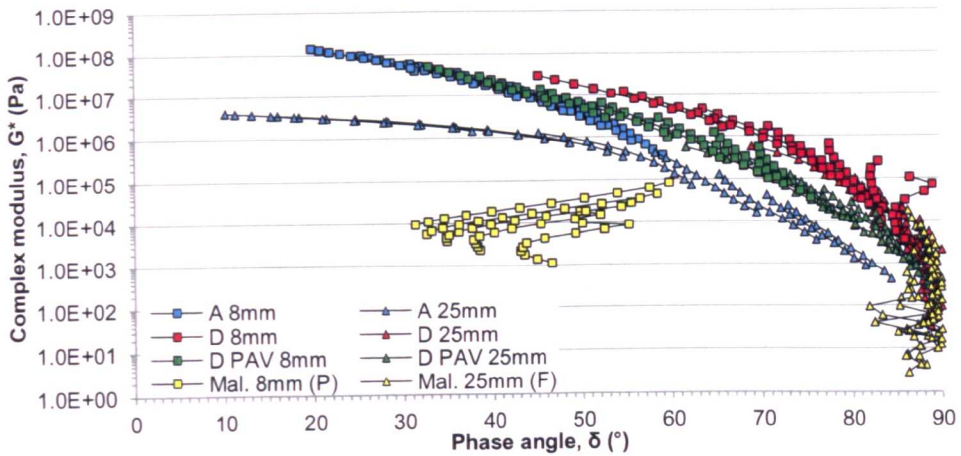


Figure 4-8: Black diagram for bitumen and maltenes (using Peltier (P) and fluid (F) cooling)

### Fatigue behaviour

The analysis of bitumen fatigue is ubiquitously acquired from cyclic strain- or stress-controlled tests using a DSR (Bahia et al., 1999; Anderson et al., 2001; Lu et al., 2003). This is extended in this thesis to investigate the maltenes.

The fatigue response of maltenes was studied in the Peltier system, to prevent contamination of the circulating fluid, at 15°C and at strains confined in the linear viscoelastic regime: 0.7% and 2.0%. Exemplary time sweeps are presented in Figure 4-9 and indicate strain hardening: material strengthening by plastic flow (Hoy and Robbins, 2006). Different physical processes have been identified as the possible cause for non-oxidative hardening in bitumen (Soenen et al., 2004). Firstly, physical hardening due to a reduction in fractional free volume. This type of

hardening is noted for amorphous polymers and occurs due to cooling to temperatures below the glass transition, when molecular motions are abated such that the equilibrium free volume state is not obtained. Secondly, thermo-reversible hardening that results from the build-up of intermolecular associations (steric hardening). In polymers, this phenomenon is observed at a temperature just above or substantially above the glass transition, depending on polymer type (Soenen and Berghmans, 1994). Thirdly, isothermal hardening occurs in bitumen due to free volume collapse by wax crystallisation (Anderson and Marasteanu, 1999). These phenomena may contribute simultaneously with hardening by molecular orientation effects: due to loading, the extension of coiled molecules stores energy by increasing tension in covalent bonds (Chui and Boyce, 1999). This could provoke additional steric effects (Harini and Deshpande, 2009). A combination of these mechanisms is cited to explain the strain hardening in maltenes.

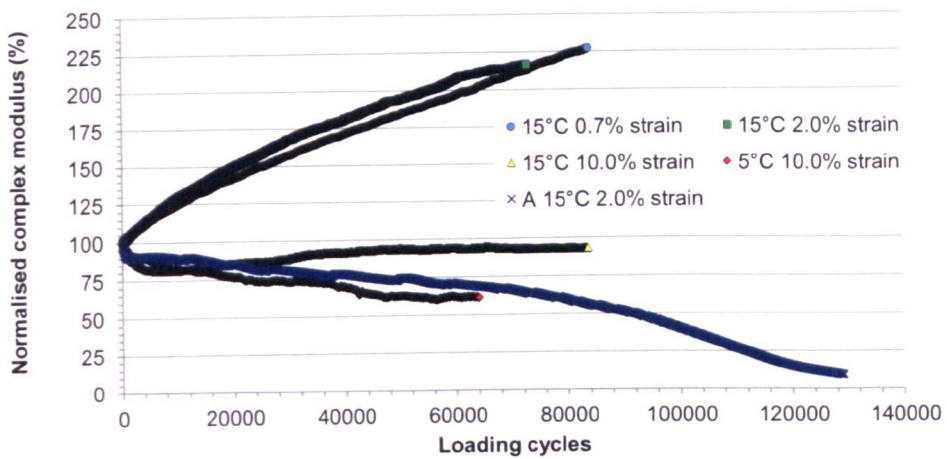


Figure 4-9: Fatigue (continuous shear) curves for maltenes and bitumen. Complex modulus is normalised to the initial (for the maltenes mean initial modulus is 17.8kPa)

In contrast to the maltenes, complex modulus evolution during fatigue of the source bitumen (bitumen A) at 15°C and 2.0% strain shows the tri-phase response described by Di Benedetto et al. (1996). That is, an initial drop in modulus (phase one) that is explained by thixotropy and sample heating due to energy dissipation (de la Roche and Marsac, 1996); a gradual decline of modulus (phase two) due to damage by microcrack growth; and macroscopic failure (phase three) due to microcrack densification (Uzan and Levenberg, 2001) (refer to Figure 4-9).

The divergent response of the materials could indicate the effect of asphaltenes on fatigue. It is known (Masson et al., 2006b) that the high molecular weight, polarity and aromaticity of the

asphaltenes in solution with maltenes modifies the glassy properties of the material. Notably, the asphaltenes order to produce an amorphous mesophase that establishes two broad glass transition temperatures, centred at 0°C and 70°C (Masson et al., 2002). Due to intermolecular bonding and free-volume effects at the test temperature (15°C) dissipation of strain energy by flow is limited in this phase (Turnbull and Cohen, 1961), and fatigue propagates by molecular rupture. This response is reported in high molecular weight polymers (Wool, 1995; Jarrousse, 2004). Devoid of asphaltenes, strain energy acquired by the maltenes can dissipate by friction (thermal energy) during plastic flow, and store in the covalent bonds (hardening). This type of behaviour is noted in low molecular weight polymers (Griffith, 1921; Rivlin and Thomas, 1953; Berry, 1961; Rosen, 1964). The effects of disrupted solubility due to asphaltene precipitation cannot be ignored, however (Martono and Bahia, 2007). To conclude, the fatigue response of the maltenes and sampled binder indicate that damage processes are governed by the glassy properties of the material. This insight is important to develop the study on damage healing.

## **4.3 RESEARCH DIAGRAM**

### **4.3.1 Introductory remarks**

In the literature review, asphalt healing is defined as the partial restoration of intrinsic bitumen structure across adjacent crack surfaces. Literature on this structuring is ambiguous however, and devoid of insight into bulk properties. Moreover, only the paper by Schmets et al. (2011) has attempted to relate the healing phenomenon to microstructure. It is also notable that, due to the complexity of ubiquitous fatigue-healing tests in the DSR, the reported healing capacity is not a true material property but is dependent on the mode of loading and test procedure. In practice, the stresses that occur in a pavement when a wheel load passes over it change with time, and include crack-producing tensile stress. This is shown in Figure 4-10. It is imperative therefore, not just to determine an artefact-free method to investigate healing, but to consider alternatives to the shear regime in the DSR.

The published literature also highlights the deficiency of microscopy techniques to study bulk structuring, yet it is this that governs behaviour. The rheological tests reported in this chapter

indicate that the contribution of any dispersed asphaltene network is negligible and moreover, that damage is governed by glassy domains. To develop a fundamental understanding of the healing process therefore, it is firstly vital to address the structural ambiguities that abound.

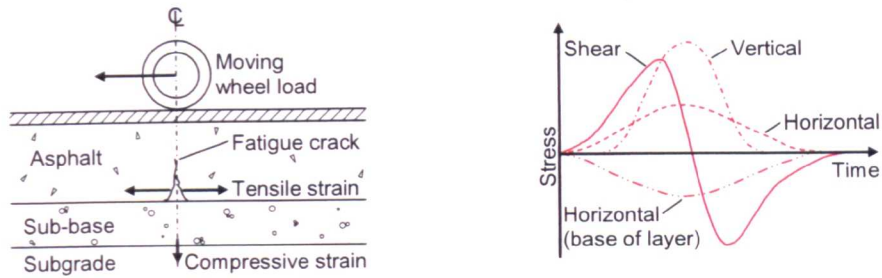


Figure 4-10: Schematic of structural failure of an asphalt pavement and stresses induced by the moving wheel load. Developed from Read and Whiteoak (2003)

#### 4.3.2 Explanation of the research process

Based on the literature review and findings from the rheology tests reported in this chapter, a research approach was produced to study and further understand the healing phenomenon of bitumen at the microstructural level. This approach is presented in Figure 4-11 and explained hereafter. Notably, detailed sub-diagrams are produced in Chapters 5 and 6.

#### Microscopy analyses (Chapter 5)

This section of the thesis focuses on relating surface structuring and bulk morphology. Firstly, this research uses ESEM to develop knowledge of the response of bitumen to irradiation. This microscope is then used with a Peltier cooling stage to form insights into the thermal variation of bitumen structure, as reported only by AFM. In order to validate the theoretical chemistry of the structure, the ESEM is lastly used to study three bitumen fractions: asphaltenes, maltenes and waxes. In order to develop understanding of bulk structuring, which preceding rheological analyses indicates is critical to damage, a novel freeze-fracture technique is used in cryogenic electron microscopy. This technique is based on the principle that freezing the sample arrests molecular processes that otherwise disrupt the physical-chemical state of the material. This is complemented by a unique study using ion milling under cryogenic conditions, which enables selective excavation of material in order to develop insight of the structure of interfacial areas. Such fundamental knowledge cannot be acquired using the available AFM methods.

### Mechanical analyses (Chapter 6)

This section of the thesis focuses on the development of an effective test method to quantify the healing of bitumen. Based on the literature review, the test methods should closely mimic the healing process that occurs between fracture surfaces. Moreover, from preceding analysis in this chapter, it is important to consider a range of fracture temperatures: rheology indicates that damage is governed by glassy properties, which depend on diverse glass transitions. To address these aims and to provide alternative loading regimes, direct tension tests and Vialit pendulum tests are used with a novel DSR approach. The direct tension test enables fracture in the vicinity of the glass transition temperature of the aromatics (-19.6°C), and the latter two tests where wax crystallisation occurs (23°C to 30°C). The effect of external factors including healing time and temperature are studied with these techniques.

### Conclusions (Chapter 7)

Based on the research of material microstructure and healing behaviour, the conclusions and recommendations for future work will be presented.

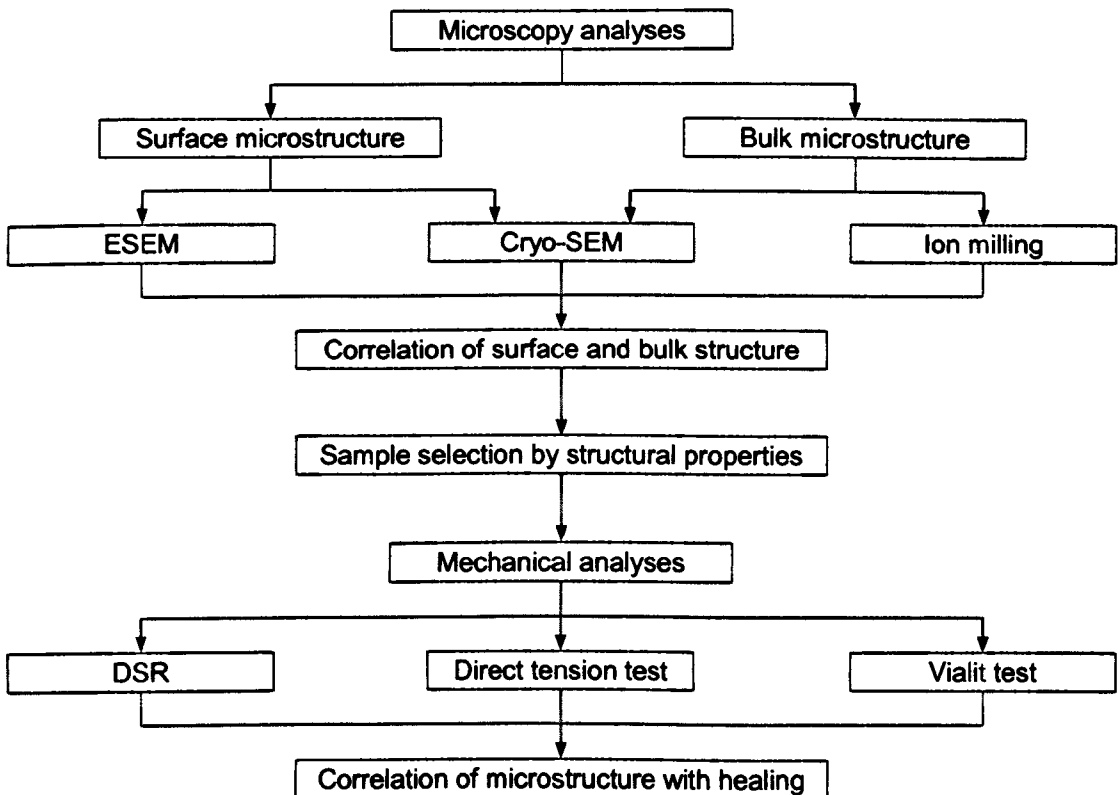


Figure 4-11: Research diagram for the experimental study on bitumen structure and healing

## 5 A STUDY ON BITUMEN AND ITS FRACTIONS BY SEM

During the four centuries since the invention of the optical microscope (Baker, 1754), a partial knowledge of the solid-state microstructure of bitumen has been developed (Speight, 2007). It is the focus of this study to continue the literary discussion on the nature of this structuring, by elaborating on the relationship between the bee-like dispersed phase and the fibrillar network. Moreover, by applying recent innovations in cryogenic preparation this research establishes a novel technique to examine bulk structures, using electron and ion microscopy. The approach for this section of the research is presented schematically in Figure 5-1.

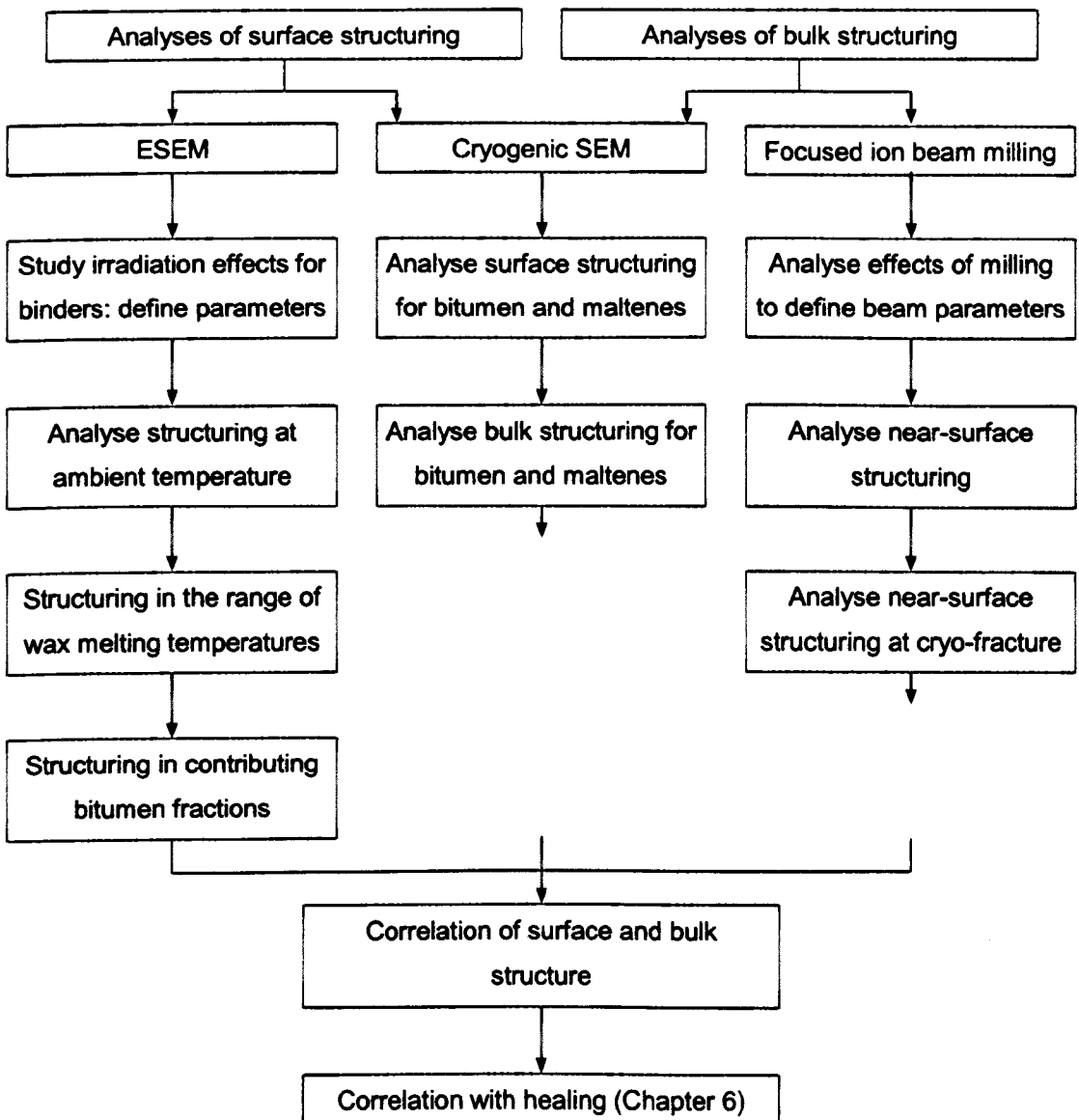


Figure 5-1: Conceptual representation of the research approach for the microscopy section

## 5.1 ENVIRONMENTAL SCANNING ELECTRON MICROSCOPY

### 5.1.1 Background

Commercial ESEM was introduced in 1986 (ElectroScan, 1989), using differential pumping in the column to establish a pressure gradient from the gun chamber to the sample chamber. In the sample chamber, a pressurised gas establishes a unique opportunity to examine hydrated matter. This retains liquid water at pressure higher than 4.6 Torr above 0°C (Sheehan, 1995; Dokland et al., 2006). The gas also suppresses accumulation of electric charge at the sample surface: as primary or secondary electrons collide with gas molecules around the sample, gas ionisation produces positive ions that drift towards its surface. This process compensates the energy from electrons embedded there and the removes artefacts due to the electric potential created (Kimseng and Meissel, 2001). The conventional conductive coating required to image insulating materials in SEM is negated therefore, which enables the study of these samples in their natural state (Danilatos, 1989; Bewick et al., 2009).

### 5.1.2 Sample preparation

The review of published microscopy research indicates various potential sample preparation methods. The methods chosen for ESEM research herein and alternative methods described in the literature are defined as follows, and summarised below in Table 5-1.

Table 5-1: A summary of key preparation methods with benefits (ben.) and drawbacks (dra.)

Preparation method	Outline and justification
Solvent precipitation (not used here)	Sample dissolved in solvent and deposited on a spinning glass slide Ben.: Film thickness used as a controlling variable (Pauli et al., 2011) Dra.: Changes the solid-state structure (Stulirova and Pospisil, 2008)
Heat-casting (bitumens)	Sample heated to liquid state and poured onto a microscope slide Ben.: Maintains solid-state microstructure (Masson et al., 2006a) Dra.: Without close temperature control, sample can oxidise rapidly
Buttering (maltenes)	Sample softened at low heat and spread onto a microscope slide Ben.: Low heat precludes oxidation effects Dra.: Handling of stiff materials alters structure (Rozeveld et al., 1997)

## **Bitumen**

In published AFM studies samples are prepared by spin-casting from a solution. Solutions are produced by dissolving bitumen in a solvent (usually toluene). For spin-cast films, the solution is deposited on a spinning glass microscope slide using a spin-caster to rotate the substrate. This method is used for research in which film thickness is a controlling variable (refer to page 24). Yet, this is known to modify sample structure (Stulirova and Pospisil, 2008). In this thesis, the samples are prepared by heat-casting in order to preserve solid-state structure.

250ml of the sampled binder was heated in an oven at 130°C and stirred regularly, to produce a homogeneous liquid with the consistency of motor oil at room temperature: pourable but not overly fluid. This enables reversal of steric hardening and thorough creep of the material with minimal thermal degradation (ageing) (Wilson et al., 2001). Thin bitumen films were prepared by pouring a continuous stream of the material, to avoid entraining distortive air bubbles, onto 12.7mm diameter aluminium sample mounts. The mounts were cleaned with toluene and then acetone to minimise contamination, and warmed to sample temperature to promote adhesion. Film thickness often varied in the range of 500 to 2000µm. This is satisfactory to minimise the potential artefactual action of the micrometre-scale (Wang et al., 2008) surface roughness of sample mounts, and the interfacial mechanisms that provoke discordant topologies in bitumen films thinner than 10µm (Pauli et al., 2011).

It is the current understanding that bitumen structure forms by mechanisms including diffusion and crystallisation (Schmets et al., 2010). These contribute to bitumen metastability and to the transition of its kinetic phases to a mature, mainly-stable state within 24 hours of annealing at 22°C (Masson and Polomark, 2001). To allow for these ordering phenomena, samples were lastly annealed at 25°C for the duration of 24 hours before microscopy investigations.

## **Maltenes**

The maltenes are solvent oils in which is suspended a high concentration of volatile fractions, waxes and resins. This fraction is hence less thermally-stable than the neat bitumen (Kopsch, 2008). The preparation method for the maltenes should surmount any potential evaporation or

thermal decomposition of the concentrated structure-sustaining components therefore, which occurs at high temperatures. The heat-casting preparation method for maltenes is unsuitable.

For investigations on structuring in the maltenes, samples were produced simply by spreading or buttering material onto aluminium sample mounts: cleaned *ut supra* and heated to ambient temperature. This physical manipulation is known to modify structure in bitumen (Rozeveld et al., 1997): images of oils indicate no similar effect (Pauli et al., 2011). The thin and translucent films of maltenes are annealed under identical conditions as bitumen films, and then stored at  $-20^{\circ}\text{C}$ : the glass transition temperature (Masson and Polomark, 2001), to inhibit steric effects.

### **Asphaltenes**

Aliquots of the wax-free asphaltenic fraction were removed from the residue in a borosilicate glass basin after evaporation of the solvent and oven-drying, by scraping (Poirier and George, 1983) the opaque solids from the evaporation vessel with a metal spatula. With stainless steel forceps, the recovered particles were deposited onto clean aluminium sample mounts coated with conductive carbon tabs to assure adhesion, then stored at  $5^{\circ}\text{C}$  to prevent age-hardening.

### **Waxes**

Papery samples of paraffin wax were recovered from the distillates obtained by the distillation of the soft binder, using stainless steel forceps to extract desiccated crystallised residue from an evaporation dish. The specimens were fixed onto clean aluminium mounts using adhesive-conductive carbon tabs, and then stored at  $5^{\circ}\text{C}$  to preclude the solid-liquid phase transition of the lowest-melting part: *n*-Heptadecane at temperatures above  $22^{\circ}\text{C}$  (Messerly et al., 1967).

#### **5.1.3 Sample testing**

The instrument used for this study was an FEI XL30 FEG-ESEM. Micrographs were collected at a partial pressure of 0.5 to 3.0 torr water vapour, using an acceleration voltage of 10keV for general imaging and 20keV for high-resolution observations (Stokes, 2011). The temperature-sensitivity of surface structure was scrutinised using an inbuilt Peltier cooling stage to create a thermal conditioning cycle. Namely, temperature was firstly reduced to  $0^{\circ}\text{C}$  on the pre-cooled

and calibrated stage; then elevated to 25°C in increments of 5°C; and lastly restored to 0°C at a nominal rate of 5°C per minute. During testing, a thermal equilibration period of ten minutes was included at each temperature prior to observations on bitumen morphology. Although any calculation of sample temperature under irradiation is convoluted by beam heating effects, the maximum temperature (25°C) is similar to that of wax appearance in wax-petroleum solutions. Bhat and Mehrotra (2004) reported this to be 23 to 30°C for solutions with wax concentrations below 10% by mass. Crystalline waxes in bitumen may be expected to show a transformation into a more stable state at the temperatures used herein. Consistent with the working theory, in which structuring is produced by waxy fractions that are swollen by occluded short aliphatic and alkylated chains, the surface of bitumen is also expected to show a structural change.

#### 5.1.4 Radiation effects in ESEM

From the literature, the expected response of the bitumen surface under excessive irradiation intensities is to relinquish an atomic layer of the material. This derives studies of near-surface topology in bitumen, which produces useful theories for understanding this mixture of myriad hydrocarbons. In this thesis, the type and amount of beam effects are shown uniquely to vary with sample temperature and asphaltene content. The examples that follow elucidate damage in three binders irradiated at an acceleration voltage of 10keV and 4000x magnification, and a working distance of 10mm. Damage phenomena were observed at television scan rates using the conditions indicated on each micrograph. This research is summarised in Table 5-2.

Table 5-2: A summary of radiation effects in bitumen with varying asphaltene (asph.) content

Sampled bitumen	Outline observations and explanation
D (7.5% asph.)	10keV radiation exposed the network: precluded by focusing dose. The unique observation of radiation resistance is due to a modification of bitumen chemistry, which preserves the amorphous original state.
B (12.0% asph.)	Irradiation at 10keV caused smoothening: at 20keV exposed network. The radiation stability is ascribed to a higher concentration of aromatic fractions, which reduces radiolysis: the process exposing the network.
A (18.3% asph.)	Prolonged irradiation at 10keV and 20keV distinguished by charging. Asphaltenes behave as a sponge-type protector, and transfer ionisation without chemical effect (e.g. loss of free radicals from paraffins).

### Bitumen D (Asphaltene content: 7.5%)

The response of the surface of low asphaltene content bitumen after two minutes irradiation is consistent with the literature: surfaces appear as networks of highly-entangled strings (refer to Figure 5-2(a)). This change was abated by previous irradiation: a focussing dose of radiation renders the sample resistant to successive electron degradation, which so retains the smooth state. Adjacent to this doubly-scanned region, the sample was modified towards the otherwise ubiquitous fibril network (refer to Figure 5-2(b)). This phenomenon is explained by a change in chemistry. Namely, the perturbation of an organic material by inelastic electron scattering may create an excited state within the interacting molecule (Fryer, 1987; Dorset, 1995), as follows.

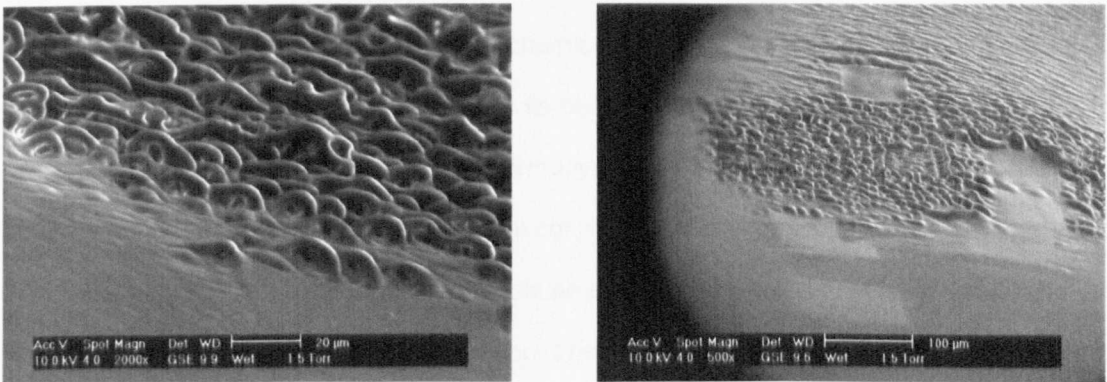


Figure 5-2: (a) ESEM micrograph of bitumen D after 2 minutes irradiation at 25°C. (b) Beam effects in bitumen D due to double irradiation at 25°C.

For the alkanes, radiolytic decomposition may stimulate cross-linking of the carbon skeleton (Kobayashi and Sakaoku, 1965). This reaction occurs in the paraffins by rupture of C-H bonds and the liberation of hydrogen, and may persist towards the production of an infusible material that increases stability under radiation (Charlesby, 1952; Alexander et al., 1955). The inelastic scattering can also yield radical groups: alcohols, carbonyls and fragments with an unpaired electron in the carbon backbone (Bludenko et al., 2007). Radicals are unstable: they decay or dimerise to form new compounds, and may be involved in hydrogen abstraction reactions with alkanes and polycyclic aromatics (Downing, 1983; Violi et al., 2004). Radical compounds also stabilise by delocalisation of unpaired electrons over an extensively-conjugated double bond system. This poly-conjugated structure derives high thermal and radiation stability due to the effect of resonance (Wu and Spence, 2003), where imbibed energy is distributed through the

aromatic rings without bond scission. It is tentatively proposed that a surface layer of radiolytic  $\pi$ -delocalised fragments preserves the amorphous state during a second irradiation process.

Discontinuous imaging with repeated photography allowed recovery of the original amorphous state of the sample. In repose from irradiation for fifteen minutes (in the microscope), imaging of the embedded fibril system was precluded by a surface layer of material: notionally, solvent oils. However, a secondary period of prolonged exposure to the electron beam volatilised the molecules concentrated at the binder surface, to reveal the string-like superstructure (refer to Figure 5-3). Analogising to the electron response of aliphatic polyester (Cairns et al., 2012) and other amorphous-crystalline polymers (Aronov and Rosenman, 2007), it is suggested that the modification of bitumen is reflected by chemical changes. These induce a thermodynamic imbalance between the irradiated area and its periphery, which causes bitumen molecules to diffuse into this area. This restores the thermodynamic equilibrium and the amorphous state of the irradiated domain. Moreover, the local concentration of aromatic fractions established in this scanned area, due to the initial volatilisation of aliphatics, could enable decomposition of this restored surface by secondary irradiation. These fractions may usurp the protective effect of delocalised electrons by a scavenging phenomenon (Fryer, 1989; Fujiyoshi, 1998).

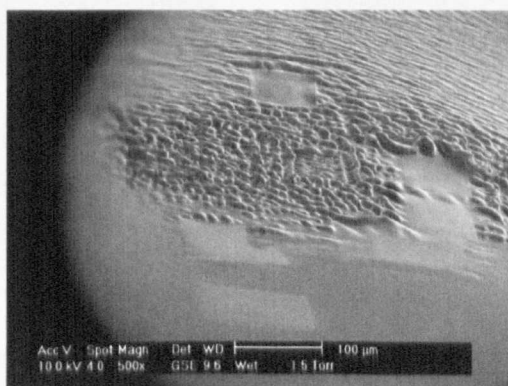


Figure 5-3: Beam effects due to discontinuous irradiation of bitumen D at 10keV and 25°C.

Dynamic phenomena of bubble formation and rupture were also observed across the sample (refer to Figure 5-4(a)). The radiolytic decomposition of weakly-combined oxygen-containing compounds in bitumen is known (Cataldo et al., 2004; Mustafaev et al., 2004) to produce light gases including carbon monoxide and methane. These segregate from irradiated zones along

paths traced in the plasticising fractions and form bubbles when trapped. The bubbles rupture when the inner pressure exceeds the interfacial tension of the material, and leave concavities that distort the string-like structure. This lends credence to the inherency of this structuring.

Local deformation of the embedded fibrils was also imaged remotely to the position of emitted radiolytic fragments (refer to Figure 5-4(b)). This is ascribed to inclusions of metallic elements that migrated to the surface under sample heating, due to the adsorption of electrons. Energy dispersive X-ray (EDX) analysis of surface precipitates revealed them to be concentrations of magnesium, silicon and potassium dispersed stably in salt form. This enclave of concentrated functional groups occurs primarily in the heavy non-volatile components. When they diffuse to the surface they drag the aromatic skeleton of constituent molecules. This backbone reduces damage (Mahoney et al., 1959) near the metals precludes exposure of network structuring.

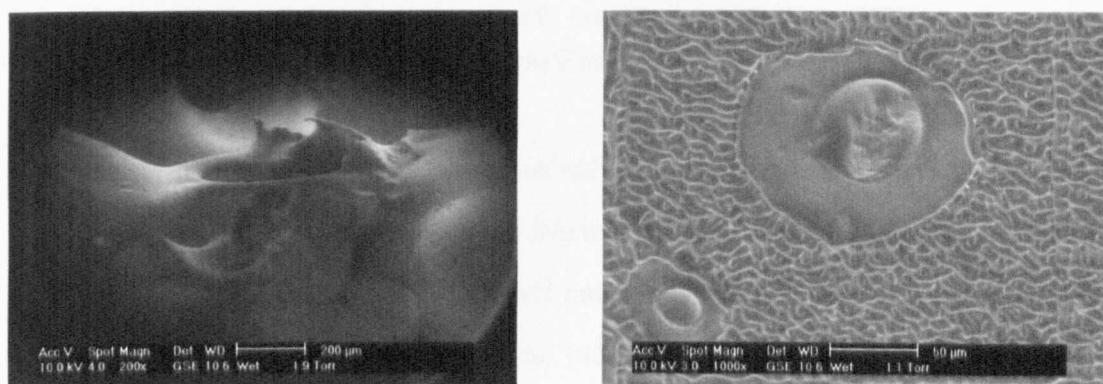


Figure 5-4: (a) Image of bubble formation and rupture in bitumen D at 25°C. (b) Distortion of entangled network components due to metallic precipitates.

### Bitumen B (Asphaltene content: 12.0%)

The radiation damage sustained by the intermediate asphaltene content bitumen, exposed to the 10keV beam for ten minutes, is juxtaposed with bitumen D. The irradiated area is defined by smoothening of the surface and peripheral accumulation of charge (refer to Figure 5-5(a)). The superior radiation stability of this sample is ascribed to a higher concentration of aromatic systems, associated with higher asphaltene content. Namely, energy adsorption in resonance structures enables radiolytic fragments to isomerise, and stabilise their electron configuration (Charlesby, 1952; Hollinghurst, 1966). This intermolecular energy transfer is offered to explain

the low radiolysis product yield from this bitumen. Analogous behaviour is reported for phenyl systems and alkyl benzenes (Pullman and Pullman, 1963; Jones et al., 1964). Incongruous to the theory published by Rozeveld et al. (1997), aromatic structures and constituent molecules are conceived as dispersed through an upper layer of aliphatics. Moreover, the phenomena of radiolysis and un-saturation are proposed in order to explain the exposure of the network.

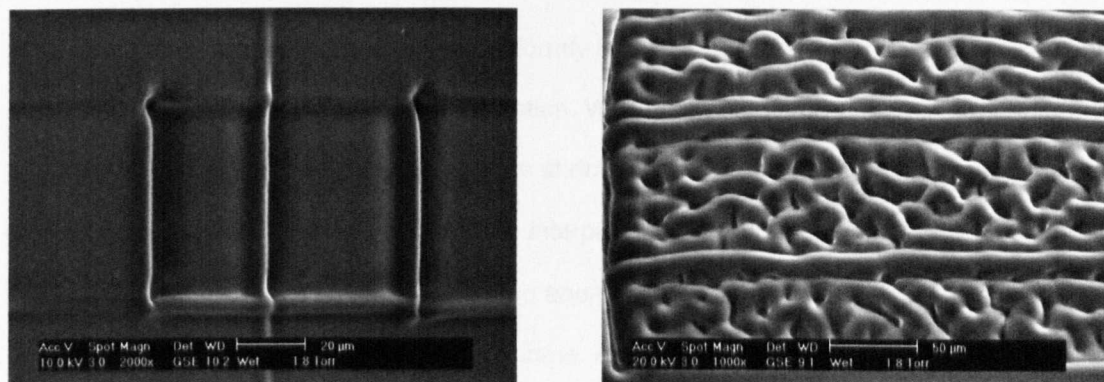


Figure 5-5: (a) Image of charging in bitumen B, irradiated at 10keV and 25°C for 10 minutes. (b) Micrograph of bitumen B irradiated at 20keV and 25°C for 5 minutes.

The radiation stability of this binder decreases with increasing incident beam voltage. Namely, samples irradiated using a 20keV beam for five minutes show a network of myriad string-like structures (refer to Figure 5-5(b)). The direct radiation effect with which this modification is associated is radiolysis (Hobbs, 1979; Howie, 1980). Radiolysis or ionisation damage occurs within each chain by the decay of electric excitation (Egerton et al., 2004). The frequency and intensity of the inelastic scattering events that produce ionisation damage vary inversely with acceleration voltage (Cosslett, 1978; Joy and Joy, 1996). The experimental evidence hereto thus contests theory that damage is proportional to energy deposited in the irradiated sample.

In the electron microscopy literature, this uncertainty is ascribed to energy threshold effects in aromatic molecules (Isaacson, 1975; Li and Egerton, 2004); to the physical extent of artefacts including shrinkage (Joy and Joy, 1996); and to changes in chemical composition (Graham et al., 1984). The carbon-K threshold effect is negligible for the incident electron energies used in this thesis (Isaacson, 1975; Howie et al., 1987; Drummy et al., 2004). Shrinkage artefacts and charging effects produce electrostatic fields that, at high beam voltages, cause dielectric

breakdown and mechanical distortion (Cazaux, 1986; Graham et al., 1994): damage effects at low beam voltages are less notable (Joy and Joy, 1996). The release of ubiquitous hydrogen atoms in the presence of high-energy radiation renders unsaturated bonds on carbon chains, which may form cross-links and glass-like structure (Charlesby, 1952). An analogous effect in polyethylene is ascribed to oxidation under radiation: a wax-like radiation-resistant membrane forms and prevents the loss of dislodged atoms (Alexander et al., 1955). This surface process is distinct from cross-linking that occurs uniformly in a sample (Charlesby, 1952). For bitumen, mass loss redounds to the surface modification. While the contribution of each superimposed mechanism cannot be separated clearly, the shrinkage effects are thought to be secondary to chemical phenomena therefore. A tentative interpretation of the experimental evidence in this thesis is that intense conversion of absorbed energy into chemical change, in the presence of oxygen, produces a diffusion-limiting membrane. At low voltage irradiation this layer captures radicals and atoms heavier than hydrogen: when produced at high voltage irradiation, it is of a higher permeability. This conclusion is accordant with previous discussion on bitumen D.

#### **Bitumen A (Asphaltene content: 18.3%)**

For the high asphaltene content samples, prolonged exposure to the electron beam using an acceleration voltage of 10keV was distinguished by charging along the periphery of the raster-scanned area. At 20keV, damage was by local adsorption of carbonaceous material liberated from the sample, which produces a depression. Consistent with prior discourse it is suggested that aromatic rings behave as sponge-type (Burton et al., 1951) protectors for aliphatics. This transfers much of the ionisation without chemical effect (Manion and Burton, 1952).

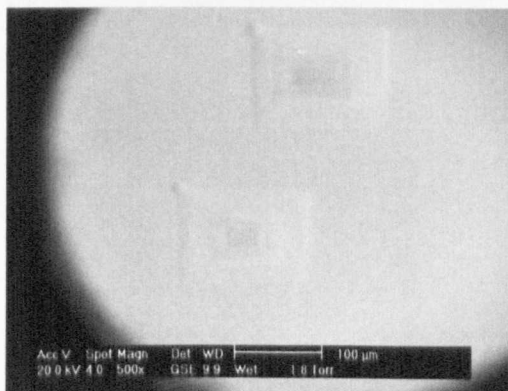


Figure 5-6: Micrograph of bitumen A following irradiation at 20keV and 25°C for 20 minutes.

### 5.1.5 The morphology of bitumen

#### Introductory remarks

In studying bitumen structuring by ESEM it is thought (Rozeveld et al., 1997) that asphaltenes contribute to the myriad entangled fibrils. However, this *a priori* conclusion requires additional empirical evidence. This is the impetus for the initial part of this research section. To quantify microstructural variation with chemistry, images are analysed using parameters introduced by Stangl et al. (2006). These are derived in that paper, and summarised as follows:

1. The mean diameter of the fibrils ( $d$ ), obtained by measurements within ESEM images;
2. The average spacing between adjacent fibrils ( $a$ ), derived from the area confined by a polygon approximating the network structure, using  $a^2 = A_{\text{polygon}}$  (refer to Figure 3-1);
3. The packing density of the fibrils ( $f_s$ ), defined by extracting the two-dimensional ESEM image to the third dimension by assuming an isotropic structure modelled by a simple frame, and then by use of the following equations.

$$f_s = \frac{V_s}{(a/2)^3} \quad \text{Equation 5-1}$$

$$V_s = 3 \times \left[ \frac{A_s}{4} \times \left( \frac{a}{2} - \frac{\sqrt{A_s}}{2} \right) \right] + \left( \frac{\sqrt{A_s}}{2} \right)^3 \quad \text{Equation 5-2}$$

$$A_s = \frac{d^2 \times \pi}{4} \quad \text{Equation 5-3}$$

These parameters are presented schematically below, in Figure 5-7.

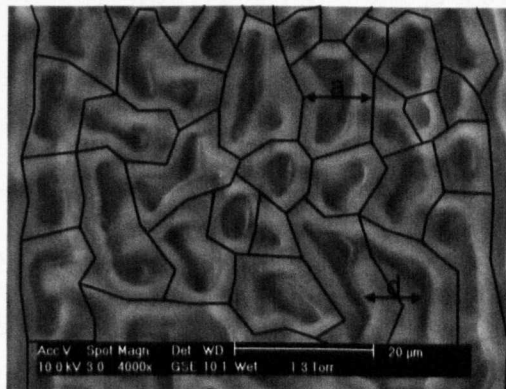


Figure 5-7: Example of quantification of properties of bitumen structure from an ESEM image

### The effect of asphaltene concentration at 25°C

Micrographs of low asphaltene content binder (D) present a continuous network of entangled fibrils undulating through surface hydrocarbons. The constituent fibrils have a mean diameter of 3.9µm (refer to Figure 5-2(a)). The emergence of the embedded network above the surface of the sample is ascribed to a superposition of low pressure and radiolysis: the destruction of intermolecular bonds that reduces cohesion and facilitates a partial expansion of the viscous system. For the intermediate asphaltene content bitumen (B) the irradiated surfaces introduce ubiquitous string-like structures with a mean diameter of 10.6µm (refer to Figure 5-5(b)). The less protrusive state partly validates the preceding explanation. Samples of high asphaltene content binder (A) retain an amorphous state (refer to Figure 5-6). This is ascribed to dilution and dispersion of oligo-aromatic asphaltenic segments within the oily solvent, and the transfer of excitation energy among the fractional molecules. This inhibits radiolysis and volatilisation.

Table 5-3: Parameters developed for ESEM quantification of sample microstructure at 25°C

Sample	Asphaltenes (%)	Fibril diameter, d (µm)		Fibril spacing, a (µm)		Density, f <sub>v</sub>
		Mean	Std. dev.	Mean	Std. dev.	
A	18.3	Samples retain an amorphous state after irradiation at 20keV				
B	12.0	10.6	2.5	27.4	5.4	0.27
D	7.5	3.9	1.2	13.3	4.5	0.17
D (PAV)	13.1	3.0	0.8	7.2	1.4	0.30
-----						
Maltenes (B)	0.0	5.4	1.3	17.3	6.0	0.19
-----						
50/70 <sup>9</sup>	21.3	8.6	1.2	23.3	6.7	0.25
50/70 (PAV) <sup>9</sup>	20.1	5.8	1.8	9.8	1.4	0.53

As with the variation of fibril diameter, the network packing density increases with asphaltene concentration and is partly reflected by penetration (refer to Table 5-3). However, comparison with such parametric description of microstructure in the literature (Masson et al., 2006a), and with samples of bitumen D subjected to oxidation by RTFOT and PAV, creates uncertainty in

<sup>9</sup> Reproduced from Masson et al. (2006a) for comparison. Asphaltenes by latroscan analysis

this correlation: the increased asphaltene content due to ageing manifests as a densification of the network structure but also as incongruous fibrillar contraction. This is explained below.

The formation of ketones, carboxylic acids or other functional groups during ageing increases the polarity of the dispersed and solvent phases in bitumen (Lu and Isacson, 2002). With the incremental reduction of the paraffinic content of the oils (Branco et al., 2001) this could raise the solubility of asphaltenes in the maltenes, which may produce this fibrillar contraction. The densification of this network appears discordant with increased compatibility however, which instead manifests as a higher degree of dispersion (Zhang et al., 2011).

The structural evolution of the interspersed solvent phase may originate from the oxidation of methyl branches, which inhibit efficient ordering during cooling (Vara and Gonzalez, 2012). As an alternative, this could arise from an increased concentration of amphipathic molecules that have both hydrophilic and hydrophobic properties. For similar chemical groups dispersed in a hydrophobic solvent, this can produce structural transitions (Luzzati and Tardieu, 1974).

In petroleum crudes, the occlusion of oils and co-precipitation of wax swells internal structure (Yang and Kilpatrick, 2005). The phase-separated asphaltenic structure in bitumen may also be enriched in these fractions, by dissolution interactions with aliphatics and immobilisation in alkylated asphaltene chains. The dissociation of alkyl or alkyl aromatic side-chains due to the oxidative transformation of resins into asphaltenes (Zhang et al., 2011) could then release the occluded saturated hydrocarbons. This is consistent with an ageing-induced increase in this fraction (Le Guern et al., 2011) and a contraction of fibril structures. This increased non-polar content of bitumen may contribute to reduced compatibility of the colloidal asphaltenes in the maltenic solvent, and thus to the flocculation of the asphaltenes that extends the space-filling character of the network. The author of this thesis suggests this to be the working hypothesis.

### **The effect of sample temperature**

The thermal sensitivity of bitumen microstructure has not created any published studies using ESEM. This has stimulated some research by atomic force microscopy, which has shown that

structure is modified by heat at temperatures coinciding with the melting and crystallisation of waxes. Motivated by this, an inceptive investigation focussed on thermal effects in bitumen D.

Micrographs were collected as samples were heated from 0 to 25°C and then cooled to 0°C, in order to define the thermal variation of surface structure (refer to Figures 5-8 to 5-10). The pronounced stippled surface of samples at 0°C and low magnification is resolved as localised ripple-textures at higher magnification. The emerging parts are 80 to 270nm in width, between immersed strips 200 to 400nm wide: dimensions are comparable with AFM literature. As the bitumen was heated from 0 to 10°C, volatilisation of radiolytic compounds gradually produced the ellipsoidal boundary of the ripples. This process ultimately conferred the impression of an interconnected network (refer to Figure 5-9(a)). On warming to 15°C an abrupt morphological transition occurred: fractions to peripheral bee-like structures coalesced to produce entangled fibrils in which rippled structures could faintly be discerned (refer to Figure 5-9(b)). Desorption phenomena and viscous relaxation at 25°C established this network without observable intra-fibril structures. As sample temperature was returned to 0°C the prevalent rippled texture was restored (refer to Figure 5-10(b)). Notably, after this thermal cycle bee-like structures showed a modified profile. The protuberant strands, initially arch-like in extreme, were almost coplanar with the surface and devoid of clear chromatographic phase boundaries; instead, demarcated by parallel ridges approximately 250nm in width. Key structural parameters are shown below.

Table 5-4: Summary of geometrical properties of dispersed bee-like structures at 5°C

Bitumen	Wax (%)	Peak width (µm)		Trough width (µm)		Ellipse area (µm <sup>2</sup> ) <sup>10</sup>	
		Mean	Std. dev.	Mean	Std. dev	Mean	Std. dev
C	1.26	0.330	0.080	0.199	0.074	-	-
D	1.65	0.249	0.086	0.104	0.047	14.33	4.35
D (RTFOT/PAV)	0.12	0.198	0.045	0.101	0.028	13.36	2.40
AAK-1 <sup>11</sup>	1.30	0.358	0.043	0.193	0.054	-	-

<sup>10</sup> Area incorporating bee-like structure and peripheral paraphase, where distinguishable

<sup>11</sup> Data from Pauli et al. (2011) for comparison. Percentage of crystalline material by DSC

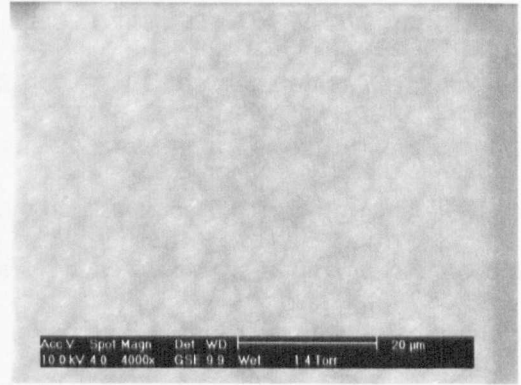
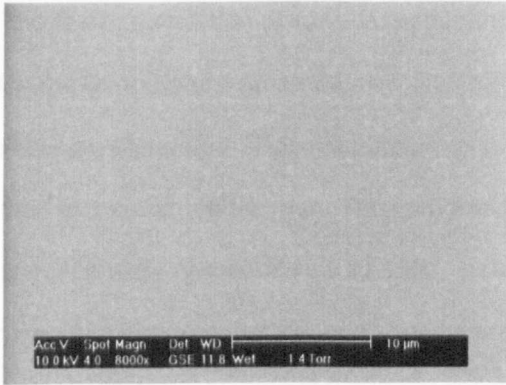


Figure 5-8: (a) Micrograph of bitumen D following irradiation at 10keV and 0°C for 2 minutes.  
 (b) Micrograph of bitumen D following irradiation at 10keV and 5°C for 2 minutes.

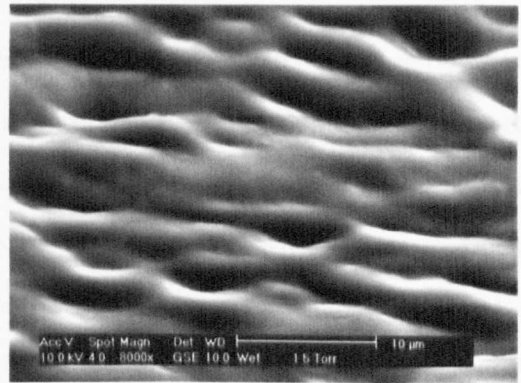
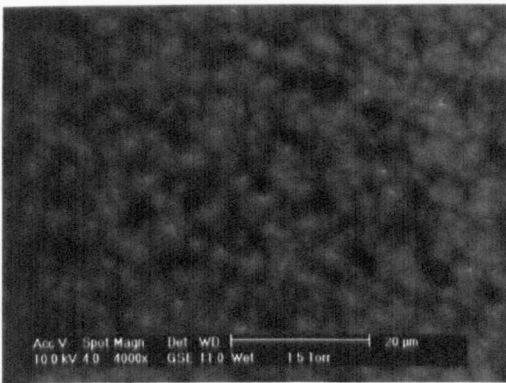


Figure 5-9: (a) Micrograph of bitumen D following irradiation at 10keV and 10°C for 2 minutes.  
 (b) Micrograph of bitumen D following irradiation at 10keV and 15°C for 2 minutes.

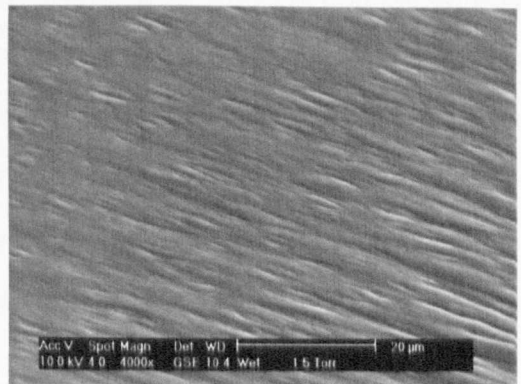
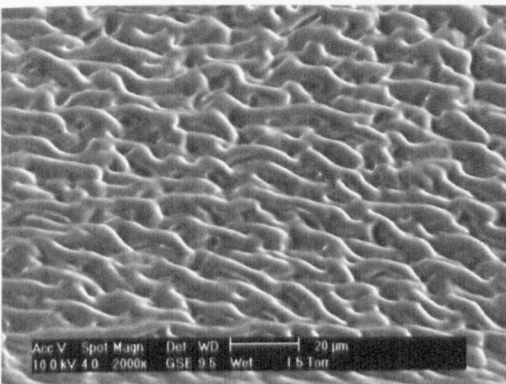


Figure 5-10: (a) Micrograph of bitumen D after irradiation at 10keV and 20°C for 2 minutes.  
 (b) Micrograph of bitumen D captured at 0°C after the thermal cycle (0°C to 25°C to 0°C).

Motivated by the images from this novel research and to bolster the working hypothesis (refer to page 118), this study focused on the thermal evolution of structure in samples of bitumen D oxidised using PAV and RTFOT. The effect of wax content is also studied, using bitumen C.

The thermal variation of surface structuring in the aged bitumen (D RTFOT/PAV) was studied for the temperature range defined above (0°C to 25°C). At 0°C the myriad bee-like structures show an elongated ellipsoidal profile with more numerous but narrower emerging segments than in the unaged bitumen. The immersed parts are of an equal width (refer to Table 5-4). As samples were heated from 0 to 15°C, localised desorption of radiolytic fragments produced a string-like boundary to the local undulations (refer to Figure 5-12(b)). This appears to connect the bee-like structures and to introduce a state of tension that develops the undulations. After warming to 25°C, the peripheral fractions coalesced to form the network that entangles at the position of rippled structures. These recurred on cooling to 0°C (refer to Figures 5-11 to 5-14).

The structural evolution of virgin and oxidised materials over this narrow temperature range is characteristic of the phase behaviour of wax-solvent mixtures (Bhat and Mehrotra, 2004). It is then incongruous that the area of individual bee-like structures is relatively constant on ageing notwithstanding the 92% loss of wax (from D to D RTFOT/PAV) (refer to Table 5-4). Perhaps the chemistry of the bee-like structures is more complex than defined in the literature. That is, different waxes and crystallisable saturated side-chains to aromatic systems may be occluded in this structure. This could in-part explain the negligible change in area due to ageing, as the aromatic fractions are less-susceptible to heating (refer to Table 2-6). The dissolution of these molecules on the periphery of the bee-like structures would explain the polarity in this domain, noted by Jäger et al. (2004), and the capacity for gelation of the waxes, as follows. The nature of interactions between wax crystals is poorly defined (Visintin et al., 2005): weak interactions are thought to occur by crystal overlap and interlock (Holder and Winkler, 1965) and networks form either by diffusion (Radlinski et al., 1996) or spontaneous alignment (Dirand et al., 1998). While the kinetics of gelation lacks clarity, it is suggested that the adsorbed aromatic sections focus attractive interactions, and hence contribute to gelation without observable interlocking.

This discussion and micrographs reported in this novel study are consistent with the working theory, that the entangled network structure in bitumen is enriched with wax. This new theory would explain the fibril contraction due to ageing. Namely, cracking of aliphatic appendages to asphaltene molecules during heating would reduce the integration of these components in the network, thereby reducing fibril diameter. It is interesting that the thermal evolution of bitumen

structure in this thesis occurred at temperatures about 20°C lower than the AFM research by Pauli et al. (2011), who reported that the bee-like structures dissolved at 43°C. This seems to validate the preceding suggestion that ESEM damage is due to radiolysis and not heating.

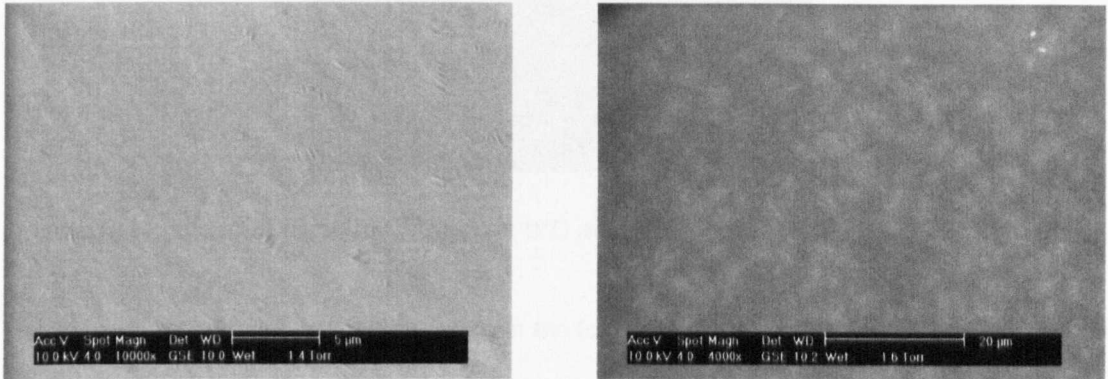


Figure 5-11: (a) Image of bitumen D (aged) after irradiation at 10keV and 0°C for 2 minutes. (b) Micrograph of bitumen D (aged) following irradiation at 10keV and 5°C for 2 minutes.

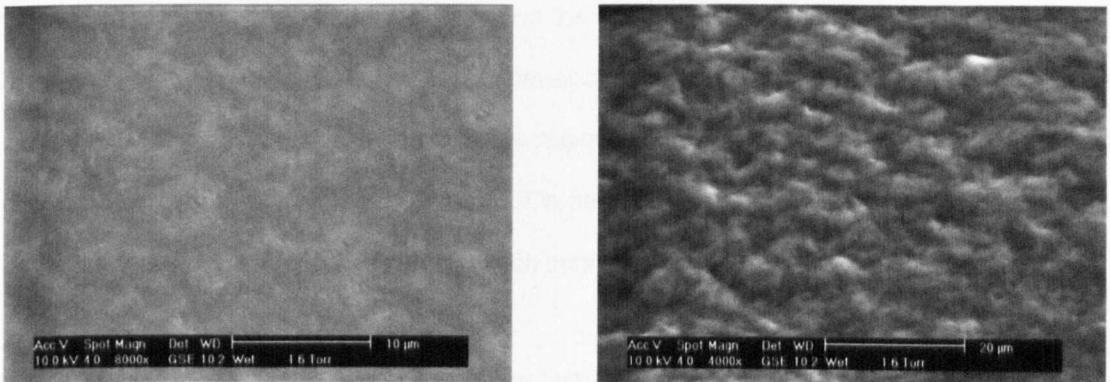


Figure 5-12: (a) Image of bitumen D (aged) after irradiation at 10keV and 10°C for 2 minutes. (b) Micrograph of bitumen D (aged) following irradiation at 10keV and 15°C for 2 minutes.

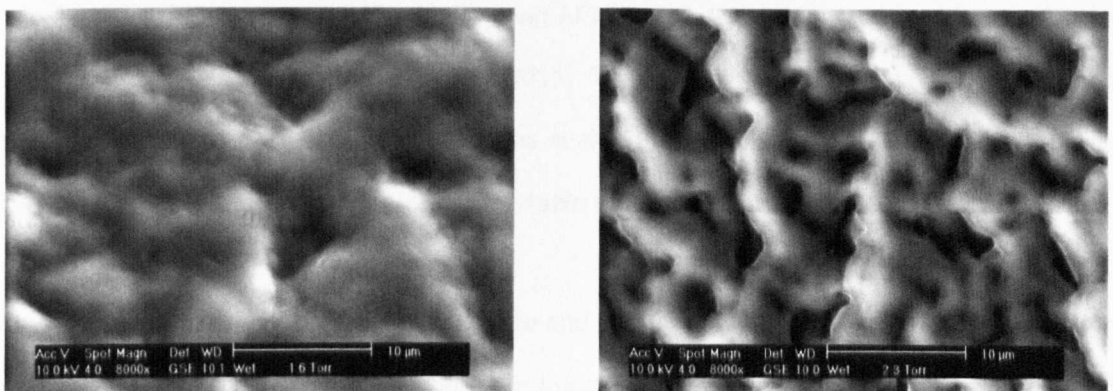


Figure 5-13: (a) Image of bitumen D (aged) after irradiation at 10keV and 20°C for 2 minutes. (b) Micrograph of bitumen D (aged) following irradiation at 10keV and 25°C for 2 minutes.

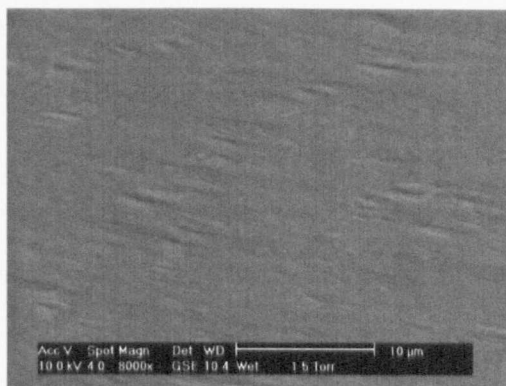


Figure 5-14: Image of bitumen D (aged) at 0°C after the thermal cycle (0°C to 25°C to 0°C).

The thermal variation of surface structure in the low wax content bitumen (C) was studied for the temperature range defined above (0°C to 25°C). Images captured at 0 to 10°C introduce seldom rippled structures hidden on polygonal regions. Micrographs also indicate well-defined pyramid-type protrusions at the surface, and snowflake-like crystals (refer to Figures 5-15 and 5-16(a)). The principal dissimilarities between the bee-like structures in bitumens C and D are the absence of ellipsoidal definition in the former sample, and the appearance of this structure in polygons. At 15°C the interaction of these regions develops pervasive ridges that appear to produce a network (refer to Figure 5-16(b)). On heating to 25°C the entangled structure forms by the consolidation of twisted strands, which confer a rope-like texture (refer to Figure 5-17).

Of the structures shown by bitumen C at low temperatures (0 to 10°C), the most interesting is the mosaic-like dispersion of rhombic plates. These resemble images of wax, but with rippled structuring at the surface of the accumulated polygonal components. Overlapping rhomboids with bee-like structures are also imaged using AFM in non-polar bitumen fractions: waxes that are suspended in solvent oils (Pauli et al., 2011). To explain the local structuring that differs to micrographs of alkanes published by Rhodes et al. (1927) and Edwards (1957), the author of this thesis proposes the inclusion of crystallisable molecules with cyclic segments, as follows.

Cyclic groups (aromatic or naphthenic) at the end of long paraffin chains disrupt crystallisation processes and create physical cross-links in the crystallites. These increase the modulus and tensile strength of this material (Harrison et al., 1992). Concentrations of irregular (Masson et al., 2002) alkane-naphthene-aromatics at the surface of the polygons could thereby produce a

modified crystal structure, which is elastically-strained to equalise to the substrate. This theory could be confirmed by the nucleation of screw dislocations near to the crystallised regions, as noted by Schmets et al. (2010), which form at interfaces due to high elastic strain (Goldthorpe et al., 2008). This strain may introduce local roughening or surface undulations (Greer, 2012), which increase in amplitude by diffusive phenomena, namely Marangoni convection.

The postulated involvement of crystallisable molecules with cyclic segments would explain the structural change of bee-like structures due to ageing, as reported in this thesis for bitumen D (refer to Table 5-4). The peaks contract as the strain energy gradient driving surface diffusion is reduced by homogenisation of the crystallite, as the aliphatic segments crack during ageing and lose cyclic groups. This also explains the absence of bee-like structure in waxy bitumens: only cyclic fractions with paraffin side-chains of sufficient length contribute to crystal growth.

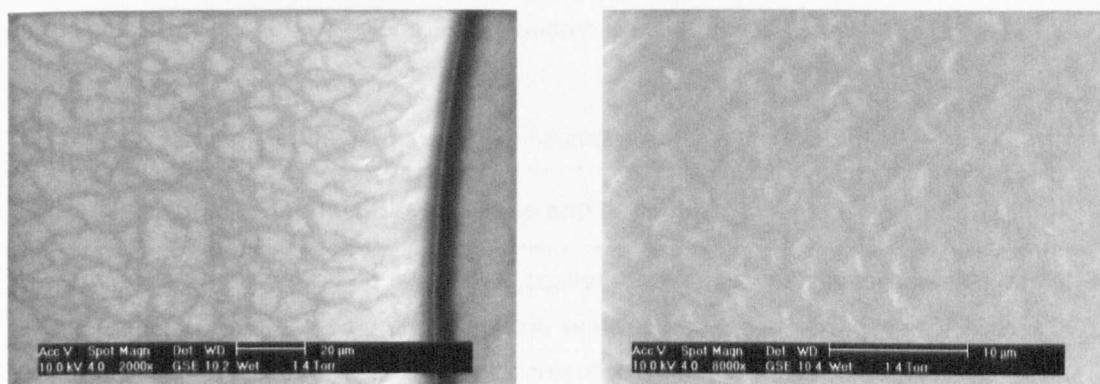


Figure 5-15: Micrographs of bitumen C after irradiation at 10keV and 0°C for 2 minutes.

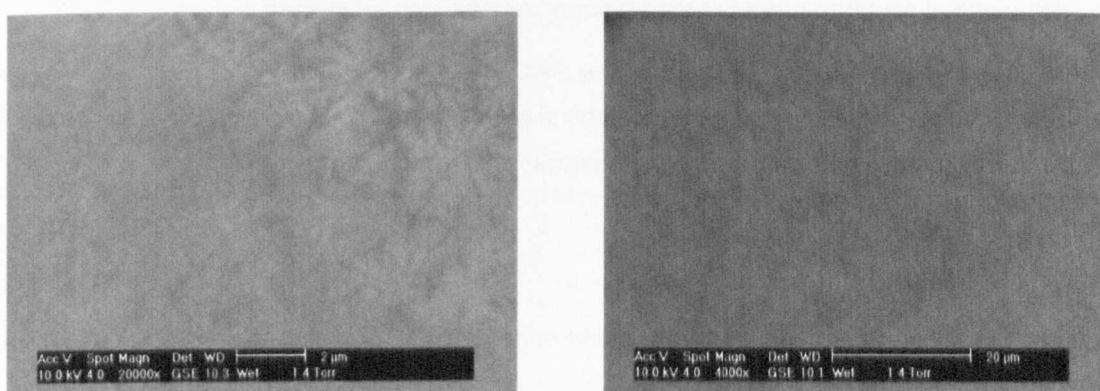


Figure 5-16: (a) Micrograph of bitumen C after irradiation at 10keV and 0°C for 2 minutes. (b) Micrograph of bitumen C following irradiation at 10keV and 15°C for 2 minutes.

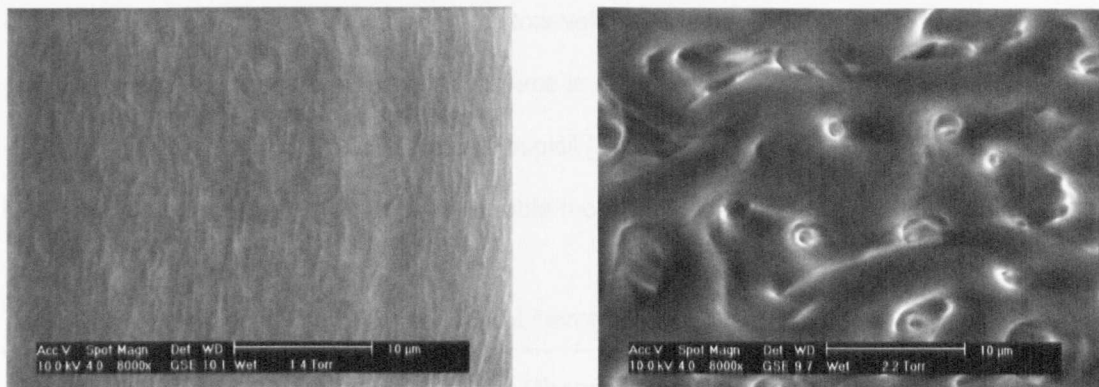


Figure 5-17: (a) Micrograph of bitumen C after irradiation at 10keV and 20°C for 2 minutes. (b) Micrograph of bitumen C following irradiation at 10keV and 25°C for 2 minutes.

### 5.1.6 The morphology of bitumen fractions

From the analysis reported in this section of the thesis and published in the literature, bitumen structure is associated with the asphaltenes, maltenes and waxes. This thesis uses the ESEM for a novel study on these fractions. This research is summarised below, in Table 5-5.

Table 5-5: A summary of the morphology of bitumen fractions using ESEM

Sampled fraction	Outline observations and explanation
Asphaltenes	Amorphous surfaces scattered with particles. Insusceptible to radiolysis The amorphous state is sustained by the solubility of asphaltenes in the solvent, and in the microscope by the protective effect of aromatics.
Maltenes	Radiolytic effects develop an entangled network analogous to bitumen. The network structure is produced in-part by low molecular weight and less polar asphaltenes, retained after chromatographic fractionation.
Waxes	Rhombic paraffin crystals with a globular structure at the surface. Secondary structuring is developed by cyclic compounds which deposit on the surface at low temperatures, in accordance with p. 124

#### Asphaltenes

Micrographs of the asphaltenes extracted from bitumen B present an amorphous surface that is insusceptible to radiolysis, after irradiation at 20keV and 25°C for up to 20 minutes (refer to Figure 5-18(a)). The stability of the sample is consistent with preceding theory that damage is reduced by aromatic fractions, which transfer ionisation without chemical effects. Notably, this

explanation differs from the conclusion of Rozeveld et al. (1997), which stated that damage is due to heating effects. The amorphous surface is inconsistent with ESEM images reported by Rozeveld et al. (1997) and Stulirova and Pospisil (2008), who showed particulate texture. This literature is summarised in Table 5-6 to enable the discussion that follows.

Table 5-6: Chronological summary of ESEM literature on asphaltene morphology

Author	Method	Observations on morphology
Rozeveld et al. (1997)	ASTM D4124-86	Virgin binder: particles of 0.2-0.3 $\mu$ m TFO/PAV aged binder: particles of 0.8-1.2 $\mu$ m
Stulirova and Pospisil (2008)	CSN 65 6073 <i>n</i> -heptane elution	Porosity destroyed by toluene evaporation Particles of 0.11-0.26 $\mu$ m, for diverse reflux times  C <sub>3</sub> part: smooth surface due to co-precipitation of semi-solid resins
Luo et al. (2010)	ASTM D2007-03	C <sub>5</sub> part: porous structure; 2.0-4.0 $\mu$ m particles C <sub>7</sub> part: smooth surface due to slow precipitation; thus, growth of aggregates with tighter structure

An explanation of the structural properties of asphaltenes that differ in this thesis compared to the literature may refer to variant elution times, and the different petroleum crude sources and chemical characteristics of this fraction. However, Stulirova and Pospisil (2008) indicated that the effect of binder-solvent contact time is minimal, and Luo et al. (2010) reported amorphous and particulate structuring in residues of both light and heavy asphaltenes (refer to Table 5-6). The author of this thesis instead proposes an explanation regarding asphaltene fractionation.

Rozeveld et al. (1997) used Corbett fractionation (ASTM D4124-86) to separate asphaltenes from AC-10 viscosity grade bitumen. Stulirova and Pospisil (2008) also extracted asphaltenes by elution in heptane, from 70/100 penetration grade bitumen. Both studies eschewed toluene dissolution of the residue which is used in this thesis according to BS 2000-143:2004. Lin and Yen (1993) and Speight (2004) showed that pre-asphaltenes, resins and reactive compounds adsorbed on the asphaltenes are only separated using toluene. Anderson and Speight (1992) indicated that separation of these constituents rearranges the residual molecular interactions, which may explain structural variation. Namely, platelet structuring of precipitated asphaltenes

could be sustained by adsorbed groups of low solubility in heptane, but perturbed by washing in toluene as molecular interactions are eliminated. This enables self-association phenomena between isolated asphalts that produce an amorphous material. Importantly, this explanation highlights the requirement for a consistent definition of the asphaltene fractionation method.

Though generally amorphous, there is a profusion of topographical detail on each surface that was fractured during the scraping process. This includes river lines that are common in cloven brittle materials (Low, 1963), and so called due to a pattern analogous to that produced by the confluence of streams (Hull, 1999). This structuring constitutes a series of steps formed at the intersection of a planar crack with a screw dislocation (Gilman, 1956), and lines parallel to the direction of crack propagation (refer to Figure 5-18(b)). These tortuous crack trajectories can also develop by crack deflection or transient arrest, which are phenomena encountered at an interface in a composite material (Gac, 1990). This structuring is particularly interesting due to its analogy to the morphology of fractured bitumen (refer to Section 5.3). This supports theory in Section 5.3 that the asphaltene contribute significantly to the brittle properties of bitumen.

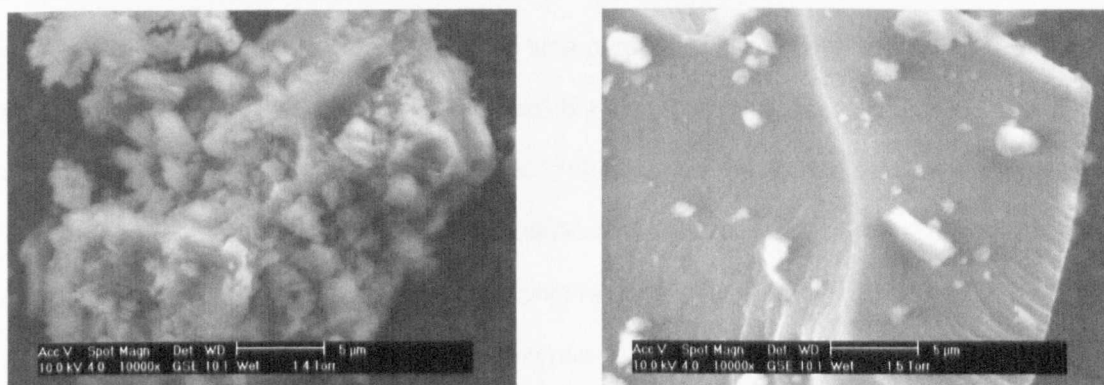


Figure 5-18: (a) Micrograph of asphaltene after irradiation at 10keV and 25°C for 2 minutes. (b) Image of fracture detail in asphaltene after irradiation at 10keV and 25°C for 2 minutes.

### Maltenes

To reduce the radiation sensitivity of the maltenes fractionated from bitumen B, samples were firstly cooled to -5°C on the Peltier stage prior to evacuation of the ESEM chamber, and then irradiated at temperatures of -10 to 0°C. Micrographs after 15 seconds exposure to the 10keV beam at -10°C indicated damage by the partial abstraction of superficial hydrocarbons. After

60 seconds of irradiation, the sample exhibited a network of highly-entangled fibrils ubiquitous in bitumens. Fibrillar definition was improved subsequent to irradiation for 120 seconds, and this radiolytic state was imaged at every temperature (refer to Figure 5-19).

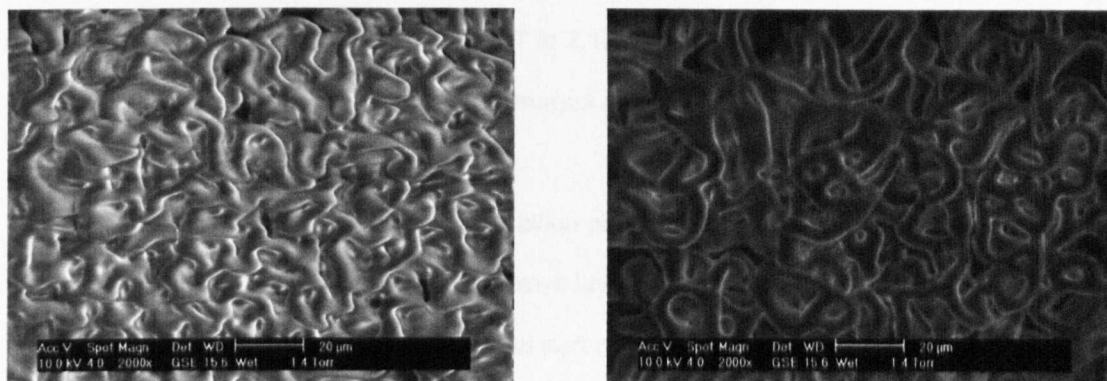


Figure 5-19: (a) Micrograph of maltenes after irradiation at 10keV and  $-10^{\circ}\text{C}$  for 1 minute. (b) Micrograph of maltenes after irradiation at 10keV and  $-10^{\circ}\text{C}$  for 2 minutes.

One explanation for this unique finding is that the network is free of heptane insoluble organic (asphaltenes) and inorganic materials. This is the antithesis of published theory. Research by Pereira et al. (2011) on the precipitation of asphaltenes in heptane suggests that this process requires elution for 250 hours at  $22^{\circ}\text{C}$ . The time parameter of asphaltene fractionation hence influences the composition of the heptane soluble components (maltenes) that are recovered after evaporation of the eluent (Speight et al., 1984). Under the elution conditions specified in BS 2000-143:2004 and used in this thesis (elution for 2 hours at  $22^{\circ}\text{C}$ ), the maltenes fraction could retain low molecular weight and low polarity asphaltenes in the dimer and trimer state (Pereira et al., 2011). These retained asphaltenes could contribute by hydrogen bonding to the network. To conclude, the asphaltenes are not the only fraction involved in this structure.

### Paraffin waxes

The paraffin waxes purified and crystallised from the distillates of binder B were cooled to and initially irradiated at  $5^{\circ}\text{C}$ , to preclude microscope contamination arising from the abstraction of liquid fractions at near-ambient temperatures (Messerly et al., 1967). Micrographs captured at low magnification present a highly-wrinkled paper-like surface (refer to Figure 5-20(a)). These succinctly evidence rhombic paraffin crystals by the footprint of the folds, which formed due to

shrinkage on cooling or by the development of curved crystals due to polydispersity (Hubbard, 1945; Edwards, 1957; Glaeser et al., 2011). Despite mechanical ambiguity, myriad creases confer a honeycomb-type texture that is suppressed along the torn periphery of the sample by fibrous structure (refer to Figure 5-20(b)). At high magnifications the inter-fold domains exhibit globular structuring: rounded particles of 0.7 to 2.1  $\mu\text{m}$  in diameter. Interestingly, the inherency of this composition is confirmed by similar images at 0 to 20°C (refer to Figure 5-21(a)).

Micrographs at 0°C define anisotropic crystalline plates that are often curled along their edges towards an acicular habit, but which are always layered (refer to Figure 5-21(b)). Discrete and interconnected globules saturate the median part of overlapping layers. These are ascribed to low molecular weight cyclic compounds that deposit mainly at low temperatures at the surface of fused material (Edwards, 1957). This structuring also persisted at 20°C, but definition of the globules was reduced perhaps due to melting by thermoelectric heating. Beam heating effects could also be involved, but citation thereof is omitted because the samples are otherwise not modified. This could indicate a high proportion of branched, aromatic and alicyclic molecules.

The novel micrographs and discussion presented in this section of the thesis are notable: the author previously postulated that crystallisable molecules with cyclic segments are involved in the bee-like structuring (refer to page 124). This microscopy study on the waxes suggests that this theory is reasonable, and that other fractions contribute to the undulating characteristic.

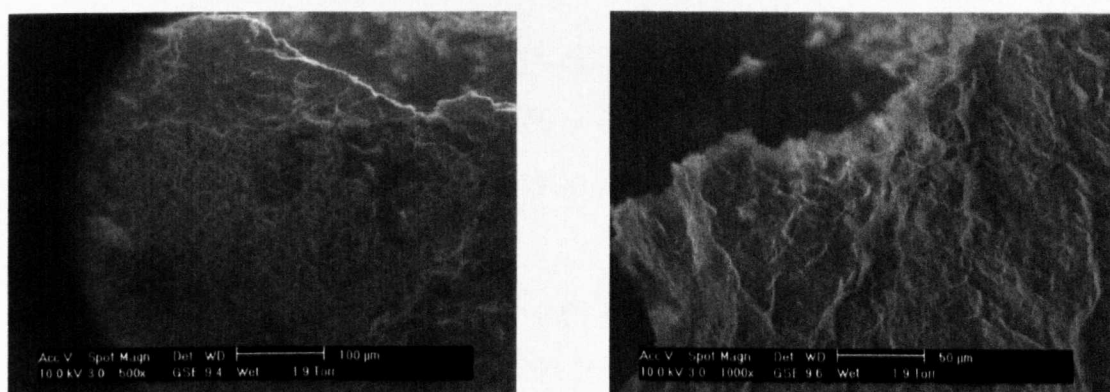


Figure 5-20: (a) Low resolution image of wax after irradiation at 10keV and 5°C for 1 minute. (b) High resolution micrograph of wax after irradiation at 10keV and 5°C for 1 minute.

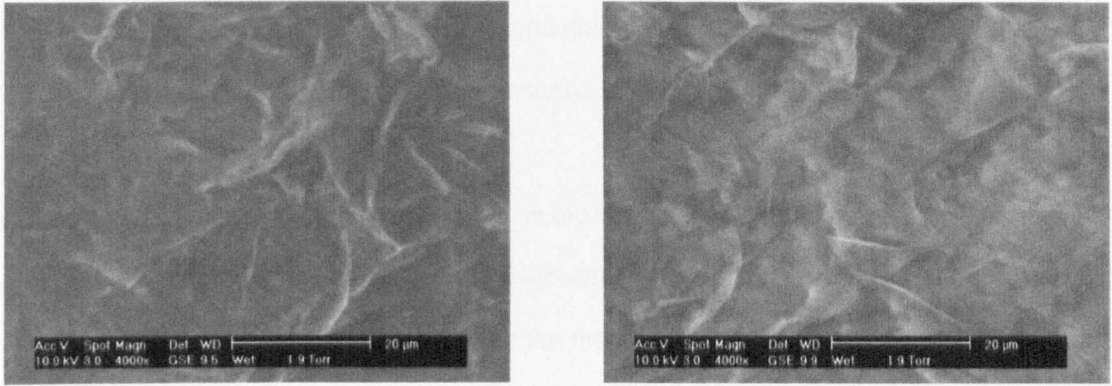


Figure 5-21: (a) Micrograph of waxes after irradiation at 10keV and 20°C for 1 minute. (b) Micrograph of waxes after irradiation at 10keV and 0°C for 1 minute.

### 5.1.7 Discussion

The sensitivity of bituminous materials to radiation damage is shown in this thesis to decrease with temperature. For the low asphaltene content bitumen B damage commenced at 5°C, and involved desorption of radiolytic fragments from between ellipsoidal dispersions. This process matured at 10°C and produced the basal globular texture of these structures. The next phase of decomposition was initiated at 15°C by the delocalisation of desorption: the vaporisation of particles evolved from the irradiated sample produced ubiquitous network structuring, but with the usual separation of fibrils obscured by beam-resistant material. For samples of this binder oxidised using RTFOT and PAV, this response was retained but shifted by 10°C. Namely, the local desorption processes persisted from 15 to 25°C, when they delocalised.

An explanation for this response that is coherent with the literature is that sample temperature superposed with beam heating coincided with thermally-activated steps in the decay process, thus producing a finite mass loss. More logical is an explanation regarding molecular mobility.

Rozeveld et al. (1997) calculated the sample temperature due to beam heating as 200°C. The mean molecular thermal energy due to this effect is analysed by the product of the Boltzmann constant and temperature: 0.034eV. For light hydrocarbons, the ionisation channels with the lowest activation energies are the losses of H, H<sub>2</sub> and C<sub>2</sub>H<sub>2</sub>, which are in the range of 4.1 to 4.6eV (Charlesby, 1952; Liang and Lifshitz, 1998). The disparity between molecular thermal

energy and beam heating effects indicates that the activated radiolytic particles are produced by inelastic electron scattering (radiolysis), and not by thermal energy (Li and Egerton, 2004). This explanation is consistent with theory reported in this section of the thesis.

It is emphasised that whilst this explanation is incongruous with the conclusion of Rozeveld et al. (1997), it does not preclude enhanced degradation by heating. Notably, the theory derived in this thesis explains the disparity between the maximum temperature attained at the surface and that required for pyrolysis (refer to Section 2.6.2). The exposure of network structure in a sample of nanometric thickness, which is hence in close thermal contact with the heat sink, is verification for this theory (refer to Figure 5-22).

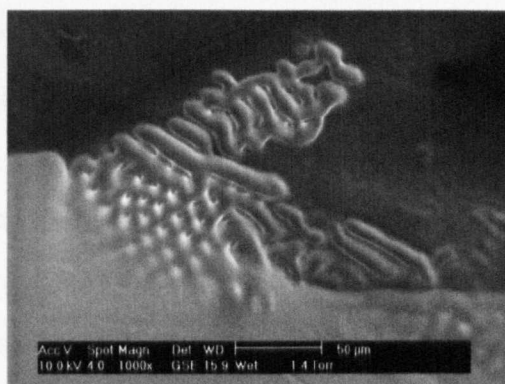


Figure 5-22: Image of thin bitumen D sample after irradiation at 10keV and 20°C for 1 minute.

### 5.1.8 Summary

The variation of damage with asphaltene content originates the theory of surface modification by radiolysis and not by heating. This highlights the protective effect of aromatic fractions and chemical alteration. Network structuring is imaged at various temperatures in bitumen and, for the first time, in the maltenes fraction. This novel use of thermal control in the ESEM suggests that this structure develops by the precipitation of crystallisable paraffinic segments, which are imaged at low temperature as ellipsoidal bee-like structures. These form due to compositional effects and catalyse gelation by the concentration of polar interactions due to co-precipitation of aromatics. The co-precipitated chains establish the elongated character of these structures.

## **5.2 CRYOGENIC SCANNING ELECTRON MICROSCOPY**

Despite many published studies on bitumen structure, knowledge of bulk structural properties remains elusive. Using a freeze-fracture preparation technique, this section describes original micrographs of the amorphous bulk of low asphaltene content bitumen (D) and maltenes from bitumen B. These materials have shown profuse topographical detail in ESEM: the aromatics in high asphaltene bitumens decrease surface structuring due to wax deposits and inhibit the observation thereof.

### **5.2.1 Background**

The simplest method to reduce deterioration of a macromolecular complex in the presence of radiation is freezing (Low et al., 1966; Taylor and Glaeser, 1973). The potential for cryogenic preparation in electron microscopy of thin layers was realised in the late 1950s and evolved in the early 1960s, towards analyses of bulk samples (Fernández-Morán, 1966; Walther, 2008). This technique is based on the principle that rapidly freezing a sample physically suspends its fluids in a vitreous ice. This lowers their vapour pressure and thereby limits the evaporation of the compounds that sustain naturally-occurring structure (Luo, 2007; Greiser, 2009). To arrest volatile fractions, avoid damage by products of radiolysis (Sheehan, 1995), and thus preserve the physicochemical state of a material during electron irradiation, the sample is immersed in sub-cooled nitrogen. This liquid and solid nitrogen slush is used for its superior heat-transfer characteristics compared to the liquid, and higher low-resolution contrast between ice crystals and biological samples (Dokland et al., 2006; The John Innes Centre, 2007; Zhou, 2008).

### **5.2.2 Review of pertinent literature**

Mikula and Munoz (2000) used cryo-SEM to study the structure of colloidal particles in water-in-oil emulsion; clay particles suspended in oil sand tailings; and refinery coke. Samples were plunged into liquid nitrogen and fractured, and imaged uncoated at  $-180^{\circ}\text{C}$ . The structuring of these materials was also studied using confocal laser-scanning microscopy. For the oil sand tailings this revealed subtle preparation artefacts associated with freezing and sublimation in cryo-SEM. That is, a flocculated system of edge-to-edge interactions between clay plates was

thought to be produced by ice crystal formation in the oil phase, and not an intrinsic structure.

In research by Wilson et al. (2000), heat-cast samples of pure and polymer-modified bitumens were cooled in sub-cooled nitrogen at  $-202^{\circ}\text{C}$ , and fractured *in vacuo* at  $-160^{\circ}\text{C}$ . The samples were then coated with 4nm of platinum using ultrapure argon gas. The internal morphology of pure binder was mainly featureless with low topographical contrast, but with irregular fracture stops: remnants of changes in the fracture plane where the crack encountered a dense phase in the matrix. In polymer-modified bitumen, styrene-butadiene block copolymer particles in the continuous bitumen phase showed plastic deformation after fracture, but the bitumen retained low contrast and a mirror-like appearance. Plasticity was explained by the more-rubbery state of the butadiene monomer on fracture due to a glass transition at  $-90^{\circ}\text{C}$ , in contrast to styrene at  $70^{\circ}\text{C}$  and bitumen at  $-27^{\circ}\text{C}$  (Wilson et al., 2000) to  $-20^{\circ}\text{C}$  (Masson and Polomark, 2001).

The authors of that published study subsequently examined the structure of polymer-modified bitumens using ESEM and cryo-SEM (Champion et al., 2001; Champion-Lapalu et al., 2002). Internal structuring was exposed by fracture using three-point flexure at  $-20^{\circ}\text{C}$ . Similar to their previous paper, the bitumen moiety retained a glassy state and the polymer particles showed plasticity. Moreover, the fractures propagated along the interface between the two phases by pull-out of the polymer micelles. The authors hence postulated that the mechanism of fracture is governed by adhesion between polymer-saturated domains and the bitumen. The inclusion of the polymer phase contributed to a toughening of the bitumen, which compelled discussion on fracture behaviour. Namely, toughening was explained by the processes of crack pinning: stiff inclusions impede or pin an approaching crack and thus augment the fracture plane and increase fracture energy (Smith and Hesp, 2000), and crack bridging: ductile particles inhibit crack opening by physically-bridging this plane (Broberg, 1999; Kotoul and Vrbka, 2003). The authors suggested that neither phenomenon fully explains fracture in bitumen, and concluded that peripheral definition of the particles indicates the transition between stable fracture in the matrix, and instability near to the polymer phase. The research also concluded that cryo-SEM extends the resolution of observations by ESEM and by ultraviolet fluorescence microscopy.

### 5.2.3 Sample preparation

The methods used to prepare microscopy samples of low asphaltene content bitumen (D) and maltenes from bitumen B are explained here. These materials showed profuse topographical detail and high susceptibility to electron damage in ESEM, and are hence the most promising for this research.

To study surface structures in bitumen, thin-film samples were prepared as defined in Section 5.1.2. The preparation method for maltenes was modified in order to prevent contamination of the vacuum by ubiquitous hydrocarbons: molecules that dissociate from the sample under an electron beam at high vacuum or at cryogenic temperatures ( $-165^{\circ}\text{C}$ ). These deposit from the vapour or solid phase onto the chamber walls and sample surface as a carbonaceous residue that limits analytical precision (Gupta and Stallcup, 2006). To reduce the irradiated area and improve sample retention, brass rivet mounts used in studies on leaf xylem and chytrid fungus (Berger et al., 2005; Johnson et al., 2009) were selected. The mounts were washed in toluene and acetone and then warmed to  $40^{\circ}\text{C}$  to ensure sample adhesion. This heating is below the glass transition temperature of the multi-ring segments common to aromatics and resins, and will thus minimise thermal distortion of intrinsic structuring. The maltenes were heated to  $40^{\circ}\text{C}$  in a borosilicate glass basin and sampled using a warm penetration needle. One large droplet was promptly delivered into each rivet. For precision of sampling and microscopy analysis the preparation time was limited to 30 seconds, and samples were annealed for 24 hours at  $25^{\circ}\text{C}$  prior to imaging (refer to page 108 for justification).

Application of the rivet mount is novel and essential: cross-sections of maltenes and bitumen samples were also produced using this cryo-assembly. For the maltenes a large droplet, cast as above (at the tip of a penetration needle), was inserted as an adhesive between two rivets that were aligned in a head-to-head orientation (refer to Figure 5-23). Bitumen samples were produced analogously, but using sampling and preparation temperatures of  $130^{\circ}\text{C}$ . Following annealing and influenced by a study on rice seedlings by Faiyue et al. (2010), the rivets were mounted onto a cryo-shuttle and plunged into sub-cooled nitrogen at  $-210^{\circ}\text{C}$ . This assembly was transferred *in vacuo* into a Quorum Technologies sample preparation system. This cryo-

trapped high vacuum preparation chamber: of  $10^{-3}$  Pa or better, ensured a contamination-free environment to produce fracture surfaces (Wilson et al., 2000). The upper rivet was displaced by a cooled knife, exposing an internal surface of each material for SEM (Berger et al., 2005).

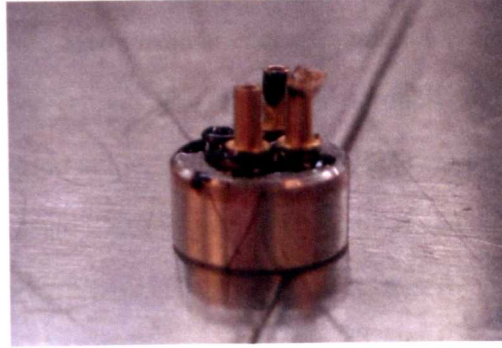


Figure 5-23: Sample pressed between two rivet mounts for fracture under cryo conditions.

#### 5.2.4 Sample testing

The microscope used for this investigation was a FEI Quanta 200 3D FEG-SEM/FIB equipped with a Quorum Technologies PP2000 preparation system. The whole or fractured specimens were etched in the preparation chamber by ice sublimation at  $-90^{\circ}\text{C}$  for up to ten minutes, and then re-cooled to  $-165^{\circ}\text{C}$ . The surfaces were sputter-coated by low energy input with platinum films of 2 to 5nm thickness, to ensure adequate electrical conductivity and secondary electron yield without loss of resolution (Wilson et al., 2000). The samples were then transferred onto the cold stage in the SEM chamber then imaged at  $-165^{\circ}\text{C}$ . Micrographs were collected using an acceleration voltage of 5 or 10keV and probe currents of 90pA, 0.12 or 0.18nA. The effects of prolonged irradiation arising from such highly beam-sensitive materials were moderated by initially focussing on an area remote to the field of interest, whilst a temperature differential of  $-25^{\circ}\text{C}$  between the cold trap and the sample surface reduced the accumulation of ionised and contaminating materials at an imaged section.

#### 5.2.5 The morphology of bitumen

Low magnification micrographs of low asphaltene content bitumen (D) reveal the dilated state of the sample: the surface is covered by bubbles that formed due to aeration and agitation on plunging into the nitrogen slush (refer to Figure 24(a)). At high magnifications, myriad bee-like

structures cover the surface, which is modified also by linear fractures (refer to Figure 24(b)). These are common in crystalline materials (Liu, 2005) and evidence of a brittle propagation of pure tensile stress at the crack tips. The primary cleavage planes are thought to have formed by anisotropic shrinkage on quenching, and involve aborted in-plane secondary fractures that produce a complex branched system within inter-ripple domains as fracture energy dissipates (refer to Figure 3-25(a)). The propagation of fractures through dispersions is most interesting: secondary cracks are arrested in the smooth matrix near to rippled structures; primary cracks traverse through both the dispersed and solvent phases but seldom along the solute-solvent interface (refer to Figure 3-25(b)).

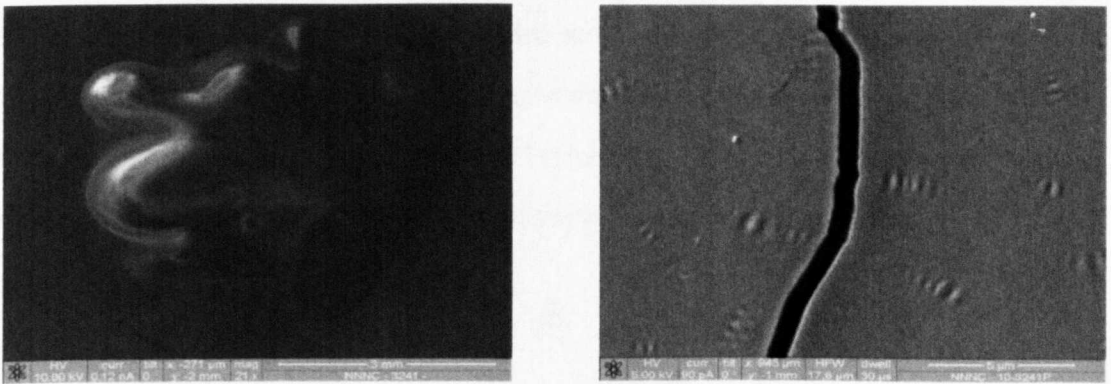


Figure 5-24: (a) Electron micrograph of bitumen D showing the effects of freezing in the slush. (b) Electron micrograph of bitumen D showing bee-like structures and cracking.



Figure 5-25: (a) Electron micrograph of bitumen D showing an aborted secondary crack. (b) Electron micrograph of bitumen D showing cracked bee-like structures.

From a mechanical perspective, an interface between elastically-incompatible parts acts as a natural stress inducer. This attracts high stresses and is prone to cracking when the material

is exposed to thermal or mechanical load (Schmets et al, 2010). The infrequent observation of solute-solvent interfacial cracks suggests that this two-phase system forms with continuously-distributed properties. This is explained by conformational effects and depletion fractionation.

In accordance with Section 5.1.5, suppose the bee-type structures form by the precipitation of waxes and then occlusion of crystallisable paraffinic appendages on aromatic molecules. The polar sections could produce a surfactant-like layer around the crystallite, in which immiscible groups align in order to compensate the energetic penalty due to the creation of the interface (Pons-Siepermann and Glotzer, 2012). The exclusion of light solvent molecules from the edge of this structure develops a depletion layer, due to a loss of conformational entropy within this region. Where two layers overlap, imbalanced osmotic pressure yields an effective attraction between the particles and a gain in free volume accessible to lighter molecules (Goulding and Hansen, 2001; Lekkerkerker and Tuinier, 2011) (refer to Figure 5-26). This mechanism could contribute to the continuum between the crystalline and amorphous phases.

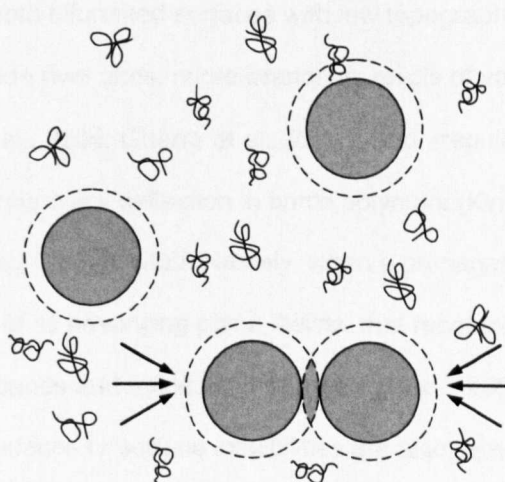


Figure 5-26: Schematic of overlapping depletion layers and unbalanced osmotic pressure (Lekkerkerker and Tuinier, 2011)

The morphology of one fractured surface indicates wax-induced phase separation in the bulk: bee-type structures are imaged to a depth of about 25 $\mu\text{m}$  scattered between depressions that were perhaps cast by pull-out of this localised structure (refer to Figure 5-27). The mean width of the strands (0.263 $\mu\text{m}$ ) is analogous to that of surface ripples (refer to Table 5-4). Suppose that the fracture occurred due to quenching; the separation and configuration of the structured

phase are not simply due to free surface-effects, but are material properties. Consistent with the literature reviewed in Section 5.1.2, the structuring is exposed by apparent incompatibility or poor adhesion with the matrix. This challenges the previous discussion.

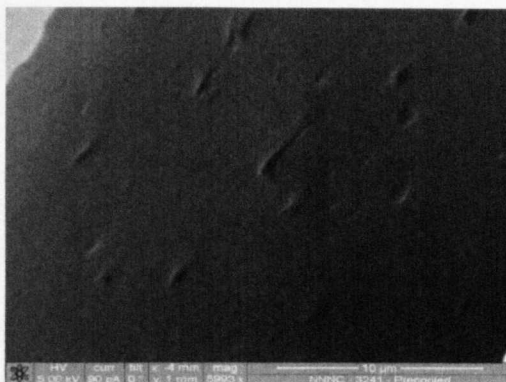


Figure 5-27: Electron micrograph of near-surface bee-type structuring in bitumen D at a crack.

### Fractured samples

Micrographs of samples fractured *in vacuo* at  $-165^{\circ}\text{C}$  show morphological features similar to published literature. Smooth bifurcated surfaces with low topographical contrast saturate slow fracture zones and precede river lines, micro-branches: relicts of variable crack plane velocity and tortuosity (Zhang et al., 2006; Guerra et al., 2011), and irregular cleavage stops (refer to Figure 5-28(a)). To describe crack deflection in brittle polymers (Kinloch and Taylor, 2006) the study of Faber and Evans (1983) is cited. Namely, when a propagating crack interacts with an inhomogeneity it tilts out of its advancing plane, twists, and recombines during re-propagation to produce brittle failure bands and relinquish fragments (Gac, 1990) (refer to Figure 5-28(b)). Discontinuous fracture surfaces or surface instabilities are also be explained by crack arrest due to plastic dissipation of fracture energy at the crack tip (Kinloch and Williams, 1980).

Domains peripheral to these surface instabilities show profuse topographical detail. Notably, faceted surfaces that are produced by cleavage due to quench-separation of chemical phases in the sample; out-of-plane pyramidal instabilities caused by crack velocity changes (Fineberg et al., 1991); and fine planar layers similar to graphite (refer to Figure 5-29(a)). This layered structure may reflect parallel pi-pi stacking within concentrations of polyaromatic segments of the molecules (refer to Figure 2-5). The stacks of nanometric thickness appear to cause long-

range order in the matrix, to the emergence of repeating layers: 2 to 10 $\mu$ m in profile. Images of parabolic protrusions and spindle-shaped cast marks at the surface indicate the distribution of stress between fracture surfaces, and ductile deformation (refer to Figure 5-29(b)).

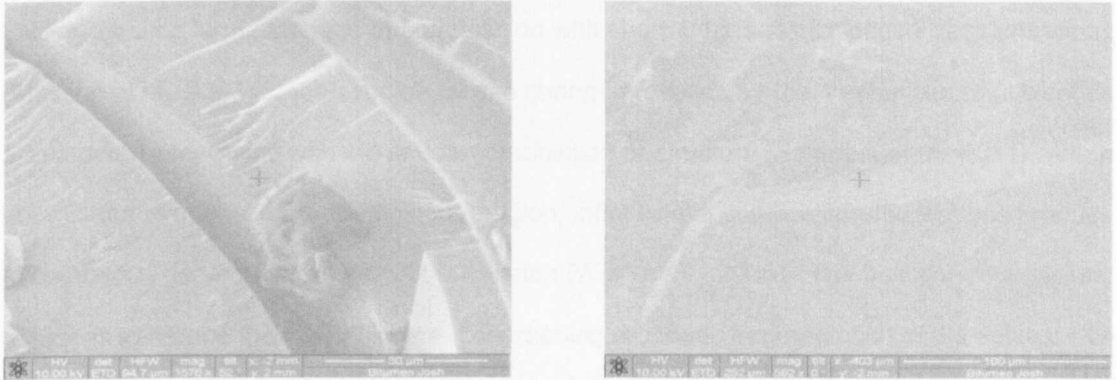


Figure 5-28: (a) Cryo-SEM micrograph of the bulk of bitumen D, produced by *in situ* fracture. (b) Micrograph of bitumen D showing the fragmented structure of the fractured surface.

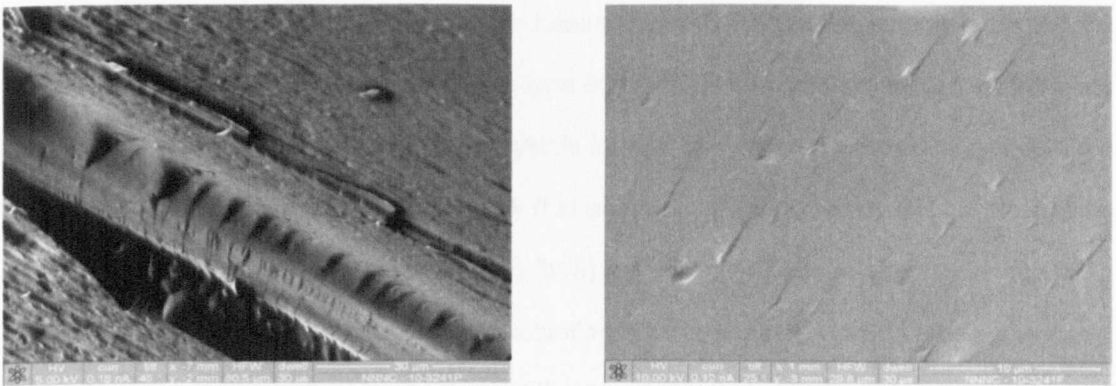


Figure 5-29: (a) Micrograph of the bulk of bitumen D showing pyramidal instabilities and planar layering. (b) Micrograph of parabolic cast marks in the bulk of bitumen D.

The internal morphology of bitumen, devoid of structuring ubiquitous in its uppermost layers, explains the enigmatic phase separation. Namely, while waxes occur throughout the material, anisotropic conformational entropy or surface tension establish the proclivity for wax diffusion towards the surface. This is detected by a turbid appearance (Knowles and Levin, 1941) and reduced surface free energy (Wei et al., 2010). This preferential wetting by waxy components produces a change in composition: so-called compositional strain (Williame et al., 1974), and the phenomenon of surface-directed spinodal decomposition that may extend into the bulk.

Spinodal decomposition in a bulk is well understood: when an initially homogenous composite is quenched into a region of thermodynamic instability, phase decomposition occurs by long-range diffusion (Wise et al., 2005). In the metastable region of the temperature-composition plane between the spinodal<sup>12</sup> and bimodal: the line delimiting phase equilibrium, a nucleation barrier requires large changes of composition with sharp interfaces for phase transformations (Masson et al., 2003). In this region, phase change proceeds by the mechanism of nucleation and growth, in domains with the critical composition or structure (Schmets et al., 2011). When the mixture is quenched to the spinodal region, infinitesimal composition fluctuations produce spontaneous decomposition without nucleation (Wise et al., 2005). The bi-continuous system coarsens to reduce the interfacial area: coarsening precedes fragmentation of the solvent-rich phase (Fujita, 2012) (refer to Figure 5-30). The kinetics of this process are modified by a free surface: short-range interactions<sup>12</sup> and thermal gradients introduce preferential segregation of one component to the surface. Conceptually, this phenomenon explains the microstructural transformation observed in bitumen D under heating in an ESEM: as the sample is cooled the fibrillar network fragments into discrete bee-type domains. The rippled profile of the inclusions is consistent with the surface of unstable crystals formed thus, which is known to evolve into a corrugated form to minimise surface energy (Liu and Metiu, 1993). Moreover, the alternating layers parallel to the free surface in Figure 5-29(a) are consistent with segregation in the initial stage of decomposition. This produces a fluctuation in the composition field perpendicular to the surface that grows to form layers parallel thereto (Wise et al., 2005).

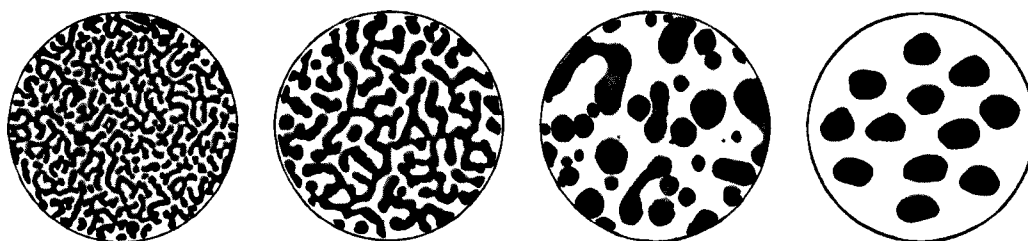


Figure 5-30: Schematic illustration of phase separation by spinodal decomposition (Masson et al., 2003; Wei et al., 2010)

---

<sup>12</sup> The limit of stability of a solution, therefore denoting the boundary of absolute instability of a solution to decompose into multiple phases

## 5.2.6 The morphology of maltenes

Micrographs of maltenes show homogenous surfaces that are interrupted by cleavage cracks and ice crystals (refer to Figures 5-31 and 5-32). Ice is indicative of inefficient quenching and sublimation. The absence of bee-type structure in this wax-concentrated fraction is intriguing: Kringos et al. (2011) published images of this structuring in maltenes using AFM.

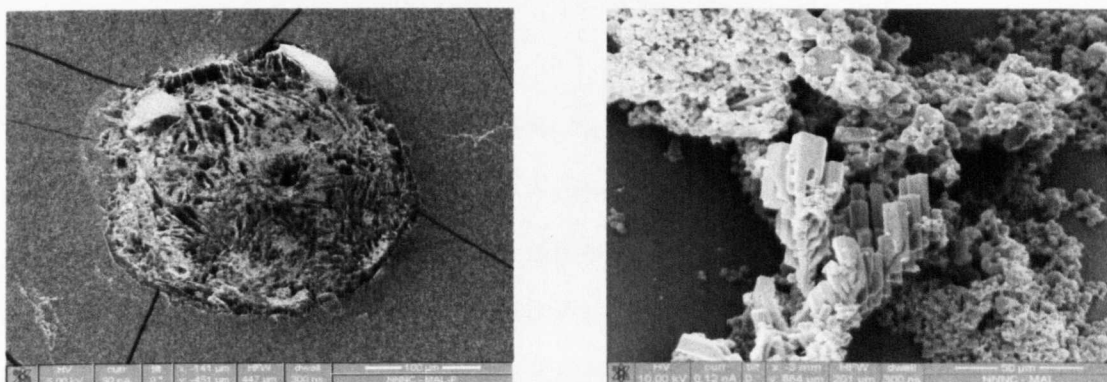


Figure 5-31: (a) Cryo-SEM micrograph of maltenes showing ice crystal growth at the surface. (b) Micrograph of maltenes indicating columnar ice crystal growth due to freezing in the slush.

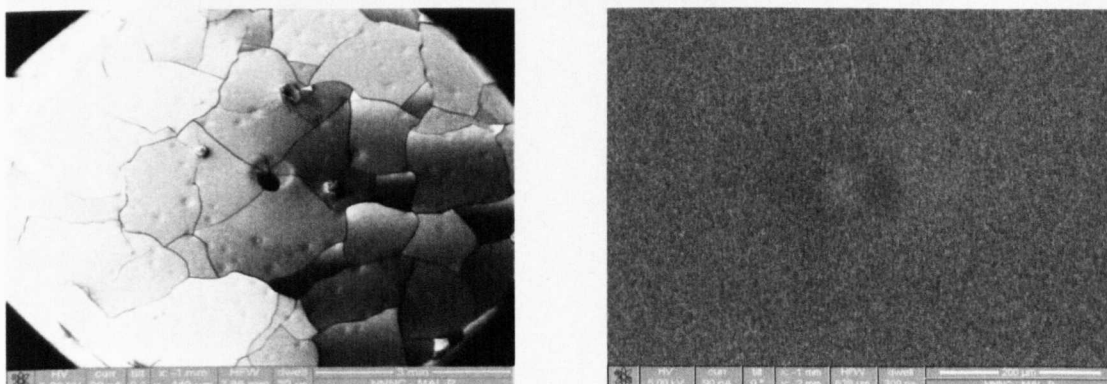


Figure 5-32: (a) Low magnification image of the surface of quenched maltenes with cleavage cracks. (b) Cryo-SEM micrograph of the amorphous surface of gradually-cooled maltenes.

The author of this thesis thought that the inability to image surface structure in maltenes using ESEM was due to instability during irradiation, which is mitigated at cryogenic conditions. For cryo-SEM, it is theorised that maltene homogeneity is produced by the quenching process. To explain, the temperature at which wax crystallisation starts (23 to 30°C) is similar to that used in this study for annealing. The rapid cooling process in the nitrogen slush may have arrested this phase separation and thus precluded the development of microstructure. This effect is not

observed in bitumen as crystallisation temperatures are raised by wax-asphaltene interactions (Kriz and Andersen, 2005), which allows for phase separation during annealing. To verify this theory, the preparation method was revised to include gradual pre-cooling: refrigeration for 60 minutes at 5°C followed by storage in an insulated chamber for that duration, using dry ice as the cooling agent. Although cracked and covered by columnar and spherical ice crystals, the otherwise smooth surface indicates that the absence of bee-type structuring is ambiguous.

### Fractured samples

The bulk of maltenes is also devoid of phase separation, but shows profuse detail: mirror-like regions enclosed by planar cracks and out-of-plane instabilities including fracture stops (refer to Figure 5-33(a)). In addition, well-defined parallel layers about 300nm in profile sandwich an amorphous segment (refer to Figure 5-33(b)). Ordering in this phase could be established by adjacent sheets of maltene-compatible polyaromatic structures of low molecular weight, which are retained after fractionation.

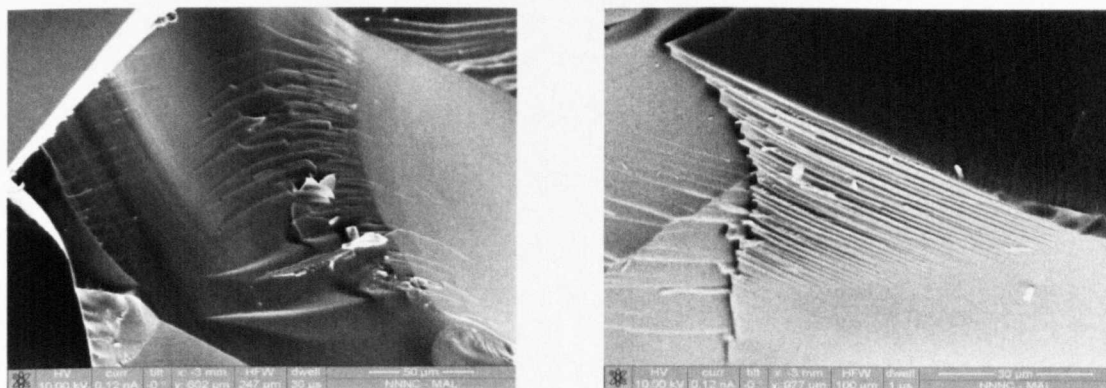


Figure 5-33: (a) Micrograph of topographic detail in the bulk of maltenes produced by fracture. (b) Cryo-SEM micrograph of planar layering in the bulk of the maltenes, exposed *in situ*.

### 5.2.7 Summary

The exposure of microstructure by radiolysis is precluded by electron irradiation at cryogenic temperatures: surfaces are modified by aeration and agitation on plunging into nitrogen slush. Low magnification micrographs of bitumen show profuse topographical detail that is explained by anisotropic shrinkage during quenching. Fractures propagated through bee-type structures indicate solute-solvent compatibility: continuum solubility is maintained from these dispersions

to the bitumen moiety. The bulk phase is glassy amorphous. The most important conclusion is that this amorphous state is perturbed by an interface or free surface: biasing effects including composition-dependent short-range interactions and thermal gradients drive phase separation and surface structure. Surface-directed spinodal decomposition enables this structuring to the depth of about 25 $\mu\text{m}$ . The absence of surface structuring in maltenes is ambiguous. However, micrographs indicate long-range order in the bulk, which is produced by low molecular weight maltene-compatible aromatic fractions and changes in the compositional field.

## 5.3 CRYOGENIC FOCUSED ION BEAM MICROSCOPY

Electron microscopy at 15°C and -165°C has produced the first images of bee-type structures using this technique. These have enabled an alternative theory for bitumen structure: bitumen is a glassy amorphous material that is perturbed due to free surfaces and then precipitation of crystallisable molecules, which produces structuring in a surface layer about 25µm thick. This theory is supported below using gallium ion irradiation. Using this method, ablated samples of bitumen D show near-surface phase separation due to crystallisation-modified solubility, and long-range ordering due to pi-pi bonding between polyaromatic molecules.

### 5.3.1 Background

Following commercialisation of SEM in 1965, developmental focus shifted to novel techniques of sample preparation and in particular, ion milling (Schiffbauer and Xiao, 2011). The focused ion beam system uses ionised inert gas for the deposition and ablation of materials (Castaing and Labourie, 1953). This system may either be a single-beam instrument, which exploits the capacity of an ion beam for sample modification and imaging, or a dual-beam instrument. This instrument integrates an ion column within another analytical microscope: a SEM in which the ion and electron columns are tilted to each other at an angle of 52° (Brunner et al., 2006).

The optics of focused ion beam microscopes resemble those of SEMs. Rather than irradiating samples from an electron source however, an extraction voltage pulls gallium from a reservoir and ionises the liquid metal by field evaporation (Stevie et al., 2005). The accelerated ions are focused on the sample by electrostatic lenses (Heaney et al., 2001). The inelastic interactions of the impinging ions with target atoms produce secondary electrons and secondary ions that are used to construct an image of the surface. The secondary electron mode is preferred for imaging applications in the dual-beam platform, because the images produced are of a higher contrast and resolution (Hatiboglu, 2006). This mode also negates sputtering of the sample: a surface layer is ablated when the momentum transferred from ions to sample atoms exceeds the binding energy of the material (Wirth, 2009). Manipulation of this sputtering phenomenon enables the selective excavation of material from a sample (refer to Figure 5-34). This method

is used in the manufacture of silicon wafers by the semiconductor industry (Kim et al., 2012), and by academia to develop knowledge of the morphology of bulk and interfacial domains of various materials (Krohn, 1961; Phaneuf, 1999; Loos et al., 2002; Adams et al., 2006; Utlaut, 2009; Schiffbauer and Xiao, 2011).

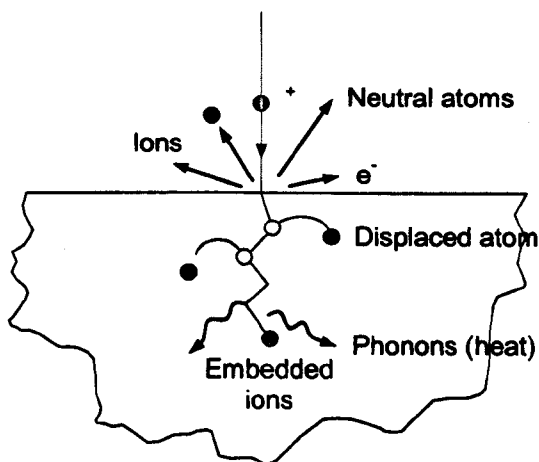


Figure 5-34: Possible interactions of the incident ion beam with a solid sample; the most important process is the release of target atoms: physical sputtering (Orloff et al., 2006)

### 5.3.2 Review of pertinent literature

Use of the focused ion beam (FIB) system in materials science is hampered by the scarcity of this platform (Phaneuf, 1999), and most applications in this field have studied metals (Kitano et al., 1995), silicon (Lugstein et al., 2003) and ceramics or other hard materials (Holzer et al., 2004). Published FIB studies of biological materials (Ishitani et al., 1995; Milani et al. 2007) or polymers (Niihara et al., 2005) are limited. This derives from the consensus that molecules of soft materials, unlike those of hard materials, could not sustain ion irradiation and would thus damage easily (Zanini et al., 2005; Brunner et al., 2006; Kochumalayil et al., 2009a). Further, the electric field established during irradiation produces radicals and molecular fragments in polymers by selective bond cleavage (Moliton et al., 1996). When liberated these particles are sputtered or emitted as a gas from a thin surface layer (Kochumalayil et al., 2009b), or diffuse in the polymer matrix and participate in chemical reactions that damage the polymer structure (Kochumalayil et al., 2009a). Amplified locally by heating during irradiation due to low thermal conductivity and limited thermal stability (Kochumalayil et al., 2009b), etching of soft polymers at room temperature was thought to be impractical (Niihara et al., 2005). Early studies on thin-

film polymers exploited the heat sink behaviour of supporting (Loos et al., 2002) or reinforcing (Brostow et al., 2007) hard components therefore, or FIB processing at cryogenic temperature (Niihara et al., 2005; Stokes et al., 2007; Fu et al., 2008; Kochumalayil et al., 2009a).

The FIB/SEM platform has been used for cross-sectional analyses of chemistry and structure. Chemistry-thickness profiles are produced by etching a sample and deriving the stoichiometry of the exposed surface by secondary ion mass spectroscopy (Adams et al., 2006b); structure-thickness profiles are produced by examining the surface using SEM. Brunner et al. (2006) for example etched multi-layered polymer laminates using an ion beam current of 20nA at 30keV and normal incidence, and then rotated the sample through 52° to define layer thicknesses by electron-mode imaging. Brostow et al. (2007) used the dual-beam platform at liquid nitrogen temperature to study aluminium particles dispersed in low density polyethylene. The authors etched samples using an ion beam current of 7nA at 30keV and imaged the cross-sections by secondary and backscattered electrons. The aluminium particles were noted as hemispherical protrusions from an amorphous matrix: this structure derives from a differential sputter yield of the fractions due to their different physical properties (Wong et al., 2010).

The structuring of polymethylmethacrylate after ion milling is similarly dependent on chemical heterogeneity. The initially amorphous flat surface was modified by ion erosion at 6.76nA and 30keV to a plate-like surface with sharp contours, and a nodular structure at a vertical scale of below 100nm (Kochumalayil et al., 2009a). The study explained the structural homogeneities by the expulsion of activated radicals from the polymer during FIB irradiation. Moreover, these topographical modifications were more pronounced in the presence of water vapour. This was ascribed to the enhanced flux of escaping fragments due to the local action of water, and free radicals that promote more intense chemical reactions and prevent the recombination of large immobile segments of polymers in the radical state.

The structural modification of a glassy epoxy polymer after ion irradiation further contributes to this knowledge. Namely, dry etching at 7nA and 30keV exposes localised regions of a sub-micrometre globular network: by milling in the presence of water, this emerges as a pervasive

system (Kochumalayil et al., 2009b). The structural inhomogeneity of this network structure is explained by the destruction of weak bonds between the polymers, from which local variation of polymer stiffness arises. The smooth surface exposed under high-vacuum conditions was attributed to the propensity for short mobile sections to recombine and deposit at the surface.

The development of surface structure by etching is also affected by the angle of the impinging ion beam. Adams et al. (2006) noted that carbon bombarded with gallium at 2.2nA and 20keV retains a smooth profile at normal incidence. The authors reported a transition to a roughened sinusoidal profile at intermediate angles ( $45^\circ$  to  $70^\circ$ ), and then to a saw-tooth cross-section as the angle of ion incidence increases above  $70^\circ$ . The rippled pattern is explained by the subtle dependence of sputter yield on surface curvature (Bradley and Harper, 1988), and smoothing processes that include thermal diffusion, viscous flow, ion-enhanced diffusion and preferential sputtering without mass flux (Adams et al., 2006). Planarisation of peaks at high ion incidence angles is attributed to the preclusion of regions of the surface to ion exposure, where a critical feature height-to-length ratio is breached (Carter, 1999).

A similar structural transition occurs in vitreous ice due to ion etching at cryogenic conditions: an environment which precludes devitrification by beam heating (Marko et al., 2006). Domes are developed by FIB milling at normal incidence and propagate parallel to the direction of the impinging ions (Fu et al., 2008). As the incidence angle is increased the domes tilt and evolve into shallow steps, and then flatten to form a smooth profile at grazing angles of  $80^\circ$  (refer to Figure 5-35). This phenomenon was also explained by the dependence of sputter yield on the angle of ion incidence (Fu et al., 2008).

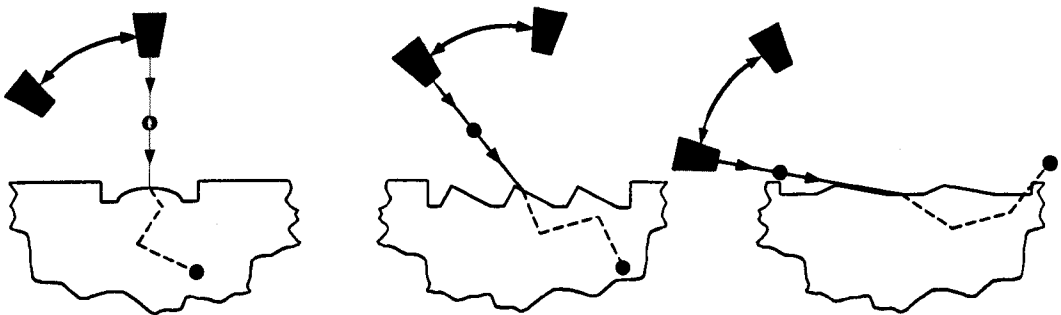


Figure 5-35: Diagram of the evolution of the surface of vitreous ice with beam incidence angle (Fu et al., 2008)

### 5.3.3 Sample testing

FIB etching is used in this thesis to study potential structuring underlying and peripheral to the surface features in samples of bitumen D and the fractionated maltenes, using an FEI Quanta 200 3D FEG-SEM/FIB. Developed from the procedure of Kochumalayil et al. (2009b), focused gallium ion etching was conducted under high vacuum at  $-165^{\circ}\text{C}$  and an acceleration voltage of 30keV; a beam current of 0.01 to 3nA; a dwell time of 1 to 20 $\mu\text{s}$ ; and ion incidence angles of  $0^{\circ}$ ,  $10^{\circ}$  or  $52^{\circ}$ . Electron micrographs of the milled areas were collected using the conditions established in cryogenic SEM investigations on the two materials (refer to Section 5.2.4).

### 5.3.4 FIB etching of bitumen

Preceding investigations on sub-surface morphology of amorphous and structured domains in the low asphaltene content bitumen (D), this thesis scrutinises the physical modifications due to different FIB parameters. This enables the author to define the limits of irradiation in which microstructural detail is preserved.

The morphology of samples prepared by pouring (defined in Section 5.1.2) and ablated using ion currents of up to 1nA at an angle of incidence of  $0^{\circ}$  showed minimal evolution to depths of 6 $\mu\text{m}$ . This depth includes the string-like network structure that is embedded at 400nm (refer to page 39). At 3nA, disc-like chains appeared 1.5 $\mu\text{m}$  below the surface (refer to Figures 5-36(a) and (b)). At the base of these sputtered regions are ring-like protrusions with tube radii of 0.05 to 0.1 $\mu\text{m}$  and major radii of 0.4 to 0.5 $\mu\text{m}$ . These geometrical properties are comparable to the overall dimensions of micelles in colloidal systems, and to the arch-type strings of the bee-like structures reported hereto (refer to page 24 and Section 5.1). The literature explains structure development during sputtering to variation in mechanical strength or phase boundaries, which establish locally-divergent thinning processes. It is thought that asphaltenes furnish hardness in bitumen (refer to Section 2.5), and novel microscopy studies reported in this thesis indicate this fraction is unsusceptible to radiolysis. The author therefore concludes that these structures are composed mainly of asphaltenes. Interestingly, the effects of FIB irradiation pervaded the periphery of the milled domain. Namely, the generation of phonons (heat), recoiled atoms and diffusing free radicals caused the initially homogeneous surface near to the irradiated domain

to phase separate. This is in the form of graduated ellipsoids that extend vertically in the high vacuum conditions (refer to Figure 5-37(a)).

Physical modifications due to impinging gallium ions were also studied for FIB angles of  $0^\circ$  to  $52^\circ$ , at a current of 3nA. Columnar disc-like structures at  $0^\circ$  developed into smooth cylindrical shapes at  $10^\circ$  that are veiled by amorphous oils and tilted to the direction of the incident ions. These evolved into subtle terraces at  $20^\circ$ , and shallow plateaus as the FIB was rotated to  $52^\circ$  (refer to Figure 5-37(b) and 5-38(a)). This angular dependence of morphology is explained by variations in the effective region of ion tracks and the stochastic nature of the impinging ions. At high incident angles, the probability that ions are reflected increases. Consequently, the ion tracks are confined to surface layers and energy deposition decreases, which reduces sputter yield and moderates microstructural changes (Fu et al., 2008).

The effects of variable dwell time were investigated using an ion current of 3nA at  $52^\circ$ . As the dwell time was increased from  $1\mu\text{s}$  to  $20\mu\text{s}$ , the morphology of the milled region evolved from terraces to a series of cylindrical structures and subtle disc-like protrusions (refer to Figure 5-38(b)). The literature explains similar observations simply, by the number of ion-sample atom interactions and thus molecular cleavages that occur during the time of irradiation on a single region or pixel. These are directly proportional to dwell time (Adams et al., 2006b). Defined by this initial study, the ion irradiation parameters used herein are a beam current of 30pA; dwell time of  $1\mu\text{s}$ ; an ion incidence angle of  $0^\circ$ ; and 30keV acceleration voltage.

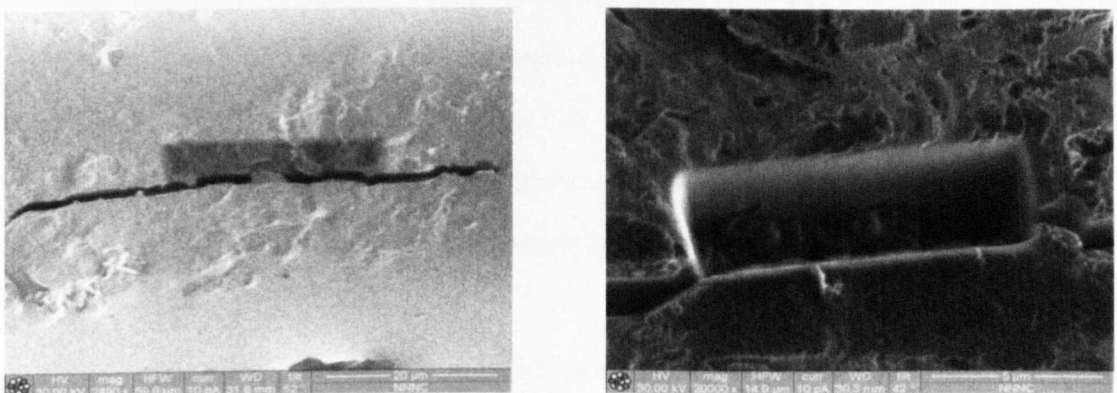


Figure 5-36: (a) Cryo-SEM image of the effects of ion bombardment of bitumen D at 1nA and  $0^\circ$  incidence. (b) Image of the effects of ion irradiation in bitumen D at 3nA and  $0^\circ$  incidence.

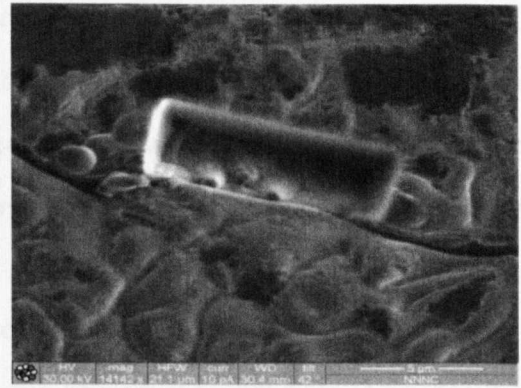


Figure 5-37: (a) Micrograph of peripheral effects of ion bombardment of bitumen D at 3nA and 0° incidence. (b) Image of the effects of ion irradiation in bitumen D at 3nA and 20° incidence.

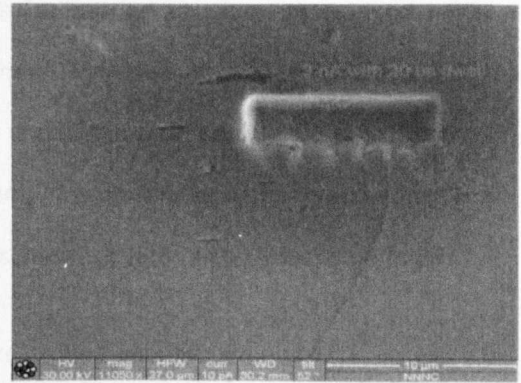
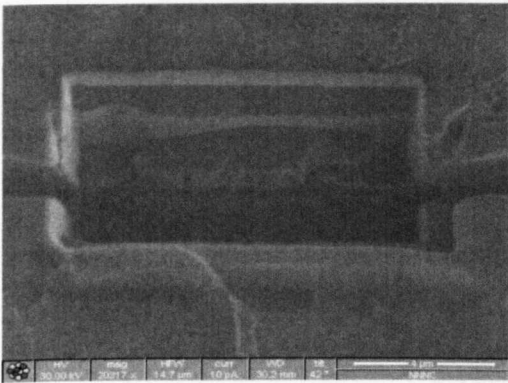


Figure 5-38: (a) Micrograph of the effects of ion bombardment of bitumen D at 3nA and 52° incidence. (b) Image of the effects of ion irradiation in bitumen D at 3nA, 52° incidence and a dwell time 20µs.

### Poured samples

Repeated FIB bombardment of a rectangular domain enclosing a cracked bee-type structure provoked sample amorphisation. That is, electronic collective effects and sputtering of chain fragments caused the decay of ripple elevation at the surface, and coarsening then refining of peripheral disperse instabilities (refer to Figure 5-39(a)). Besides amorphisation, bright spots formed in an adjacent and initially-homogeneous domain indicate the implantation of gallium ions, or the redistribution of the platinum coating due to heating.

Electron micrographs of morphological deformations produced by prolonged FIB irradiation in a rectangle overlapping a second bee-type structure are intriguing. Notably, differences in the sputtering rates of the apex and base of each ripple produce a series of non-interacting string-

like forms, which stitch the milled side-walls (refer to Figure 5-39(b)). To differentiate intrinsic sub-surface structuring from artefacts of the etching process, rectangular FIB irradiation was used to erode a third bee-type structure. This study also shows discrete strings that connect the milled side-walls. These correspond in position to the trough of the periodic waveform, but to a lesser extent to width (refer to Figure 5-40(a) and Table 5-7). Consistent with the working theory, in which bitumen microstructure is produced by wax and crystallisable saturated side-chains on aromatic molecules (refer to page 118), the differential sputter rates show chemical heterogeneity in this domain. Perhaps immiscibility of the naphthene-aromatic end-groups on the crystallised paraffins or mutual repulsion between the outward-stretching cyclic segments introduces micro-phase separation into stripes. Similar banded structure is reported by Wilson (2001) for siloxane side-chain liquid crystal polymers. Moreover, the alternating hill-valley or undulating structure could form as the composite crystals curl on cooling (refer to page 130). Length mismatch between cyclic and paraffinic parts may contribute when the conformational entropy gain by molecular alignment compensates interface formation (refer to page 29).

Table 5-7: Geometrical properties of un-etched and etched bee-like structures

Sample	Preparation	Peak width ( $\mu\text{m}$ ) <sup>13</sup>		Trough width ( $\mu\text{m}$ )	
		Mean	Std. dev.	Mean	Std. dev
D (ESEM) <sup>14</sup>	Peltier cooling	0.249	0.086	0.104	0.047
D (FIB/SEM)	Cryo-freezing	0.313	0.084	0.160	0.037
D (FIB/SEM)	Gallium ion etching	0.117	0.012	0.391	0.183

The relative stiffness of the apex and base of the undulating structure is antithetical to studies by AFM in pulsed force mode, noted by Jäger et al. (2004). Perhaps phase separation occurs in an intermediate layer and propagates the disrupted crystallisation process to the surface of the crystal, thereby establishing sinusoidal roughening due to elastic strain (refer to Section 5.1.5, page 124). However, similar structuring in the amorphous moiety that is exposed by ion bombardment near to the bee-type structure may indicate an alternative mechanism. Namely,

<sup>13</sup> For the etched sample, the peak refers to residual material and the trough to voided areas

<sup>14</sup> Data from Table 5-4

inhomogeneous contraction induced in sub-surface string-like parts and the continuous phase may provoke the rippling perceived in crystallised domains. This may be precluded elsewhere by stress relaxation within the surface oils.

### Fractured samples

Ion irradiation of surfaces that were produced by fracture, using the method defined in Section 5.2.3, did not indicate significant morphological anomalies. Notably, metal redistribution or re-deposition of sputtered material produced discontinuities at the first-milled edge of the trench, which otherwise retained low contrast (refer to Figure 5-40(b)). This strongly suggests that the solubility continuum in the bulk maintains the dispersed and diluted state of the SARA fraction molecules. This also indicates that the continuum is perturbed at a surface by precipitation of wax, which stimulates near-surface phase separation in the form of interconnected ellipsoids.

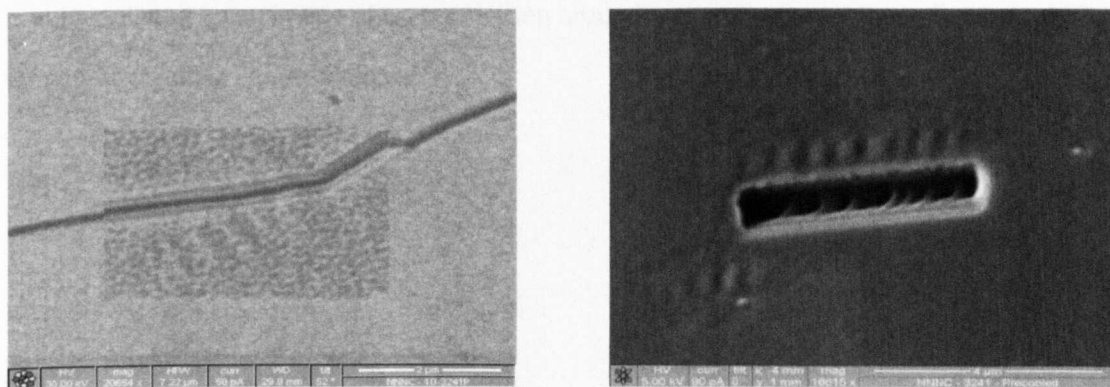


Figure 5-39: (a) Micrograph of the effects of ion bombardment bee-type structure 30pA and 0° incidence. (b) Image of the effects of prolonged FIB irradiation of another bee-type structure.

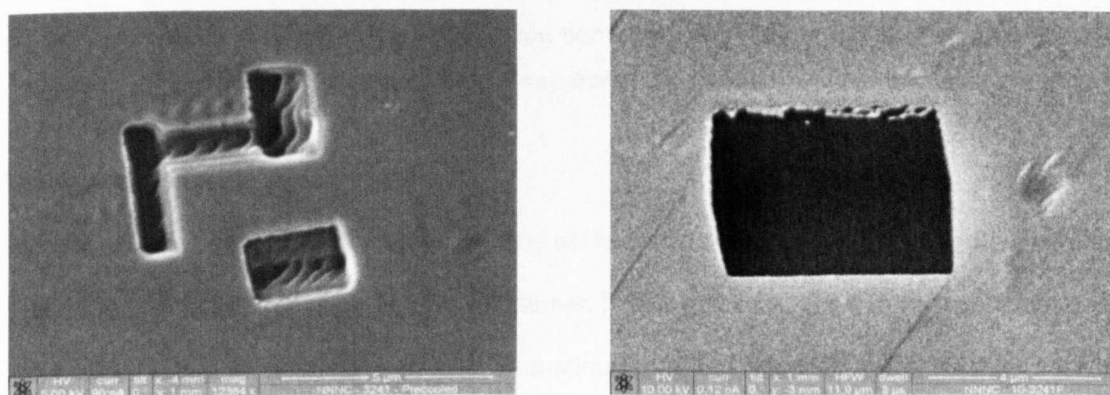


Figure 5-40: (a) Image of the effects of ion irradiation of structured and amorphous domains at 30pA and 0° incidence. (b) Image of the effects of ion irradiation in the bulk of bitumen D.

### 5.3.5 FIB etching of maltenes

#### Penetration needle-dropped samples

Ion bombardment of quenched samples, prepared as in Section 5.2.3, produced domains that are devoid of morphological heterogeneity. The fractions in this system thus dilute each other; perhaps by physical dispersion and hydrogen transfer (refer to Figure 5-41(a)). FIB irradiation in a rectangle spanning the edge of a bubble, which formed at the surface of gradually-cooled samples, reveals lenticular layers in the maltenes covering the void (refer to Figure 5-41(b)). It is also shown that peripheral phase separation occurs in the form of discrete cylinders. These indicate that the slower rate of cooling, compared to the quenched samples, enables diffusive domain segregation although unobserved at its surface. The protuberant structures appear to develop by the suction-extension of maltenes-compatible polyaromatic fractions that establish layering, when intermolecular cohesion is modified by the sputtering of saturates. This theory is substantiated by an image of layers twisting around and protruding at these flower bud-like structures (refer to Figure 5-42(a)).

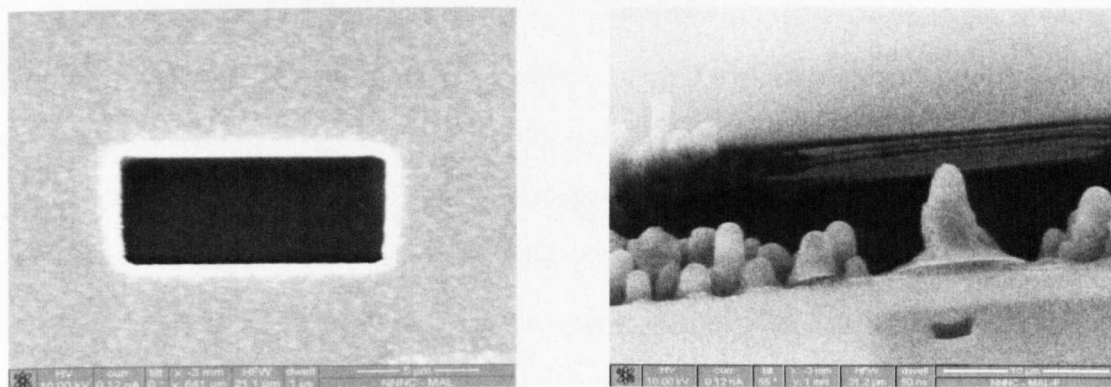


Figure 5-41: (a) Micrograph of the effect of ion bombardment of the surface of quench-cooled maltenes. (b) Image of near-surface phase separation in gradually-cooled maltenes.

#### Fractured samples

Rectangular FIB irradiation of various regions at the fractured surface did not produce notable morphological heterogeneities. Similar to bitumen D, the eroded regions were featureless with the exception of peripheral damage and discontinuities at the first-milled edge of the trenches (refer to Figure 5-42(b)). While this could be explained by unperturbed solubility continuum, it is acknowledged that quenching of this sample (according to Section 5.2.4) may contribute by

inhibiting the development of structuring through diffusive phenomena.

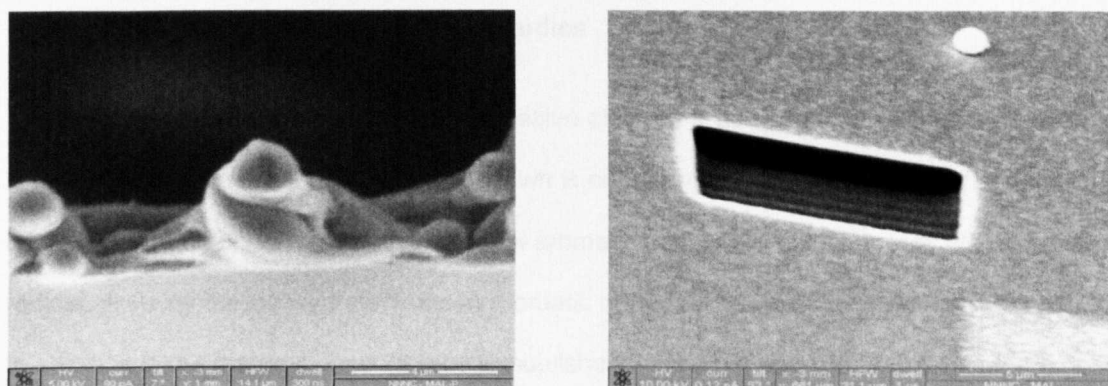


Figure 5-42: (a) High-magnification of the phase separation along the ion-eroded edge of the surface in gradually-cooled maltenes. (b) Micrograph of the effects of ion bombardment in the bulk of quench-cooled maltenes

### 5.3.6 Summary

This thesis reports the first use of focused ion beam etching to study structure in bitumen and maltenes. On bitumen, ion-induced structural evolutions of amorphous surfaces into complex protrusions indicate dispersed concentrations of asphaltenes. Electron micrographs of etched bee-type structures indicate differential sputtering rates, which are explained by micro-phase separation of constituents due to immiscibility of occluded aromatics and length mismatch. An inhomogeneous volume contraction during cooling may also contribute. The central finding of this research is that amorphous fracture surfaces indicate that the material is glassy: structure occurs at free surfaces in air and at super-cryogenic temperatures due to perturbed solubility and surface effects. The absence of structure in the maltenes is consistent with ESEM studies reported in this thesis, and indicates homogenous chemistry. However, this is uncertain since cooling rate effects contribute: slow cooling enables phase separation that quenching inhibits.

## **5.4 CONCLUSIONS AND RECOMMENDATIONS**

### **5.4.1 Conclusions from microscopy studies**

The expected response of bitumen to excessive electron irradiation is to relinquish an atomic layer of the surface. This radiolytic breakdown is common but is prevented in high asphaltene content bitumen due to a protective effect of aromatic fractions. That is, energy adsorbed from radical alkyls by delocalised electrons in aromatic structures enables these radiolytic products to stabilise in the material. Incongruous to published theory it is concluded that these aromatic fractions are dispersed through the aliphatics, in order for this phenomenon to be widespread, and do not simply produce concentrations. It is also concluded that radiation damage occurs by radiolysis and not by beam heating, which is suggested in the literature.

Microscopic analysis of bitumen and heptane-soluble fractions at 20°C show that asphaltenes contribute to network structure, but not to the exclusion of aliphatics as noted in literature. The first use of thermal control in ESEM indicates that this network is replaced at 0°C by dispersed bee-type structures. These coalesce into network structure as temperature rises, in response to compositional fluctuations. This phenomenon is explained by spinodal decomposition. The ellipsoidal geometry of the dispersions is explained by concentrations of aromatic compounds along their edge. Cracking of crystallisable aliphatic side-chains on these molecules catalyses the disconnection of this component from the entangled network, that explains contraction of the string-like structures due to ageing. This theory is reported uniquely in this thesis.

Radiolysis is arrested by irradiation at cryogenic temperatures: continuous network structuring is not exposed after prolonged irradiation with electrons. Anisotropic shrinkage during quench cooling propagates fractures through the dispersed inclusions, which indicates solute-solvent compatibility. This enables the solubility continuum that maintains the amorphous state of the bulk, which is reported only in this thesis using a new freeze-fracture preparation method. The important conclusion is that this state is perturbed by a free surface: biasing effects including composition-dependent short-range interactions catalyse phase separation and near-surface structuring. The absence of an elastic plateau in rheology data confirms that this structuring is

space-bound: diffusing particles are limited in depth. The absence of structure in maltenes is concluded to indicate a shift of phase change behaviour due to separation from asphaltenes. Long-range order (parallel thin-layers) in near-surface regions of this fraction is reminiscent of unstable binary composites that segregate by spinodal decomposition.

From the preceding conclusions the absence of surface structuring in high asphaltene content bitumen is explained by the highly-aromatic composition of the upper layer. That is, aromatics dispersed through the crystallisable aliphatics inhibit wax crystal growth and thus structuring.

Electron micrographs of FIB irradiated amorphous bitumen evidence differential sputtering in the form of graduated discs. Bee-type inclusions also show this phenomenon, which indicates micro-phase separation. For the latter structure, this indicates micro-phase separation due to immiscibility of occluded aromatics or length mismatch between crystallisable materials. The relative stiffness of the alternating ripple components is antithetical to the literature: the micro-phase separation phenomenon occurs in an intermediate layer and propagates the disrupted process to the surface. Analogous structuring exposed by ion bombardment peripheral to the bee-type parts indicates contribution from anisotropic contraction. The absence of rate effects in the bulk is consistent with structure formation by surface biasing: spinodal decomposition.

#### **5.4.2 Recommended further electron microscopy studies**

The research in this thesis has concentrated on low temperature tests of bitumen. To develop a broader understanding of microstructural characteristics, microscopy analyses at moderate temperatures are advised. This could include tests using cryo-SEM or ESEM at temperatures closely aligned to the glass transitions of chromatographic fractions. This was avoided in this thesis due to rational concerns for microscope contamination by radiolytic fragments.

Micrographs of the asphaltenes reported in this thesis introduce an amorphous surface. This featureless morphology is inconsistent with particulate texture noted in the literature review. It is concluded that this difference is due to physicochemical effects that control self-association behaviour, and to elution processes. Importantly, the structural characteristics are susceptible

to the arbitrary definition of this fraction. It is suggested that microscopic analysis on the effect of eluent type are undertaken to produce a reliable and stable definition. This research should extend to investigate the effects of precipitation time.

The cryogenic fracture preparation technique used in this research provides a novel approach to investigate bulk structure. However, ice crystal growth during quenching partially obscured microscopy analyses. Slam freezing is recommended as an alternative. Ion bombardment of the surface could be extended to prepare films for transmission electron microscopy, in order to negate the preparation artefacts associated with solvent precipitation.

## 6 A STUDY ON FRACTURE HEALING IN BITUMEN

The response of bitumen to repeated load is the degradation of mechanical properties, which is explained by thixotropy and damage. Damage occurs due to a dislocation of microstructural segments and molecular scission, and produces failure: the three-dimensional densification of dispersed cracks. The healing of cohesive fractures is studied most efficiently at reproducible single crack interfaces. Accordingly, using a combination of three shear and tension tests, this thesis studies bitumen healing across a defined crack. The approach is shown in Figure 6-1.

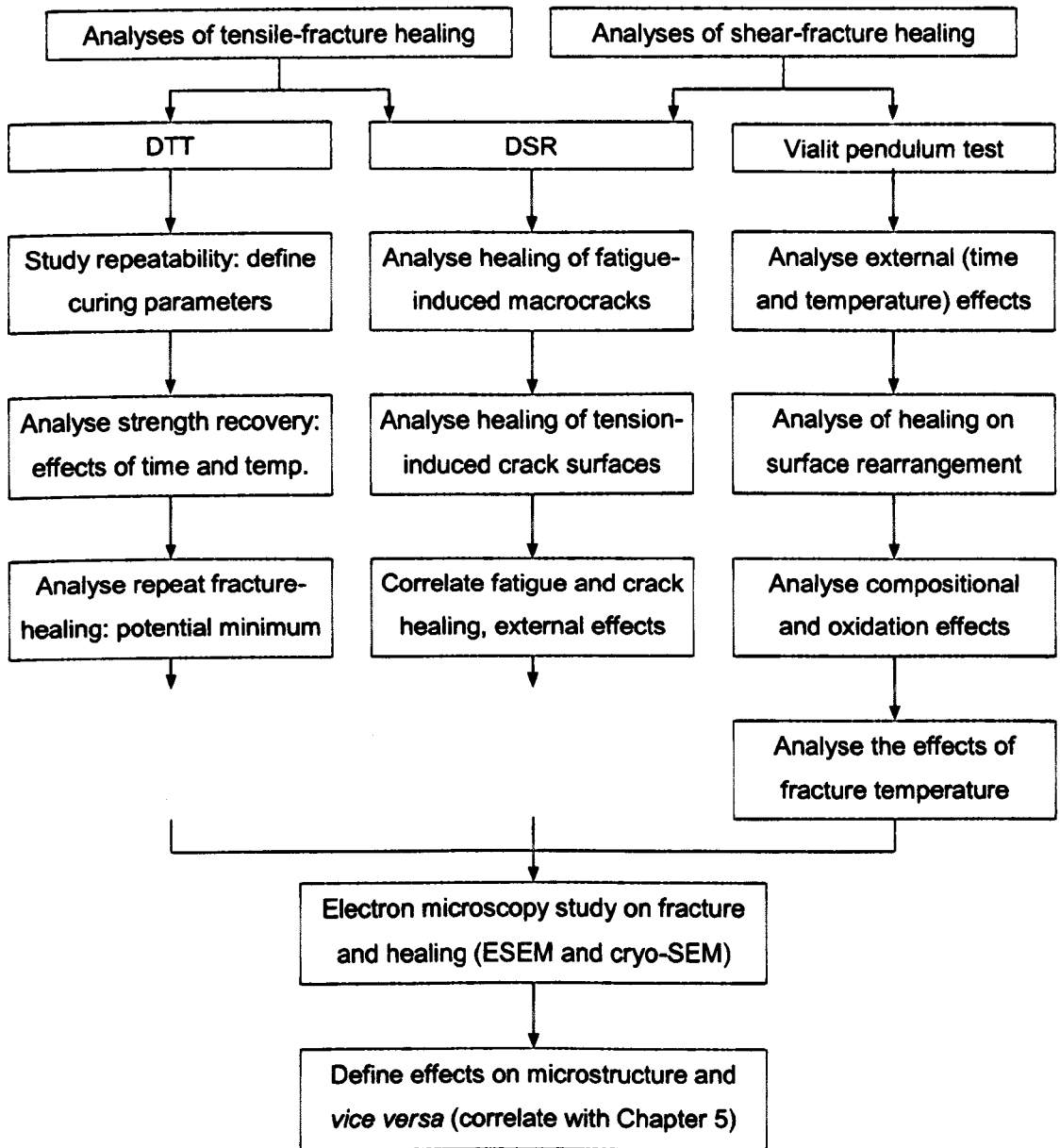


Figure 6-1: Conceptual representation of the research approach for the mechanical section

## **6.1 INTRODUCTORY REMARKS**

The first test is the direct tension test, which simulates the crack-opening stress regime at the base of asphalt in flexible pavements (refer to Figure 4-10). The second test is an evolution of the two-piece healing method using DSR: this approach studies healing across tensile failure surfaces using shear. The third test uses the Vialit pendulum apparatus to investigate healing at shear failures. The shear stress distribution under loading initially increases with depth from the pavement surface to a maximum at 60mm, after which it decreases (Su et al., 2009). This surface-concentrated stress condition produces top-down cracking in longitudinal wheel paths and is simulated using the DSR and Vialit pendulum test.

## **6.2 DIRECT TENSION TESTING**

### **6.2.1 Background**

The direct tension test (DTT) was developed by the Strategic Highways Research program to characterise the low temperature failure properties of bitumen. These are a critical indicator of asphalt behaviour in cold environments, thus an essential and prevalent design consideration (Anderson and Dongré, 1995). The test procedure is used to assure ductile failure. The brittle properties of dumbbell-shape samples of bitumen are acquired by the application of a uniaxial monotonic stress state and continuous strain measurements, using a fluid-based temperature control system to produce accurate results (Dongré et al., 1997). From the stress-strain curve, brittle fracture at temperatures below the glass transition of bitumen (-15°C to -35°C) (Masson et al., 2002) is defined by the maximum stress (refer to Figure 6-2). This often corresponds to a failure strain of 1% or less (Anderson and Dongré, 1995). The inherent capacity of the DTT to fracture samples and to measure failure-related properties compelled its use for this study.

### **6.2.2 Review of pertinent literature**

#### **General**

The repeatability of bitumen testing is a particular concern. For the DTT, this is defined by two aspects: stress-strain curves and failure values (refer to Figure 6-2). For diverse bitumens the

coefficient of variation of failure stress and strain is usually on the order of 10% (Dongré et al., 2003), but decreases with increasing test temperature (Osman, 2004). This is ascribed by Ho and Zanzotto (2001) to the alignment polar molecules within samples during preparation. The authors of that paper hence introduced an alternative preparation method, which is shown to improve repeatability. Namely, a slow cooling mechanism for the mould filled with bitumen is provided by an arrangement of heated ceramic tiles and empty moulds. This allows the polar fractions to stabilise with aligned dipoles before quenching to a state with limited diffusion. It is concluded (Ho et al., 2003) that this method more-accurately simulates the thermal condition in bitumen after paving.

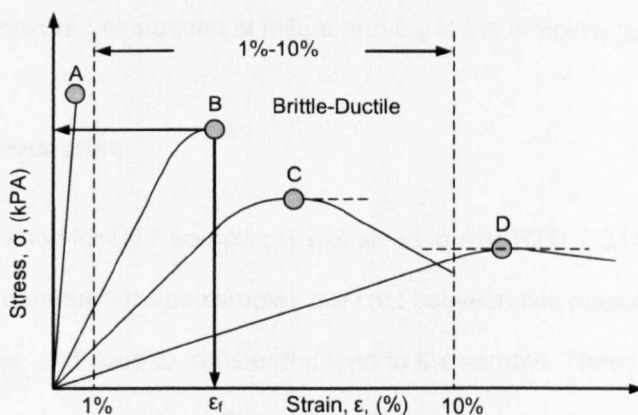


Figure 6-2: Various stress-strain behaviours of bitumen in the DTT, where the failure stress in each example is denoted by grey circles

The effect of sample cross-section and length on the variability of DTT data, collected for high polymer content bitumen sealants, is also published (Al-Qadi et al., 2008). Notably, the effect of a 50% reduction in cross-section is negligible, and similar to length effects for samples that are elongated at an equal rate of strain. The tensile response of pure bitumen is also sensitive to strain rate, which displaces failure to lower stress and strain at higher rates (Osman, 2004). Moreover, the type and molecular weight distribution of waxes contributes to tensile behaviour (Ho et al., 2003). Namely, at temperatures in the region of vitrification, microcrystalline waxes shift the failure stress and strain to lower values. Paraffin waxes with low polydispersity cause an abrupt decline in failure properties at temperatures below  $-16^{\circ}\text{C}$ . This contribution reduces with broadening molecular weight distribution, due to slow crystallisation over a wider range of temperatures (Ho et al., 2003). It is notable that a paper by Marasteanu and Anderson (2001) demonstrated nonlinear behaviour (refer to Section 3.3.5) at large strain values.

### Calculations of stress and strain

The stress and strain in the gauge length of the specimen are calculated using equations 6-1 and 6-2 respectively (Al-Qadi et al., 2008). The effective gauge length is defined as that with the same cross-section of the gauge, which yields the same strain energy as that of the entire dumbbell-shaped sample between the plastic inserts (Dongré et al., 1996).

$$\sigma_f = P_f / A_0 \quad \text{Equation 6-1}$$

$$\epsilon_f = \Delta L_f / L_{\text{eff}} \quad \text{Equation 6-2}$$

where  $\sigma_f$  is failure stress,  $P_f$  is load at failure,  $A_0$  is the initial cross-sectional area,  $\epsilon_f$  is failure strain,  $\Delta L_f$  is the measured elongation at failure and  $L_{\text{eff}}$  is the effective gauge length.

### 6.2.3 Sample preparation

The preparation method for DTT samples is explained in AASHTO T 314-02 and described in brevity below. The dumbbell-shape samples are cast between two plastic inserts cleaned with toluene and acetone, and used to transfer the load to the sample. These are positioned at the ends of an aluminium mould (refer to Figure 6-3). Teflon-coated paper is placed on the mould and used with a silicon-based release agent to prevent bitumen-mould adhesion.

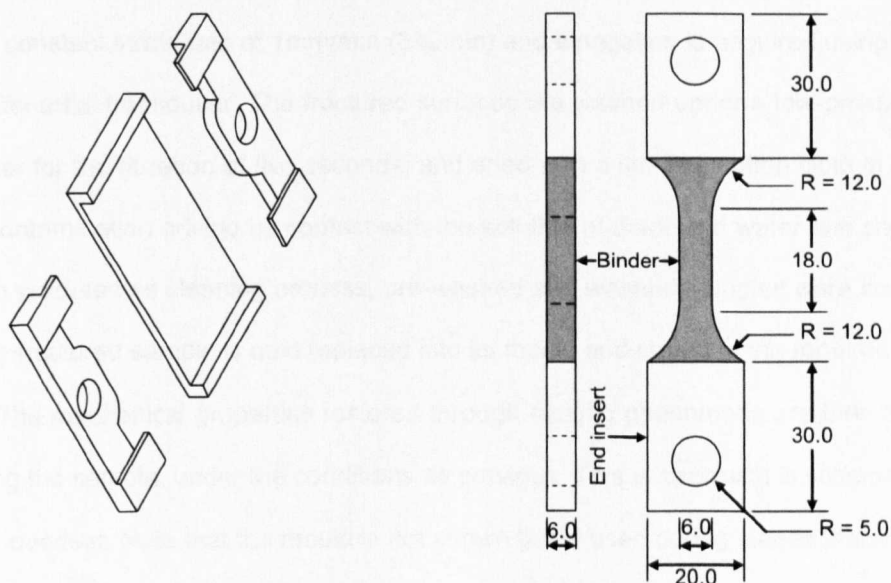


Figure 6-3: Direct tension test aluminium mould and sample geometry (AASHTO T 314-02)

For this study bitumen B was selected: it is the intermediate asphaltene content sample and is

shown to have microstructural properties that are quantifiable using ESEM. This is a required consideration, according to the research approach in Figure 6-1.

The sampled binder is heated at 135°C and stirred regularly, to produce a homogenous liquid with the consistency of motor oil at room temperature. The bitumen is poured into pre-warmed moulds in a continuous stream, in order to prevent air entrainment and high thermal gradients due to the drop in bitumen temperature. The samples are then cooled at room temperature for the duration of one hour according to the AASHTO standard, which enables satisfactory data reproducibility (Dongré et al., 2002). The samples are then trimmed level with the mould using a hot straightedge. The AASHTO protocol specifies that the samples are then stored at room temperature for ten to fifteen minutes before testing. However, to allow for structural ordering phenomena the filled moulds are stored at 25°C in a dehumidified chamber for 24 hours prior to testing (refer to page 95). The samples are de-moulded and conditioned in the cooling bath for  $60 \pm 10$  minutes, and tested immediately thereafter.

#### **6.2.4 Sample testing**

After conditioning at the test temperature of -25°C, a sample is mounted onto the loading pins whilst remaining submerged in the cooling fluid. Each of the six replicate samples is loaded to failure at a constant strain rate of 1mm/min (3%/min) and elongation is acquired using a linear variable differential transducer. The fractured surfaces are washed under a low-pressure flow of cold water for the duration of five seconds, and dried with a lint-free cotton cloth in order to minimise contamination arising by contact with the solution of deionised water and potassium acetate. To validate this cleaning process, pre-washed and washed samples were imaged by ESEM. The fractured sample is next replaced into its mould and stored at the required healing condition. The mechanical properties restored through healing phenomena are then acquired by re-testing the sample, under the conditions as previous. This approach is schematised in Figure 6-4, overleaf. Note that the mould is not shown but is used during stages 2 and 3.

After this test, the bitumen sample is discarded and the end tabs are soaked in a solvent, and rinsed with a detergent solution to remove any oil residue left by the mineral spirit cleaner.

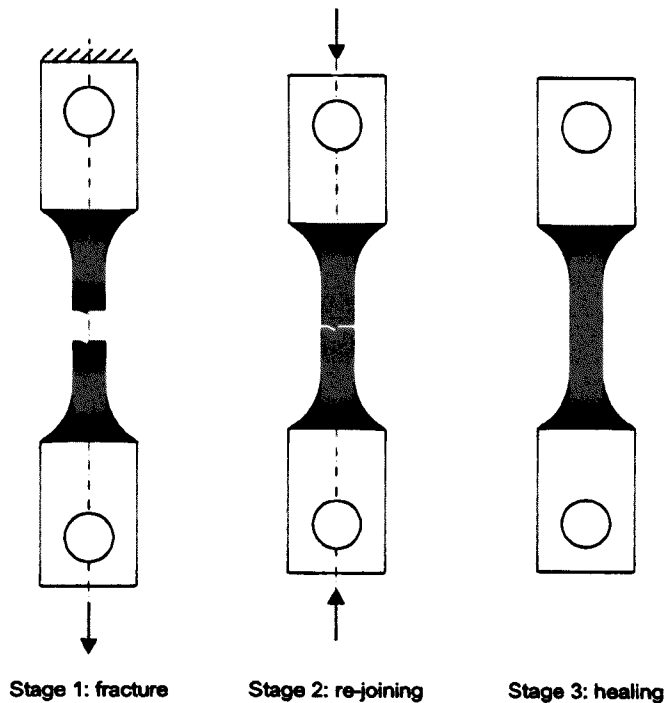


Figure 6-4: Schematic of the healing test on bitumen using the DTT

## 6.2.5 Results and discussion

### Repeatability of the tensile fracture test

The repeatability of the fracture test on bitumen B is analysed using true stress (related to the current cross-sectional area), true strain (the summation of strain increments) and toughness, for curing times of 1, 24 and 48 hours. This enables the evaluation of microstructural changes (refer to Figures 6-5 to 6-7).

The microstructural evolution of bitumen is illustrated by the change in failure values upon the application of load. For example, mean strength increases from 1.69MPa under the AASHTO protocol to 3.12MPa after a 48 hour curing period (refer to Table 5-1). This could be explained by transformations in the metastable state by isothermal densification of amorphous domains below 60°C, due to partial ordering of aromatics of increasing molecular weight (Masson and Polomark, 2001). The crystallisation of waxes on cooling to the cloud point: 23 to 30°C (Bhat and Mehrotra, 2004), could also contribute. ESEM micrographs for the short and intermediate curing times indicate time-dependent changes of the fibrillar network (refer to Table 6-2). This is consistent with the working hypothesis (refer to page 118) that this structure forms (rapidly)

by ordering of crystallisable groups, and evolves (slowly) by adsorption of simple aromatics.

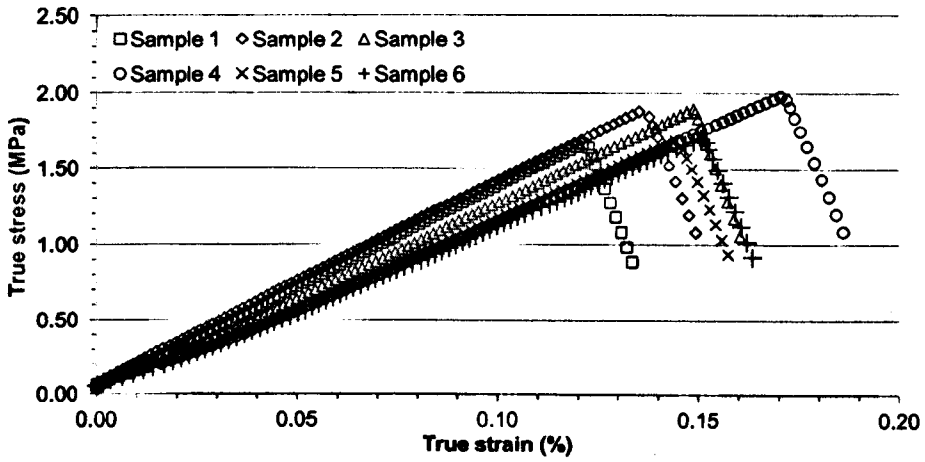


Figure 6-5: Repeatability of DTT at -25°C after one hour annealing at 25°C

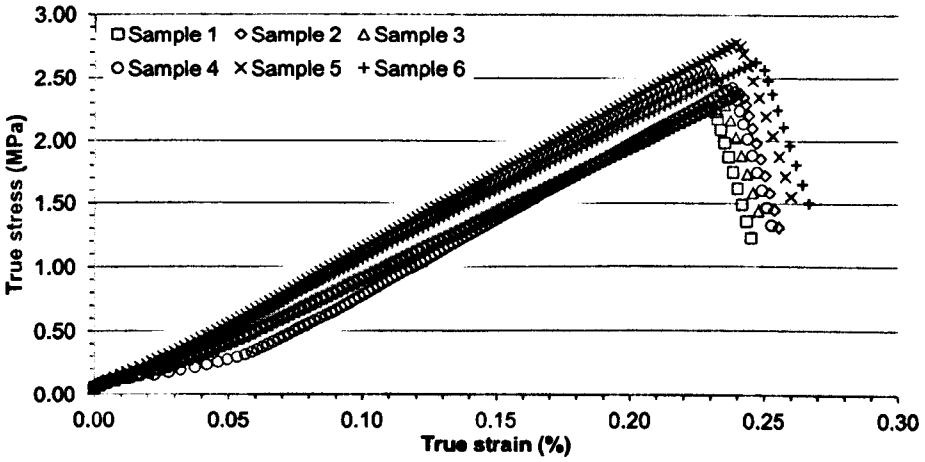


Figure 6-6: Repeatability of DTT at -25°C after 24 hours annealing at 25°C

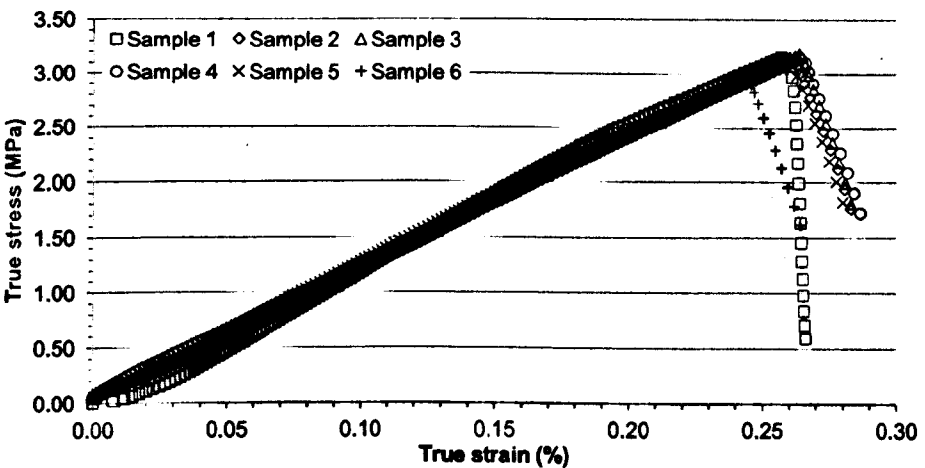


Figure 6-7: Repeatability of DTT at -25°C after 48 hours annealing at 25°C

Table 6-1: Variability of failure properties at 3%/min and -25°C (bitumen B)

Curing time (hours)	Strength (MPa)			Failure strain (%)			Toughness (MJ/m <sup>3</sup> )		
	Mean	Std. dev.	Co. var.	Mean	Std. dev.	Co. var.	Mean	Std. dev.	Co. var.
0.25 (AASHTO)	1.69	0.20	9.82	0.14	0.02	11.15	0.12	0.02	18.32
1	1.80	0.13	7.33	0.15	0.02	11.34	0.13	0.02	16.04
24	2.51	0.18	7.38	0.24	0.01	2.73	0.29	0.03	11.99
48	3.12	0.10	3.09	0.26	0.01	3.01	0.41	0.03	6.33

Table 6-2: Parameters for ESEM quantification of sample microstructure (bitumen B)

Curing time (hours)	Fibril diameter, d (µm)		Fibril spacing, a (µm)		Density, f <sub>s</sub>
	Mean	Std. dev.	Mean	Std. dev.	
1	9.6	2.1	31.1	7.0	0.18
24	10.6	2.5	27.4	5.4	0.27

For the following tests a 24 hour curing time was selected in order to ensure data repeatability and experimental feasibility.

### Strength recovery

The healing behaviour of the cracked interface is quantified by the ratio of recovered-to-initial fracture strength rather than toughness, for which the data is statistically more disperse (refer to Table 6-1). The time-dependent strength recovery was studied at the healing temperatures of 20°C and 40°C (refer to Figure 6-9), for the fracture temperature of -25°C. Healing data are described using a time-dependent model that is a modified form of the Christensen-Anderson equation (refer to Equation 6-3). This equation is used regularly for master curves of complex modulus (Christensen and Anderson, 1992; Woldekidan et al., 2010; Qiu, 2012).

$$H(t) = \sigma_{h,asy(l)} + \frac{\sigma_{h,asy(u)}}{\sigma_f} \times \left[ 1 + \left( \frac{m}{t} \right)^{\log 2/n} \right]^{n/\log 2} \quad \text{Equation 6-3}$$

where  $\sigma_{h,asy(l)}$  is the lower asymptotic healed strength (an s-shaped curve),  $\sigma_{h,asy(u)}$  is the upper

asymptotic healed strength,  $\sigma_f$  is the initial fracture strength,  $m$  and  $n$  are model parameters.

Preceding the discussion on the time-dependence of restored strength it is important to report two problems that limited the success of this study. Firstly, due to a uniform stress distribution in the gauge length the fracture test sporadically produced two cracks, which complicated the re-moulding stage. Notably, replacing the sample into a mould introduced damage and stress concentrations due to bending of the sample, which precluded further healing and re-fracture. Secondly, in order to study crack healing the re-fracture surface is required to be the same as the initial fracture surface. Using callipers to measure the length of sample fragments, it was established that the position of the crack surfaces occasionally deviated after healing (refer to Figure 6-8). This mechanistic research of fracture healing is confounded by spatial variation of crack-limiting interfaces: these problems introduced significant deviations among data points. These data are hence excluded from the time-dependent model of the healing process.

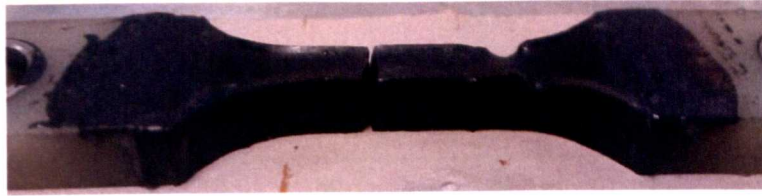


Figure 6-8: Profile photograph of a fractured, healed and re-fractured DTT sample. Note the two crack trajectories: the healed crack near the right end-tab, and the central re-fracture.

Figure 6-9 shows the time-dependent variation of restored strength, which evidences healing phenomena at 20°C and 40°C. At both temperatures, the precipitous recovery at short times precedes an asymptotic limit at 48 hours that indicates cessation of diffusive processes. The Christensen-Anderson Model predicts that the crossover time, to wit, the interchange of short- and long-term healing rates, is reduced by increased healing temperature (refer to Table 5-5). That is early-stage healing is a viscosity-limited process. This is ostensibly verified by periodic measurement of crack width, whereby closure is noticeably independent of the global healing function. The strength recovery curve is shifted to shorter times at the higher temperature and the plateau value increases from 25% to 30%. This indicates molecular scission processes or irrecoverable damage, which is unreported in the literature (refer to Chapter 3). To explain, it

is known that the crystallisable fractions could experience phase change or physical-chemical reactions at the higher healing temperature (refer to Chapter 2). This may in part establish the increased limiting tangent to recovery, and confirm the dissipative thermodynamic concept by Kringos et al. (2009) (refer to Section 3.3.4). This is consistent with theory on the involvement of aliphatic fractions in healing (refer to Table 4-1). Contributions due to the isotropisation and disordering of amorphous domains cannot be ignored, as suggested by the study on curing. It is concluded that strengthening processes including steric hardening or ageing are negligible, as inferred from coincidental pre- and post-healing stress-strain graphs. This indicates healing is not simply an expression of stiffening, as is reported in the literature (refer to Section 3.3.5).

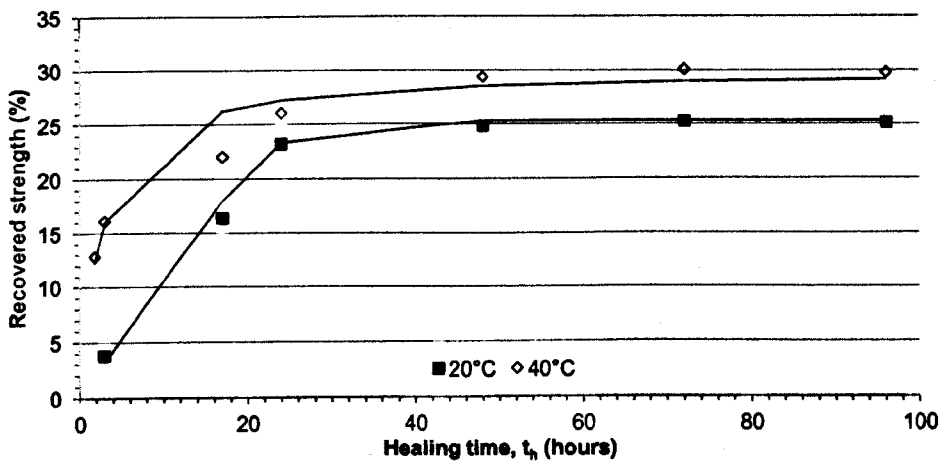


Figure 6-9: Variation of strength recovery with time modelled using the modified Christensen-Anderson Model, for healing temperatures of 20°C and 40°C and fracture at -25°C

Table 6-3: Parameters developed for the modified Christensen-Anderson Model

Heating temperature (°C)	$\sigma_{h,asy} / \sigma_f$ (%)	Crossover time, m (hours)	n (-)
20	25.33	23.75	0.038
40	29.76	2.85	0.280

### Repeat fracture-healing tests

Calliper measurements on the position of fracture planes established that post-healing crack paths are often identical to the initial damage event. Accordingly, a novel DTT investigation is reported in this thesis in order to evaluate repeated dissociation between the fragments.

This study used three healing cycles (four fracture tests) and the healing temperature of 20°C for 24 hours, which corresponds to the plateau in Figure 6-9 and hence cessation of diffusion. This informed two new insights. Firstly, the magnitude of strength recovery during successive healing periods decreases (refer to Figure 6-10). This indicates that the capacity of bitumen to resist an applied force is degraded by crack propagation through the healed interface (verified to within 500µm). To explain, it is theorised in this research that the molecules bridging across and peripheral to the fracture plane progressively shorten due to consecutive scissions; thus, their ability to participate in network-building processes reduces. This arises macroscopically as reduced strength recovery. Secondly, five of the six samples show limiting tangents to their recovery curves: the mean limiting value is about 13.2%. This is comparable to the re-fracture strength restored after complete optical closure of the crack: at 40°C this required 1.83 hours at which time 12.8% strength was restored. Consistent with the literature review, this material-specific boundary to healing is explained by the thermodynamic work of cohesion.

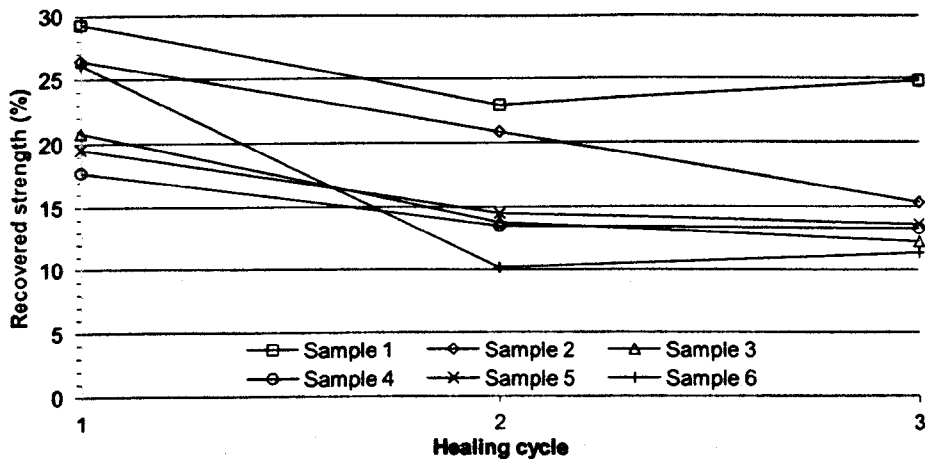


Figure 6-10: The effect of repeated fracture-healing on recovered strength: healing cycles are 24 hours at 20°C, and fracture is at -25°C

### 6.2.6 Electron microscopy study on short-term healing

To analyse optically the microstructural effects of healing, material was sampled from bitumen B that was fractured using DTTs and healed at 20°C for three hours. According to Figure 6-8, this corresponds to mean strength recovery of 3.80%. For shorter healing times, the fractured material would disintegrate when handled. Moreover, the interface was isolated from the bulk

using a hot blade to cut the bitumen, and then mounted onto an aluminium holder. The ESEM was constrained by sample thickness: 5.0mm compared to poured films of 0.5 to 2.0mm. This required a long working distance<sup>15</sup> and hence degraded the resolution of the micrographs.

Using the irradiation conditions defined in Section 5.1, the void between the crack surfaces is shown to be bridged by irregular bitumen strands that enable interfacial transmission of stress (refer to Figure 6-11(a)). This micrograph verifies the bridge-healing mechanism postulated by de la Roche et al. (2003) and identified using acoustic emissions (refer to page 79). Driven by the propensity for an interface to shrink and reduce its area and free energy (Mullins, 1958), it is concluded that bridges form by flow: the profile suggests flow originates from both surfaces.



Figure 6-11: (a) Image of the bridge-healing mechanism in bitumen B (10 seconds exposure). (b) Micrograph of the interfacial bridge after 5 minutes irradiation at 20keV and 20°C.

After five minutes irradiation at 20keV the fibril network structure was exposed (refer to Figure 6-11(b)). Towards the midpoint of the bridge longer fibrils align axially-parallel, but adjacent to the crack surfaces the network morphology is random and densely entangled. Analysing this micrograph using the parameters introduced by Stangl et al. (2006) (refer to Section 5.1.5 and Table 6-4) shows that fibril diameter and density increase along the bridge, with distance from its midpoint: with time after cessation of flow. This structure develops in two phases: firstly by flow (or bulk translation) and cooling of crystallisable molecules and aromatic side-chains, and secondly by diffusive build-up of entanglement. Notably, the density of fibrils peripheral to the bridge (at the crack surface) is restored after this healing, but diametrical recovery is partial. It

<sup>15</sup> The distance between the target and the base of the objective lens (Goldstein et al., 2002)

is also interesting that although this structuring is limited to the surface (refer to Section 5.2.5) it mimics on a microscopic scale the interdiffusion model for polymer healing (refer to Section 3.3.2). This provides a commonality between polymer and bitumen healing.

Table 6-4: Parameters for ESEM quantification of healed and initial structuring in bitumen B

Distance along strand ( $\mu\text{m}$ )	Fibril diameter, $d$ ( $\mu\text{m}$ )		Fibril spacing, $a$ ( $\mu\text{m}$ )		Density, $f_s$
	Mean	Std. dev.	Mean	Std. dev.	
18.8	3.0	0.8	10.5	2.2	0.16
81.3	4.3	0.7	14.6	4.4	0.17
116.1	4.9	1.0	12.6	2.6	0.28
-----					
Un-fractured sample	10.6	2.5	27.4	5.4	0.27

A high-resolution image captured after 5 minutes irradiation on a poorly-washed section of the interface shows the effects of filler: potassium crystals. Namely, the highly-entangled network is interrupted by inclusions that also prevent contact of the fracture surfaces (refer to Figure 6-12). This could in part confirm the known loss of healing in bitumen-fine aggregate mastics.

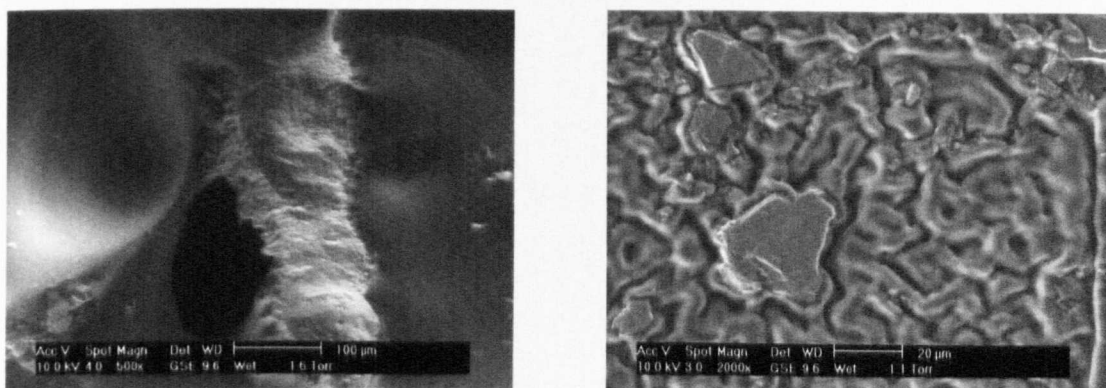


Figure 6-12: (a) Low magnification image of interruption to healing due to potassium crystals. (b) High resolution of disruption to microstructure due to potassium crystals.

## 6.2.7 Summary

The direct tension test was used to describe crack healing behaviour in bitumen B: a fracture-healing-re-fracture procedure using tensile strength recovery to define the effects of healing. It

is shown that healing is a viscosity-driven and thermally-accelerated process, which is altered by phase change and physical-chemical reactions of crystallised molecules and disordering of amorphous domains. Repeated re-propagation of remnant crack planes provides evidence for the contribution of molecular entanglements to healing, which is consistent with the postulated local condensation of high molecular weight chains. The surface-concentrated network shows diffusive build-up of entanglement that enables strength recovery and remnants of damage, to which partial healing is ascribed.

## **6.3 DYNAMIC SHEAR RHEOMETRY**

### **6.3.1 Background**

Analysis of bitumen healing in the literature is acquired ubiquitously by cyclic strain- or stress-controlled tests using a DSR, with regular (intermittent-type) or periodic (storage recuperation) interruption of continuous shear. Due to complexity of the test, the evidenced healing capacity is spurious and susceptible to procedural artefacts particularly the mode of loading. Moreover, constant oscillation at low amplitude during recovery is informative but thought-provoking: the kneading action could contribute to healing (refer to Uchida et al. (2002) on p. 72). An efficient rheology study on fatigue healing should instead adopt the analysis method established in the polymer state-of-the-art review. Namely, the production of recovery graphs by acquiring data using numerous samples healed for manifold times, or regular but ephemeral characterisation of the response of replicates. Both methods are used in this thesis. Inspired by the literature a novel study using the DSR then aims to decompose fatigue-healing into a fracture singularity. This is developed from the method noted by Bommavaram et al. (2009) (refer to Figure 3-15).

### **6.3.2 Fatigue-healing tests**

#### **Preamble**

Initial focus of this study is on the ability of fatigued binder to recover mechanical performance during rest periods, with the aim to characterise the effect of damage induced in the regime of macrocrack growth. Studies of healing in this regime of fatigue are not found in any literature. According to Section 6.2 and Figure 6-1 bitumen B was selected for this work. The rheological behaviour of this intermediate asphaltene content bitumen was examined using Bohlin Gemini and CVO dynamic shear rheometers equipped with 8mm diameter parallel plates. Samples of the material were prepared by the method detailed under Section 4.2.4.

#### **Test methodology**

To ensure that rheological testing is conducted in the region of linear viscoelastic response, a strain sweep was produced for bitumen B at 20°C (refer to Figure 6-13). The temperature was selected to correlate with DTTs on this material, and is in the region of wax crystallisation and

phase transition temperatures: 22 to 30°C (refer to Section 5.1.2). This enables contributions to healing due to these phenomena, which are reported elsewhere in this thesis. Accordingly, microscopic deformation is developed by continuous shear at a strain confined in this domain (1.5% oscillated at 25Hz and 20°C). This is arrested at a level of damage defined by the ratio of current-to-initial complex modulus. The recovery of rheological properties is analysed intra-healing by regular measurements on replicates (similar to the protocol of Bommavaram et al. (2009) on page 78), and post-healing by studying re-fatigue of healed samples (similar to the method of Phillips (1999) on page 83).

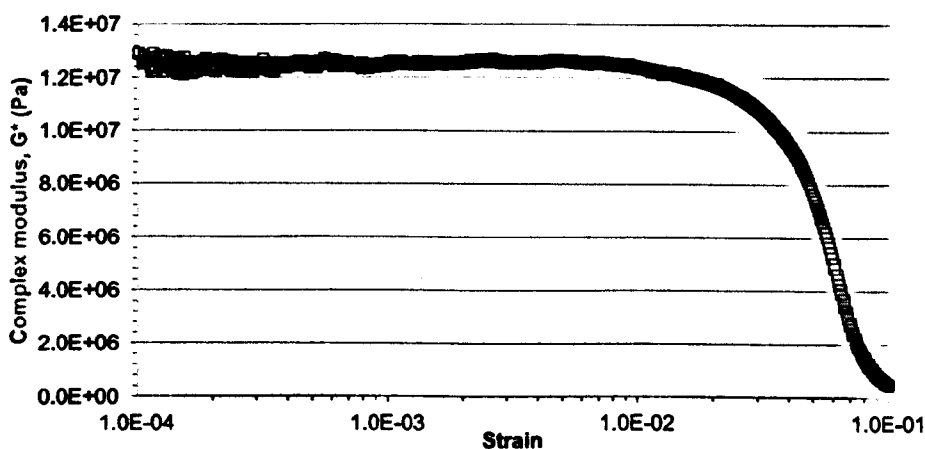


Figure 6-13: Strain sweep for bitumen B at 20°C and 25Hz, using a Bohlin Gemini rheometer

### Results and discussion

The evolution of complex modulus during fatigue evidences the ubiquitous tri-phasic response explained in Section 4.2.4. This is summarised as: mechanical property loss due to thixotropy and heating (phase one); the nucleation and growth of microcracks (phase two); and fracture due to microcrack densification (phase three) (refer to Figure 6-14). To isolate the beginning of fracture, the energy-based approach published by Rowe and Bouldin (2000) was applied to these data (refer to Figure 6-14). That is, when plotting the product of loading cycles (N) and complex modulus ( $G^*$ ) ( $N.G^*$ ) versus load cycles, a distinct maximum occurs at failure: crack initiation. For bitumen B this occurs at the 40% loss of initial complex modulus. This novel use of the energy concept enables precursory theory on the mechanism of healing: by comparing the normalised complex modulus value at the onset of recovery with that at fracture ( $0.60G^*$ ), the damage mechanism is identified. To adjust focus from microcrack to macrocrack healing,

storage recuperation-type rest periods are hence introduced to fatigue tests at below  $0.60G^*$ .

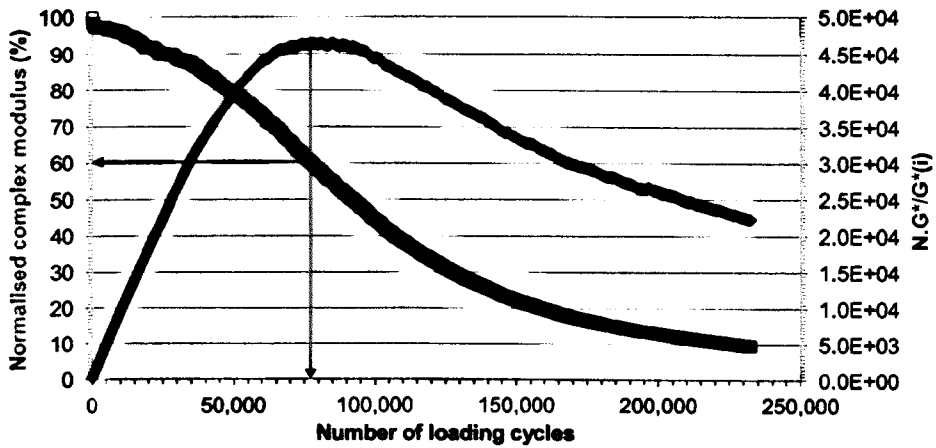


Figure 6-14: Variation of normalised complex modulus ( $G^*(n) / G^*(i)$ ) in continuous oscillation, showing the fatigue failure point defined by Rowe and Bouldin (2000)

The healing response was studied at  $20^\circ\text{C}$ , in order to remove thermal effects associated with temperature changes between fatigue and healing. The loading conditions are 0.015% strain oscillated at 25Hz intermittently for five seconds per minute, to reduce the interposition of data capture (kneading action) on healing. From the graphical presentation of mean data collected for rest periods that are introduced at various damage conditions, it is noted that the recovery of complex modulus (defined by Equation 6-4) is linearly-dependent on time to a limiting initial value of  $0.55G^*$  (refer to Figure 6-15). The plateau thereafter could suggest different healing kinetics in the regime of initial microcrack densification. This is explained by the convolution of dispersion effects and irrecoverable microstructural changes and thixotropy. It is notable that the time-dependence of the steady-state segments is not constant with the fourth root of time, as is predicted by the interdiffusion model for healing (refer to Figures 3-5 and 6-16).

Healing index: 
$$HI = \frac{G^*(t)}{G^*_{\text{initial}}} \times 100\% \quad \text{Equation 6-4}$$

where  $G^*(t)$  is the current complex modulus and  $G^*_{\text{initial}}$  is that previous to fatigue.

Moreover, there is an exponential drop in the mean healing rate with increased damage (refer to Figure 6-17). This response is explained by crack face separation distance: development of interfacial strength firstly requires contact between fracture surfaces, from which it follows that

increased crack opening displacement impedes recovery. This is ostensibly substantiated by the decline in instantaneous (cohesive-type) healing with damage.

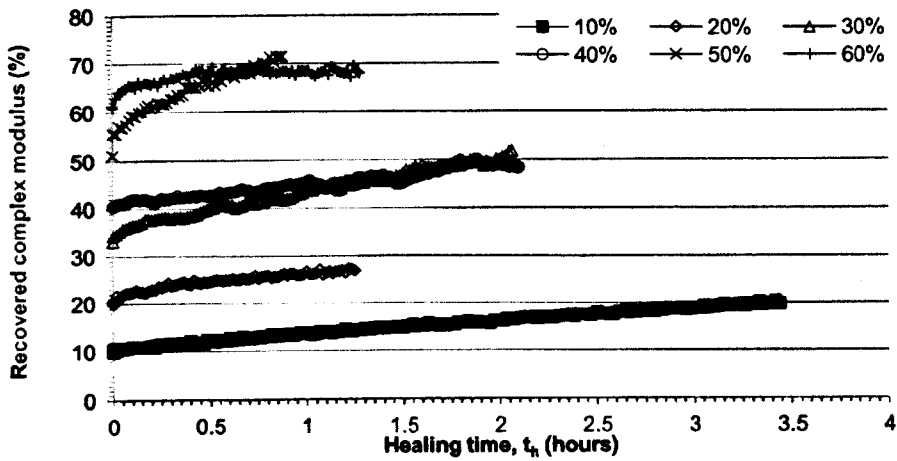


Figure 6-15: Complex modulus recovery plots for healing at 20°C from various damage levels

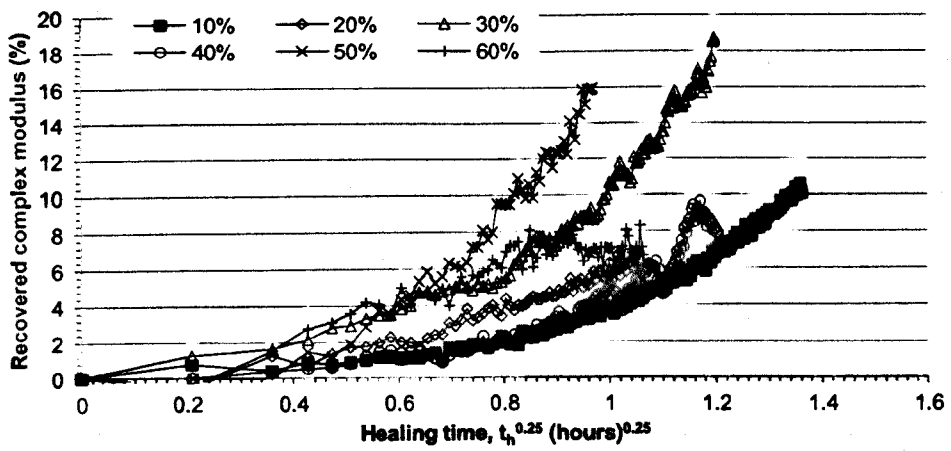


Figure 6-16: Variation of complex modulus recovery with the fourth root of healing time

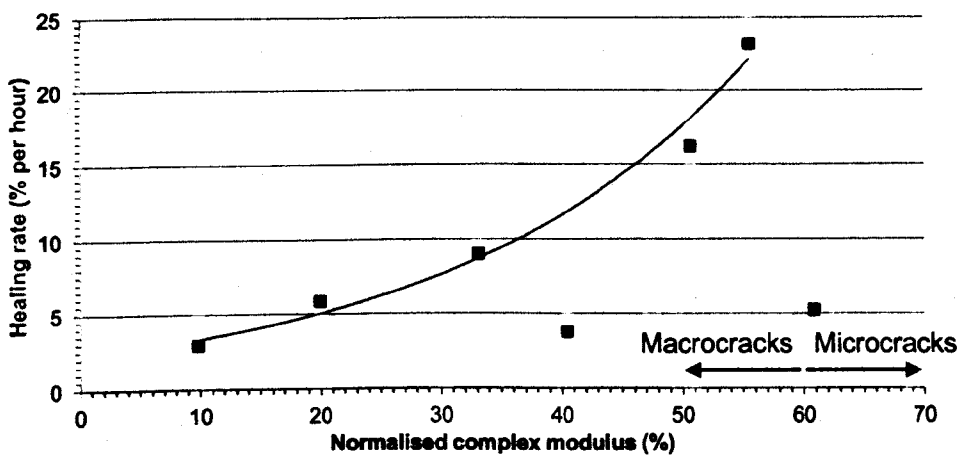


Figure 6-17: Recovery rate of complex modulus with damage level at the onset of healing

Following this initial study and in accordance with literature on polymer healing, an alternative test protocol is produced for higher healing temperatures. This is to prevent the interruption of healing by edge effects, which occur due to softening during rest period oscillation (kneading). The fatigued bitumen disc is instead healed in the cooling fluid in repose from strain. Healing is quantified by subsequent re-fatigue in terms of recovered complex modulus (at the onset of the loading phase) and fatigue life. This recovery phase is inserted on cessation of continuous shear after a 90% loss in complex modulus, and uses the strain conditions defined previously. This is the closest point to sample failure that can be studied without ambiguities in these data due to shearing of the fractured sample. The time-dependence of healing was studied thus at 20°C and 40°C.

At the low temperature the restored complex modulus derives a sigmoidal curve that appears to plateau at 70%. At 40°C the intermediate segment shifts to shorter times and the recovery graph exhibits an increased tangential limit (refer to Figure 6-18). This thermal transposition is consistent with diffusive healing kinetics and the higher (apparent) plateau could be explained by perturbation of the thermodynamic state of the crystallised chains. That is, loss of cracking is thought (Kringos et al., 2009) to require rearrangement, by phase transition, of precipitated wax that starts at 23 to 30°C. Similar to the literature, recovery of fatigue life is protracted and appears to plateau at 28% after 24 hours at 40°C. The significant difference between complex modulus and fatigue life recovery indicates unique or non-synergistic mechanisms of healing, as follows. With reference to the concept of interdiffusion, the restoration of modulus could be explained by cohesion (wetting), interfacial diffusion of chains and bulk relaxation or ordering. Inefficient recovery of fatigue life may be ascribed to the inability of ruptured chains to interact and resist further damage. This response establishes additional sites for crack nucleation that explains post-healing life decay.

The time-dependent model for healing processes suggested by Bhasin et al. (2009) is applied to these data (refer to Equation 3-20 and Figure 6-18) using the parameters in Table 5-2. It is shown thus that healing due to interfacial molecular diffusion is dependent on temperature, to wit the convolution of the constants  $q$  and  $r$  indicate increased flux or reduced time to plateau.

The parameter  $p$  varies inversely with short-term recovery and shows that cohesive healing at the crack interface, in addition to diffusion during the time increment to initial measurement, is expedited by thermal effects.

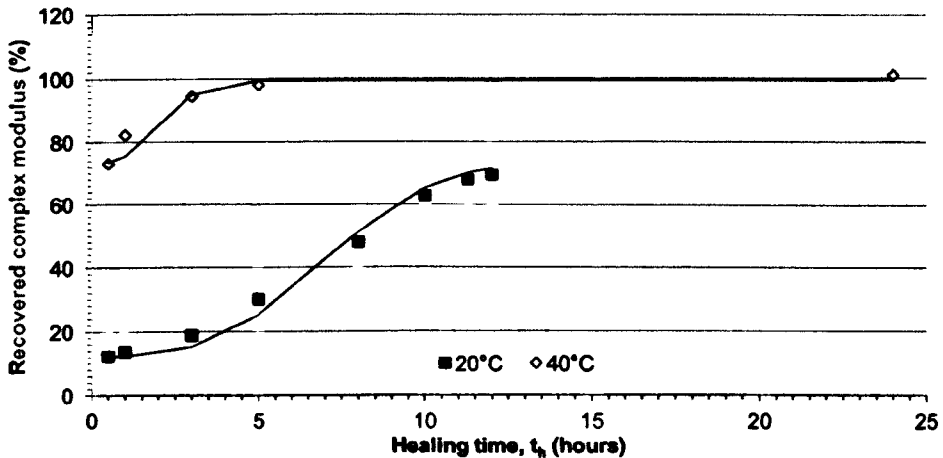


Figure 6-18: Variation of complex modulus recovery with time modelled using the equation by Bhasin et al. (2009), for healing temperatures of 20°C and 40°C and fatigue at 20°C

Table 6-5: Parameters developed for the healing function for bitumen B

Healing temperature (°C)	$R_0$ (%)	$p$ (-)	$q$ (-)	$r$ (-)
20	12.27	61.32	0.002	3.07
40	73.16	26.32	0.095	2.65

From mechanical considerations and insights from repeat fracture-healing using DTTs, failure is explained by stress-concentration at microscopic flaws. It is instructive to examine repeated fatigue-healing therefore, to evaluate the recovery capacity of the re-propagated macroscopic fracture surface. Using the fatigue conditions described above samples are firstly damaged to catastrophic failure: a 90% loss of complex modulus, and then healed in repose from strain at 40°C for one hour. The disc is then re-fatigued to an equal complex modulus value, when this protocol is repeated for four additional fatigue tests. It was found that the efficiency of healing phenomena decreases during successive healing cycles (refer to Figure 6-19). This response is explained by the progressive decay in the capacity for network-building phenomena, due to molecule contraction by consecutive scission events. It is consistent with previous discussion

in this section that fatigue life is most sensitive to this process.

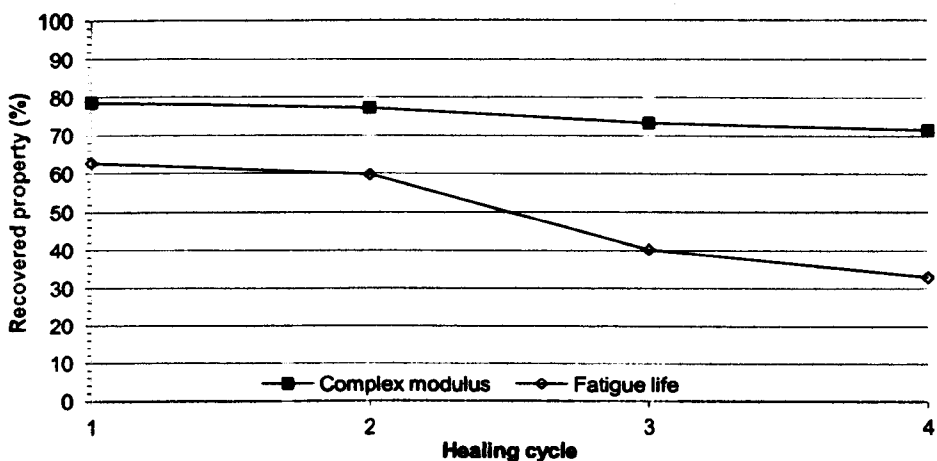


Figure 6-19: The effect of repeated fatigue-healing cycles on rheological property recovery

### 6.3.3 Fracture-healing tests

#### Preamble

To characterise the component of healing acquired by a wetted crack interface and caused by molecular diffusion and mixing, wetting should be instantaneous (Wool, 1995). The simulative DSR test proposed by Bhasin et al. (2009), to compress bitumen discs attached to the spindle and base plate, efficiently achieves this aim. The capacity of this method to study true healing is questioned. Notably, this method describes in fact welding: the contact of two surfaces with uniform molecular weight distribution (Wool, 1995). This protocol hence produces data devoid of fracture effects including modification of molecular weight distribution and surface topology. This thesis hence introduces an evolution of this protocol to study healing in cracked samples.

#### Test methodology

A modified silicone mould method is used for sample preparation. Namely, a defined mass of bitumen B is heated to the consistency of motor oil at room temperature; poured into a 25mm diameter mould; cooled and then annealed for 24 hours at 25°C. The  $4.0 \pm 0.1$ mm thick disc is mounted onto the base plate of the rheometer and warmed to its softening point previous to compression to 3.4mm. The suitability of this dimension is validated by Qiu (2012). The disc is trimmed and then stiffened by thermal conditioning at 5°C for 60 minutes, using inundation of

the circulating fluid bath. As this equilibration time elapses, the bath is drained and the spindle grip is loosened to allow the DSR head to be raised. To fracture the brittle disc a tensile force is applied to the spindle, which is then re-fixed into the top grip. After curing in air at 20°C, the fragmented sections are brought into contact by lowering the spindle, to produce the required disc thickness: 3.4 to 3.0mm. This creates a wetted interface. The sample is immersed in the aqueous cooling solution chilled to 20°C, and rheology is measured by periodic oscillation of 0.015% strain at 25Hz. To exclude steric effects and creep from rheological changes during crack healing, the complex modulus of an un-broken disc of equal geometry is measured. The analysis of healing is achieved by normalising the response of the fractured disc thereto. This novel approach is schematised in Figure 6-20, below.

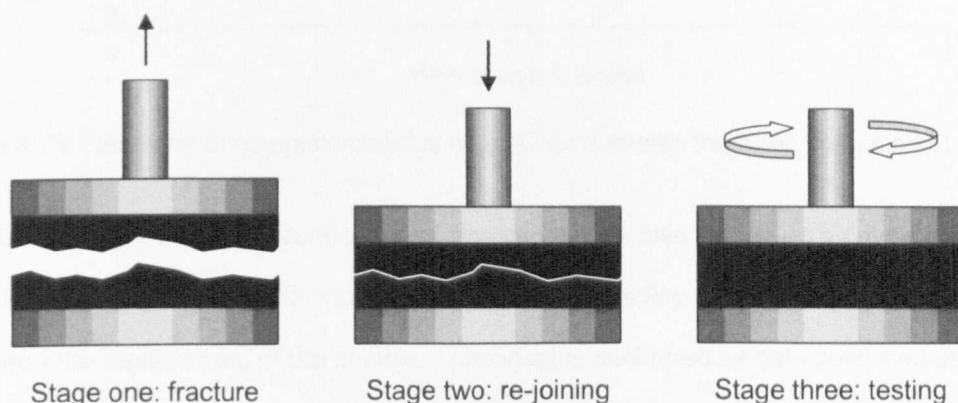


Figure 6-20: Schematic of the (tensile) fracture (shear) healing test on bitumen B using the dynamic shear rheometer

## Results and discussion

Figure 6-21 presents typical data from the fracture-healing tests. This indicates two phases: a primary (immediate) phase controlled by gap closure and a secondary time-dependent phase. This is consistent with the model introduced by Bhasin et al. (2009), which describes bitumen healing as the convolution of wetting (instant) and diffusion (temporal) phenomena. Complex modulus restored during the primary healing phase varies with disc thickness: this increment increases to 120% at 3.2mm, from 17% at 3.4mm. The compressive stress applied to the disc is uncontrolled, but the confinement effect produced as thickness is reduced transfers energy to the binder. This ensures interfacial contact and wetting by elastic-plastic deformation of the surfaces. Moreover, the time-dependent component of healing could be affected by relaxation of residual stresses (creep). The apparently incongruous data at the gap width of 3.0mm are

explained by load-induced flow to peripheral regions of the interface. This produces molecular orientation and reduces contributions from chemical bonds or molecular entanglement. This is consistent with the behaviour of low-viscosity polymers (refer to Section 3.3.2).

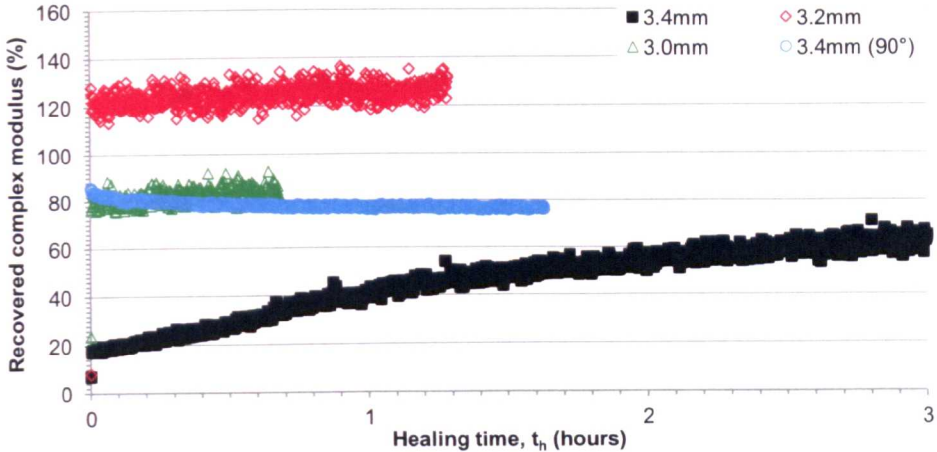


Figure 6-21: Recovery of complex modulus at 20°C for samples fractured in tension at 5°C

Notwithstanding the effect of confinement, data variation is also explained by misalignment of crack surfaces. That is, the affine state of topology produced by fracture propagation could be modified after replacement of the spindle. This effect is confirmed by data produced using the 3.4mm geometry and rotating the spindle 90° after fracture (denoted 3.4mm (90°)). Moreover, the linear gain of complex modulus shown by the 3.0mm and 3.2mm discs is contradictory to the sigmoidal response of the 3.4mm disc. These samples restored about 66% of pre-fracture complex modulus after three hours, from an initial value of approximately 20%.

### 6.3.4 Correlation of fatigue- and fracture-healing

Figure 6-22 presents the collated data. Notably, complex modulus is restored in the fractured samples at 20°C at shorter times than required to achieve equal recovery in the fatigue tests, also at 20°C. This unexpected result could be explained by the contribution of low molecular weight fracture remnants to rapid healing, and the absence of network separation (thixotropy) after prolonged mechanical agitation of van der Waals forces. The author recognises that this conclusion may be susceptible to confinement effects and an inability to accurately reproduce a purely-cohesive fracture surface, and dispersed fatigue damage that could reduce complex

modulus recovery. It is also notable that for the fractured samples, the percolation of cooling solution through the disc could reduce interfacial cohesion (Zollinger, 2005) and hence modify (reduce) the measurable healing capacity.

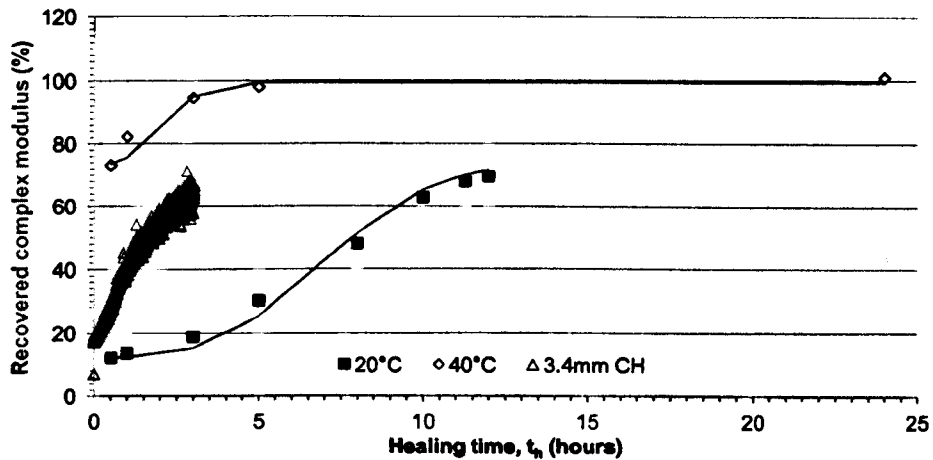


Figure 6-22: Data for complex modulus recovery from fatigue-healing tests for healing at 20°C and 40°C, and a fracture-healing test on 3.4mm thick samples at 20°C

### 6.3.5 Summary

Initial DSR investigations in this thesis focused on healing in fatigued bitumen. These showed that healing restores macro-cracks, and that full recovery of complex modulus requires phase transition (melting and crystallisation) of crystallised groups. Irrecoverable molecular damage and irreversible thixotropic effects preclude complete restoration of fatigue life, which requires a different time-dependence and non-synergistic healing phenomena. A new fracture-healing test was introduced, which indicated that compressive stress expedites recovery. Collation of these data suggests that the healing time is reduced by low molecular fragments of fracture, but increased by thixotropy and dispersed damage.

## 6.4 VIALIT PENDULUM TEST

### 6.4.1 Background

The Vialit pendulum test was developed in the 1990s to simulate cohesive fracture of bitumen where aggregate is in direct contact with traffic stress: in surface dressings and rolled asphalt surface courses, for example (FEHRL, 2006). The principle of this test is to measure the peak energy absorbed by the fracturing of a binder film under specific conditions of impact (Bononi, 1988). The Vialit test provides a novel method to study true (fracture) healing, therefore.

The Vialit pendulum test involves placing a thin film of bitumen between two steel cubes, and measuring the energy required to remove the upper cube. The Vialit apparatus consists of a pendulum that is raised to the vertical and released through its arc to strike a steel cube. This cube is fixed to a second cube by a 1mm thick layer of bitumen. The cube is displaced by the impacting pendulum, which fractures the bitumen film. The absorbed fraction of kinetic energy is defined in terms of the angle swept after impact ( $\alpha$ ) (Airey et al., 2002). Notably, the surface of the cubes is textured (roughness 700 $\mu\text{m}$ ) in order to ensure that cracks occur in the binder (cohesive), and not at the steel-bitumen interface (adhesive). This protocol is standardised in EN 13588:2008. The general layout of this shear-type test is shown in Figure 6-23, below.

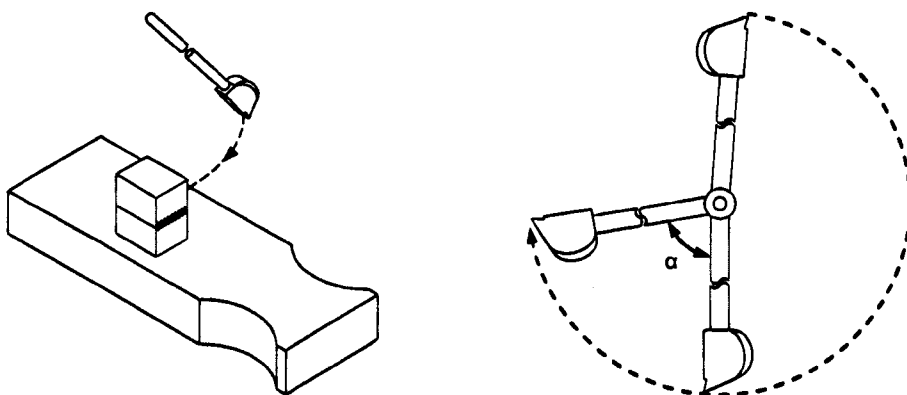


Figure 6-23: Schematic of Vialit pendulum cohesion test (developed from EN 13588:2008)

Cohesive energy curves are produced on a linear scale with temperature. The graphs indicate thermal variation (refer to Figure 6-25) and for most binders tend to a low temperature ( $< 0^{\circ}\text{C}$ ) asymptote of  $0.2\text{J}/\text{cm}^2$  (Waters, 2008). In this regime the film fails according to brittle fracture:

above the temperature of peak cohesion failure is viscous in nature. The effect of oxidation is to increase the temperature of maximum cohesion (Widyatmoko et al., 2002). Moreover, the cohesive energy across the entire temperature range is raised by polymer modification of the bitumen, although comparability between data published by different analysts is limited.

#### **6.4.2 Sample preparation**

The preparation method for Vialit pendulum films is explained in EN 13588:2008. In summary, the cubes are washed using mineral spirit cleaner, rinsed with an aqueous solution containing ethanol and then dried in an oven. The sampled binder is heated to a temperature not greater than 90°C above its ring and ball softening point and stirred often, to produce a homogeneous liquid with a consistency at which it can be spread. Using a spatula, the bitumen is applied to the textured faces of the cube and support (pre-heated to  $60 \pm 5^\circ\text{C}$  for 60 minutes), which are immediately joined with the serrations facing each other. Excess binder is removed from cube surfaces by scraping with a knife and the test assemblies are cured at 25°C in a dehumidified environment for 24 hours, to allow for ordering of bitumen microstructures. Prior to testing, the geometry is conditioned in a fluid bath at the required test temperature for 90 minutes.

#### **6.4.3 Sample testing**

After thermal conditioning at 5 to 80°C, the assembly is transferred to the cohesion tester and the pendulum is released. The time for this process is less than 20 seconds and the replicates are tested in a 10 minute period. The swing-through angle ( $\alpha'$ ) is recorded to the nearest 0.5°, and the cube faces in contact with bitumen are investigated for evidence of adhesive failure: if an area of exposed metal greater than 5mm<sup>2</sup> is visible the result is discarded.

In standard tests the base plate is replaced and the cube inverted on a clean base and tested as above, in order to determine the absorbed energy of impact and bitumen cohesion (refer to Equation 6-5 and Figure 6-24). For the healing study reported in this thesis the detached cube is replaced onto the support and stored in an oven under the required conditions, and then re-conditioned in a fluid bath before re-fracture. By this method approach of the fracture surfaces

(crack closure) is simulated by replacing the upper cube. Flanges on the cube (refer to Figure 6-24) should stop this compression from being transferred to the film. The healing response of bitumen is quantified by the ratio of recovered-to-initial cohesion. Notably, conditioning effects are removed by tests for zero healing: fractured samples are cured for 90 minutes in the bath.

$$C = mgr(\cos\alpha - \cos\alpha')/s \quad \text{Equation 6-5}$$

where C is the cohesive energy, m is the pendulum mass, g is acceleration due to gravity, r is the radius at the centre of gravity of the pendulum and s is the breaking area ( $100\text{mm}^2$ ).



Figure 6-24: Profile photograph of a fractured Vialit pendulum sample (bitumen A)

#### 6.4.4 Results and discussion

##### Preamble

It has been discussed in work that healing requires phase transitions of waxes and interacting aromatic groups (refer to Section 6.2.7, for example). These processes occur at temperatures on the order of  $-10^{\circ}\text{C}$  to  $50^{\circ}\text{C}$ , as described on page 40. For bitumens B and C, healing at the upper temperature of  $50^{\circ}\text{C}$  could produce spurious data due to a loss of sample volume: their softening points are  $51.8^{\circ}\text{C}$  and  $39.2^{\circ}\text{C}$ , respectively. Bitumen A was instead selected for the initial tests reported in this section: it has a high softening point ( $72.0^{\circ}\text{C}$ ) that enables healing above  $40^{\circ}\text{C}$  (refer to Table 4-2 for physical properties). This effect is defined in detail below.

##### Repeatability of cohesion with pendulum test

The repeatability between six successive tests on binder A is analysed at temperatures in the range of  $5$  to  $80^{\circ}\text{C}$  (refer to Figure 6-25). Data in the domain of brittle failure, at temperatures below the peak cohesion at  $62.3^{\circ}\text{C}$ , have a standard deviation of  $0.002$  to  $0.031\text{J}/\text{cm}^2$ . This is

comparable to EN 13588:2008. Data are more variable in the ductile domain, which conforms to a review of repeatability published in the literature (Soerensen, 2009). The Vialit pendulum cohesion curve for bitumen A shows the temperature-limiting tangent below 20°C and peak of 0.63J/cm. This is similar to cohesion values noted for low penetration bitumens (Widyatmoko et al., 2002). To achieve highly accurate data and produce analyses that are comparable with DSR studies, samples are conditioned at 20°C for crack healing tests. Variability of cohesion data is increased by healing phenomena, but at healing times longer than 24 hours standard deviations are similar to the original population: 0.012 to 0.039J/cm<sup>2</sup> for healing temperatures of 20°C to 50°C.

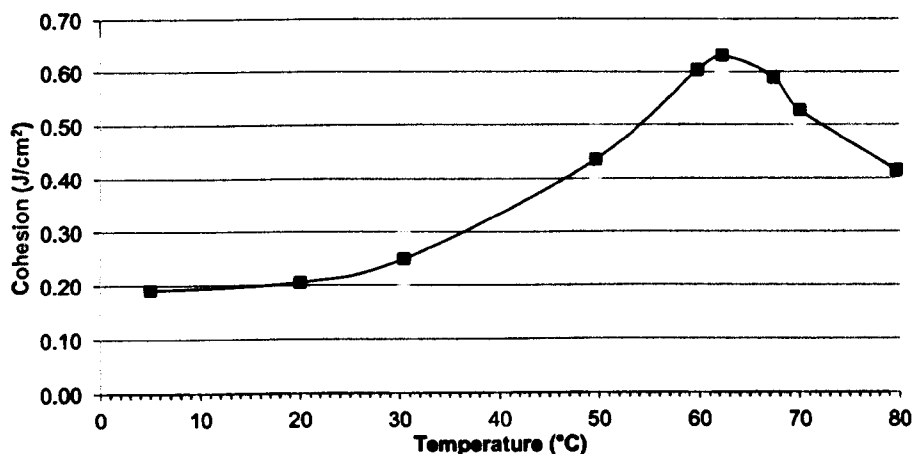


Figure 6-25: Vialit pendulum curve for bitumen A: the variation of cohesion with temperature

### Cohesion recovery

The time-dependence of the recovered cohesive energy was studied for bitumen A: the upper viscosity bound, at temperatures of 20°C, 30°C, 40°C and 50°C (refer to Figure 6-26). At the lowest temperature restored cohesion increases from a tangent at 2% to 33% after healing for 120 hours. As the healing temperature is raised, the asymptotic recovery domain is displaced to times beyond the scope of this study. Moreover, the intermediate steady-state region shifts to shorter times and a plateau forms at 80%. The principle of time-temperature superposition is applied to these data in order to construct a healing master curve at 40°C. This is modelled using the modified Christensen-Anderson equation (Equation 6-3), with the parameters noted in Table 6-6. The sigmoidal curve presented in log-log space indicates a cohesive asymptote occurring at short healing times, and partial recovery at long times (refer to Figure 6-27).

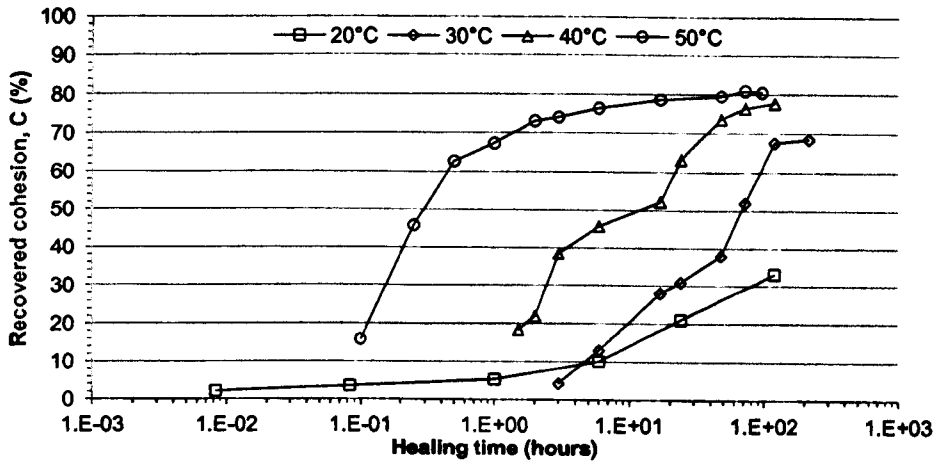


Figure 6-26: Cohesion recovery curves for bitumen A at 20°C, 30°C, 40°C and 50°C

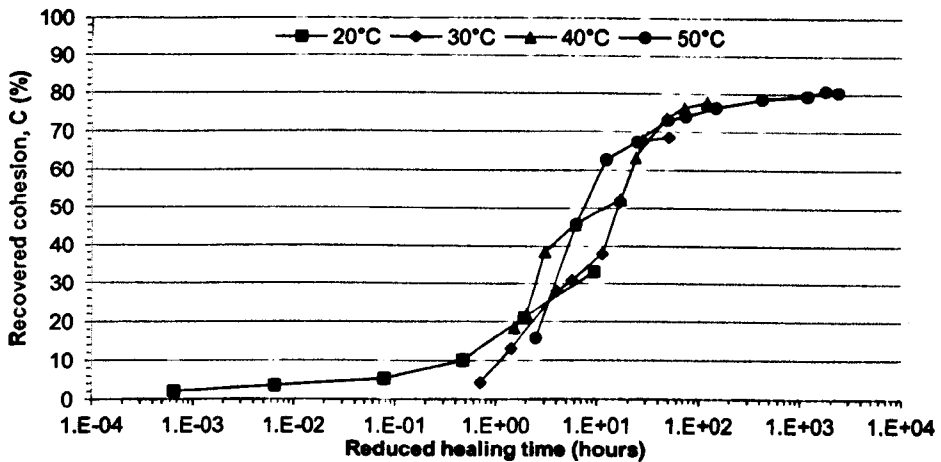


Figure 6-27: Cohesion recovery master curve produced for bitumen A at 40°C

Table 6-6: Parameters developed for the modified Christensen-Anderson Model

Heating temperature (°C)	$\sigma_{h,asy} / \sigma_f$ (%)	Crossover time, m (hours)	n (-)
40	80.29	0.24	0.78

### Surface rearrangement effects

To study the effects of surface rearrangement phenomena on the evidenced healing capacity, the fracture surfaces were separated for several days at -20°C using the configuration shown in Figure 6-24. The detached cube is then replaced onto the support and healed for 24 hours at 40°C previous to re-fracture. Compared to the control tests in which the crack surfaces are immediately rejoined, the recovered cohesive energy is reduced by delayed healing (refer to

Figure 6-28). This is explained by relaxation, diffusive inward migration and reaction of broken molecules, or contamination and smoothening of the surfaces that modify (reduce) wettability.

According to literature on polymer healing, this response indicates that the interpenetration of ruptured bitumen molecules or chain termini drives diffusion, which reduces in efficiency due to thermodynamic or structural homogenisation. Moreover, it is notable that the effect appears to plateau after 28 days delay at 72% recovered cohesion, which is similar to the second point of inflection on the recovery master curve. This could suggest that the polar (Lewis acid-base) component of surface energy that governs long-term healing of bitumen (refer to Table 4-1) is neutralised by reactions during delay, or is altered by rupture of the aromatic groups between which hydrogen bonds form (refer to Section 2.4).

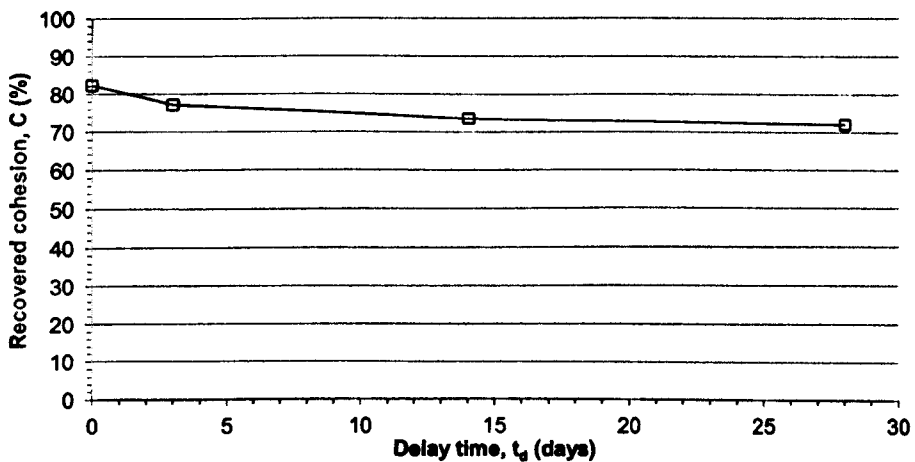


Figure 6-28: The effect of delay between re-contact of fracture surfaces on asymptotic healing

### Compositional effects

The time-dependence of recovered cohesion was also studied at 40°C for samples of binders B and D, to investigate the effect of composition (asphaltene concentration). Recovery graphs produced on a log-time axis evidence the intermediate or steady-state domain and asymptotic limit at 80% restored cohesion, which are consistent with bitumen A (refer to Figure 6-29). It is notable that an increase in asphaltene concentration shifts the curves to longer healing times, and decelerates diffusive healing phenomena: causes the curves to rotate towards the x-axis. That is, the rate of diffusion varies in inverse proportion to the n parameter of the Christensen-

Anderson model, which increases with asphaltene content (refer to Table 6-7). The viscosity-building interactions between asphaltene molecules appear to suppress the healing process.

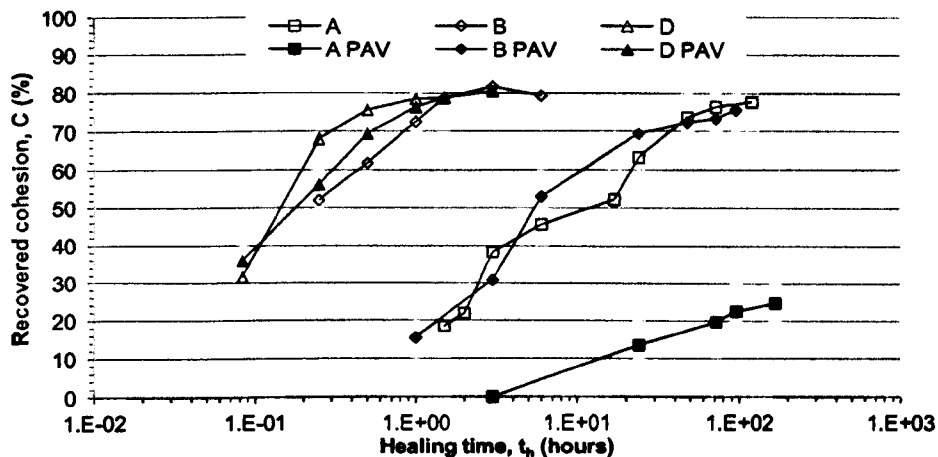


Figure 6-29: Cohesion recovery curves for virgin and oxidised bitumens heated at 40°C

Table 6-7: Parameters for the Christensen-Anderson model at a healing temperature of 40°C

Sample (oxidised)	$\sigma_{h,asy} / \sigma_f$ (%)	Crossover time, m (hours)	n (-)
A (PAV)	77.68 (24.76)	5.23 (20.92)	0.27 (0.28)
B (PAV)	80.53 (75.59)	0.23 (4.04)	0.21 (0.26)
D (PAV)	80.51 (80.55)	0.21 (0.10)	0.13 (0.28)

It is interesting to compare the recovery of cohesion and strength (DTT) for bitumen B at 40°C (refer to Figure 6-9 and 6-28). The rate and tangential magnitude of restored cohesion exceed recovery of fracture strength. This could indicate different and non-synergistic healing kinetics as discussed above, but may also be explained by two differences between the test methods. Firstly, the stress condition: in the Vialit pendulum test mode two in-plane shear produces the fracture, and in the DTT mode one tension at a rate of 3%/min. The deformation zones could contain molecular remnants of the fracture that are aligned in different orientations. Literature on polymer healing shows that molecular orientation effects modify healing (refer to page 51). Secondly, the mode of surface approach (crack closure): this is simulated for Vialit pendulum samples by application of compression to the replaced cube, and by flow in the DTT test. The surface rearrangement effects or structural homogenisation pending crack closure by flow of

bitumen molecules may hence contribute to the reduced healing capacity of DTT samples.

Also intriguing is the asymptotic limit to healing that is constant at 80% for the three materials. This could be explained by temperature effects during impact that establish the propensity for fracture by molecular scission. This would explain the tangential low-temperature cohesion at  $0.2\text{J}/\text{cm}^2$  for manifold bitumens. This is the working hypothesis: the null hypothesis is that this recovery plateau forms by flow attenuation due to differential viscosity on healing.

To refute the null hypothesis, aliquots of the three binders were fractured at  $20^\circ\text{C}$  and healed for one to six hours at equi-viscous temperature: the softening point (refer to Table 4-1). The recovery of cohesive energy for the three materials was about 80% at short and intermediate healing times, but diverged for bitumens A and B after six hours due to stiffening and the loss of sample volume by flow (refer to Figure 6-30). To study the effects of flow and softening on cohesion recovery, Vialit samples of bitumen A were prepared for cubes modified with wider grooves in the surface. It was found that this modified geometry allowed for greater loss of the sample material, during healing at  $50^\circ\text{C}$ . Notably, the mean initial cohesion ( $0.213\text{J}/\text{cm}^2$ ) was similar to that for the standard cube ( $0.205\text{J}/\text{cm}^2$ ), but the restoration of cohesion was shifted to longer time and a lower limit due to less-confined flow (refer to Figure 6-31). The maximum healing capacity of bitumen is not susceptible to viscosity effects: differences are explained by void formation due to thermally-activated flow. This is consistent with the working hypothesis.

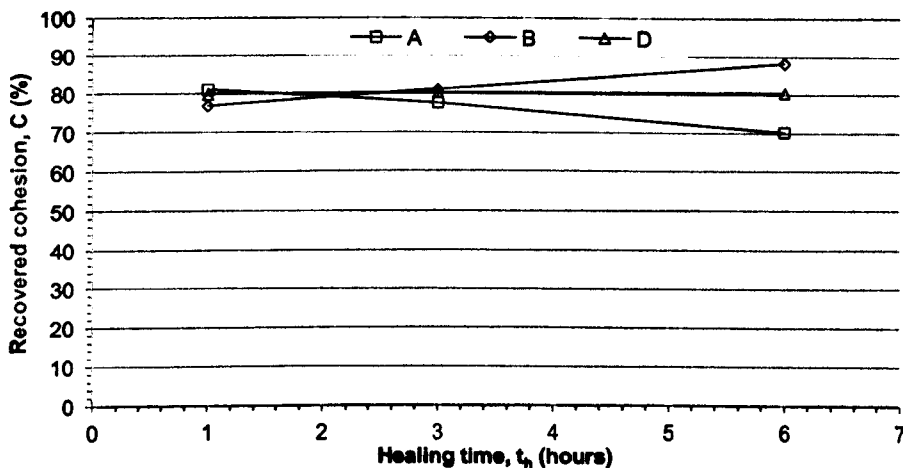


Figure 6-30: Cohesion recovery curves produced by healing the bitumen softening points

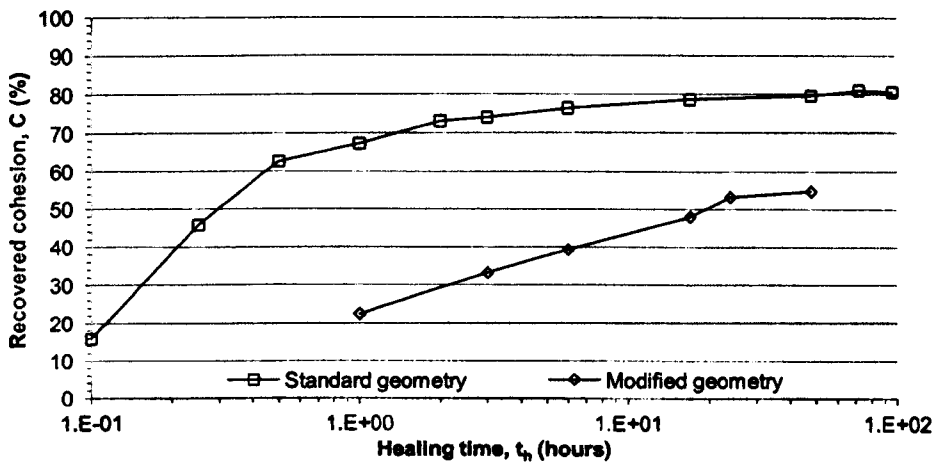


Figure 6-31: The effect of base plate roughness on the healing of bitumen A at 50°C

### Fracture temperature effects

To confirm the working hypothesis that the healing limit is sensitive to the molecular response of bitumen to external stress, samples of binder A were fractured at 5°C and 60°C and healed at 50°C. The recovery curves indicate a shift to shorter healing times and an increased limit to restored cohesive energy with raised impact temperature (refer to Figure 6-32). According to the literature on polymer and bitumen fracture kinetics, molecular dislocation above the glass transition is bounded by melting of van der Waals forces. Below this temperature, this process is limited by the stretching or bending of intermolecular and main-chain bonds and thus chain scission. These data could then be explained by this varying crack mechanism: chain rupture is reduced as bitumen is warmed through the glass transition temperature of resins (14.7°C) and simple asphaltenes. This allows for an increased volume of molecular interpenetration to the depth required for complete interfacial stress transfer, and reduces irreparable damage in the molecules: the healing capacity increases. Consistent with the dissipative thermodynamic model (refer to Section 3.3.4) and discussion in the DTT study, the rearrangement or merging into the matrix of crystallised fractions above 23°C may contribute.

### Oxidation (ageing) effects

The effects of compositional changes due to oxidation were studied for bitumens A, B and D at the healing temperature of 40°C. Samples were produced using RTFOT and PAV (refer to Section 4.2.2 and Table 4-1). The increase in asphaltene concentration retards the diffusive

processes that define the steady-state portion of the graph: curves rotate towards the x-axis. For bitumens A and B ageing shifts healing to longer times; for bitumen D the curves for virgin and aged samples are almost coincidental (refer to Figure 6-29 ). The parameters developed for the Christensen-Anderson models for each sample (refer to Table 6-7) are plotted against asphaltene concentration (refer to Figure 6-33). This produces two unique curves that indicate that asphaltenes act as healing inhibitors: the parameters vary inversely with healing capacity but directly with asphaltene concentration. The model for bitumen healing noted by Bhasin et al. (2009) is also applied to the data: parameters  $p$  and  $q$  are independent of composition, but the constant  $q$  shifts to lower values due to ageing and oxidation.

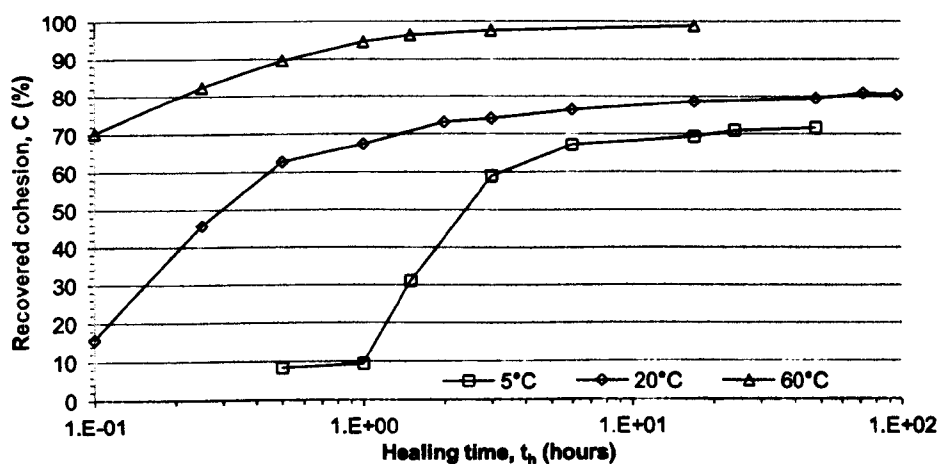


Figure 6-32: The effect of fracture temperature on restored cohesion for healing of bitumen A at 40°C

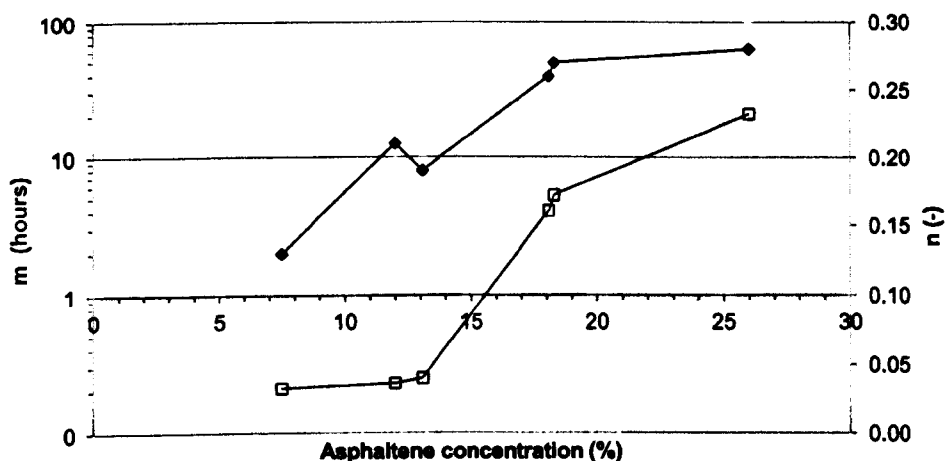


Figure 6-33: Variation of Christensen-Anderson model parameters with asphaltene content ( $m$  is denoted by the open squares, and  $n$  is denoted by the filled diamonds)

### **A comment on Vialit pendulum testing**

Cohesion is a performance measure of bitumen and the Vialit pendulum test allows for unique study on healing for brittle and ductile response. However, in her review on the Vialit cohesion test and other methods to measure related properties, Soerensen (2009) could not produce a formal correlation of data. This could prevent interchange of healing theory between tests. It is also notable that the cohesion healing test reported above is a lengthy and involved process.

### **6.4.5 Summary**

A Vialit pendulum test was introduced to characterise crack healing in bitumen using cohesion to quantify its effects. The data indicate that healing conforms to a sigmoidal model on double logarithmic axes: the lower tangent evidences wetting kinetics and the upper plateau partial or maximum healing. The diffusion regime is suppressed by network-building interactions among asphaltene molecules and the tangential limit is sensitive to fracture temperature. Notably, the glassy state of bitumen molecules at low fracture temperatures limits the healing response.

## 6.5 COLLATION OF MECHANICAL TEST DATA

Figure 6-34 presents results derived for binder B using rheometry, tension and cohesion tests for the healing temperature of 40°C. It is shown that the restoration of complex modulus after prolonged fatigue is generally inconsistent with fracture data: the mechanisms of stiffness and strength recovery are non-synergistic. This could be explained by the dependency of strength on the distribution of stress, which concentrates at local discontinuities and is thus sensitive to residual damage. Data from tension tests are coincidental to fatigue life recovery: the inability of ruptured molecules to interact and resist damage is a limiting factor in the healing kinetics of both properties therefore. The discussion on page 188 cannot be overlooked: differences in the stress conditions between the tests and the mode of crack closure could be involved.

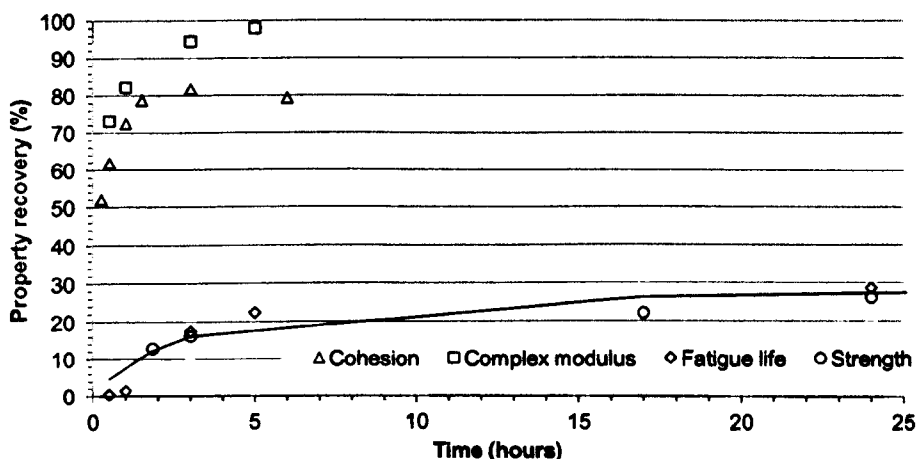


Figure 6-34: Collation of data for bitumen B healed at 40°C, and tested using Vialit pendulum (cohesion), DSR (complex modulus and fatigue life) and DTT (strength)

The stress-response of viscoelastic materials on fracture varies with temperature: evidence of this effect in bitumen is shown in Figure 6-35. This graph introduces combined cohesion and DTT data for the tangential limit (asymptote) to healing in bitumen B with an additional DTT at -18°C. The abrupt rise in maximum healing after -20°C is prominent and correlates highly with the glass transition of aromatic molecules: -19.6°C (refer to Table 2-6). More efficient healing above this temperature is explained by the increase in free volume or conformational entropy in the liquid parts, which facilitates sliding of elastically-bonded segments. This confirms that crack healing seldom occurs by reformation of ruptured bonds in molecular skeletons; instead

by attraction between contacting molecules. The ostensibly unique curve for bitumen A and B indicates that healing is limited by a convolution of the glassy characteristics of the fractions.

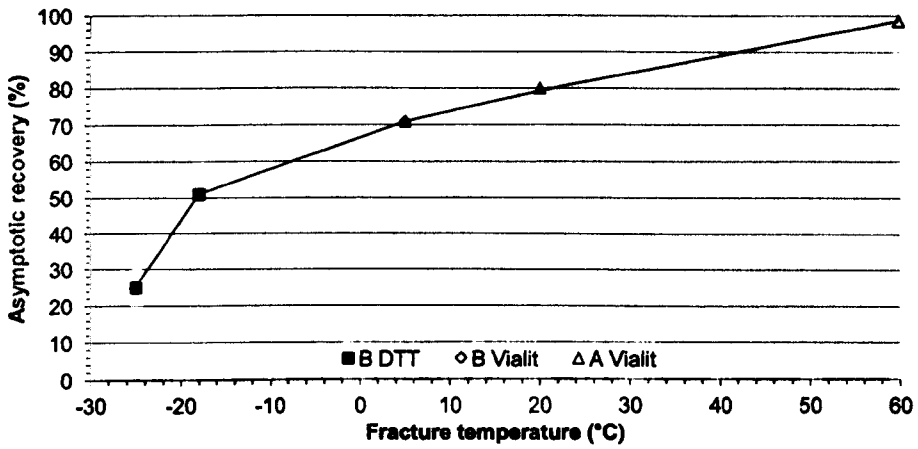


Figure 6-35: Variation of healing asymptote (strength and cohesion) with fracture temperature for bitumens A and B healed at 40°C

## 6.6 ELECTRON MICROSCOPY STUDY ON FRACTURE HEALING

### 6.6.1 Preamble

To complement the mechanical analyses of bitumen healing, cryo-SEM and ESEM were used to study the structural changes produced by fracture and healing mechanisms. For this optical research, a new sample preparation technique is proposed and explained below. To correlate with the range of mechanical tests used in this thesis, bitumen B was selected for this study.

Thin discs of bitumen are firstly prepared according to the silicone mould method for rheology tests. This is explained in Section 4.2.4. The 2000 $\mu\text{m}$  thick samples are cooled in air and then stored at 25°C for 24 hours, to allow for molecular ordering. The discs are then transferred to a freezer and stored at -25°C for 6 hours. The brittle discs are then fractured by hand and the splintered material is promptly restored to its initial configuration, in order to simulate closure of the crack. The re-formed sample is fixed to an aluminium holder coated with a conductive carbon tab to assure adhesion. This approach is schematised in Figure 6-36. These samples are stored at the required healing conditions previous to imaging, and then cooled at -25°C to minimise viscous flow and quench micro-structuring processes

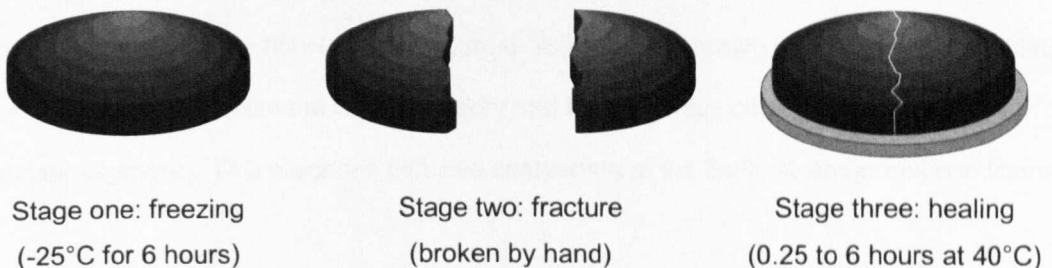


Figure 6-36: Schematic of the approach used to prepare fractured-healed samples for electron microscopy studies

### 6.6.2 Precursory cryo-SEM study on healing

The sample was imaged using the irradiation conditions defined in Section 5.3 after healing at 40°C for 15 minutes. This corresponds to cohesive energy recovery of ca. 52%. The partially-healed interface is well-defined and shows bridges that confer a seam-type pattern: the crack surfaces appear stitched together (refer to Figure 6-37). The cohesive strength evolved within

this wetted domain assures the interfacial transfer of applied stress.

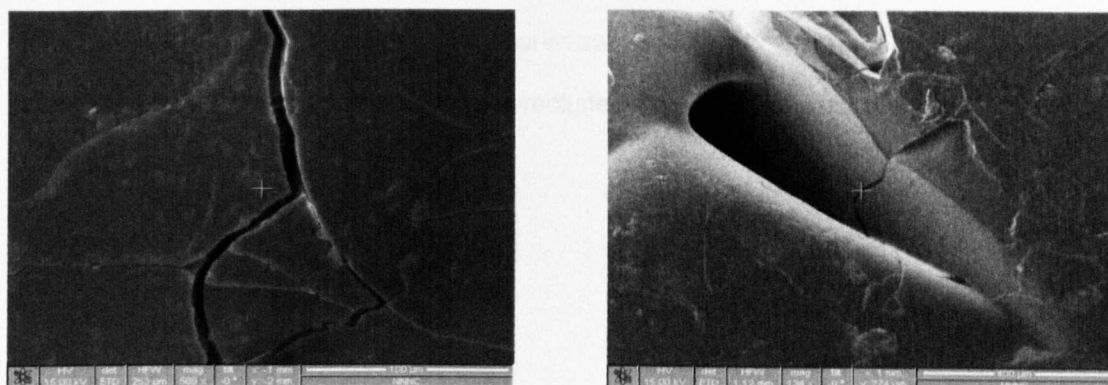


Figure 6-37: Cryo-SEM images of bitumen B fractured and healed for 0.25 hours at 40°C

### 6.6.3 ESEM study on healing

Samples for ESEM study on the microstructural effects of healing at 40°C were irradiated at a partial pressure of 0.6 to 1.4 torr water vapour, using the parameters defined in Section 5.2.4. In the intermediate domain of cohesion recovery (0.5 hours: 62% healing), the parabolic state of adjacent crack surfaces indicates viscous flow under the influence of gravity (refer to Figure 6-38(a)). After prolonged irradiation individual fibrils of the network are found to interpenetrate the plane healing plane, forming a zip-like structure by protrusion in a direction normal to the crack face and parallel to flow (refer to Figure 6-38(b)). The narrowed mean diameter of fibrils (refer to Table 6-8) bolsters the working theory that healing firstly occurs by interpenetration of molecular segments. This precedes diffusive coarsening of the fibrils at isothermal conditions.

Optical study on healing in the asymptotic region of restored cohesion (6 hours: 80% healing) was complicated by an inability to recognise the healing interface using microscopy. This was resolved by fixing aluminium tape to the sample mount at this location. The network structure was exposed in this plane after irradiation for 5 minutes 20keV. This structure is ubiquitously-entangled and three-dimensional but with apparent residual orientation effects (refer to Figure 6-39). By analysing this micrograph using the technique defined in Section 5.1.5 and collating with previous data, it is shown that fibril diameter and density increase with healing time (refer to Table 6-8). The enhanced interfacial transmission of load correlates with these processes,

namely condensation and randomisation. Moreover, the incomplete recovery of cohesion and other mechanical property correlates to changes in the dimensional and spatial distribution of the microstructure, when compared with poured samples. It is thought that this structuring is modified by molecular rupture, which may preclude network-building interactions.

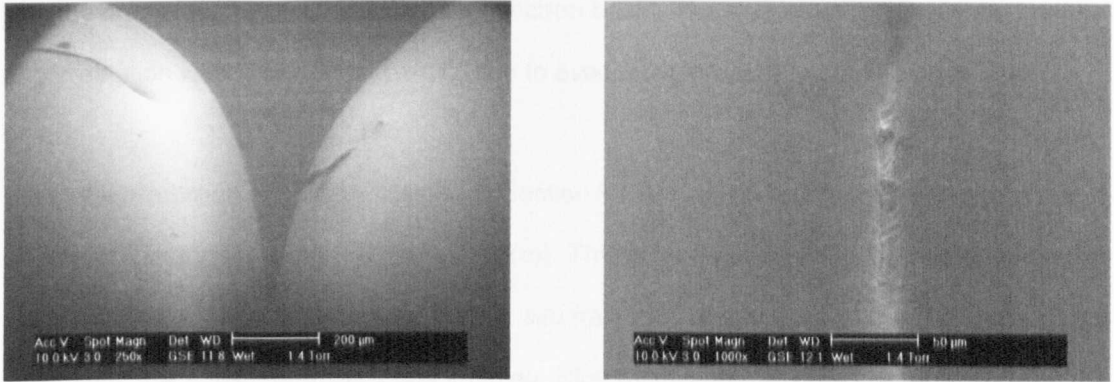


Figure 6-38: (a) Low magnification image of a crack interface after 0.5 hours healing at 40°C. (b) High magnification micrograph of the crack interface after 0.5 hours healing at 40°C.

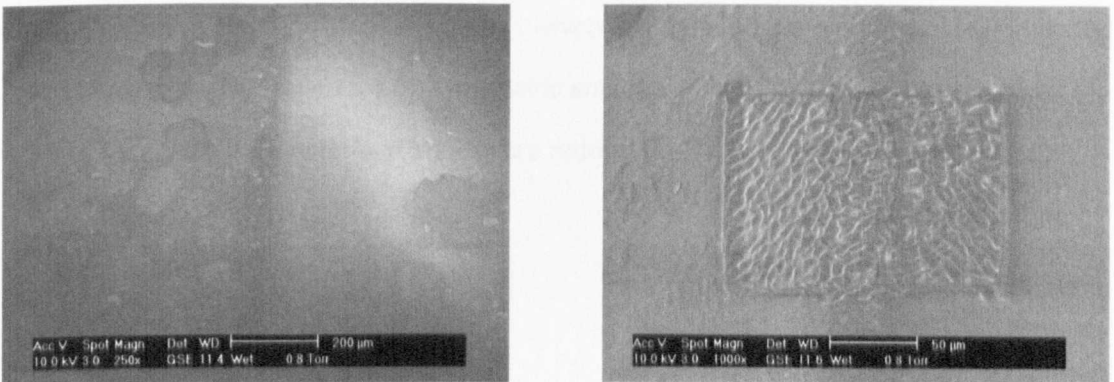


Figure 6-39: (a) Low magnification image of a crack interface after 6.0 hours healing at 40°C. (b) High magnification micrograph of the crack interface after 6.0 hours healing at 40°C.

Table 6-8: Parameters for ESEM quantification of healed and initial structuring in bitumen B (data derived from micrographs produced at 20°C)

Healing time (hours)	Cohesion at 20°C (J/cm <sup>2</sup> )	Fibril diameter, d (μm)		Fibril spacing, a (μm)		Density, f <sub>s</sub>
		Mean	Std. dev.	Mean	Std. dev.	
0.5	0.128	2.8	0.5	-	-	-
6.0	0.164	4.4	0.9	13.6	2.7	0.20
Un-fractured	0.207	10.6	2.5	27.4	5.4	0.27

#### 6.6.4 ESEM study on fracture

To study the working theory: that agitation of intermolecular forces and scission of main-chain bonds could produce an altered microstructure, a fractured surface was imaged using ESEM. This sample was produced as described in Section 6.5.1, and fixed onto an aluminium mount with the crack face aligned normal to the electron beam. The maximum time between fracture and irradiation was 0.10 hours at 20°C, due to evacuating the ESEM sample chamber.

Using the irradiation conditions defined in Section 5.2.4, low resolution images indicate microvoiding at the surface (refer to Figure 6-40(a)). This is incongruous with abundant topological detail reported by cryo-SEM research on *in situ* fracture (refer to Section 5.3.5), and evidence of viscous flow between fracture and imaging. High resolution micrographs captured after five minutes irradiation show the three-dimensional network of entangled fibrils common to poured samples (refer to Figure 6-40(b)). This image also shows effects of anisotropic conformational entropy: diffusive proliferation of structuring, which compares to the amorphous bulk reported in this study (refer to Section 5.3.5). Parametric analysis of this structure is consistent with the working theory: fibril diameter and density are reduced by fracture (refer to Table 6-9).

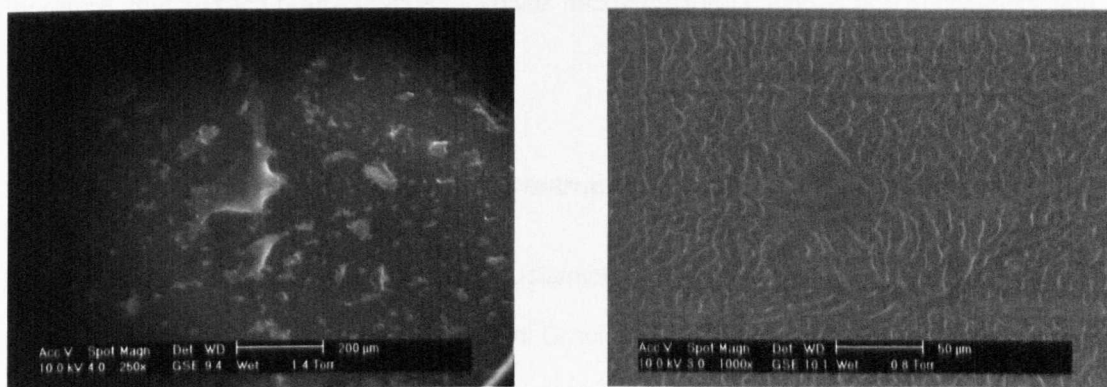


Figure 6-40: (a) Low magnification image of a crack surface after 0.1 hours exposure at 20°C. (b) High magnification micrograph of the crack surface after 0.1 hours exposure at 20°C.

The author recognises that cohesion data produced at 20°C may not compare accurately with images of fractures produced at -25°C. That is, data progression is reasonable but the degree of accuracy could be increased by equi-thermal tests. This is not feasible for these methods.

Table 6-9: Parameters for ESEM quantification of fractured and poured structure in bitumen B (data derived from micrographs produced at 20°C)

Sample preparation method	Fibril diameter, $d$ ( $\mu\text{m}$ )		Fibril spacing, $a$ ( $\mu\text{m}$ )		Density, $f_s$
	Mean	Std. dev.	Mean	Std. dev	
Fractured at -25°C	4.5	2.2	18.0	2.9	0.13
Poured	10.6	2.5	27.4	5.4	0.27

### 6.6.5 A comment on the effects on microstructure

The solubility continuum in the bulk maintains the dispersed and diluted state of the fractions. This is perturbed by fracture, which stimulates near-surface wax crystallisation and separation of aromatic fractions in the form of a network. This response could explain the suppression of healing by delayed closure of the crack. That is, the flocculation of associating particles upon fracture catalyses molecular interactions at the surface. This aggregation reduces the number of potential interaction sites, and precludes the interfacial development of network structuring. This hypothesis is confirmed by micrographs including Figure 6-39(b), which indicate that the proclivity for entanglement across the interface is lower than in poured samples. It is thought therefore, that surface rearrangement involves microstructural changes due to crystallisation and flocculation.

### 6.6.6 Discussion on the effects of microstructure

The preferential segregation of structure-sustaining compounds to the fractured surface is an important aspect of mechanical deformation. Crack propagation introduces a fluctuation in the composition field that evolves into the form of the fibrillar network, which is aligned parallel to the surface. This is consistent with surface-directed spinodal decomposition as concluded in Chapter 5. Loss of fibril diameter, entanglement and density is evidence of a reduced capacity for molecular interaction due to scission and de-cohesion of supra-molecular structures during crack growth. Rheology tests in Section 4.2 explain this by the contribution of glassy aromatic segments to damage. The time-dependent coarsening and densification of the network during delay to healing indicate long-range diffusion (refer to Table 6-10). These changes explain the

lower healing capacity associated with delayed crack closure: the growth of network structure before re-contact of the two surfaces reduces potential interaction sites for interfacial healing.

Table 6-10: Parameters for ESEM quantification of the effects of fracture-delay-healing on the microstructure of bitumen B (data derived from micrographs produced at 20°C)

Delay (hours)	Tangential limit (%)	Diameter, d (µm)		Spacing, a (µm)		Density
		Mean	Std. dev.	Mean	Std. dev.	
1	82.22	4.5	2.2	18.0	2.9	0.13
24	80.60	5.2	0.5	17.1	1.8	0.18

To develop an understanding of the effect of bitumen morphology, it is theorised that structure at the fractured surfaces is proportional to the character of intrinsic microstructure. Table 6-11 introduces the parameters developed to quantify microstructure and model healing at 40°C. It is shown that the diffusion rate, which is inversely proportional to the n parameter, is reduced by network densification: this gel-like system reduces healing by spatial interference. Build-up of the network during surface rearrangement could similarly prevent percolation of structuring through the healing interface. This is consistent with suppression of healing due to asphaltene molecules, which are thought to contribute to this structure (refer to Chapter 5), and polymer networks in modified bitumens (refer to Chapter 3). Additional testing is required.

Table 6-11: Parameters for ESEM quantification of initial structure and healing (data derived from micrographs produced at 20°C and using the Christensen-Anderson model)

Sample	Asp. (%)	Wax (%)	n (-)	Diameter, d (µm)		Spacing, a (µm)		Density
				Mean	Std. dev.	Mean	Std. dev.	
B	12.0	-	0.21	10.6	2.5	27.4	5.4	0.27
D	7.5	1.65	0.13	3.9	1.2	13.3	4.5	0.17
D RTFOT/PAV	13.1	0.12	0.28	3.0	0.8	7.2	1.4	0.30

### **6.6.7 Summary**

This thesis reports the first use of microscopy to study fracture-healing in bitumen. Cryo-SEM indicates that early healing enables the interfacial transfer of force by the formation of bridges due to flow. ESEM studies on the structural effects of healing indicate that this phenomenon firstly occurs by interpenetration of molecular segments, and then diffusive coarsening of the network at isothermal conditions. The incomplete recovery of cohesion and other mechanical properties correlates to fracture-induced changes in the spatial distribution of this structuring. It is also thought that the flocculation of associating particles on fracture catalyses molecular interactions at the surface. This precludes the interfacial development of network structuring, with which is associated a reduced capacity for healing due to delayed crack closure.

## **6.7 CONCLUSIONS AND RECOMMENDATIONS**

### **6.7.1 Conclusions from mechanical analyses of crack healing**

Three new tests are introduced to study fracture healing in bitumen. These are complemented by the first microscopy analyses on the microstructural effects of this phenomenon.

The direct tension test was used to develop the first new crack-healing study. The data shows that healing is a viscosity-driven (thermally-accelerated) process that is enhanced by physical and chemical reactions (phase transition) of crystallised waxes, and disordering of amorphous regions. This thesis also firstly studied consecutive re-propagation of remnant crack surfaces. This test provided evidence for the contribution of molecular entanglements to healing, which introduces a commonality between polymer and bitumen healing. This is also consistent with the postulated concentrations of high molecular weight aromatics near to bee-type structures.

Dynamic shear rheometer studies show that recovery of complex modulus is inconsistent with fracture data. This is explained by its dependency on bulk mechanical properties or dispersion effects, and informs the conclusion that complex modulus is an unreliable parameter to define healing. Notably, this novel research on macro-crack healing indicated that full recovery of the mechanical properties requires phase transition of crystallised chains. The second new crack-healing test was developed using this apparatus. This test suggested that healing phenomena are enhanced by compressive stress. Collation of the fatigue and fracture data indicates that healing time is reduced by low molecular products of fracture: it is imperative to study healing at cracked surfaces.

The third new test introduced in this thesis used the Vialit pendulum apparatus. This enabled characterisation of healing at reproducible fracture surfaces. These data indicate that healing conforms to a sigmoidal model, in which the diffusive phenomena are suppressed by network-building interaction between asphaltenes. Moreover, this test uniquely identified the incapacity of broken molecules to interact and resist damage: this is a limiting factor in the mechanism of healing. In accordance with this conclusion, this test identified that the molecular response of

bitumen to fracture varies with temperature. In the glassy regime, immobilisation of aromatic-containing fractions and imbibed saturates explains the concentrated scission processes that reduce healing. As fracture temperature is raised above their glass transition chain separation by thermal expansion enables sliding of elastically-bonded components without scission. The capacity for network-building interactions is sustained and full healing is possible: recovery is precluded by the glassy fractions.

### **6.7.2 Conclusions from microscopic analyses of crack healing**

Unique electron microscopy analyses of healed surfaces shows the distinctive bridge-healing mechanism: parabolic strands evolve by flow of the bitumen and enable interfacial transfer of stress. Prolonged irradiation of the bridges indicates that the network structure heals firstly by diffusive densification of the fibrils, and secondly by entanglement. This mimics the healing of polymers. Further analysis of this network indicates residual damage due to molecule scission that correlates with the partial recovery of mechanical properties. Surface rearrangement due to flocculation reduces the number of potential sites for interfacial molecular interactions. This reduces the capacity for healing.

### **6.7.3 Recommended further studies on healing**

The tests introduced in this thesis indicate uniquely the importance of fracture temperature on healing, and highlight the complexities associated with quantification of this process. From the correlation of property recovery with fracture temperature, it is suggested to test at the glass transition temperatures of the fractions as defined using differential scanning calorimetry. The analysis of healing behaviour should be conducted by strength recovery.

The rheological simulation method for fractured bitumen is imprecise but a logical progression of the literature: it allows for collation of fracture and fatigue-healing. To improve repeatability of this test the shear platform could be adjusted to include an extensional rheometer.

It is also instructive to study the effects of delayed healing in order to develop understanding of the molecular interactions that are critical to this process.

## 7 CONCLUSIONS

The core aim of this study was to understand the relationship between bitumen microstructure and fracture healing. This thesis accordingly focused on three aspects: the surface and bulk structure of bitumen; the healing phenomenon and its effective measurement; and the effects of fracture and healing on structure. Some of the novel findings associated with these parts of the research are summarised below, in Table 7-1, and the conclusions from these as follows.

Table 7-1: Summary of the important novel findings of this research

Test method	Page	Outline observations and explanation
ESEM	110	The beam effects are shown to vary with asphaltene content: this is consistent with radiolysis and not heating as reported in literature.
	119	The first use of thermal control shows that structuring is modified by heat: the entangled asphaltene network is enriched with wax.
Cryo-SEM	136	Cracks propagated through bee-type dispersions during quenching: shows solute-solvent compatibility that is not noted in the literature.
	138	The bulk of bitumen is amorphous: this state is altered by interfaces that catalyse surface-directed spinodal decomposition.
Cryo-FIB/SEM	149	Modifications due to irradiation include ion-resistant domains: these indicate that asphaltenes are well-dispersed in non-polar fractions.
	152	Amorphous bulk surfaces indicate constant sputtering: structuring occurs at free surfaces in air, which is unreported in the literature.
DTT	167	Fracture healing is higher above wax crystallisation temperatures: healing involves physical-chemical reactions of these molecules.
	168	Repeat fracture-healing tests show healing is reduced by cracking of healed interfaces: evidence for the contribution of entanglement.
DSR	175	Healing restores macrocracks: healing was noted in the literature to restore micro-damage only.
	179	A tensile fracture-healing test shows that cracks recover faster than fatigue damage: healing time is reduced by fragments of fracture.
Vialit pendulum	187	Cohesion recovery is reduced by delayed crack closure: formation of structure at the formerly amorphous surface reduces healing.
	190	Incomplete recovery relates to changes in structure: glassy state of molecules at low fracture temperatures limits the healing response.

## 7.1 CONCLUSIONS FROM MICROSCOPY STUDIES

The main difference between published atomic force microscopy and environmental scanning electron microscopy studies is the representation of bitumen surface. In work using the former method, dispersed ellipsoidal groups of undulations are imaged. The literature concludes that waxes are responsible for this structure. In electron microscopy papers, surface oils covering a continuous network of polar molecules are volatilised by beam heating effects. Notably, the understanding of these structures is incomplete, and evidence of bulk structuring in bitumen is missing. In consideration of the literature, an approach using three electron microscopy-based methods was used in this thesis to acquire insights of surface and bulk structure.

The first of these three methods was environmental scanning electron microscopy (ESEM). In microscopy analyses of bitumen at 20°C it was shown that surface decomposition varies with asphaltene content, due to the protective effect of aromatic groups. Incongruous to published theory it is concluded that these aromatic fractions are well-dispersed through a surface layer of oils, in order for this effect to be widespread, and do not simply produce concentrations. As surfaces were exposed to prolonged irradiation the network structure was exposed. This was also observed for the first time in the maltenes fraction. Also contrasting with the literature it is therefore concluded that asphaltenes do contribute to this structure but not to the exclusion of other fractions. As the sample temperature was reduced to 0°C, this network was replaced by dispersed bee-type structures; as temperature is increased these coalesce into the network. It is concluded from this original use of thermal control that bitumen microstructure develops in two stages. Firstly, by precipitation of crystallisable paraffinic segments due to compositional effects, and secondly by diffusion of aromatics that catalyse gelation by polar interactions.

The second method of optical study was cryogenic scanning electron microscopy (cryo-SEM). Analysis of bitumen at -165°C noted the first images of bee-type structures using this method, and identified that fractures propagated through these dispersions during cooling. With insight acquired from a mechanical perspective, it is concluded that the two-phase system forms with continuously-distributed properties: the solute and solvent are compatible. This is incongruous with the literature, which suggests that the two phases are essentially incompatible. The study

then used a new *in situ* fracture preparation technique, in order to investigate bulk structure. It was shown that surface structure occurs to a depth of about 25 $\mu$ m, below which the bulk is in a glassy amorphous state. The important conclusion is that this amorphous state is perturbed by an interface or a free surface: biasing effects including composition-dependent short-range interactions and temperature gradients drive phase separation and surface structure. Surface-directed spinodal decomposition enables this structuring in near-surface domains.

This thesis then reported the first use of focused ion beam (FIB) etching to study structure in bitumen and maltenes at cryogenic temperatures. Electron micrographs of ion irradiated bee-type structure evidence differential sputtering: the peak of the rippled structure is etched more readily than the trough. In accordance with ESEM study, it is concluded that this micro-phase separation occurs due to immiscibility of the waxes and co-precipitated aromatic fractions that constitute this structure. FIB irradiated sections of the amorphous bulk do not show these rate effects. Consistent with cryo-SEM work it is therefore concluded that structure observed at the surface of bitumen is limited to that layer, and occurs due to surface biasing effects.

## **7.2 CONCLUSIONS FROM MECHANICAL STUDIES**

Published researches of bitumen healing exemplify the complexity of this phenomenon and its dependency on various factors, namely bitumen chemistry and healing time, temperature and damage. The literature reports three models for healing. The viscoelastic continuum damage model uses thermodynamics of irreversible processes to explain damage, and defines healing as the recovery of damage variables. The model embodies the contributions of van der Waals and Lewis acid-base interactions to healing. The multi-step model was refined from rudiments of polymer healing and defines two basic stages: crack closure due to flow and intermolecular forces, which restore stiffness; and interfacial diffusion that restores strength. Bridging these models, the dissipative thermodynamic model explains damage at the scale where chemistry meets mechanics. This model explains healing by rearrangement of phase-separated wax.

Two main methods are used to develop these models and study healing: fatigue-healing tests using storage recuperation protocols, and fatigue-healing tests by intermittent loading. These

tests have developed useful knowledge of fatigue healing, but crack healing is poorly defined in the literature. In consideration of this an approach incorporating three fracture-healing tests was used in this thesis in conjunction with SEM, to acquire insight of microstructural recovery.

The first of these three methods was a direct tension test (DTT). A fracture-healing-re-fracture procedure was used with tensile strength recovery to study healing. Consistent with published literature by dynamic shear rheometry, the data indicated that strength increases with healing time and temperature. However, healing was partial at the fracture temperature of  $-25^{\circ}\text{C}$ , and increased only slightly (from 25% to 30%) by doubling healing temperature (from 20 to  $40^{\circ}\text{C}$ ). This effect is not reported in the literature. It is concluded that healing is a viscosity-driven and thermally-accelerated process that is enhanced by phase transition of crystallised waxes. This thesis also found that post-healing crack trajectories are usually identical to the initial damage event. This finding derived a study on consecutive re-propagation of remnant crack surfaces, which provided evidence for the contribution of molecular entanglements to healing. This new result introduces a commonality between polymer and bitumen healing.

This thesis next reported the use of dynamic shear rheometry (DSR). Initial investigations with the DSR focused on healing in fatigued bitumen. These identified that healing restores macro-cracks and that recovery of complex modulus and fatigue life are inconsistent. It is concluded that this indicates different primary healing mechanisms: the recovery of modulus is explained by wetting and bulk effects, and fatigue life by interfacial molecular interaction. A new fracture healing test was introduced using the DSR. This established that healing is separated into two phases: an instantaneous phase that mimics crack closure, and a time-dependent phase due to diffusion. This test suggested that healing phenomena are enhanced by compressive force. Collation of these data indicated that healing time is lower for fracture than fatigue damage. It is concluded that the healing time is reduced by low molecular weight products of fracture and increased by thixotropy and dispersed damage: it is vital to study healing at cracked surfaces.

The third test introduced in this study used the Vialit pendulum apparatus. The data show that healing produces a sigmoidal curve on a log-time axis. As the asphaltene content of bitumen

is increased these curves are shifted to longer times. It is concluded that diffusion phenomena drive strength recovery, and that these are suppressed through viscosity-building interactions between asphaltenes. This is consistent with the literature and the multi-step healing model in particular. The upper plateau to these curves was generally constant for each material at 80% cohesion recovery, at 40°C healing. This result was also found for oxidised samples. To study further this notably unexpected finding, the thesis then introduced a study on variable fracture temperature. It was identified that as fracture temperature is increased the rate and maximum recovery also increased. In accordance with the research in this thesis on bitumen structure, it is concluded that this unique finding indicates that the glassy or non-glassy state of the bulk is the limiting factor to healing. This is due to different failure mechanisms at the molecular level. Of the other novel findings in this research, the most important was that delayed crack closure also reduces this plateau. Consistent with the findings from cryo-SEM, it is concluded that this is an effect of structure formation due to fracture of the amorphous bulk.

This thesis lastly reports the first use of microscopy to study fracture-healing in bitumen. Cryo-SEM identifies that early healing is enabled by bridges across the interface. From the profile of these bridges it is concluded that they form by flow, which is consistent with the multi-step model for healing. ESEM studies after long healing times indicate that this phenomenon firstly occurs by interpenetration of microstructural segments at the interface, and then by diffusive build-up of structure. This mimics the healing of polymers. The healed microstructure showed dimensional changes compared to poured samples. After correlating this with the recovery of mechanical properties it was concluded that these changes indicate residual damage, due to molecular scission. This conclusion is consistent with the Vialit pendulum study.

### **7.3 OVERALL CONCLUSION**

The central finding of this thesis is that the bulk of bitumen is amorphous: the healing capacity of bitumen is governed by the glassy and non-glassy state of this phase, due to the molecular kinetics of fracture. However, fracture propagation produces a free surface where, at elevated temperatures, the modified solubility enables near-surface structuring. This structure reduces the capacity for healing as the number of potential sites for interfacial molecular interactions is

decreased. Complete recovery of mechanical properties also requires phase transition of the crystallised fractions that contribute to this structure. Notably, none of the models proposed in the literature fully explain these findings. A combination of the multi-step and thermodynamic models would be more accurate, but must be modified to account for fracture temperature.

## **7.4 CONCLUSIONS WITH REGARD TO ASPHALT PAVEMENTS**

The literature review has shown that healing is important in an asphalt pavement: cracks are repaired through healing and the service life of the pavement is extended. This behaviour can be optimised to produce asphalt with enhanced durability, while maintaining the structural and functional performance requirements of the material.

Considering healing at different depths in a pavement it could be concluded that cracks in the base courses heal better than at the surface. That is, the ingress of water and dirt and effects arising from oxidation reduce the capacity for healing, and these processes are more intense at the surface. However, from the studies reported in this thesis it would also be reasonable to conclude that cracks at the surface could heal better than in the base. This work has identified that compression enhances healing. The traffic stresses at the surface have a kneading effect and thereby close fracture planes; these loads propagated through to the base are of a crack-opening type. It is also essential to consider the stress type producing the fracture, therefore.

This research is the first to compare healing of tensile and shear fractures. Collation of these data indicates that shear cracks heal better than tensile cracks. It is concluded that the ability for healing in asphalt varies not only with depth, due to the stress distribution in the pavement, but also with the proximity of the wheel load to any plane in the material. That is, shear stress is lowest under the wheel load, where the tensile stress is highest (refer to Figure 4-10).

When examining healing in asphalt it is also important to consider the design of the mixture. It is known that dense asphalt mixtures are rich in bitumen and cohesive cracks are hence likely to heal. In contrast mixtures with higher void contents could be expected to show less healing. It is important to recall that in each case the service temperatures of the pavement will govern

the healing capacity due to the effect of temperature on the fracture mechanism. Considering the influence of fracture size on healing it is concluded that micro-cracks enable rapid healing. Notably, closure of the cracks is limited by binder viscosity and delays to healing allow for the development of surface structuring that reduces healing. In attempts to optimise the healing of asphalt the maximum benefit is thus realised when effects of damage and healing equilibrate.

## LIST OF REFERENCES

Abdallah, D. J. and Weiss, R. G. (2000) *n*-alkanes gel *n*-alkanes (and many other organic liquids). *Langmuir*, Vol. 16, pp. 352-355.

Abdallah, D. J., Sirchio, S. A. and Weiss, R. G. (2000) Hexatriacontane organogels: the first determination of the conformation and molecular packing of a low molecular mass organogel in its gelled state. *Langmuir*, Vol. 16, pp. 7558-7561.

Abraham, H. (1938) *Asphalts and allied substances: their occurrence, modes of production, use in the arts and methods of testing*. Fourth edition, D van Nostrand Company, New York.

Adorjányi, K. and Füleki, P. (2011) Performance evaluation of bitumens at high temperature with multiple stress recovery creep test. *Hungarian Journal of Industrial Chemistry*, Vol. 39, No. 2, pp. 195-199.

Adams, D. P., Mayer, T. M., Vasile, M. J. and Archuleta, K. (2006b) Effects of evolving surface morphology on yield during focused ion beam milling of carbon. *Applied Surface Science*, Vol. 252, Issue 6, pp. 2432-2444.

Adamsmair, S. (2008) *Digital processing for a bi-modal atomic force microscope (AFM)*. [http://www.emt.jku.at/research/research\\_projects\\_ongoing/phd\\_projects/afm\\_adamsmair/afm\\_adamsmair.html](http://www.emt.jku.at/research/research_projects_ongoing/phd_projects/afm_adamsmair/afm_adamsmair.html) Date accessed 3 November 2011.

Airey, G.D. (1997) *Rheological characteristics of polymer modified and aged bitumens*. The University of Nottingham, PhD Thesis.

Airey, G. D. (1999) Dynamic shear rheometry, fluorescent microscopy and chemical evaluation of polymer modified bitumens. In: *The 7th Conference on Asphalt Pavements for Southern Africa*.

Airey, G. D. (2002) Use of black diagrams to identify inconsistencies in rheological data. *The International Journal of Road Materials and Pavement Design*, Vol. 3, No. 4, pp. 403-424.

Airey, G. D. (2003) Rheological properties of styrene butadiene styrene polymer modified road bitumens. *Fuel*, Vol. 82, pp. 1709-1719.

Airey, G. D. (2004) Styrene butadiene styrene polymer modification of road bitumens. *Journal of Materials Science*, Vol. 39, pp. 951-959.

Airey, G. D. (2005) A review of 10 years DSR testing at Nottingham. *Journal of Applied Asphalt Binder Technology*, Vol. 4, pp. 2-30.

Airey, G. D. (2010) Bituminous materials. In P. Domone and J. Illston (Eds.) *Construction materials: their nature and behaviour*. Oxon: Spon Press, pp. 209-210.

Airey, G. D. and Hunter, A. E. (2003) Dynamic mechanical testing of bitumen: sample preparation methods. *ICE Transport*, Vol. 156, Issue TR2, pp. 85-92.

Airey, G. D., Mohammed, M. H. and Fichter, C. (2008) Rheological characteristics of synthetic road binders. *Fuel*, Vol. 87, pp. 1763-1775.

Airey, G. D., Singleton, T. M. and Collop, A. C. (2002) Properties of polymer modified bitumen after rubber-bitumen interaction. *Journal of Materials Science in Civil Engineering*, Vol. 14, No. 4, pp. 344-354.

Al-Balbissi, A. H. (1983) *A comparative analysis of fracture and fatigue properties of asphalt concrete sulphlex*. PhD Thesis, Texas A&M University.

Al-Balbissi, A. and Little, D.N. (1990) Effect of fracture healing on laboratory-to-field shift factor. *Transportation Research Record: Journal of the Transportation Research Board*, Vol. 1286, pp. 173-181.

Alexander, P., Black, R. M. and Charlesby, A. (1955) Radiation induced changes in the structure of polyisobutylene. *Proceedings of the Royal Society of London, Series A: Mathematical and Physical Sciences*, Vol. 232, pp. 31-48.

Al-Qadi, I. L., Yang, S.-H., Masson, J.-F. and McGhee, K. K. (2008) Characterisation of low temperature mechanical properties of crack sealants utilising direct tension test. Illinois Center for Transportation, Series No. 08-028.

American Association of State and Highway Transportation Officials (2007) Standard method of test specification for determining the fracture properties of asphalt binder in direct tension. AASHTO T 314-07.

American Association of State and Highway Transportation Officials (2007) Standard method of test specification for determining the creep compliance and strength of hot mix asphalt using the indirect tensile test device. AASHTO T 322-07.

Anderson, D. A. and Dongré, R. (1995) The SHRP direct tension specification tests: its development and use. *ASTM publication*, No. 04-012410-08, pp. 51-66.

Anderson, D. A. and Knechtel, K. (1997) Factors affecting the precision of the dynamic shear and bending beam rheometers. In H. Di Benedetto and L. Francken (Eds.) *Proceedings of the Fifth International RILEM Symposium, Mechanical Test for Bituminous Materials: Recent Improvements and Future Prospects*, Rotterdam: AA Balkema, pp. 79-86.

Anderson, D. A. and Marasteanu, M. O. (1999) Physical ageing of asphalt binders relative to their glass transition temperature. *Transportation Research Record: Journal of the Transportation Research Board*, Vol. 1661, pp. 27-34.

Anderson, D. A., Christensen, D. W., Bahia, H. U., Dongre, R., Sharma, M. G., Antle, C. E. and Button, J. (1994) *Binder Characterisation and Evaluation, Volume 3: Physical Characterisation*. SHRP-A-369, Strategic Highways Research Program, National Research Council, Washington D.C.

Anderson, D., Le Hir, Y., Marasteanu, M. O., Planche, J. P., Martin, D. and Giles, G. (2001) Evaluation of fatigue criteria for asphalt binders. *Transportation Research Record: Journal of the Transportation Research Board*, Vol. 1766, pp. 48-56.

Andrews, E.H. and King, N.H. (1978) Surface energetics and adhesion. In A.T. Clark and W.J. Feast (Ed.) *Polymer Surfaces*, Wiley Interscience, pp. 47-63.

Ardenne, M. Van. and Beischer, D. (1940) Untersuchung von Metalloxyd-Rauchen mit dem Universal-Elektronenmikroskop. *Zeitschrift für Elektrochemie und angewandte physikalische Chemie*, Vol. 46, Issue 4, pp. 270-277.

Aronov, D. and Rosenman, G. (2007) Surface energy modification by electron beam. *Surface Science*, Vol. 601, Issue 21, pp. 5042-5049.

Artamendi, I. and Khalid, H. (2005) Characterisation of fatigue damage for paving asphaltic materials. *Fracture and Fatigue of Engineering Materials and Structures*, Vol. 28, pp. 1113-1118.

- Awanti, S.S., Amarnath, M.S. and Veeraragavan, A. (2007) Influence of rest periods on fatigue characteristics of SBS polymer modified bituminous concrete mixtures. *International Journal of Pavement Engineering*, Vol. 8, No. 3, pp. 177-186.
- Babcock, G.B., Statz, R. J. and Larson, D. S. (1998) Study of asphalt binders using lap shear bonds. *Proceedings of the 43<sup>rd</sup> Annual Conference of Canadian Technical Asphalt Association*, Vancouver, pp. 1-15.
- Bahia, H.U. and Anderson, D.A. (1995). The Pressure Aging Vessel (PAV): A Test to Simulate Rheological Changes Due to Field Aging. ASTM Special Technical Publication 1241, Hardin, J.C., ed. American Society for Testing and Materials. West Conshohocken, PA.
- Bahia, H. U., Zhai, H., Bonnetti, K. and Kose, S. (1999) Non-linear viscoelastic and fatigue properties of asphalt binders. *Journal of the Association of Asphalt Paving Technologists*, Vol. 68, pp. 1-38.
- Baker, H. (1754) *The microscope made easy*. Fourth edition. London: R. and J. Dodsley.
- Barber, P. and Atkinson, J.R. (1972) Some microstructural features of the welds in butt-welded materials. *Journal of Materials Science*, Vol. 7, pp. 1131-1136.
- Barbour, R. V. and Peterson, J. C. (1974) Molecular interactions of asphalt: an infrared study of the hydrogen-bonding basicity of asphalt. *Analytical Chemistry*, Vol. 46, No. 2, pp. 273-277.
- Bassim, N. D., De Gregorio, B. T., Kilcoyne, A. D. L., Scott, K., Chou, T., Wirick, S., Cody, G. and Stroud, R. M. (2012) Minimising damage during FIB-TEM sample preparation of soft materials. *Journal of Microscopy*, Vol. 245, Issue 3, pp. 288-301.
- Bassett, D. C. (1981) *Principles of polymer morphology*. Cambridge: Cambridge University Press, pp. 38-71.
- Bastien, L.J. and Gillespie Jr., J.W. (1991) A non-isothermal model for strength and toughness of fusion bonded joints of amorphous thermoplastics. *Polymer Engineering and Science*, Vol. 31, pp. 1720-1730.
- Bates, M. A. and Frenkel, D. (1998) Influence of polydispersity on the phase behaviour of colloidal liquid crystals: a Monte Carlo simulation. *Journal of Chemical Physics*, Vol. 109, No. 14, pp. 6193-6199.
- Bauget, F., Langevin, D. and Lenormand, R. (2001) Dynamic surface properties of asphaltenes and resins at the oil-air interface. *Journal of Colloid and Interface Science*, Vol. 239, pp. 501-508.
- Bazin, P. and Saunier, J.B. (1967) Deformability, fatigue and healing properties of asphalt mixtures. *Proceedings of the Second International Conference on the Structural Design of Asphalt Pavements*, Vol. 4, pp. 566-570, Ann Arbor.
- Bearsley, S., Forbes, A. and Haverkamp, R. G. (2004) Direct observation of the asphaltene structure in paving-grade bitumen using confocal laser-scanning microscopy. *Journal of Microscopy*, Vol. 215, Issue 2, pp. 149-155.
- Becker, J. R. (1997) *Crude oil waxes, emulsions and asphaltenes*. Tulsa: PenWell Publishing Company, pp. 209-250.
- Becker, Y., Muller, A. J. and Rodriguez, Y. (2003) Use of rheological compatibility criteria to study SBS modified asphalts. *Journal of Applied Polymer Science*, Vol. 90, pp. 1772-1782.
- Benbouzid, M. and Hafsi, S. (2008) Thermal and kinetic analysis of pure and oxidised bitumens. *Fuel*, Vol. 87, pp. 1585-1590.

- Bengisu, M., Inal, O. T. and Tosyali, O. (1991) On whisker toughening in ceramic materials. *Acta Metallurgica et Materialia*, Vol. 39, Issue 11, pp. 2509-2517.
- Bennema, P., Liu, X. Y., Lewtas, K., Tack, R. D., Rijpkema, J. J. M. and Roberts, K. J. (1992) Morphology of orthorhombic long chain normal alkanes: theory and observations. *Journal of Crystal Growth*, Vol. 121, pp. 679-696.
- Benson, F. (1988) *Correlation among asphalt concrete mechanical healing, asphalt cement dispersion, FT-IR chemical functional groups and NMR chemical structure*. PhD Thesis, Texas A&M University.
- Berger, L., Hyatt, A. D., Speare, R. and Longcore, J. E. (2005) Life cycle stages of the amphibian chytrid *Batrachochytrium dendrobatidis*. *Diseases of Aquatic Organisms*, Vol. 68, pp. 51-63.
- van den Bergh, W. (2011) *The effect of ageing on the fatigue and healing properties of bituminous mortars*. PhD Thesis, Delft University of Technology.
- Berry, J. P. (1961) Strength of glass polymer. *Journal of Polymer Science*, Vol. 50, pp. 107.
- Beuving, E. (2004) Moderators Report: Conclusions of the Third Eurasphalt and Eurobitume Congress. *Proceedings of the Third Eurasphalt and Eurobitume Congress*, Vienna [http://www.eecongress.org/2004/uk/ModeratorsReports/Conclusions\\_new.doc](http://www.eecongress.org/2004/uk/ModeratorsReports/Conclusions_new.doc) Date accessed 24 April 2009.
- Bewick, S., Edge, J., Forsythe, T. and Parsons, R. (2009) *CK12 Chemistry*. The CK12 Foundation, p. 536. <http://www.ck12.org/flexbook/book/808> Date accessed 18 August 2011
- Bhairampally, R.K., Lytton, R.L. and Little, D.N. (2000) Numerical and graphical method to assess permanent deformation potential for repeated compressive loading of asphalt mixtures. *Transportation Research Record: Journal of the Transportation Research Board*, Vol. 1723, pp. 150-156.
- Bhasin, A., Bommavaram, R., Greenfield, M. and Little, D. (2011) Use of molecular dynamics to investigate self-healing mechanisms in asphalt binders. *Journal of Materials in Civil Engineering*, Vol. 23, Issue 4, pp. 485-492.
- Bhasin, A., Bommavaram, R., Little, D.N. and Greenfield, M. (2009) Intrinsic healing in asphalt binders: measurement and impact of molecular morphology. *Proceedings of the Sixth International Conference on Maintenance and Rehabilitation of Pavements and Technological Control*, Torino.
- Bhasin, A., Howson, J., Masad, E., Little, D.N. and Lytton, R.L. (2007) Effect of modification processes on bond energy of asphalt binders. *Transportation Research Record: Journal of the Transportation Research Board*, Vol. 1998, pp. 29-37.
- Binnig, G., Quate, C. F. and Gerber, Ch. (1986) Atomic Force Microscope. *Physical Review Letters*, Vol. 56, Issue 9, pp. 930-933.
- Blair, C. M. (1960) Interfacial films affecting the stability of petroleum emulsions. *Chemistry and Industry*, pp. 538-544.
- Bludenko, A. V., Ponomarev, A. V., Chulkov, V. N., Yakushev, I. A. and Yarullin, R. S. (2007) Electron beam decomposition of bitumen-gas mixtures at high dose rates. *Mendeleev Communications*, Vol. 17, Issue 4, pp. 227-229.

- Bodin, D., Soenen, H. and de la Roche, C. (2004) Temperature effects in binder fatigue and healing tests. *Proceedings of the Third Eurasphalt and Eurobitume Congress*, Vol. 136, Vienna.
- Boëda, E., Bonilauri, S., Connan, J., Jarvie, D., Mercier, N., Tobey, M., Valladas, H., al Sakhel, H. and Muhesen, S. (2008) Middle Palaeolithic use of bitumen at Umm el Tiel around 70,000 BP. *Antiquity*, Vol. 82, pp. 853-861.
- Boiko, Y.M. (2000) Self-adhesion of amorphous polymers and their miscible blends. *Mechanics of Composite Materials*, Vol. 36, No. 1, pp. 79-82.
- Bolzan, P.E. and Huber, G. (1993) Direct tension test experiments. *Strategic Highways Research Program*, Report No. A-641.
- Bommavaram, R.R., Bhasin, A. and Little, D.N. (2009) Use of dynamic shear rheometer to determine the intrinsic healing properties of asphalt binders. *Proceedings of the 88<sup>th</sup> Meeting of the Transport Research Board*, Washington, D.C.
- Bonnaure, F. P., Huibers, A. H. and Boonders, A. (1982) A laboratory investigation of the influence of rest periods on the fatigue characteristics of bituminous mixes. *Journal of the Association of Asphalt Paving Technologists*, Vol. 51, pp. 104-128.
- Bononi, A. (1988) Methodologie de caracterisation des liants modifies. *Proceedings of the RILEM residential seminar*, Dubrovnik, pp. 119-133.
- Bradley, R. M. and Harper, J. M. E. (1988) Theory of ripple topography induced by ion bombardment. *Journal of Vacuum Science and Technology A*, Vol. 6, Issue 4, pp. 2390-2395.
- Branco, V. A. M., Mansoori, G. A., Xavier, L. C. D. A., Park, S. J. and Manafi, H. (2001) Asphaltene and collapse from petroleum fluids. *Journal of Petroleum Science and Engineering*, Vol. 32, pp. 217-230.
- Braun, R. L. and Burnham, A. K. (1993) *Chemical reaction model for oil and gas generation from type I and type II kerogen*. Livermore: Lawrence Livermore National Laboratory.
- Breen, J. J. and Stephens, J. E. (1967) The glass transition temperature and the mechanical properties of asphalt. *Proceedings of The Annual Conference of the Canadian Technical Asphalt Association*, Report No. JHR-67-16.
- Breyse, D., de la Roche, C., Domec, V. and Chauvin, J.J. (2003) Influence of rest time on recovery and damage during fatigue tests on bituminous composites. *Materials and Structures*, Vol. 36, pp. 648-651.
- Briggs, M. H. (1962) Meteorites and planetary organic matter. *The Observatory*, Vol. 82, pp. 216-218.
- Briscoe, B.J. (1978) Some aspects of the autoadhesion of elastomers. In A.T. Clark and W.J. Feast (Ed.) *Polymer Surfaces*, Wiley Interscience, pp. 25-44.
- Broberg, K. B. (1999) *Cracks and Fracture*. San Diego: Academic Press, pp. 565-569.
- Brostow, W., Gorman, B. P. and Olea-Mejia, O. (2007) Focussed ion beam milling and scanning electron microscopy characterisation of polymer-metal hybrids. *Materials Letters*, Vol. 61, pp. 1333-1336.
- Brown, H. R. (1991) A molecular interpretation of the toughness of glassy polymers. *Macromolecules*, Vol. 24, pp. 2752-2756.
- Brown, H.R. and Russel, T.P. (1996) Entanglements at polymer surfaces and interfaces. *Macromolecules*, Vol. 29, pp. 798-800.

- Brulé, B. and Gazeau, S. (1996) *Characterisation of rheological and thermal behaviour of asphalt cements modified by ethylene copolymers*. Proceedings of the ACS Symposium on Modified Asphalts, Orlando, Florida, pp. 1289-1295.
- Brunner, S., Gasser, Ph., Simmler, H. and Wakili, K. G. (2006) Investigation of multilayered aluminium-coated polymer laminates by focussed ion beam (FIB) etching. *Surface and Coatings Technology*, Vol. 200, pp. 5908-5914.
- Bucknall, C.B., Drinkwater, I.C. and Smith, G.R. (1980) Hot-plate welding of plastics: factors affecting weld strength. *Polymer Engineering and Science*, Vol. 20, pp. 432-440.
- Bueche, F. (1955) Tensile strength of plastics above the glass transition. *Journal of Applied Physics*, Vol. 26, No. 9, pp. 1133-1140.
- Burke, J. (1984) Solubility parameters: theory and application. *The Book and Paper Group Annual*, Vol. 3.  
<http://cool.conservation-us.org/coolaic/sg/bpg/annual/v03/bp03-04.html> Date accessed 28 October 2011.
- Burton, M., Gordon, S. and Hentz, R. R. (1951) Effect of ring on radiation chemistry of alkyl-substituted benzenes. *Journal de Chimie Physique et de Physico-Chimie Biologique*, Vol. 48, pp. 190-194.
- Cairns, M.-L., Dickson, G. R., Orr, J. F., Farrar, D., Hardacre, C., Sa, J., Lemoine, P., Mughal, M. Z. and Buchanan, F. J. (2012) The potential of electron beam radiation for simultaneous surface modification and bioresorption control of PLLA. *Journal of Biomedical Materials Research Part A*.
- Campbell, F. C. (2008) *Elements of metallurgy and engineering alloys*. Materials Park: ASM International, pp. 53-75.
- Carpenter, S. H., Ghuzlan, K. and Shen, S. (2003) A fatigue endurance limit for highway and airport pavements. *Transportation Research Record: Journal of the Transportation Research Board*, Vol. 1832, pp. 131-138.
- Carpenter, S.H. and Shen, S. (2005) Energy concepts for fatigue analysis of airport pavement: impact of rest period between loads. *Proceedings of the FAA COE Fourth Annual Joint Meeting*, Orlando.
- Carpenter, S.H. and Shen, S. (2006) Dissipated energy approach to study hot-mix asphalt healing in fatigue. *Transportation Research Record: Journal of the Transportation Research Board*, Vol. 1970, pp. 178-185.
- Carter, G. (1999) The effects of surface ripples on sputtering erosion rates and secondary ion emission yields. *Journal of Applied Physics*, Vol. 85, Issue 1, pp. 455-459.
- Castaing, R. and Labourie, P. (1953) Examen direct des métaux par transmission au microscope électronique. *Comptes Rendues Académie des Sciences*, Vol. 237, pp. 1330-1332.
- Castro, M. and Sánchez, J.A. (2006) Fatigue and healing of asphalt mixtures: discriminate analysis of fatigue curves. *Journal of Transportation Engineering*, Vol. 132, pp. 168-174.
- Cataldo, F., Keheyani, Y. and Baccaro, S. (2004) The effect of gamma-irradiation of anthracite coal and oil bitumen. *Journal of Radioanalytical and Nuclear Chemistry*, Vol. 262, No. 2, pp. 443-450.
- Cazaux, J. (1986) Some considerations on the electric field induced in insulators by electron bombardment. *Journal of Applied Physics*, Vol. 59, Issue 5, pp. 1418-1431.

- Champion, L., Gerard, J.-F., Planche, J.-P., Martin, D. and Anderson, D. (2001) Low temperature fracture properties of polymer-modified asphalts relationship with morphology. *Journal of Materials Science*, Vol. 36, pp. 451-460.
- Champion-Lapalu, L., Wilson, A., Fuchs, G., Martin, D. and Planche, J.-P. (2002) Cryo-scanning electron microscopy: a new tool for interpretation of fracture studies in bitumen/polymer blends. *Energy and Fuels*, Vol. 16, pp. 143-147.
- Chang, H.-L., Wong, G. K., Lin, J.-R. and Yen, T. F. (2000) Electron spin resonance study of bituminous substances and asphaltenes. In T. F. Yen and G. V. Chilingar (Eds.) *Asphaltenes and asphalts*. London: Elsevier Science B.V., pp. 229-280.
- Charlesby, A. (1952) Cross-linking of polyethylene by pile radiation. *Proceedings of the Royal Society of London, Series A: Mathematical and Physical Sciences*, Vol. 215, pp. 187-214.
- Chen, J., Wang, J., Han, E. and Ke, W. (2008) ESEM observation of the process of hydrogen generation around the micro-droplets forming on AZ91 magnesium alloy. *Electrochemistry Communications*, Vol. 10, Issue 4, pp. 577-581.
- Cheng, D., Little, D.N., Lytton, R.L. and Holste, J.C. (2003) Moisture damage evaluation of asphalt mixtures by considering both moisture diffusion and repeated-load conditions. *Transportation Research Record: Journal of the Transportation Research Board*, Vol. 1832, pp. 42-49.
- Cherry, B.W. (1981) *Polymer Surfaces*, Cambridge: Cambridge University Press, pp. 18-33.
- Cheung, C.Y. and Cebon, D. (1997) Deformation mechanisms of pure bitumen. *Journal of Materials in Civil Engineering*, Vol. 9, pp. 117-129.
- Chinnov, E. A. and Kabov, O. A. (2007) Marangoni effect on wave structure in liquid films. *Microgravity Science and Technology*, Vol. XIX, Issue 3/4, pp. 18-22.
- Christensen, D. W. and Anderson, D. A. (1992) Interpretation of dynamic mechanical test data for paving grade asphalt cements. *Journal of the Association of Asphalt Paving Technologists*, Vol. 61, pp. 67-116.
- Chowdary, V., Krishnan, J.M. and Rengaraju, V.R. (2005) Laboratory investigation on healing of sand asphalt mixtures. *Proceedings of the R. Lytton Symposium on Mechanics of Flexible Pavements*, pp. 95-102, Louisiana.
- Chuang, J., Grosberg, A.Y. and Tanaka, T. (2000) Topological repulsion between polymer globules. *Journal of Chemical Physics*, Vol. 112, pp. 6434-6442.
- Chui, C. and Boyce, M. C. (1999) Monte Carlo modelling of amorphous polymer deformation: evolution of stress with strain. *Macromolecules*, Vol. 32, pp. 3795-3808.
- Chung, F., Sarathi, P. and Jones, R. (1991) *Modelling of asphaltene and wax precipitation*. Bartlesville: IIT Research Institute.
- Cicerone, M. and Soles, C. (2004) Fast dynamics and stabilisation of proteins: binary glasses of trehalose and glycerol. *Biophysical Journal*, Vol. 86, Issue 6, pp. 3836-3845.
- Claessen, H. J. M. and Oosten, J. G. (1996) *Ideology and formation of early states*. Leiden: E. J. Brill, pp. 173-175.
- Claffey, W. J. and Parsons, D. F. (1972) Electron diffraction study of radiation damage in coronene. *Philosophical Magazine*, Vol. 25, Issue 3, Special Issue, pp. 637-643.

- Claudy, P., Létouffé, J. M., Rondelez, F., Germanaud, L., King, G. N. and Planche, J. P. (1992) A new interpretation of time dependent physical hardening in asphalt based on DSC and optical thermoanalysis. *ACS Symposium on Chemistry and Characterisation of Asphalts, Washington, D.C.* pp. 1408-1426.
- Cointe, F. and Monnoye, R. (1995) *Correlation between two dynamic rheometers: Rheometrics RDA II and Bohlin CS 50*. Proceedings of the Rheology of Bituminous Binders European Workshop, Brussels, Paper No. 4.
- Colinet, P. (2010) Interfacial patterns and waves in liquid layers and thin films. In P. Colinet and A. Nepomnyashchy (Eds.) *Pattern Formation at Interfaces*, New York: Springer Wien, pp. 3-37.
- Collins, H. J. and Hart, C. A. (1936) *Principles of road engineering*. London: Edward Arnold Publishers, Ltd.
- Coney, D. and Croney, P. (1998) *Design and Performance of Road Pavements*. New York: McGraw-Hill, pp. 23-28.
- Connan, J. (1999) Use and trade of bitumen in antiquity and prehistory: molecular archaeology reveals secrets of past civilisations. *Philosophical Transactions of the Royal Society B: Biological Sciences*, Vol. 354, pp. 33-50.
- Corbett, L. C. (1969) Composition of asphalt based on generic fractionation using solvent deasphalting, elution-adsorption chromatography and densimetric characterisation. *Analytical Chemistry*, Vol. 41, pp. 576-579.
- Corbett, L.W. and Merz, R.E. (1975). Asphalt Binder Hardening in the Michigan Test Road After 18 Years of Service. Transportation Research Record 544. Transportation Research Board, National Research Council, Washington, D.C. pp. 27-34.
- Cosslett, V. E. (1978) Radiation damage in the high resolution microscopy of biological materials: a review. *Journal of Microscopy*, Vol. 113, pp. 113-129.
- Cottrell, A. H. (1956) The effects of irradiation on the physical properties of solids. *British Journal of Applied Physics*, Vol. 7, Supplement 5, pp. S43-S49.
- Csanyi, L.H. (1962) Functions of fillers in bituminous mixes. *Transportation Research Record: Journal of the Transportation Research Board*, Vol. 329, pp. 1-5.
- Cui, J., Wang, R., Sinclair, A.N. and Spelt, J.K. (2003) A calibrated finite element model of adhesive peeling. *International Journal of Adhesion and Adhesives*, Vol. 23, pp. 199-206.
- D'Angelo, J., Klutz, R. and Dongre, R. N. (2007) Revision of the SuperPave high temperature binder specification: the multiple stress recovery test. *Journal of the Association of Asphalt Paving Technologists*, Vol. 76, pp. 123-162.
- Daley, R.E., Evett, D., Halstead, E., Schwan, J.J., Stewart, J. and Zumstein, R. (1993) Polymers: Glossary. *Materials and Science Technology Teachers Workshop* <http://matse1.mse.uiuc.edu/polymers/glos.html>, Date accessed 16 September 2009.
- Daniel, J.S. and Kim, Y.R. (2001) Laboratory evaluation of fatigue damage and healing of asphalt mixtures. *Journal of Materials in Civil Engineering*, Vol. 13, pp. 434-440.
- Danilatos, G. D. (1985) Design and construction of an atmospheric or environmental SEM 3. *Scanning*, Vol. 7, pp. 26-42.
- Danilatos, G. D. (1989) Environmental SEM: a new instrument a new dimension. *Proceedings of the Institute of Physics Electron Microscopy and Analysis Group and Royal Microscopical Society Conference*, London, Series No. 98, Chapter 10, pp. 455-458.

- Danilatos, G. D. (2012) *ESEM Science and Technology*.  
<http://www.danilatos.com/> Date accessed 25 January 2012.
- Danilatos, G. D. and Robinson, V. N. E. (1979) Principles of scanning electron microscopy at high specimen pressures. *Scanning*, Vol. 2, pp. 72-82.
- Davidson, M. W. (2010) *Microscopy basics: resolution*.  
<http://www.microscopyu.com/articles/formulas/formulasresolution.html> Date accessed 9 June 2011.
- Dawson, I. M. (1952) The study of crystal growth with the electron microscope 2. The observation of growth steps in the paraffin *n*-hectane. *Proceedings of the Royal Society of London, Series A: Mathematical and Physical Sciences*, Vol. 214, pp. 72-79.
- Dawson, I. M. (1954) Croissance des cristaux. *Acta Crystallographica, Series B*, Vol. 7, pp. 668-669.
- De la Roche, C., Hammoum, F., Piau, J.-M. and Stéfani, C. (2003) Behaviour of a thin film of bitumen at the pseudo-contact between two aggregates. *Bulletin des laboratoires des Ponts et Chaussées*, Vol. 242, pp. 3-14.
- De La Roche C. and Marsac P. (1996) *Caractérisation expérimentale de la dissipation thermique dans un enrobé bitumineux sollicité en fatigue*. Proceedings of the First International Eurobitume and Euroasphalt Congress, Strasbourg.
- De Moraes, M. B., Pereira, R. B., Simão, R. M. and Leite, L. F. (2010) High temperature AFM study of CAP 30/45 pen grade bitumen. *Journal of Microscopy*, Vol. 239, Part 1, pp. 46-53.
- Delaporte, B., Van Rompu, J., Di Benedetto, H., Chaverot, P. and Gauthier, G. (2008) New procedure to evaluate fatigue of bituminous mastics using an annular shear rheometer. In I.L. Al-Qadi, T. Scarpas and A. Loizos (Ed.) *Pavement Cracking*, London: Taylor & Francis Group, pp. 457-466.
- Department for Transport (DfT) (2008) *Road expenditure statistics: regional expenditure on roads: 2007/2008*.  
<http://www.dft.gov.uk/pgr/statistics/datatablespublications/roads/condition/> Date accessed 7 March 2011.
- Deveraj, N. (1974) Dependence of surface tension of liquid helium 1 on the temperature and the density. *Proceedings of the Indian Academy of Science*, Volume 43, pp. 208-209.
- Di Benedetto, H., Soltani, A. A. and Chaverot, P. (1996) Fatigue damage for bituminous mixtures: a pertinent approach. *Journal of the Association of Asphalt Paving Technologists*, Vol. 65, pp. 142-158.
- Dickie, J. P., Haller, M. N. and Yen, T. F. (1969) Electron microscopic investigations on the nature of petroleum asphaltics. *Journal of Colloid and Interface Science*, Vol. 29, pp. 475-484.
- Diessel, C. F. K. and Gammidge, L. (1998) Isometamorphic variations in the reflectance and fluorescence of vitrinite: a key to depositional environment. *International Journal of Coal Geology*, Vol. 36, pp. 167-222.
- Dieter, G.E. (2001) *Mechanical Metallurgy*. New York: McGraw-Hill.
- Dignac, J. J. (2002) *More about bitumen*. Total Bitumen in the United Kingdom  
[http://www.bitumen.total.co.uk/cb/cbunitedkingdom.nsf/VS\\_OPM/C12572D60029B00FC125719600341C15?OpenDocument](http://www.bitumen.total.co.uk/cb/cbunitedkingdom.nsf/VS_OPM/C12572D60029B00FC125719600341C15?OpenDocument) Date accessed 17 June 2011.

- van Dijk, W. (1969) Practical fatigue characterisation of bituminous mixtures. *Proceedings of the Association of Asphalt Paving Technologists*, Vol. 38, pp. 423-456.
- van Dijk, W. and Visser, W. (1977) Energy approach to fatigue for pavement design. *Journal of the Association of Asphalt Paving Technologists*, Vol. 46, pp. 1-40.
- Dirand, M., Chevallier, V., Provost, E., Bouroukba, M. and Petitjean, D. (1998) Multi-component paraffin waxes and petroleum solid deposits: structural and thermodynamic state. *Fuel*, Vol. 77, No. 12, pp. 1253-1260.
- Dodd, C. G. (1960) The rheological properties of films at crude petroleum-water interfaces. *Journal of Physical Chemistry*, Vol. 64, No. 5, pp. 544-550.
- Dokland, T., Hutmacher, D. W., Ng, M. M. L. and Schantz, J.-T. (2006) *Techniques in microscopy for biomedical applications*. London: World Scientific Publishing Co. Pte. Ltd., pp. 114-120.
- Dongré, R., Button, J. W., Kluttz, R. Q. and Anderson, D. A. (1997) Evaluation of Superpave binder specification with performance of polymer-modified asphalt pavements. *ASTM Special Technical Publication*, Vol. 1322, pp. 80-100.
- Dongré, R., D'Angelo, J. and McMahon, S. (1996) Implementation of the Superpave direct tension device. *Proceedings of the Eurasphalt and Eurobitume Congress*, Strasbourg, Session 5.154.
- Dooling, P. J., Buckley, C. P., Rostami, S. and Zahlan, N. (2002) Hot-drawing of poly(methyl methacrylate) and simulation using a glass-rubber constitutive model. *Polymer*, Vol. 43, Issue 8, pp. 2451-2465.
- Dorrence, S. M., Barbour, F. A. and Peterson, J. C. (1974) Direct evidence of ketones in oxidised asphalt. *Analytical Chemistry*, Vol. 46, pp. 2242-2244.
- Dorset, D. L. (1986) Sectorisation in n-paraffin crystals. *Journal of Macromolecular Science: Part B*, Vol. 25, pp. 1-20.
- Dorset, D. (1995) *Structural electron crystallography*. New York: Plenum Press, pp. 160-166
- Dorset, D. L. (2005) *Crystallography of the polymethylene chain: an inquiry into the structure of waxes*. International Union of Crystallography Monographs on Crystallography. Vol. 17, Oxford: Oxford University Press.
- Dorset, D. L. and Snyder, R. G. (1996) Crystal structure of modulated n-paraffin binary solids. *The Journal of Physical Chemistry, Series A*, Vol. 100, pp. 9848-9853.
- Dourado, E. R., Simao, R. A. and Leite, L. F. M. (2012) Mechanical properties of asphalt binders evaluated by atomic force microscopy. *Journal of Microscopy*, Vol. 245, Part 2, pp. 119-128.
- Downing, K. H. (1983) Temperature dependence of the critical electron exposure for hydrocarbon monolayers. *Ultramicroscopy*, Vol. 11, Issue 4, pp. 229-237.
- Drummy, L. F., Yang, J. and Martin, D. C. (2004) Low-voltage electron microscopy of polymer and organic molecular thin films. *Ultramicroscopy*, Vol. 99, Issue 4, pp. 247-256.
- Dukat, E. L. and Anderson, D. A. (1980) The effect of various fillers on the mechanical behaviour of asphalt and asphalt concrete. *Proceedings of the Association of Asphalt Paving Technologists*, Vol. 49, pp. 530-549.

- Dunhill, S.T. (1999) *Modelling the deterioration mechanisms of UK lightly trafficked roads*. The University of Nottingham, First Year Progress Report.
- Duvall, J. J. and Jensen, H. B. (1977) The radiation chemistry of some simple pyrroles. *Radiation Research*, Vol. 72, pp. 402-413.
- Dwiggins Jr., C. W. (1965) A small angle X-ray scattering study of the colloidal nature of petroleum. *Journal of Physical Chemistry*, Vol. 69, pp. 3500-3506.
- Edwards, R. T. (1957) Crystal habit of paraffin wax. *Industrial and Engineering Chemistry*, Vol. 49, No. 4, pp. 750-757.
- Egerton, R. F. (1980) Measurement of radiation damage by electron energy-loss spectroscopy. *Journal of Microscopy*, Vol. 118, Issue 4, pp. 389-399.
- Egerton, R. F. (2005) *Physical principles of electron microscopy: an introduction to TEM, SEM and AFM*. New York: Springer Science and Business Media, Inc.
- Egerton, R. F., Li, P. and Malac, M. (2004) Radiation damage in the TEM and SEM. *Micron*, Vol. 35, Issue 6, pp. 399-409.
- ElectroScan (1989) GE investigates the new possibilities of environmental microscopy. *ElectroScanner*, Vol. 1, pp. 1-4.  
<http://www.danilatos.com/electroscanner.htm> Date accessed 17 August 2011.
- Elworthy, P. H. and Mysels, K. J. (1966) The surface tension of sodium dodecylsulfate solutions and the phase separation model of micelle formation. *Journal of Colloid and Interface Science*, Vol. 21, pp. 331-347.
- Ensley, E. K. (1975) A kinetic investigation of association in asphalt. *Journal of Colloid and Interface Science*, Vol. 53, No. 3, pp. 452-460.
- Ensley, K. (1975) A kinetic investigation of association in asphalt. *Journal of Colloid and Interface Science*, Vol. 53, No. 3, pp. 452-460.
- Escovitz, W. H., Fox, T. R. and Levi-Scetti, R. (1975) Scanning transmission ion microscope with a field ion source. *Proceedings of the National Academy of Sciences*, Vol. 72, No. 5, pp. 1826-1828.
- Eurobitume (1996) Glossary of rheological terms – a practical summary of the most common concepts. *Rheology of Bituminous Binders*, Brussels: Eurobitume.
- Eurobitume and Asphalt Institute (2008) *The bitumen industry – a global perspective: production, chemistry, use, specification and occupational exposure*.
- European Asphalt Producers Association (EAPA) (2008) *Asphalt in figures: 2008*.  
[http://www.eapa.org/usr\\_img/asphalt/AsphaltinFigures2008.pdf](http://www.eapa.org/usr_img/asphalt/AsphaltinFigures2008.pdf) Date accessed 10 February 2011.
- Eustathopoulos, N. Nicholas, M.G. and Drevet, B. (1999) *Wettability at high temperatures*. Oxford: Elsevier Science Limited, pp. 44 and 148.
- Evans, A. G. and Hutchinson, J. W. (1995) The thermomechanical integrity of thin films and multilayers. *Acta Metallurgica et Materialia*, Vol. 43, Issue 7, pp. 2507-2530.
- Faber, K. and Evans, A. G. (1983) Crack deflection processes one: theory. *Acta Metallurgica*, Vol. 31, Issue 4, pp. 565-576.

- Faiyue, B., Al-Azzawi, M. J. and Flowers, T. J. (2010) The role of lateral roots in bypass flow in rice (*Oryza sativa* L.). *Plant, Cell and Environment*, Vol. 33, pp. 702-716.
- Fazilov, T. I. (1965) Investigation of bitumen by luminescence microscopy. *Chemistry and Technology of Fuels and Oils*, Vol. 1, No. 2, pp. 148-149.
- FEHRL (2006) *BitVal: analysis of available data for validation of bitumen tests. Report on phase 1 of the BitVal project.* Forum of European National Highway Research Laboratories, C. Nicholls (Ed.), TRL, UK.
- Fernández-Morán, H. (1960) Direct study of ice crystals and of hydrated systems by low-temperature electron microscopy. *Journal of Applied Physics*, Vol. 31, p. 2.
- Fernández-Morán, H. (1966) High-resolution electron microscopy with superconducting lenses at liquid helium temperatures. *Proceedings of the National Academy of Sciences of the United States of America*, Vol. 56, Issue 3, pp. 801-808.
- Ferry, J. D. (1980) *Viscoelastic Properties of Polymers.* New York: John Wiley & Sons.
- Finn, F., Saraf, C., Kulkarni, R., Nair, K., Smith, W. and Abdullah, A. (1977) The use of distress prediction subsystems for the design of pavement structures. *Proceedings of the Fourth International Conference on Structural Design of Asphalt Pavements*, pp. 3-38, Ann Arbor.
- Flewitt, P.E.J. and Wild, R.K. (1984) *Some techniques of optical microscopy.* The University of Cambridge: Department of Materials Science and Metallurgy  
<http://bunter.msm.cam.ac.uk/phase-trans/2006/optical.microscopy.pdf>, Date accessed 1 August 2009.
- Forbes, R. J. (1964) *Bitumen and petroleum in antiquity.* Leiden: E. J. Brill, pp. 1-78.
- Forbes, R. J. (1993) *Studies in ancient technology.* Leiden: E. J. Brill, pp. 144-149.
- Forsythe, G. (2005) *A critical history of early Rome.* London: University of California Press, Ltd., p. 309.
- Frank, F. C. (1970) The strength and stiffness of polymers. *Proceedings of the Royal Society of London, Series A: Mathematical and Physical Sciences*, Vol. 319, pp. 127-136.
- Franzen, S. (2004) *Flory-Huggins Theory.* North Carolina State University: Department of Chemistry  
<http://chsfpc5.chem.ncsu.edu/~franzen/CH7951/lectures/fht/sld001.htm>, Date accessed 7 September 2009.
- Frolov, A. F., Frolova, E. A., Ovchinnikova, V. N. and Vasil'eva, V. V. (1983) Strength and structure of asphalt films. *Chemistry and Technology of Fuel and Oils*, Vol. 19, pp. 415-419.
- Fryer, J. R. (1987) The effect of dose rate on imaging aromatic organic crystals. *Ultramicroscopy*, Vol. 23, Issues 3/4, pp. 321-327.
- Fryer, J. R. (1989) High-resolution imaging of organic crystals. *Journal of Electron Microscopy Technique*, Vol. 11, pp. 310-325.
- Fryer, J. R. (1993) Molecular arrays and molecular structure in organic thin films observed by electron microscopy. *Journal of Applied Physics D: Applied Physics*, Vol. 26, pp. B137-B144.
- Fryer, J. R. and Holland, F. (1984) High resolution electron microscopy of molecular crystals. III. Radiation processes at room temperature. *Proceedings of the Royal Society of London, Series A: Mathematical and Physical Sciences*, Vol. 393, pp. 353-369.

- Fryer, J. R., McConnell, C. H., Zemlin, F. and Dorset, D. L. (1992) Effect of temperature on radiation damage to aromatic organic molecules. *Ultramicroscopy*, Vol. 40, Issue 2, pp. 163-169.
- Fu, J., Joshi, S. B. and Catchmark, J. M. (2008) A study of angular effects in focussed ion beam milling of water ice. *Journal of Micromechanics and Microengineering*, Vol.18, No. 9 pp. 1-8.
- Fujita, K. (2012) Development of non-siliceous porous materials and emerging applications. *Bulletin of the Chemical Society of Japan*, Vol. 85, pp. 415-432.
- Fujiyoshi, Y. (1998) The structural study of membrane proteins by electron crystallography. *Advances in Biophysics*, Vol. 35, pp. 25-80.
- Gabriel, B. L. (1985) *SEM: a user's manual for materials science*. Metal's Park: American Society for Metals, p. 30.
- Gac, F. D. (1990) Is there anything of practical value hidden amongst the composite-toughening theories? A Jim Mueller perspective. *Proceedings of the 14<sup>th</sup> Annual Conference on Composites and Advanced Ceramic Materials, Part 1 of 2: Ceramic Engineering and Science Proceedings*, Vol. 11, Issue 7/8, pp. 551-570.
- Gaestal, C., Smadja, R. and Lamminan, K.A. (1971) Contribution a la connaissance des bitumes routiers. *Revue Generale des Routes et Aerodromes*, No. 466.
- Galloway Group (2004) *Atomic force microscopy: a guide to understanding and using the AFM*.  
<http://uweb.txstate.edu/~ab35/manuals/AFMmanuals/AFMLabManual.pdf> Date accessed 10 June 2011
- García, M., Orea, M. and Carbognani, L. (2001) The effect of paraffinic fractions on crude oil wax crystallisation. *Petroleum Science and Technology*, Vol. 19, pp. 189-196.
- Gauthier, G., Bodin, D., Chailleux, E. and Gallet, T. (2010) Non-linearity in bituminous materials during cyclic tests. *International Journal of Road Materials and Pavement Design*, Vol. 11, Sup. 1, pp. 379-410.
- Gawrys, K. L. and Kilpatrick, P. K. (2005) Asphaltenic aggregates are polydisperse oblate cylinders. *Journal of Colloid and Interface Science*, Vol. 288, pp. 325-334.
- Genin, G. and Cebon, D. (2000) Failure mechanism in asphalt concrete. *International Journal of Road Materials and Pavement Design*, Vol. 1, pp. 419-450.
- de Gennes, P.G. (1971) Reptation of a polymer chain in the presence of fixed obstacles. *The Journal of Chemical Physics*, Vol. 55, pp. 572-579.
- de Gennes, P.G. (1983) Entangled polymers. *Physics Today*, Vol. 36, No. 6, pp. 33-39.
- Ghuzlan, K. A. and Carpenter, S. H. (2000) Energy-derived, damage-based failure criterion for fatigue testing. *Transportation Research Record: Journal of the Transportation Research Board*, Vol. 1723, pp. 141-149
- Gillespie, W. M. (1855) *A manual of the principles of road-making: the location, construction and improvement of roads and rail-roads*. New York: A. S. Barnes and Co., pp. 224-228.
- Glaeser, R. M., McMullan, G., Faruqi, A. R. and Henderson, R. (2011) Images of paraffin monolayer crystals with perfect contrast: minimisation of beam-induced specimen motion. *Ultramicroscopy*, Vol. 111, pp. 90-100.

- Glasby, G. P. (2006) Abiogenic origin of hydrocarbons: an historical overview. *Resource Geology*, Vol. 56, No. 1, pp. 85-98.
- Gluyas, J. G. and Underhill, J. R. (2003) The Staffa Oil Field, Block 3/8b, UK North Sea. *The Geological Society, London Memoirs*, Vol. 20, pp. 327-333.
- Goldstein, J., Newbury, D., Joy, D., Lyman, C., Echlin, P., Lifshin, E., Sawyer, L. and Michael, J. (2003) *Scanning electron microscopy and X-ray microanalysis*. New York: Springer Science and Business Media, Inc., pp. 1-10.
- Goldthorpe, I. A., Marshall, A. F. and McIntyre, P. C. (2008) Synthesis and strain relaxation of Ge-core/Si-shell nanowire arrays. *Nano Letters*, Vol. 8, No. 11, pp. 4081-4086.
- Goodhew, P. J., Humphreys, F. J. and Beanland, R. (2001) *Electron microscopy and analysis*. London: Taylor and Francis, pp. 122-129.
- Gorman, B. P., Sahu, L., Shaito, A. and D'Souza, N. A. (2006) FIB/FESEM investigations of polymer/inorganic composites. *Microscopy and Microanalysis*, Vol. 12, Supplement 2, pp. 1000-1001.
- Graham, J., Butt, C. R. M. and Vigers, R. B. W. (1984) Sub-surface charging, a source of error in microprobe analysis. *X-Ray Spectrometry*, Vol. 13, Issue 3, pp. 126-133.
- Grant, T. P. (2001) Determination of asphalt mixture healing rate using the Superpave indirect tensile test. Master's Thesis, University of Florida.
- Gratzer, W. (2009) *Giant molecules: from nylon to nanotubes*. Oxford: Oxford University Press, pp. 3-12.
- Greer, J. (2012) *Imperfections in crystals: sources of dislocation*.  
<http://www.jrgreer.caltech.edu/content/teaching/MS161Files/Notes/Lect2MS161JRG.pdf> Date accessed 18 May 2012.
- Greiser, J. (2009) *Advances in cryo-SEM: from micrometres to nanometres*.  
<http://new.americanlaboratory.com/914-Application-Notes/577-Advances-in-Cryo-SEM-From-Micrometers-to-Nanometers/> Date accessed 15 July 2011.
- Griffith, A. A. (1921) The phenomenon of rupture and flow in solids. *Philosophical Transactions of the Royal Society of London A: Mathematical and Physical Sciences*, Vol. 221, pp. 163-198.
- Griffen, R. L., Simpson, W. C. and Miles, T. K. (1959) Influence of composition of paving asphalts on viscosity, viscosity-temperature susceptibility, and durability. *Journal of Chemistry and Engineering Data*, Vol. 4, pp. 349-354.
- Gross, L., Mohn, F., Moll, N., Liljeroth, P. and Meyer, G. (2009) The chemical structure of a molecule resolved by atomic force microscopy. *Science*, Vol. 325, No. 5944, pp. 1110-1114.
- Grundke, K. (2008) Characterisation of polymer surfaces by wetting and electrokinetic measurements – contact angle, interfacial tension, zeta potential. In M. Stamm (Ed.) *Polymer Surfaces and Interfaces*, Berlin: Springer-Verlag, pp. 103-138.
- Guerrero, A., Partal, P. and Gallegos, C. (1998) Linear viscoelastic properties of sucrose ester-stabilised oil-in-water emulsions. *Journal of Rheology*, Vol. 42, Issue 6, pp. 1375-1388.
- Guo, A., Zhang, X. and Wang, Z. (2008) Simulated delayed coking characteristics of petroleum residues and fractions by thermogravimetry. *Fuel Processing and Technology*, Vol. 89, pp. 643-650.

- Gupta, R. and Stallcup, R. (2006) Introduction to in situ nanomanipulation for nanomaterials engineering. In W. Zhou and Z. Wang (Eds.) *Scanning Microscopy for Nanotechnology: Techniques and Applications*. New York: Springer Science and Business Media, pp. 192-224.
- Hall, M. G. and Lloyd, G. E. (1983) The SEM examination of geological samples with a semiconductor backscattered-electron detector: reply. *American Mineralogist*, Vol. 68, pp. 843-844.
- Hansen, C. M. (2007) *Hansen solubility parameters: a user's handbook*. Boca Raton: CRC Press, pp. 1-7.
- Harini, M. and Deshpande, A. P. (2009) Rheology of poly(sodium acrylate) hydrogels during cross-linking with and without cellulose microfibrils. *Journal of Rheology*, Vol. 53, Issue 1, pp. 31-47.
- Harrison, I. R., Wang, G. and Hsu, T. C. (1992) *A differential scanning calorimeter study of asphalt binders*. SHRP report A-612, Washington D. C.: National Research Council.
- Harvey, J.A.F. and Cebon, D. (2000) Bitumen films in tension. *SCI Lecture Paper Series*.
- Harvey, J.A.F. and Cebon, D. (2003) Failure mechanisms in viscoelastic films. *Journal of Materials Science*, Vol. 38, pp. 1021-1032.
- Hatiboglu, B. (2006) *Mechanical properties of individual polymeric micro and nano fibres using atomic force microscopy (AFM)*. MSc Thesis, North Carolina State University, pp. 47-51.
- Hayton, B., Airey, G. D., Elliott, R. and Raynor, C. S. (1999) *Long term ageing of bituminous binders*. Proceedings of the Eurobitume Workshop 99, Luxembourg. Paper No. 126.
- Heaney, P. J., Vicenzi, E. P., Giannuzzi, L. A. and Livi, K. J. T. (2001) Focussed ion beam milling: a method of site-specific extraction for microanalysis of Earth and planetary materials. *American Mineralogist*, Vol. 86, pp. 1094-1099.
- Heavens, J. W., Keller, A., Pope, J. M. and Rowell, D. M. (1970) Beam-induced changes in the scanning electron microscopy of poly(oxyethylene). *Journal of Materials Science*, Vol. 5, No. 1, pp. 53-62.
- Hefer, A. and Little, D.N. (2005) Adhesion in bitumen-aggregate systems and quantification of the effects of water on the adhesive bond. *The International Centre for Aggregates Research*, Report No. 505-1, p. 37.
- Henderson, R. M., Edwardson, J. M., Geisse, N. A. and Saslowsky, D. E. (2004) Lipid rafts: feeling is believing. *News in Physiological Sciences*, Vol. 19, No. 2, pp. 39-43.
- Herzog, P., Tchoubar, D. and Espinat, D. (1987) Macrostructure of asphaltene dispersions by small angle X-ray scattering. *Fuel*, Vol. 67, Issue 2, pp. 245-250.
- Hesp, S. A. M., Iliuta, S. and Shirokoff, J. W. (2007) Reversible ageing in asphalt binders. *Energy & Fuels*, Volume 21, Issue 2, pp. 1112-1121.
- Ho, S. M. S., Klesken, B. and Zanzotto, L. (2003) Direct tension tests: a useful tool to study the low-temperature properties of wax-containing asphalt. *Proceedings of the 82<sup>nd</sup> TRB Annual Meeting*, Paper No. 03-3157.
- Ho, S. M. S. and Zanzotto, L. (2001) Sample preparation for direct tension testing: improving determination of asphalt binder failure stress and test repeatability. *Transportation Research Record: Journal of the Transportation Research Board*, Vol. 1766, pp. 15-23.

- Hobbs, L. W. (1979) Radiation effects in analysis of inorganic specimens by TEM. In J. J. Hren, J. J. Goldstein and D. C. Joy (Eds.) *Introduction to Analytical Electron Microscopy*. New York: Plenum Press, p. 437.
- Holder, G. A. and Winkler, J. (1965) Wax crystallisation from distillate fuels, part 1: cloud and pour phenomena exhibited by solutions of binary *n*-paraffin mixtures. *Journal of the Institute of Petroleum*, Vol. 51, pp. 228-234.
- Hollinghurst, R. (1966) Radiation-resistant fluids and lubricants. *Journal of the Institute of Petroleum*, Vol. 52, pp. 9-29.
- Holtz, R.D. and Kovacs, W.D. (1981) *An Introduction to Geotechnical Engineering*. New Jersey: Prentice Hall.
- Holzer, L., Indutnyi, F., Gasser, P., Münch, B. and Wegmann, M. (2004) Three-dimensional analysis of porous BaTiO<sub>3</sub> ceramics using FIB nanotomography. *Journal of Microscopy*, Vol. 216, Part 1, pp. 84-95.
- Howie, A. (1980) Radiation damage problems in electron microscopy. *Revue de Physique Appliquée*, Vol. 15, pp. 291-295.
- Howie, A., Mohd Muhid, M. N., Rocca, F. J. and Valdre, U. (1987) Beam damage in organic crystals.
- Hoy, R. S. and Robbins, M. O. (2006) Strain hardening of polymer glasses: effect of entanglement density, temperature and rate. *Journal of Polymer Science Part B: Polymer Physics*, Vol. 44, pp. 3487-3500.
- Huang, Y.H. (2004) *Pavement Analysis and Design*. New Jersey: Prentice Hall, pp. 368-376.
- Hubbard, P. (1910) *Dust preventives and road binders*. New York: John Wiley and Sons.
- Hubbard, B. (1945) Some observations on the optical properties of long-chain normal paraffins. *American Mineralogist*, Vol. 30, Nos. 11-12, pp. 645-672.
- Isaacson, M. (1975) Inelastic scattering and beam damage in biological materials. In B. M. Siegel and D. R. Beaman (Eds.) *Physical Aspects of Electron Microscopy and Microbeam Analysis*. New York: Wiley, pp. 247-258.
- Isaacson, M., Johnson, D. and Crewe, A. V. (1973) Electron beam excitation and damage of biological molecules; its implications for specimen damage in electron microscopy. *Radiation Research*, Vol. 55, No. 2, pp. 205-224.
- Ishitani, T., Hirose, H. and Tsuboi, H. (1995) Focussed ion beam digging of biological specimens. *Journal of Electron Microscopy*, Vol. 44, pp. 110-114.
- Izaola, Z. and Russina, M. (2010) Virtual design of the neutron guide for the TOF spectrometer NEAT. *Journal of Physics: Conference Series*, Vol. 251, No. 1, pp. 1-4.
- Jarrousse, G. (2004) Self adhesion of semi-crystalline polymers between their glass transition temperature and their melting temperature. PhD Thesis, l'université Paris, pp. 16-61.
- Jäger, A., Lackner, R., Eisenmenger-Sittner, Ch. And Blab, R. (2004) Identification of four material phases in bitumen by atomic force microscopy. *Road Materials and Pavement Design (EATA)*, Vol. 5, pp. 9-24.
- Jiménez-Mateos, J. M., Quintero, L. C. and Rial, C. (1996) Characterisation of petroleum bitumens and their fractions by thermogravimetric analysis and differential scanning calorimetry. *Fuel*, Vol. 75, No. 15, pp. 1691-1700.

- Johnson, R. (1996) *Environmental Scanning Electron Microscopy: An introduction to ESEM*, El Dorado Hills: Robert Johnson Associates, pp. 5-17.
- Johnson, D. M., Meinzer, F. C., Woodruff, D. R. and McCulloh, K. A. (2009) Leaf xylem embolism detected, acoustically and by cryo-SEM, corresponds to decreases in leaf hydraulic conductance in four evergreen species. *Plant, Cell and Environment*, Vol. 32, pp. 828-836.
- Jones, D. R. and Kennedy, T. W. (1991) The asphalt model: results of the SHRP asphalt research program. *Proceedings of the Conference, Strategic Highways Research Program and Traffic Safety on Two Continents, Part Four*, Gothenberg.
- Jones, K. H., van Dusen, W. and Theard, L. M. (1964) Intermolecular and intramolecular energy transfer in gamma-irradiated alkylbenzenes and related mixtures. *Radiation Research*, Vol. 23, pp. 128-134.
- José-Alberto, M.-H. and Jorge, A. (2011) Current knowledge of and potential applications of ionic liquids in the petroleum industry. In A. Kokorin (Ed.) *Ionic Liquids: Applications and Perspectives*. Rijeka: InTech, pp. 439-458.
- Jovanović, J. A. (2000) Models of an asphaltene aggregate and a micelle of the petroleum colloid system. *Chemistry and Industry*, Vol. 54, No. 6, pp. 270-275.
- Joy, D. C. and Joy, C. S. (1996) Low voltage scanning electron microscopy. *Micron*, Vol. 27, No. 3-4, pp. 247-263.
- Jud, K. and Kausch, H.H. (1979) Load transfer through chain molecules after interpenetration at interfaces. *Polymer Bulletin*, Vol. 1, No. 10, pp. 697-709.
- Jud, K. and Kausch, H.H. (1981) Fracture mechanics studies of crack healing and welding of polymers. *Journal of Materials Science*, Vol. 16, pp. 204-210.
- Kalloniatīs, M. and Luu, C. (2007) *The organisation of the retina and visual system: visual acuity*. <http://webvision.med.utah.edu/book/part-viii-gabac-receptors/visual-acuity/> Date accessed 15 December 2011.
- Kané, M., Djabourov, M., Volle, J.-M., Lechāire, J.-P. and Frebourg, G. (2003) Morphology of paraffin crystals in waxy crude oils cooled in quiescent conditions and under flow. *Fuel*, Vol. 82, No. 2, pp. 127-135.
- Katti, S.S. and Schultz, J.M. (1982) The microstructure of injection-moulded semi-crystalline polymers. *Polymer Engineering and Science*, Vol. 22, pp. 1001-1017.
- Katz, D. L. and Beu, K. E. (1945) Nature of Asphaltic Substances. *Industrial and Engineering Chemistry*, Vol. 37, No. 2, pp.195-200.
- Kausch, H.H. and Dettenmaier, M. (1982) On some mechanical effects in glassy polymers attributed to chain entanglements. *Colloid and Polymer Science*, Vol. 260, pp. 120-123.
- Kausch, H.H., Nguyen, T.Q. and Petrovska-Delacrétaz, D. (1991) Chain interdiffusion: macromolecules between Rouse and de Gennes. *Physica Scripta*, Vol. T35, pp. 57-60.
- Kausch, H.H., Petrovska-Delacrétaz, D., Landel, R. F. and Monnerie, L. (1987) Intermolecular interaction in polymer alloys. *Polymer Engineering and Science*, Vol. 27, No. 2, pp. 149-154.
- Kavanagh, G. M. and Ross-Murphy, S. B. (1998) Rheological characterisation of polymer gels. *Progress in Polymer Science*, Vol. 23, pp. 533-562.

- Kawanaka, S., Park, S. J. and Mansoori, G. A. (1991) Organic deposition from reservoir fluids. *Society of Petroleum Engineers Journal of Reservoir Engineering*, May, pp. 185-192.
- Keentok, M. and Xue, S.C. (1999) Edge fracture in cone-plate and parallel plate flows. *Rheological Acta*, Vol. 38, pp. 321-348.
- Khan, O., Aronovsky, I., Belcher, W., Biagi, P., Clark, S. R., Cook, G., Dani, A. H., Kenoyer, J. M., Mahadevan, I., Meadow, R. H., Mulchandani, A., Parpola, A., Sharma, B. B., Shukla, D. and Franke-Vogt, U. (2001) *The Ancient Indus Civilisation*. <http://www.harappa.com/har/indus-saraswati.html> Date accessed 20 October 2011.
- Kim, B. and Roque, R. (2006) Evaluation of healing property of asphalt mixture. *Transportation Research Record: Journal of the Transportation Research Board*, Vol. 1970, pp. 84-91.
- Kim, C.-S., Ahn, S.-H. and Jang, D.-Y. (2012) Review: developments in micro/nanoscale fabrication by focussed ion beams. *Vacuum*, Vol. 86, pp. 1014-1035.
- Kim, Y.H. and Wool, R.P. (1983) A theory of healing at a polymer-polymer interface. *Macromolecules*, Vol. 16, pp. 1115-1120.
- Kim, Y.R. (2008) Micromechanics modelling of performance of asphalt concrete based on surface energy. In *Modelling of Asphalt Concrete*, New York: McGraw-Hill, pp. 355-390
- Kim, Y.R. and Little, D.N. (1989) Evaluation of healing in asphalt concrete by means of the theory of nonlinear viscoelasticity. *Transportation Research Record: Journal of the Transportation Research Board*, Vol. 1228, pp.198-210.
- Kim, Y. R. and Little, D. N. (1990) One-dimensional constitutive modelling of asphalt concrete. *Journal of Engineering Mechanics*, Vol. 116, No. 4, pp. 751-772.
- Kim, Y. R., Little, D. N. and Benson, F. C. (1990) Chemical and mechanical evaluation on healing mechanism of asphalt concrete. *Journal of the Association of Asphalt Paving Technologists*, Vol. 59, pp. 240-275.
- Kim, Y.R., Little, D. N. and Burghardt, R.C. (1991) SEM analysis on fracture and healing of sand-asphalt mixtures. *Journal of Materials in Civil Engineering*, Vol. 3, pp. 140-153.
- Kim, Y.-R., Little, D.N. and Lytton, R.L. (2003) Fatigue and healing characterisation of asphalt mixtures. *Journal of Materials in Civil Engineering*, Vol. 15, pp. 140-153.
- Kim, Y.R., Whitmoyer, S.L. and Little, D.N. (1995) Healing in asphalt concrete pavements: is it real? *Transportation Research Record: Journal of the Transportation Research Board*, Vol. 1454, pp. 89-96.
- Kimseng, K. and Meissel, M. (2001) *Short overview about the ESEM: environmental scanning electron microscope*. <http://www.calce.umd.edu/TSFA/ESEM.pdf> Date accessed 15 August 2011.
- Kinloch, A.J. (1980) The science of adhesion, part one: surface and interfacial aspects. *Journal of Materials Science*, Vol. 15, pp. 2141-2166.
- Kinloch, A.J. (1982) The science of adhesion, part two: mechanics and mechanisms of failure. *Journal of Materials Science*, Vol. 17, pp. 617-651.
- Kinloch, A. J. and Taylor, A. C. (2006) The mechanical properties and fracture behaviour of epoxy-inorganic micro- and nano-composites. *Journal of Materials Science*, Vol. 41, pp. 3271-3296.

- Kinloch, A. J. and Williams, J. G. (1980) Crack blunting mechanisms in polymers. *Journal of Materials Science*, Vol. 15, pp. 987-996.
- Kitano, Y., Fujikawa, T., Kamino, T., Yaguchi, H. and Saka, T. (1995) TEM observation of micrometer-sized Ni powder particles thinned by FIB cutting technique. *Journal of Electron Microscopy*, Vol. 44, Issue 5, pp. 410-413.
- Klemme, H. D. and Ulmishek, G. F. (1991) Effective petroleum source rocks of the world: stratigraphic distribution and controlling depositional factors. *American Association of Petroleum Geologists Bulletin*, Vol. 75, pp. 1809-1851.
- Kline, D.B. and Wool, R.P. (1988) Polymer welding relations investigated by a lap shear joint method. *Polymer Engineering and Science*, Vol. 28, pp. 52-57.
- Klosterman, D. H. (1984) Fatigue healing studies in polystyrene and short fibre reinforced polymers. PhD Thesis, University of Illinois.
- Kobayashi, K. and Sakaoku, K. (1965) Irradiation changes in organic polymers at various accelerating voltages. *Laboratory Investigation*, Vol. 14, pp. 1097-1114.
- Kochumalayil, J. J., Meiser, A., Soldera, F. and Possart, W. (2009a) Focussed ion beam irradiation: morphological and chemical evolution in PMMA. *Surface and Interface Analysis*, Vol. 41, pp. 412-420.
- Kochumalayil, J. J., Meiser, A., Soldera, F. and Possart, W. (2009b) Focussed ion beam irradiation: morphological and chemical evolution in epoxy polymers. *Surface and Interface Analysis*, Vol. 41, pp. 931-940.
- Köhler, A. (1904) Mikrophotographische Untersuchungen mit ultraviolettem Licht. *Zeitschrift für wissenschaftliche Mikroskopie und mikroskopische Technik*, Vol. 21, pp. 129-165 and 273-304.
- Koldewey, R. (1914) *Excavations at Babylon*. London: Macmillan & Co., Ltd., p. 54.
- van der Kooij, F. M., Kassapidou, K. and Lekkerkerker H. N. W. (2000) Liquid crystal phase transitions in suspensions of polydisperse plate-like particles. *Nature*, Vol. 406, pp. 868-871.
- Kopsch, H. (2008) *Thermal Methods in Petroleum Analysis*. Weinheim: VCH Verlagsgesellschaft mbH, pp. 97-261.
- Kotoul, M. and Vrbka, J. (2003) Crack bridging and trapping mechanisms used to toughen brittle matrix composite. *Theoretical and Applied Fracture Mechanics*, Vol. 40, Issue 1, pp. 23-44.
- Kriech, A. J., Kurek, J. T. and Wissel, H. L. (1992) Effect of mode of generation on the composition of asphalt fumes. *Asphalt Institute*, pp. 1-3.  
[http://www.asphaltinstitute.org/public/engineering/PDFs/Environmental/Effects\\_Mode\\_Generation\\_Composition\\_Fumes.pdf](http://www.asphaltinstitute.org/public/engineering/PDFs/Environmental/Effects_Mode_Generation_Composition_Fumes.pdf) Date accessed 15 June 2011.
- Kringos, N., Schmets, A., Scarpas, A. and Pauli, T. (2011) Towards an understanding of the self-healing capacity of asphaltic mixtures. *HERON*, Vol. 56, No. 1/2, pp. 45-74.
- Kringos, N., Scarpas, A., Pauli, T. and Robertson, R. (2009) A thermodynamic approach to healing in bitumen. *Proceedings of the Seventh International RILEM Symposium*, pp. 123-132, Rhodes.
- Krishnan, J. M. (2006) *The physical and chemical structure of asphalt: with a brief history of their usage and availability*. Department of Civil Engineering, IIT Madras.

<http://www.karlin.mff.cuni.cz/~prusv/ncmm/workshops/wog/download/krishnan/physicalAndChemicalStructureOfAsphalt.pdf> Date accessed 24 October 2010

Kriz, P. and Anderson, S. I. (2005) Effect of asphaltenes on crude oil wax crystallisation. *Energy and Fuels*, Vol. 19, pp. 948-953.

Krohn, V. E. (1961) Liquid metal droplets for heavy particle propulsion. *Progress in Astronomy and Rocketry*, Vol. 5, pp. 73-80.

Krupp, H. (1976) Particle adhesion: theory and experiment. *Advances in Colloid and Interface Science*, Vol. 1, pp. 111-239.

Kumar, K., Nikolov, A. D. and Wasan, D. T. (2001) Mechanisms of stabilisation of water-in-crude oil emulsions. *Industrial and Engineering Chemistry Research*, Vol. 40, pp. 3009-3014.

Kumaraguruparan, K. (2010) Seeing at the atomic level. *The Stony Brook Young Investigators Review*, Vol. 2, Issue 2, pp. 22-23.

Kvenvolden, K. A. (2006) Organic geochemistry: a retrospective of its first 70 years. *Organic Geochemistry*, Vol. 37, pp. 1-11.

Lancaster, I.M. (2006) Bitumen Demystified. *NYNAS*

<http://www.soci.org.uk/SCI/groups/cmt/2006/reports/pdf/Lancaster.pdf>, Date accessed 8 June 2009.

Lawrence, S., Zhang, L. Y., Xu, X. and Masliyah, J. H. (2004) Langmuir and Langmuir-Blodgett asphaltene films at heptane-water interface. *The Canadian Journal of Chemical Engineering*, Vol. 82, pp. 821-828.

Le Guern, M., Chailleux, E., Farcas, F., Dreessen, S., Planche, J.-P. and Débarre, D. (2011) Identification of chemical species and molecular organisation of bitumens. *Proceedings of the RILEM Technical Committee TC 231 workshop on micro- and nano-characterisation and modelling of bituminous materials*, Duebendorf.

Le Guern, M., Chailleux, E., Farcas, F., Dreessen, S. and Mabile, I. (2010) Physico-chemical analysis of five hard bitumens: identification of chemical species and molecular organisation before and after artificial ageing. *Fuel*, Vol. 89, pp. 3330-3339.

Lekarp, F., Isacson, U. and Dawson, A. (2000) State of the art one: resilient response of unbound aggregates. *Journal of Transportation Engineering*, Vol. 126, pp. 66-75.

Lekkerkerker, H. N. W. and Tunier, R. (2011) *Colloids and the depletion layer*. Lecture Notes in Physics. Berlin: Springer Science and Business Media.

Lenoble, C., Vercoe, T. and Soto, T. (1993) *Rheology as a performance indicator for modified bitumen*. Proceedings of the 5<sup>th</sup> Eurobitume Congress, Stockholm, Volume 1A, 1.10, pp. 71-75.

Lerf, A., Buchsteiner, A., Pieper, J., Schöttl, S., Dekany, I., Szabo, T. and Boehm, H. (2006) Hydration behaviour and dynamics of water molecules in graphite oxide. *Journal of Physics and Chemistry of Solids*, Vol. 67, Issues 5-6, pp. 1106-1110.

Leseur, D., Gerard, J.-F., Claudy, P., Letoffe, J.-M., Planche, J.-P. and Martin, D. (1996) A structure-related model to describe asphalt linear viscoelasticity. *The Journal of Rheology*, Vol. 40, pp. 813-836.

Li, L., Xu, J., Tinsley, J., Pethica, B. A., Huang, J. S., Prud'homme, R. K. and Guo, X. (2011) Improvement of oil flowability by assembly of comb-type copolymers with paraffin and asphaltene. *Journal of The American Institute of Chemical Engineers*.

- Li, P. and Egerton, R. F. (2004) Radiation damage in coronene, rubrene and p-terphenyl, measured for incident electrons of kinetic energy between 100 and 200keV. *Ultramicroscopy*, Vol. 101, Issues 2-4, pp. 161-172.
- Li, X., Shew, C.-Y., Liu, Y., Pynn, R., Liu, E., Herwig, K. W., Smith, G. S., Robertson, J. L. and Chen, W.-R. (2010) Theoretical studies on the structure of interacting colloidal suspensions by spin-echo small angle neutron scattering. *Journal of Chemical Physics*, Vol. 132, Issue 17, pp. 174509 1-14.
- Li, Y. and Metcalf, J.B. (2002) Crack initiation model from asphalt slab tests. *Journal of Materials in Civil Engineering*, Vol. 14, pp. 303-310.
- Liang, W. Y. (1970) Excitons. *Physics Education*, Vol. 5, pp. 226-228.
- Liang, T.-N., Zhang, Z.-Q., Li, T. and Yang, X.-Z. (2004) Interpenetration of two polymer chain globules. *Polymer*, Vol. 45, pp. 1365-1371.
- Ling, Y. and Lifshitz, C. (1998) Time-dependent mass spectra and breakdown graphs: C<sub>14</sub>H<sub>10</sub> isomers. *Journal of Physical Chemistry, Part A*, Vol. 102, Issue 4, pp. 708-716.
- Little, D.N. and Bhasin, A. (2007) Exploring mechanism of healing in asphalt mixtures and quantifying its impact. In S. van der Zwaag (Ed.) *Self Healing Materials: an Alternative Approach to 20 Centuries of Materials Science*, AA Dordrecht: Springer, pp. 205-218.
- Little, D.N. and Jones, D.R. (2003) Chemical and mechanical mechanisms of moisture damage in hot mix asphalts. *California Department of Transportation: Materials Engineering and Testing*  
[http://www.dot.ca.gov/hq/esc/Translab/pubs/NSMS2003/Presentation2\\_ChemicalMechanisms](http://www.dot.ca.gov/hq/esc/Translab/pubs/NSMS2003/Presentation2_ChemicalMechanisms), Date accessed 14 May 2009.
- Little, D.N., Lytton, R.L., Williams, D. and Chen, C.W. (2001) Microdamage healing in asphalt and asphalt concrete, volume one: microdamage and microdamage healing, project summary report. *The Federal Highway Administration*, Report No. RD-98-141, pp. 9-24.
- Little, D.N., Lytton, R.L., Williams, D. and Kim, Y.R. (1999) An analysis of the mechanism of microdamage healing based on the application of micromechanics first principles of fracture and healing. *Proceedings of the Association of Asphalt Paving Technologists*, Vol. 68, pp. 501-542.
- Little, D., Prapnnachari, S., Letton, A. and Kim, Y. (1993) *Investigation of the microstructural mechanisms of relaxation and fracture healing in asphalt*. Texas A&M University, Report No. AFOSR-89-0520.
- Liu, X. Y., Bennema, P. and van der Eerden, J. P. (1992) Rough-flat-rough transitions of crystal surfaces. *Nature*, Vol. 356, pp. 778-780.
- Loeber, L., Muller, G., Morel, J. and Sutton, O. (1998) Bitumen in colloid science: a chemical, structural and rheological approach. *Fuel*, Vol. 77, pp. 1443-1450.
- Loeber, L., Sutton, O., Morel, J., Valleton, J.-M. and Muller, G. (1996) New direct observations of asphalts and asphalt binders by scanning electron microscopy and atomic force microscopy. *Journal of Microscopy*, Vol. 182, Part 1, pp. 32-39.
- Loos, J., Van Duren, J. K. J., Morrissey, F. and Janssen, R. A. J. (2002) The use of the focussed ion beam technique to prepare cross-sectional transmission electron microscopy specimen of polymer solar cells deposited on glass. *Polymer*, Vol. 43, pp. 7493-7496.
- Lotz, B. (1994) Crystallographic and structural roots of variation in polymer morphology. *Philosophical Transactions of the Royal Society of London, Series A: Physical Sciences and Engineering*, Vol. 348, No. 1686, pp. 19-28.

- Low, B. W., Chen, C. C., Berger, J. E., Singman, L. and Pletcher, J. F. (1966) Studies of insulin crystals at low temperatures: effects on mosaic character and radiation sensitivity. *Proceedings of the National Academy of Sciences*, Vol. 56, pp. 1746-1750.
- Lu, X. and Isacson, U. (2002) Effect of ageing on bitumen chemistry and rheology. *Construction and Building Materials*, Vol. 16, pp. 15-22.
- Lu, X., Langton, M., Olofsson, P. and Redelius, P. (2005) Wax morphology in bitumen. *Journal of Materials Science*, Vol. 40, pp. 1893-1900.
- Lu, X. and Redelius, P. (2007) Wax morphology in bitumen. *Journal of Materials Science*, Vol. 40, Issue 8, pp. 1893-1900.
- Lu, X., Soenen, H. and Redelius, P. (2003) Fatigue and healing characteristics of bitumens studied using dynamic shear rheometer. *Proceedings of the Sixth International RILEM Symposium on Performance Testing and Evaluation of Bituminous Materials*, pp. 408-415.
- Lugstein, A., Basnar, B., Smoliner, J. and Bertagnolli, E. (2003) FIB processing of silicon in the nanoscale regime. *Applied Physics A: Materials Science and Processing*, Vol. 76, Number 4, pp. 545-548.
- Luminari, M. and Fidato, A. (1998) State of the art report on mix design. In L. Francken (Ed.) *Bituminous binders and mixes: state of the art and interlaboratory tests on mechanical behaviour and mix design*, RILEM Report 17, London: E & FN Spon, pp 69-95.
- Lundstrom, R., Di Benedetto, H. and Isacson, U. (2004) Influence of asphalt mixture stiffness on fatigue failure. *Journal of Materials in Civil Engineering*, Vol. 16, pp. 516-525.
- Luo, H. (2007) *Microstructure development in particulate composite coatings by cryo-SEM*. Ann Arbor: ProQuest Information and Learning Company, pp. 26-27.
- Luzzati, V. and Tardieu, A. (1974) Lipid phases: structure and structural transitions. *Annual Review of Physical Chemistry*, Vol. 25, pp. 79-94.
- Lytton, R. L., Uzan, J., Fernando, E. G., Roque, R., Hiltunen, D. and Stoffels, S. M. (1993) *Development and validation of performance prediction models and specifications for asphalt binders and paving mixes*. SHRP-A-357, Strategic Highways Research Program, National Research Council, Washington D.C.
- Mack, C. J. (1932) Colloid chemistry of asphalts. *Journal of the Institute of Petroleum Technologists*, Vol. 36, pp. 2901-2914.
- Mahmoud, R., Gierycz, P., Solimando, R. and Rogalski, M. (2005) Calorimetric probing of *n*-alkane petroleum-asphaltene interactions. *Energy and Fuels*, Vol. 19, pp. 2474-2479.
- Mahoney, C. L., Barnum, E. R., Kerlin, W. W., Sax, K. J. and Saari, W. S. (1959) *Effect of radiation on the stability of synthetic lubricants*. Proceedings of the 5<sup>th</sup> World Petroleum Congress, New York, Paper No. 13
- Maillard, S., de la Roche, C., Hammoum, F., Such, P. and Piau, J. (2004) Bitumen healing investigation using a specific fracture test. *International Journal of Road Materials and Pavement Design*, Vol. 5, pp. 45-63.
- Manion, J. P. and Burton, M. (1952) Radiolysis of hydrocarbon mixtures. *Journal of Physical Chemistry*, Vol. 56, pp. 560-569.
- Mansoori, G. A. (1997) Modelling of asphaltene and other heavy organic deposits. *Journal of Petroleum Science and Engineering*, Vol. 17, pp. 101-111.

- Marasteanu, M. O. and Anderson, D. A. (2000) Comparison of moduli for asphalt binder obtained from different test devices. *Journal of the Association of Asphalt Paving Technologists*, Vol. 69, pp. 574-607.
- Marasteanu, M.O., Li, X. and Labuz, J.F. (2004) Low temperature fracture test for asphalt mixtures. *Proceedings of the Fifth International RILEM Conference*, pp. 249-256, Limoges.
- Marko, M., Hsieh, C., Moberlychan, W., Mannella, C. A. and Frank, J. (2006) Focussed ion beam milling of vitreous water: prospects for an alternative to cryo-ultramicrotomy of frozen-hydrated biological samples. *Journal of Microscopy*, Vol. 222, Issue 1, pp. 42-47.
- Martono, W. and Bahia, H. U. (2007) *Considering pavement temperature and structure in defining asphalt fatigue behaviour*. Proceedings of the 18<sup>th</sup> Engineering Mechanics Division Conference of the American Society of Civil Engineers, Blacksburg.
- Martono, W., Bahia H.U. and D'Angelo, J. (2007) Effect of testing geometry on measuring fatigue of asphalt binders and mastics. *Journal of Materials in Civil Engineering*, Vol. 19, pp. 746-752.
- Masson, J.-F., Collins, P., Robertson, G., Woods, J. R. and Margeson, J. (2003) Thermodynamics, phase diagrams and stability of bitumen-polymer blends. *Energy and Fuels*, Vol. 17, pp. 714-724.
- Masson, J.-F. and Gagné, M. (2008) Ionic pairs in polyphosphoric acid modified bitumen: insights from model compounds. *Energy and Fuels*, Vol. 22, No. 5, pp. 3390-3394.
- Masson, J.-F., Leblond, V. and Margeson, J. (2006) Bitumen morphologies by phase-detection atomic force microscopy. *Journal of Microscopy*, Vol. 221, No. 1, pp. 17-29.
- Masson, J.-F., Leblond, V., Margeson, J. and Bundalo-Perc, S. (2007) Low-temperature bitumen stiffness and viscous paraffinic nano- and micro-domains by cryogenic AFM and PDM. *Journal of Microscopy*, Vol. 227, Part 3, pp. 191-202.
- Masson, J.-F. and Polomark, G.M. (2001) Bitumen microstructure by modulated differential scanning calorimetry. *Thermochimica Acta*, Vol. 374, No. 2, pp. 105-114.
- Maxwell, B. and Guimon, C. (1962) Dynamic mechanical spectra and limit of linear viscoelasticity of high polymers. *Journal of Applied Polymer Science*, Vol. 6, Issue 19, pp. 83-93.
- McLeish, A. (1992) *Geological science*. Walton-on-Thames: Thomas Nelson & Sons Ltd., pp. 285-287.
- McMullan, D. (1993) Scanning electron microscopy: 1928-1965. *Proceedings of the 51<sup>st</sup> Annual Meeting of the Microscopy Society of America, Cincinnati*.
- McMullan, D. (1995) Scanning electron microscopy: 1928-1965. *Scanning*, Vol. 17, Issue 3, pp. 175-185.
- Medlin, D. L. and Howitt, D. G. (1992) Radiation damage processes affecting electron beam lithography of inorganic materials. *Scanning*, Vol. 14, Issue 2, pp. 86-90.
- Medlin, D. L., Thomas, L. E. and Howitt, D. G. (1989) Decomposition of refractory carbides in the analytical electron microscope. *Ultramicroscopy*, Vol. 29, Issues 1-4, pp. 228-235.
- Megson, T.H.G. (2004) *Structural and Stress Analysis*. London: Arnold, pp. 181-199.

- Menard, K. P. (2008) *Dynamic mechanical analysis: a practical introduction*. Denton: CRC Press, pp. 37-56.
- Merdrignac, I. and Espinat, D. (2007) Physicochemical characterisation of petroleum fractions: state of the art. *Oil & Gas Science and Technology*, Rev. IFP, Vol 62, pp. 7-32.
- Messerly, J. F., Guthrie, G. B., Todd, S. S. and Finke, H. L. (1967) Low-temperature thermal data for *n*-Pentane, *n*-Heptadecane and *n*-Octadecane: revised thermodynamic functions for the *n*-Alkanes C<sub>5</sub>-C<sub>18</sub>. *Journal of Chemical and Engineering Data*, Vol. 12, No.3, pp. 338-346.
- Meyer, R. F. and de Witt, W. (1990) Definition and world resources of natural bitumens. *U.S. Geological Survey Bulletin*, No. 1944, pp. 1-14.
- Mikula, R. J. and Munoz, V. A. (2000) Characterisation of emulsions and suspensions in the petroleum industry using cryo-SEM and CLSM. *Colloids and Physical Sciences A: Physicochemical and Engineering Aspects*, Vol. 174, Issues 1-2, pp. 23-36.
- Milani, M., Drobne, D. and Tatti, F. (2007) How to study biological samples by FIB/SEM? In A. Mendéz-Villas and J. Díaz (Eds.) *Modern Research and Educational Topics in Microscopy*, Formatex, pp. 787-794.
- Mkhoyan, K. A., Silcox, J., Maguire, M. A. and Disalvo, F. J. (2006) Radiolytic purification of CaO by electron beams. *Philosophical Magazine*, Vol. 86, No. 19, pp. 2907-2917.
- Mnyukh, Y. V. (1960) The structure of normal paraffins and of their solid solutions. *Journal of Structural Chemistry*, Vol. 1, No. 3, pp. 346-365.
- Mo, L.T., Huurman, M., Wu, S.P. and Molenaar, A.A.A. (2007) Finite-element analysis and experimental study on tensile fatigue behaviour of bitumen-stone adhesion. *Fatigue and Fracture of Engineering Materials and Structures*, Vol. 30, pp. 823-831.
- Moavenzadeh, F. (1967) Asphalt fracture. *Journal of the Association of Asphalt Paving Technologists*, Vol. 36, pp. 51-79.
- Mohammad, S. N. (2012) Thermodynamic imbalance, surface energy and segregation reveal the true origin of nanotube synthesis. *Advanced Materials*, Vol. 24, Issue 9, pp. 1262-1275.
- Mokhatab, S., Poe, W. A. and Speight, J. G. (2006) *Handbook of natural gas transmission and processing*. Oxford: Gulf Professional Publishing, pp. 149-151.
- Moliton, J. P., Jussiaux, C., Trigaud, T., Lazzaroni, R., Lhost, O., Bredas, J. L., Kihn, Y. and Sevely, J. (1996) Relation between plasmons and the valence-band density of states in polymethylmethacrylate: influence of ion irradiation on damage selectivity. *Philosophical Magazine Part B*, Vol. 73, Part 5, pp. 763-778.
- Moon, M.-W., Lee, S. H., Sun, J.-Y., Oh, K. H., Vaziri, A. and Hutchinson, J. W. (2007) Wrinkled hard skins on polymers created by focussed ion beam. *Proceedings of the National Academy of Sciences of the United States of America*, Vol. 104, No. 4, pp. 1130-1133.
- Morris, V. J., Kirby, A. R. and Gunning, A. P. (1999) *Atomic force microscopy for biologists*, London: Imperial College Press.
- Mott, N. F. (1932) The polarisation of electrons by double scattering. *Proceedings of the Royal Society of London, Series A: Mathematical and Physical Sciences*, Vol. 135, pp. 429-458.
- Mott, N. F. (1950) Theory of crystal growth. *Nature*, Vol. 165, No. 4191, pp. 295-297.

- Muench, S.T., Mahoney, J.P. and Pierce, L.M. (2003) Asphalt. *WDOT Pavement Guides* [http://training.ce.washington.edu/WSDOT/Modules/03\\_materials/03-3\\_body.htm](http://training.ce.washington.edu/WSDOT/Modules/03_materials/03-3_body.htm), Date accessed 01 April 2009.
- Mullins, O. C., Betancourt, S. S., Cribbs, M. E., Dubost, F. X., Creek, J. L., Andrews, A. B. and Venkataramanan, L. (2007) The colloidal structure of crude oil and the structure of oil reservoirs. *Energy and Fuels*, Vol. 21, pp. 2785-2794.
- Murugan, P., Mani, T., Mahinpey, N. and Dong, M. (2012) Pyrolysis kinetics of Athabasca bitumen using a TGA under the influence of reservoir sand. *The Canadian Journal of Chemical Engineering*, Vol. 90, Issue 2, pp. 315-319.
- Mustafayev, I., Chichek, F. and Yuzbashov, E. (2011) Gas formation regularities at the consecutive and simultaneous impact of ionising radiations and heat on Turkish lignites. *Fuel*, Vol. 90, Issue 8, pp. 2555-2559.
- Mustafaev, I., Jabbarova, L., Yagubov, K. and Gulieva, N. (2004) Radiation: thermal refining of oil-bituminous rocks. *Journal of Radioanalytical and Nuclear Chemistry*, Vol. 262, No. 2, pp. 509-511.
- Nellensteyn, F.J. (1923) *Bereiding en constitutie van asphalt (Manufacture and constitution of asphaltic bitumen)*. Dissertatie Technische Hoogeschool, Delft.
- Nellensteyn, F. J. (1924) The constitution of asphalt. *Journal of the Institute of Petroleum Technology*, Vol. 10, pp. 311-325.
- Nepomnyashchy, A., Simanovski, I. and Legros, J. C. (2012) *Interfacial convection in multilayer systems*. New York: Springer Science and Business Media, pp. 123-125.
- Niihara, K., Kaneko, T., Suzuki, T., Sato, Y., Nishioka, H., Nishikawa, Y., Nishi, T. and Jinnai, H. (2005) Nanoprocessing and nanofabrication of a structured polymer film by the focussed ion beam technique. *Macromolecules*, Vol. 38, pp. 3048-3050.
- Noel, F. and Corbett, L. W. (1970) A study of the crystalline phase in asphalts. *Journal of the Institute of Petroleum*, Vol. 56, pp. 261-268.
- NYT (1940) *Death ray for planes*. New York Times, September 22.
- O'Connor, K. M. (1984) *Crack healing in polymers*. PhD Thesis, University of Illinois.
- O'Connor, K.M. and Wool, R.P. (1980) Optical studies for void formation and healing in styrene-isoprene-styrene block copolymers. *Journal of Applied Physics*, Vol. 51, pp. 5075-5079.
- Oatley, C. W. (1982) The early history of the scanning electron microscope. *Journal of Applied Physics*, Vol 53, pp. 1-13.
- Office for National Statistics (ONS) (2008) *Construction statistics annual: 2008*. [http://www.statistics.gov.uk/downloads/theme\\_commerce/CSA\\_2008\\_final.pdf](http://www.statistics.gov.uk/downloads/theme_commerce/CSA_2008_final.pdf) Date accessed 7 March 2011.
- Oliveira, G. E., Mansur, C. R. E., Lucas, E. F., González, G. and de Souza, W. F. (2007) The effect of asphaltenes, naphthenic acids and polymeric inhibitors on the pour point of paraffin solids. *Journal of Dispersion Science and Technology*, Vol. 28, pp. 349-356.
- de Oliveira, J.R.M. (2006) *Grouted macadam – material characterisation for pavement design*. The University of Nottingham, PhD Thesis.

- Orloff, J. H. and Swanson, L. W. (1975) Study of a field-ionisation source for microprobe applications. *Journal of Vacuum Science & Technology*, Vol. 12, Issue 6, pp. 1209-1213.
- Orloff, J., Uttaut, M. and Swanson, L. (2003) *High resolution focussed ion beams: FIB and its applications*. New York: Kluwer Academic/Plenum Publishers, pp. 123-125.
- Osman, S.A. (2006) *The Role of Bitumen/Filler Mortar in Bituminous Mixture Fatigue*. The University of Nottingham, PhD Thesis.
- Overfield, R. E., Sheu, E. Y., Sinha, S. K. and Liang, K. S. (1989) SANS study of asphaltene aggregation. *Fuel Science and Technology International*, Vol. 7, Issue 5-6, pp. 611-624.
- Padgett, F. W., Hefley, D. G. and Henriksen, A. (1926) Wax crystallisation: a preliminary report. *Industrial and Engineering Chemistry*, Vol. 18, p. 832.
- Park, S. J. and Mansoori, G. A. (1988) Aggregation and deposition of heavy organics in petroleum crudes. *Energy Sources*, Vol. 10, Issue 2, pp. 109-125.
- Paso, K., Senra, M., Yi, Y., Sastry, A. M. and Fogler, H. S. (2005) Paraffin polydispersity facilitates mechanical gelation. *Industrial and Chemical Engineering Research*, Vol. 44, pp. 7242-7254.
- Pauli, T., Beemer, A. and Miller, J. (2005) Asphalt solidification theory. *Proceedings of the 43<sup>rd</sup> Peterson Asphalt Research Conference*, Laramie.
- Pauli, T., Grimes, W., Boysen, R. and Kringos, N. (2011) Chemo-mechanics of bituminous materials. *Proceedings of the RILEM Technical Committee TC 231 workshop on micro- and nano-characterisation and modelling of bituminous materials*, Duebendorf.
- Pauling, L. (1988) *General Chemistry*. New York: Dover Publications Incorporated, pp. 197-198.
- Pell, P.S. (1962) *Fatigue Characteristics of Bitumen and Bituminous Mixes*. Nottingham: Shell International Publications Company Limited, pp. 19-31.
- Perkins, T.T., Smith, D.E. and Chu, S. (1994) Direct observation of tube-like motion of a single polymer chain. *Science*, Vol. 264, pp. 819-822.
- Peterson, J.C. (1984) Chemical composition of asphalt as related to asphalt durability: state of the art. *Transportation Research Record: Journal of the Transportation Research Board*, Vol. 999, pp. 13-30.
- Peterson, J. C. (2000) Chemical composition of asphalt as related to asphalt durability. In T. F. Yen and G. V. Chilingar (Eds.) *Asphaltenes and asphalts*. London: Elsevier Science B.V., pp. 363-399.
- Peterson, J. C. (2009) A review of the fundamentals of asphalt oxidation: chemical, physicochemical, physical property and durability relationships. *Transportation Research Circular*, No. E-C140.
- Peterson, J. C., Robertson, R. E., Branthayer, J. F., Hamsberger, P. M., Duvall, J. J. and Kim, S. S. (1994) *Binder characterisation and evaluation: volume 1*. SHRP report A-367, Washington D. C.: National Research Council.
- Peterson, J. C., Robertson, R. E., Branthaver, J. F., Harnsberger, P. M., Duvall, J. J., Kim, S. S., Anderson, D. A., Christensen, D. W., Bahia, H. U., Dongre, R., Sharma, M. G., Antle, C. E., Button, J. W. and Glover, C. J. (1994) *Binder Characterisation and Evaluation, Volume 4: Test Methods*. SHRP-A-370, Strategic Highways Research Program, National Research Council, Washington D.C.

- Peralta, E. J. F. (2009) *Study of the interaction between bitumen and rubber*. Universidade do Minho, Masters Dissertation.
- Pfeiffer, J.P.H. and Saal, R.N.J. (1939) Asphaltic bitumen as colloid system. *The Journal of Physical Chemistry*, Vol. 44, No. 2, pp. 139-149.
- Phaneuf, M. W. (1999) Applications of focussed ion beam microscopy to materials science specimens. *Micron*, Vol. 30, Issue 3, pp. 277-288.
- Phillips, M.C. (1999) Multi-step models for fatigue and healing, and binder properties involved in healing. *Proceedings of the Eurobitume Workshop: Performance Related Properties for Bituminous Binders*, Paper No. 115, Luxembourg.
- Planche, J.-P., Anderson, D.A., Gauthier, G., Le Hir, Y.M. and Martin, D. (2004) Evaluation of fatigue properties of bituminous binders. *Materials and Structures / Matériaux et Constructions*, Vol. 37, pp. 356-359.
- Poirier, M.-A. and George, A. E. (1983) Thin layer chromatographic method for determination of asphaltene content in crude oils and bitumens. Vol. 7, Issue 2, pp. 165-176.
- Poulidakos, L. D. (2011) *A multi-scale fundamental investigation of moisture induced deterioration of porous asphalt concrete*. ETH Zurich, PhD Thesis.
- Prager, S. and Tirrell, S. (1981) The healing process at polymer-polymer interfaces. *Journal of Chemical Physics*, Vol. 75, pp. 5194-5197.
- Prinsen, P. and van der Schoot, P. (2003) Shape and director-field transformation of tactoids. *Journal of the American Physical Society, Physical Review E*, Vol. 68, pp. 021701-01-021701-11.
- Pullman, B. and Pullman, A. (1963) *Quantum Biochemistry*. New York: Interscience.
- Qi, X. (2006) *Integrated optical devices for telecommunications*, University of Minnesota: PhD Thesis, pp. 16-18.
- Qiu, J. (2012) Self-healing of asphalt mixtures: towards a better understanding of the mechanism. PhD Thesis, Technische Universiteit Delft.
- Quéré, D. (2008) Wetting and roughness. *The Annual Review of Materials Research*, Vol. 38, pp. 71-79.
- Radlinski, A. P., Barré, L. and Espinat, D. (1996) Aggregation of *n*-alkanes in organic solvent. *Journal of Molecular Structure*, Vol. 383, pp. 51-56.
- Raithby, K.D. and Sterling, A.B. (1970) The effect of rest periods on the fatigue performance of a hot-rolled asphalt under reversed axial loading. *Proceedings of the Association of Asphalt Paving Technologists*, Vol. 39, pp. 134-152.
- Raithby, K.D. and Sterling, A.B. (1972) Some effects of loading history on the fatigue performance of rolled asphalt. *Transport and Road Research Laboratory*, Report No. LR-496.
- Raki, L., Masson, J.-F. and Collins, P. (2000) Rapid bulk fractionation of maltenes into saturates, aromatics and resins by flash chromatography. *Energy & Fuels*, Vol. 14, Issue 1, pp. 160-163.
- Ramond, G., Pastok, M. and Suck, C. (1993) *Recherche des performances d'un liant a partir de son module complexe*. Proceedings of the 5<sup>th</sup> Eurobitume Congress, Stockholm, Abstracts and Reports, p. 81.

- Ramsay, J. D. F. (1992) Characteristics of inorganic colloids. *Pure and Applied Chemistry*, Vol. 64, No. 11, pp. 1709-1713.
- Rassamdana, H., Dabir, B., Nematy, M., Farhani, M. and Sahimi, M. (1996) Asphalt flocculation and deposition: 1. The onset of precipitation. *Journal of The American Institute of Chemical Engineers*, Vol.42, No. 1, pp. 10-22.
- Ravey, J. C., Ducouret, G. and Espinat, D. (1988) Asphaltene macrostructure by small angle neutron scattering. *Fuel*, Volume 67, pp. 1560-1567.
- Read, J.M. (1999) New method for measuring crack propagation in asphalts. *International Journal of Pavement Engineering*, Vol. 1, pp. 15-34.
- Read, J.M. and Whiteoak, D. (2003) *The Shell Bitumen Handbook*. London: Thomas Telford Publishing, pp. 195-208.
- Redelius, P. (2006) The structure of asphaltenes in bitumen. *International Journal of Road Materials and Pavement Design*, Special Issue: EATA 2006, pp. 143-162.
- Redelius, P. (2007) Hansen solubility parameters of asphalt, bitumen and crude oils. *Hansen solubility parameters: a user's handbook*. Boca Raton: CRC Press, pp. 151-158.
- Redelius, P. (2011) *Relation between bitumen chemistry and performance*. *Proceedings of the RILEM Technical Committee TC 231 workshop on micro- and nano-characterisation and modelling of bituminous materials*, Duebendorf.
- Redelius, P. and Soenen, H. (2005) Correlation between bitumen polarity and rheology. *International Journal of Road Materials and Pavement Design*, Vol. 6, No. 3, pp. 385-405.
- Refined Bitumen Association (RBA) (2011) *Bitumen manufacture*. <http://www.bitumenuk.com/bitumen-manufacture.asp> Date accessed 15 June 2011.
- Reimer, L. (1975) Review of the radiation damage problem of organic specimens in electron microscopy. *Physical Aspects of Electron Microscopy and Microbeam Analysis*. New York: Wiley.
- Rek, V. and Barjaktarović, Z.M. (2002) Dynamic mechanical behaviour of polymer modified bitumen. *Materials Research Innovation*, Vol. 6, No. 2, pp. 39-43.
- Rekvelde, M. T., van Dijk, N., Grigoriev, S., Kraan, W. H. and Bouwman, W. G. (2006) Three-dimensional magnetic spin-echo small-angle neutron scattering and neutron depolarisation: a comparison. *Review of Scientific Instruments*, Vol. 77, pp. 073902 01-10.
- Rhodes, F. H., Mason, C. W. and Sutton, W. R. (1927) Crystallisation of paraffin wax. *Industrial and Engineering Chemistry*, Vol. 19, No. 8, pp. 935-938.
- Rivlin, R. S. and Thomas, A. G. (1953) Rupture of rubber one: characteristic energy for tearing. *Journal of Polymer Science*, Vol. 10, Issue 3, pp. 291-318.
- Robards, A. W. and Wilson, A. J. (1998) *Procedures in Electron Microscopy*. New York: John Wiley and Sons.
- Robinson, V. N. E. (1975) A wet stage modification to a scanning electron microscope. *Journal of Microscopy*, Vol. 103, Issue 1, pp. 71-77.
- Robertson, R. E. (1991) *Chemical properties of asphalts and their relationship to pavement performance*. Washington, D.C.: Western Research Institute, Strategic Highways Research Program, National Research Council

- Robertson, R. E., Branthaver, J. F. and Peterson, J. C. (1992) Development of a performance related chemical model of petroleum asphalt for SHRP. *American Chemical Society Division of Fuel Chemistry Preprints*, Vol. 37, Issue 3, pp. 1272-1278.
- Rohli, R. V. and Vega, A. J. (2012) *Climatology*. Sudbury: Jones & Bartlett Learning, pp. 153-156.
- van Rompu, J., Di Benedetto, H., Gauthier, G. and Gallet, T. (2009) New fatigue test on bituminous binders and mastics using an annular shear rheometer and waves propagation. *Proceedings of the Seventh International RILEM Symposium*, pp. 69-79, Rhodes.
- Rosen, B. (Ed.) (1964) *Fracture processes in polymeric solids: phenomena and theory*. New York: Wiley.
- Rosinger, A. (1914) Beiträge zur Kolloidchemie des Asphalts. *Kolloid-Zeitschrift*, Vol. 15, pp. 177-179.
- Rowe, G.M. (1996) *Application of the Dissipated Energy Concept to Fatigue Cracking in Asphalt Pavements*. The University of Nottingham, PhD Thesis, pp. 3.19-3.30.
- Rowe, G.M. and Bouldin, M.G. (2000) Improved techniques to evaluate the fatigue resistance of asphalt mixtures. *Proceedings of the Second Eurasphalt and Eurobitume Congress*, Book One, pp. 754-763, Barcelona.
- Ruska, E. (1986) *Ernst Ruska: Autobiography*. The Nobel Foundation  
[http://nobelprize.org/nobel\\_prizes/physics/laureates/1986/ruska-autobio.html](http://nobelprize.org/nobel_prizes/physics/laureates/1986/ruska-autobio.html) Date accessed 5 June 2011.
- Salih, S. M. and Cosslett, V. E. (1975) Radiation damage in electron microscopy of organic materials: effect of low temperatures. *Journal of Microscopy*, Vol. 105, No. 3, pp. 269-276.
- Santagata, E., Baglieri, O., Dalmazzo, D. and Tsantilis, L. (2009) Rheological and chemical investigation on the damage and healing properties of bituminous binders. *Journal of the Association of Asphalt Paving Technologists*, Vol. 78, pp. 567-596.
- Sawyer, L. C. and Grubb, D. T. (1996) *Polymer Microscopy*. London: Chapman and Hall, pp. 70-77.
- Sawyer, L. C., Grubb, D. T. and Meyers, G. F. (2008) *Polymer microscopy*. New York: Springer Science and Business Media, pp. 194-196.
- Schapery, R.A. (1984) Correspondence principles and a generalised J integral for large deformation and fracture analysis of viscoelastic media. *International Journal of Fracture*, Vol. 25, pp. 195-223.
- Schiffbauer, J. D. and Xiao, S. (2011) Palaeobiological applications of focussed ion beam electron microscopy (FIB-EM): an ultrastructural approach to the (micro) fossil record. In M. Laflamme, J. D. Schiffbauer and S. Q. Dornbos (Eds.) *Quantifying the evolution of early life*, New York: Springer Science and Business Media, Inc., pp. 322-325.
- Schmets, A., Kringos, N., Pauli, T., Redelius, P. and Scarpas, T. (2010) On the existence of wax-induced phase separation in bitumen. *International Journal of Pavement Engineering*, Vol. 11, No. 6, pp. 555-563.
- Schonhorn, H. (1978) Surface modification of polymers for adhesive bonding. In A.T. Clark and W.J. Feast (Ed.) *Polymer Surfaces*, Wiley Interscience, pp. 213-234.
- Schweitzer, P.A. (2007) *Fundamentals of Metallic Corrosion: Atmospheric and Media Corrosion of Metals*, Boca Raton: CRC Press, p. 12.

- Scriven, L. E. and Sterling, C. V. (1960) The Marangoni effects. *Nature*, Vol. 187, pp. 186-188.
- Seo, Y. and Kim, Y.R. (2008) Using acoustic emission to monitor fatigue damage and healing in asphalt concrete. *Korean Society of Civil Engineers Journal of Civil Engineering*, Vol. 12, pp. 237-243.
- Shan, L., Tan, Y., Underwood, S. and Kim, Y. R. (2010) Application of thixotropy to analyse fatigue and healing characteristics of asphalt binder. 2010 Annual Meeting of the Transportation Research Board.
- Sheehan, J. G. (1995) Electron microscopy. In J. V. Koleske (Ed.) *Paint and coating testing manual*. Philadelphia: American Society for Testing and Materials, pp. 815-825.
- Shen, S. and Carpenter, S.H. (2005) Application of the dissipated energy concept in fatigue endurance limit testing. *Transportation Research Record: Journal of the Transportation Research Board*, Vol. 1929, pp. 165-173.
- Shen, S. Chiu, H.-M. and Huang, H. (2009) Fatigue and healing in asphalt binders. *Proceedings of the Transportation Research Board 88<sup>th</sup> Annual Meeting*, Report No. 09-1338.
- Shen, S., Chiu, H.-M. and Huang, H. (2010) Characterisation of fatigue and healing in asphalt binders. *Journal of Materials in Civil Engineering*, Vol. 22, pp. 846-852.
- Shim, M.-J. and Kim, S.-W. (1997) Characteristics of polymer welding by healing process. *Materials Chemistry and Physics*, Vol. 48, pp. 90-93.
- Shkrob, I. A., Sauer, M. C. and Trifunac, A. D. (2001) Radiation chemistry of organic liquids: saturated hydrocarbons. In C. D. Jonah and B. S. Rao (Eds.) *Radiation Chemistry: Present Status and Future Trends*, Amsterdam: Elsevier Science, pp. 175-221.
- Si, Z., Little, D.N. and Lytton, R.L. (2002) Characterisation of microdamage and healing of asphalt concrete mixtures. *Journal of Materials in Civil Engineering*, Vol. 14, pp. 461-470.
- Siangchaew, K. and Libera, M. (1999) The influence of fast secondary electrons on the aromatic structure of polystyrene. *Philosophical Magazine A*, Vol. 80, Issue 4, pp. 1001-1016.
- Siegel, (1972) Der Einfluss tiefer Temperaturen auf die Strahlenschädigung von organischen Kristallen durch 100 keV-Elektronen. *Zeitschrift für Naturforschung A*, Vol. 27, pp. 325-332.
- da Silva, J. A. L. and Couthino, J. A. P. (2004) Dynamic rheological analysis of the gelation behaviour of waxy crude oils. *Rheological Acta*, Vol. 43, Issue 5, pp. 433-441.
- Silva, E. and Ulm, F.-J. (2002) A bio-chemo-mechanics approach to bone resorption and fracture. *Proceedings of the 15<sup>th</sup> American Society of Civil Engineers Engineering Mechanics Conference*, Columbia University.
- Simpson, W. C., Griffin, R. L. and Miles, T. K. (1961) Relationship of asphalt properties to chemical constitution. *Journal of Chemical and Engineering Data*, Vol. 6, No. 3, pp. 426-429.
- Singh, P. and Fogler, H. S. (1999) Prediction of the wax content of the incipient wax-oil gel in a pipeline: an application of the controlled stress rheometer. *Journal of Rheology*, Vol. 43, pp. 1437-1459.
- Singh, P., Venkatesan, R., Fogler, H. S. and Nagarajan, N. (2000) Formation and ageing of thin film wax-oil gels. *Journal of The American Institute of Chemical Engineers*, Vol. 46, No. 5, pp. 1059-1074.

- Smith, B.J. and Hesp, S.A.M. (2000) Crack pinning in asphalt mastic and concrete. *Transportation Research Record: Journal of the Transportation Research Board*, Vol. 1728, pp. 75-81.
- Smith, B.J. and Hesp, S.A.M (2000b) Crack pinning in asphalt mastic and concrete: effect of rest periods and polymer modifiers on the fatigue life. *Proceedings of the Second Eurasphalt and Eurobitume Congress*, Book Two, pp. 539-546, Barcelona.
- Smoot, R.C., Price, J. and Barrett, R. L. (1983) *Chemistry: A Modern Course*. Charles E. Merrill Books, pp. 239-240.
- Soenen, H. and Berghmans, H. (1994) Phase behaviour and gelation of solutions of poly(vinyl chloride). *Polymer Gels and Networks*, Vol. 2, pp. 159-172.
- Soenen, H., Ekblad, J. and Redelius, P. (2004) Isothermal hardening in bitumen and in asphalt mixtures. *Proceedings of the Third Eurasphalt and Eurobitume Congress*, Vienna .
- Soenen, H., Visscher, J., Vanelstraete, A. and Redelius, P. (2006) Influence of thermal history on rheological properties of various bitumen. *Rheological Acta*, Vol. 45, pp. 729-739.
- South, J. T., Case, S. W. and Reifsnider, K. L. (2002) Crack growth of natural rubber using a modified double cantilever beam. *Mechanics of Materials*, Vol. 34, Issue 8, pp. 451-458.
- Sourty, E. D., Tamminga, A. Y., Michels, M. A. J., Vellinga, W.-P. and Meijer, H. E. H. (2011) The microstructure of petroleum vacuum residue films for bituminous concrete: a microscopy approach. *Journal of Microscopy*, Vol. 241, Part 2, pp. 132-146.
- Speight, J. G. (2007) *The chemistry and technology of petroleum*. Fourth edition. Boca Raton: CRC Press, pp. 293-294.
- Sperling, L. H. (2006) Introduction to physical polymer science. New Jersey: John Wiley & Sons, pp. 585-600.
- Srivastava, S. P., Handoo, J., Agrawal, K. M. and Joshi, G. C. (1993) Phase transition studies in *n*-alkanes and petroleum-related waxes: a review. *Journal of Physics and Chemistry of Solids*, Vol. 54, Issue 6, pp. 639-670.
- Stangl, K., Jäger, A. and Lackner, R. (2004) Microstructure-based identification of bitumen performance. *International Journal of Road Materials and Pavement Design*, Vol. 5, pp. 111-142.
- Starkova, O. and Aniskevich, A. (2007) Limits of linear viscoelastic behaviour of polymers. *Mechanics of Time-Dependent Materials*, Vol. 11, pp. 111-126.
- Starov, V.M. (2008) *Current problems in kinetics of wetting and spreading*. Presentation at The University of Nottingham.
- Starov, V.M., Verlade, M.G. and Radke, C.J. (2007) *Wetting and spreading dynamics (surfactant science)*. Boca Raton: CRC Press, pp. 1-3.
- Steffe, J. F. (1996) *Rheological methods in food process engineering*. East Lansing: Freeman Press, pp. 1-93.
- Stevie, F. A., Giannuzzi, L. A. and Prenitzer, B. I. (2005) The focussed ion beam instrument. In L. A. Giannuzzi and F. A. Stevie (Eds.) *Introduction to focussed ion beams instrumentation, theory, techniques and practice*, New York: Springer Business and Media, pp. 1-12.

- Stokes, D. J. (2008) *Principles and practice of variable pressure/environmental scanning electron microscopy*. Chichester: John Wiley & Sons, pp. 1-12.
- Stokes, D. (2011) *ESEM: imaging tissue cultured cells*. Hillsboro: FEI Company, Application Note 032, pp. 3-14.
- Stokes, D. J., Reyntjens, S., Jiao, C., Hayles, M. F. and Hubert, D. H. W. (2007) New characterisation techniques for the study of nanoscale polymeric systems in two- and three-dimensions. *Technical Proceedings of the 2007 NSTI Nanotechnology Conference and Trade Show*, Volume 2, pp. 45-48.
- Storm, D. A., Barresi, R. J. and Sheu, E. Y. (1995) Rheological study of Ratwai vacuum residue in the 298-673K temperature range. *Energy Fuels*, Vol. 9, pp. 168-176.
- Stulirova, J. and Pospisil, K. (2008) Observation of bitumen microstructure changes using scanning electron microscopy, *International Journal of Road Materials and Pavement Design*, Vol. 9, No. 4, pp 745-754.
- Svedberg, T. (1921) *The formation of colloids*. New York: D. Van Nostrand Company, pp. 9-14.
- Swanson, J. M. (1942) A contribution to the physical chemistry of the asphalts. *Journal of Physical Chemistry*, Vol. 46, pp. 141-150.
- Sybilski, D., Vanelstraete, A. and Partl, M. N. (2004) Recommendation of RILEM TC 182-PEB on bending beam and rheometer measurements of bituminous binders. *Materials and Structures*, Vol. 37, pp. 539-546.
- Tangella, S., Craus, J., Deacon, J. A. and Monismith, C. L. (1990) *Summary report on fatigue response of asphalt mixtures*. TM-UCB-A-003A-89-3, Strategic Highways Research Program, National Research Council, Washington D.C.
- Tarefder, R. A., Arifuzzaman, M. and Uddin, W. (2010) Determining hardness and elastic modulus of asphalt by nanoindentation. *International Journal of Geomechanics*, ASCE, Vol. 10, No. 2, pp. 106-116.
- Taylor, K. A. and Glaeser, R. M. (1973) Hydrophilic support films of controlled thickness and composition. *Review of Scientific Instruments*, Vol. 44, pp. 1546-1547.
- Taylor, K. A. and Glaeser, R. M. (2008) Retrospective on the early development of cryo-electron microscopy of macromolecules and a perspective on opportunities for the future. *Journal of Structural Biology*, Vol. 163, Issue 3, pp. 214-223.
- Teugels, W. and Gustavsson, B. (1995) *Practical experience in working with a controlled stress rheometer*. Proceedings of the Rheology of Bituminous Binders European Workshop, Brussels, Paper No. 3.
- Teugels, W. and Nilsson, A. M. (1995) *Comparison of two different temperature control systems on a controlled stress rheometer*. Proceedings of the Rheology of Bituminous Binders European Workshop, Brussels, Paper No. 3.
- Teunou, E. and Fitzpatrick, J.J. (2000) Effect of storage time and consolidation on food powder flowability. *Journal of Food Engineering*, Vol. 43, pp. 97-101.
- Thom, N.H. (2007) *Railway Engineering: ballast properties*. The University of Nottingham, Civil Engineering Course Notes, pp. 12-25.

- Thom, N.H. (2008) *Principles of Pavement Engineering*. London: Thomas Telford Publishing Limited, pp. 10, 118-120, 282, 349.
- Thom, N.H., Osman, S., Collop, A.C. and Airey, G.D. (2006) Fracture and fatigue of binder and binder / filler mortar. *Proceedings of the Tenth International Conference on Asphalt Pavements*, pp. 10-26, Quebec City.
- Tinsley, J. F., Jahnke, J. P., Dettman, H. D. and Prud'home, R. K. (2009) Waxy gels with asphaltenes 1: characterisation of precipitation, yield stress and morphology. *Energy and Fuels*, Vol. 23, pp. 2056-2064.
- Toda, A., Okamura, M., Hikosaka, M. and Nakagawa, Y. (2005) Three-dimensional shape of polyethylene single crystals grown from dilute solutions and from the melt. *Polymer*, Vol. 46, pp. 8708-8716.
- Traxler, R. N. (1936) The physical chemistry of asphaltic bitumen. *Chemical Review*, Vol. 19, No. 2.
- Traxler, R. N. and Coombs, C.E. (1935) The colloidal nature of asphalt as shown by its flow properties. *The Journal of Physical Chemistry*, Vol. 44, pp. 149-165.
- Tseng, K. and Lytton, R. (1990) Fatigue damage properties of asphalt concrete pavements. *Transportation Research Record: Journal of the Transportation Research Board*, Vol. 1286, pp. 84-97.
- Turnbull, D. and Cohen, M. H. (1961) Free-volume model of the amorphous phase: glass transition. *The Journal of Chemical Physics*, Vol. 34, No. 1, pp. 120-125.
- Turner, W. R. (1971) Normal Alkanes. *Industrial Engineering Chemistry Product Research and Development*, Vol. 10, No. 3, pp. 238-260.
- Uchida, K., Kurokawa, T., Himeno, K. and Nishizawa, T. (2002) Healing characteristics of asphalt mixture under high temperature conditions. *Proceedings of the 9<sup>th</sup> Conference on Design of Asphalt Pavements*, International Society for Asphalt Pavements, Copenhagen.
- Ulm, F.-J. (2003) Chemomechanics of concrete at finer scales. *Materials and Structures*, Vol. 36, pp. 426-438.
- U.S. Energy Information Administration, EIA (2009) *Top world oil producers, 2009*. <http://www.eia.gov/countries/> Date accessed 17 June 2011.
- Utlaut, M. (2009) Focussed ion beams. In J. Orloff (Ed.) *Handbook of charged particle optics*. Second edition. Boca Raton: CRC Press, pp. 523-536.
- Uzan, J. (1997) Evaluation of fatigue cracking. *Transportation Research Record: Journal of the Transportation Research Board*, Vol. 1570, 99. 89-95.
- Uzan, J. and Levenberg, E. (2001) Strain measurements in asphalt concrete specimens towards the development of a fracture model. *International Journal of Pavement Engineering*, Vol. 2, pp. 243-258.
- Vara, L. A. A. and Gonzalez, E. B. (2012) Experimental study of the influence of solvent and asphaltenes on liquid-solid phase behaviour of paraffinic model systems by using DSC and FT-IR techniques. *Journal of Thermal Analysis and Calorimetry*, Vol. 107, pp. 1321-1329.
- Venkatesan, R., Singh, P. and Fogler, H. S. (2002) Delineating the pour point and gelation temperature of waxy crude oils. *Journal of The Society of Petroleum Engineers*, Vol. 7, No. 4, pp. 349-352.

- Verstraeten, J. (1991) Fatigue of bituminous mixes and bitumen thixotropy. *Proceedings of the 19<sup>th</sup> World Road Congress*, AIPCR, Marrakech, pp. 766-769.
- Violi, A., Truong, T. N. and Sarofim, A. F. (2004) Kinetics of hydrogen abstraction reactions from polycyclic aromatic hydrocarbons by H atoms. *Journal of Physical Chemistry, Part A*, Vol. 108, pp. 4846-4852.
- Visintin, R. F., Lapasin, R., Vignati, E., D'Antona, P. and Lockhart, T. P. (2005) Rheological behaviour and structural interpretation of waxy crude oil gels. *Langmuir*, Vol. 21, pp. 6240-6249.
- Walther, P. (2008) High resolution cryoscanning electron microscopy of biological samples. In H. Schatten and J. B. Pawley (Eds.) *Biological low-voltage scanning*. New York: Springer Science and Business Media, Inc., pp. 245-262.
- Wagoner, M.P., Buttlar, W.G. and Paulino, G.H. (2005) Disc-shaped compact tension test for asphalt concrete fracture. *Experimental Mechanics*, Vol. 45, pp. 270-277.
- Wang, H., Feng, H., Liang, W., Luo, Y. and Malyarchuk, V. (2009) Effect of surface roughness on retention and removal of *Escherichia coli* 0157:H7 on surfaces of selected fruits. *Journal of Food Sciences E: Food Engineering and Physical Properties*, Vol. 74, No. 1, pp. 8-15.
- Waters, J. C. (2008) *Developing and trialling a climate-based selection guideline for chipseal binders*. New Zealand Transport Agency, Research Report 358, pp. 28-30.
- Wei, J., Huang, X. and Zhang, Y. (2010) Influence of commercial wax on performance of asphalt. *Journal of Materials in Civil Engineering*, Vol. 22, Issue 8, pp. 760-766.
- Wekumbura, C., Strastna, J. and Zanzotto, L. (2007) Destruction and recovery of internal structure in polymer-modified asphalts. *Journal of Materials in Civil Engineering*, Vol. 19, pp. 227-232.
- Widyatmoko, I., Elliott, R. C., Heslop, M. W. and Williams, J. T. (2002) Ageing characteristics of some low penetration grade binders. In S. E. Zoorob, A. C. Collop and S. F. Brown (Eds.) *Performance of bituminous and hydraulic materials in pavements*, Lisse: Swets and Zeitlinger, pp. 13-24.
- Williams, D., Little, D. N., Lytton, R. L., Kim, Y. R. and Kim, Y. (2001) Microdamage and microdamage healing in asphalt concrete, volume two: laboratory and field testing to assess and evaluate microdamage and microdamage healing. *The Federal Highway Administration*, Report No. RD-98-144.
- Wilson, M. (2001) *Simulations of side-chain liquid crystal polymers and dendrimers*. Durham University: The Wilson Group  
[http://www.dur.ac.uk/mark.wilson/polymers\\_and\\_dendrimers.html](http://www.dur.ac.uk/mark.wilson/polymers_and_dendrimers.html) date accessed 7 May 2012.
- Wilson, A., Fuchs, G., Scramoncin, C., Martin, D. and Planche, J. P. (2000) Localisation of the polymer phase in bitumen/polymer blends by field emission gun cryo-scanning electron microscopy. *Energy and Fuels*, Vol. 14, pp. 575-584.
- Wirth, R. (2009) Focussed ion beam (FIB) combined with SEM and TEM: advanced analytical tools for studies of chemical composition, microstructure and crystal structure in geomaterials on a nanometre scale. *Chemical Geology*, Vol. 261, Issues 3-4, pp. 217-229.
- Wise, S. M., Kim, J. S. and Johnson, W. C. (2005) Surface-directed spinodal decomposition in a stressed, two-dimensional thin film. *Thin Solid Films*, Vol. 473, pp. 151-163.

- Woldekidan, M. F., Huurman, M. and Mo, L. T. (2010) Testing and modelling of bituminous mortar response. *Journal of Wuhan University of Technology: Materials Science Edition*, Vol. 25, No. 4, pp. 637-640.
- Wong, K. C., Haslauer, C. M., Anantharamaiah, N., Pourdeyhimi, B., Batchelor, A. D. and Griffis, D. P. (2010) Focussed ion beam characterisation of bicomponent polymer films. *Microscopy and Microanalysis*, Vol. 16, Issue 3, pp. 282-290.
- Wool, R.P. (1979) Crack healing in semicrystalline polymers, block copolymers and filled elastomers. *Polymer Science and Technology*, Vol. 12A, pp 341-362.
- Wool, R. P. (1990) *Strength of polymer interfaces*. US Army Research Office, Report No. 22966-MS, pp. 3-40.
- Wool, R. P. (1993) Polymer entanglements. *Macromolecules*, Vol. 26, pp. 1564-1569.
- Wool, R.P. (1995) *Polymer Interfaces: Structure and Strength*. New York: Carl Hanser Verlag.
- Wool, R.P. and O'Connor, K.M. (1981) A theory of crack healing in polymers. *Journal of Applied Physics*, Vol. 52, No. 10, pp. 5953-5963.
- Wu, J. (2009) The influence of mineral aggregates and binder volumetrics on bitumen ageing. The University of Nottingham, PhD Thesis.
- Wu, S. (1982) *Polymer Interface and Adhesion*. New York: Marcel Dekker Incorporated, pp. 29-65.
- Wu, S., Pang, L., Liu, G. and Zhu, J. (2010) Laboratory study on ultraviolet radiation ageing of bitumen. *Journal of Materials Science in Engineering*, Vol. 22, No. 8, pp. 767-772.
- Wu, J. and Spence, J. C. H. (2003) Low-dose, low-temperature convergent-beam electron diffraction and multiwavelength analysis of hydrocarbon films by electron diffraction. *Microscopy and Microanalysis*, Vol. 9, pp. 428-441.
- Xiao, F., Punith, V. S. and Amirghanian, S. N. (2012) Effects of non-foaming WMA additives on asphalt binders at high performance temperatures. *Fuel*, Vol. 94, pp. 144-155.
- Xu, T. and Huang, X. (2012) Combustion properties of asphalt binder containing flame retardant. *Fire and Materials*, Vol. 36, pp. 97-106.
- Xu, W. and Li, G. (2010) Constitutive modelling of shape memory polymer based self-healing syntactic foam. *International Journal of Solids and Structures*, Vol. 47, pp. 1306-1316.
- Yang, S.-H. and Al-Qadi, I.L. (2009) Direct observation of bitumen-aggregate interface. *Proceedings of the 88<sup>th</sup> Meeting of the Transport Research Board*, Washington, D.C.
- Yang, X. and Kilpatrick, P. (2005) Asphaltenes and waxes do not interact synergistically and co-precipitate in solid organic deposits. *Energy and Fuels*, Vol. 19, pp. 1360-1375.
- Yoder, E.J. and Witczak, M.W. (1975) *Principles of Pavement Design*. John Wiley & Sons Incorporated, pp. 16-18
- Zaikin, Y. A. and Zaikina, R. F. (2008) New trends in the radiation processing of petroleum. In A. N Camilleri (Ed.) *Radiation Physics Research Progress*, New York: Nova Science, pp. 17-103.
- Zanini, S., Riccardi, C., Orlandi, M., Esena, P., Tontini, M., Milani, M. and Cassio, V. (2005) Surface properties of HMDSO plasma treated polyethylene terephthalate. *Surface and Coatings Technology*, Vol. 200, pp. 953-957.

Zaki, N., Schoning, P. C. and Rahimian, I. (2000) Effect of asphaltene and resins on the stability of water-in-waxy oil emulsions. *Petroleum Science and Technology*, Vol. 18, Nos. 7-8, pp. 945-963.

Zhang, F., Ouyang, J., Wang, D. and Feng, X. (2012) Mechanism of high-carbon paraffin deposition and preventing methods. *Advanced Materials Research*, Vols. 396-398, pp. 1102-1105.

Zhang, L. Y., Xu, Z. and Masliyah, J. H. (2003) Langmuir and Langmuir-Blodgett films of mixed asphaltene and a demulsifier. *Langmuir*, Vol. 19, pp. 9730-9741.

Zhang, H. L., Yu, J. Y., Feng, Z. G., Xue, L. H. and Wu, S. P. (2011) Effect of ageing on the morphology of bitumen by atomic force microscopy. *Journal of Microscopy*, Vol. 246, Issue 1, pp. 11-19.

Zhou, Z. H. (2008) Towards atomic resolution structural determination by single-particle cryo-electron microscopy. *Current Opinion in Structural Biology*, Vol. 18, pp. 218-228.

Zollinger, C. J. (2005) Application of surface energy measurements to evaluate moisture susceptibility of asphalt and aggregates. Master's Thesis, Texas A&M University.